Towards high-volume, primary bonded, lightweight automotive structures.

by

Richard John Roy Woodward

Innovation Report

Submitted to the University of Warwick in partial fulfilment of the degree of

Doctor of Engineering

Wednesday 31st October 2018

Abstract

Increasing pressures upon high-volume automotive manufacturers has led to the requirement for lightweight body structures. These increasingly require the introduction of lightweight materials, such as fibre reinforced polymer composites. As a result, effective joining technologies are a key automotive industry requirement to enable the introduction of optimal, lightweight material combinations to automotive body structures. Following an extensive literature review, adhesive bonding techniques were identified as a potentially suitable joining solution. However, two key barriers to the adoption of adhesive only, primary bonded, structural joints within the high-volume automotive industry were identified. These were the requirement for optimal surface treatment methods for composites, applied prior to adhesive bonding and a technique to achieve rapid joint handling strength during manufacture. These industrial requirements formed the primary areas of research for this project.

An extensive investigation was performed to identify suitable surface pre-treatment methods, for high-volume adhesive bonding of composites. A particular focus was placed on the use of atmospheric pressure plasma surface treatment. It was identified that this process can effectively increase the surface free energy of both a thermoset and thermoplastic composite through modification of the surface chemistry. No significant increase in adhesive bond strength was found upon a thermoset substrate. The process can however effectively influence the adhesive joint failure mode upon a thermoplastic FRP surface, with joint durability implications. Limitations of the process were identified with respect to surface contamination removal.

Electromagnetic induction heating was identified as a method to rapidly heat composite and metallic substrates. As such the process was potentially suitable for accelerating the cure and strength development of structural adhesives. Equipment was specified and a bespoke testing methodology developed to identify the rate of joint strength development following optimised induction heating cycles. A full sized CFRP floor/sill joint sub-assembly was used to demonstrate the achievable joint handling strength within a sub one-minute cure cycle for a primary bonded composite intensive joint. It was demonstrated that manufacturing cycle time limitations are achievable with a load well in excess of a typical body in white weight applied prior to joint failure. As a result, the work has identified and developed, a potential high-volume joining solution to a present challenge facing the automotive industry.

Declaration

This innovation report is submitted to the University of Warwick in support of my application for the degree of Engineering Doctorate. It has been composed by myself and has not been submitted in any previous application for any degree. The work presented (including data generated and data analysis) was carried out by the author.

Engineering doctorate supervisors

Academic supervisors (WMG);

Professor Ken Kendall and Dr Darren Hughes.

Industrial supervisors (Jaguar Land Rover);

Paul Bristo (2013 – 2016), Adrian Hughes (2013 – 2016) and Eissa Senan.

Table of contents

List of figures

List of tables

Nomenclature

1K – One component

2K – Two component

ABR – Abraded surface

ACC – AC Current

AL - Aluminium

ANOVA – Analysis of variance

APPT – Atmospheric pressure plasma treatment

AR – As received

BE – Binding energy

CFRP – Carbon fibre reinforced polymer

CI – Confidence interval

CTE – Coefficient of thermal expansion

DIC – Digital image correlation

DoF – Degrees of freedom

DSC – Differential scanning calorimetry

DW – Dry wipe

EMF – Electromagnetic field

EPSRC - The Engineering and Physical Sciences Research Council

FEA – Finite element analysis

FRP – Fibre reinforced polymer

GF – Glass fibre

HP-RTM – High pressure resin transfer moulding

IPA - Isopropyl alcohol

IPS – In plane shear

JLR – Jaguar Land Rover

MS – Mean square

NCF – Non-crimp fabric

NVH – Noise, vibration and harshness

OWRK – Owens Wendt and Kaelble method of surface energy calculation

PA6 – Polyamide 6

PI – Prediction interval

Riv-bonded – A joining solution combining a rivet and structural adhesive

SEM – Scanning electron microscopy

SFE – Surface free energy

SLS – Single lap shear

SMC – Sheet moulding compound

SMR – Solvent based mould release

SPR – Self piercing rivet

SS – Sum of squares

Tg – Glass transition temperature

TP – Thermoplastic

TS – Thermoset

VG – Vacuum grease

WD – Working distance - the distance between the plasma torch tip and the workpiece

WMG – Warwick Manufacturing Group

WMR – Water based mould release

XPS – X-ray photoelectron spectroscopy

Acknowledgments

There are a number of people who have greatly contributed to the success of this project, and to who I would like to express my sincere gratitude. Firstly, to my academic supervisors Dr Darren Hughes and Professor Ken Kendall who have provided invaluable support and guidance from the project outset. Similarly, to Dr Helen Ascroft who has provided great deal of much appreciated advice upon many occasions.

I would like to thank the EPSRC and Jaguar Land Rover for sponsoring the project and giving me the opportunity to develop a great deal of knowledge over its duration. In particular I would like to thank my industrial supervisors, Paul Bristo, Adrian Hughes and Eissa Senan. Through their involvement with this project they have provided much industrial insight and assistance in ensuring the industrial value and progression of the project. Similarly, to many of their colleagues within Jaguar Land Rover who have provided many thought provoking discussions along the way.

There are a great number of people within WMG who I would like to thank for giving me their time and valuable experience. Neil Reynolds has helped no end with his extensive knowledge of composite materials and mechanical testing methods. Martyn Wilkins, Darren Stewardson and all of the WMG technicians who are a great source of assistance and enthusiasm. Further to my fellow doctoral students, especially Corentin Pasco and Rich Powe with whom it has been a pleasure to work with over the past years.

I would finally like to thank all of the adhesive suppliers who have supported my research and provided invaluable advice over the project duration. This includes; 3M, Henkel, Lohmann and Sika. Without their support, the research outcomes would have been severely restricted.

1. Chapter one - Introduction

As pressures upon automotive manufacturers grow, particularly in terms of weight reduction, increasing use of more exotic material combinations becomes inevitable as a method to deliver lighter body structures. Multi-material body structures bring a number of increased engineering challenges over traditional metallic based body structures, which must be overcome. One of these challenges is multi-material joining. Accordingly, joining solutions must be developed to assemble these multi-material structures, within a high-volume manufacturing environment. As such, efficient joining methods for automotive structures are of critical importance to ensure optimal performance of the vehicle and a cost-effective manufacturing process.

Jaguar Land Rover have an interest in the adoption of lightweight materials within their body structures and recognise the need for improved joining techniques. This requirement forms the basis for this project. The work presented within this document primarily addresses adhesive bonding techniques for the joining of carbon fibre reinforced polymer composite (CFRP) intensive joints, for use within high-volume automotive body construction. CFRP's provide specific challenges compared to traditional metallic joints and development of this area is a key requirement of the automotive industry at present. Two of the most challenging areas related to adhesive bonding consist of the development of optimal surface pre-treatment processes and acceleration of the adhesive curing process to meet high-volume cycle time requirements. Accordingly, chapter three is devoted to the optimisation of surface pre-treatment of CFRP prior to adhesive bonding. The second area of work consists of rapid adhesive curing technologies to quickly develop joint strength during manufacture and is presented within chapter four.

The combination of these two areas of research contribute to increased knowledge of efficient multi-material joining techniques, addressing a key industrial problem facing the high-volume automotive industry. This was achieved through the application of innovative adhesive products and existing processes to a new, challenging area of CFRP intensive high-volume joining. The conclusions of the research work, and the process developed were demonstrated to Jaguar Land Rover through a full-sized component sub-assembly. This highlighted the achievable joint strength and cycle time with a primary bonded (adhesive only) composite intensive joint. This is presented within chapter five, along with a high-level overview of the business case for the joining strategy presented as part of this work.

1.1. Research objectives

Industrial sponsors of this work, Jaguar Land Rover, have a specific requirement for improved joining techniques for use with CFRP intensive and multi-material body structures. Some of the key industrial requirements are that joining techniques must meet minimal assembly cycle times, prove reliable in service and meet a range of design criteria. The current joining technique used by Jaguar Land Rover for structural assemblies consists of the combination of self-piercing rivets and structural adhesive. This technique was identified as less suited to the joining of CFRP intensive structures. Primary bonded (adhesive only) joints provide an alternative solution, more suited to CFRP materials. However, reliable surface preparation techniques used prior to adhesive bonding and reducing the cycle time for adhesive cure were identified as major roadblocks in the adoption of primary bonded, lightweight automotive structures. Thus, development of these areas formed the underlying objectives of this work.

The first sub-objective was the identification of suitable surface pre-treatment techniques for the manufacture of reliable, primary bonded, CFRP intensive adhesive joints at high-volume. To achieve this various pre-treatment techniques were investigated upon CFRP substrates through an extensive test programme. Identification of the most appropriate surface pre-treatment technique required an assessment of the adhesive bond strength following treatment as well as consideration of the joint failure mode and durability performance. Investigation of other key considerations to Jaguar Land Rover were also required. This included an assessment of the effect of surface contamination on a bond surface, cycle time implications, as well as the effect of a delay between surface pre-treatment and bonding.

The second key sub-objective consisted of the identification of the minimal cure cycle time to achieve a specified joint strength during manufacture. To achieve this a variety of structural adhesive products were selected and extensive analysis performed using a customised electromagnetic induction heating set up to accelerate the adhesive cure cycle. Joint strength following various thermal cycles was identified for each adhesive product. Further industrial considerations were also analysed in detail. These included the effect of joint temperature upon the joint strength and the evaluation of strength loss caused due to an initial rapid curing step.

The combined outcomes of these research objectives provided Jaguar Land Rover with an enhanced understanding of suitable surface pre-treatment techniques for primary bonded,

CFRP intensive joints. Further, manufacturing and design implications for primary bonded structural joints were highlighted. These two outcomes contribute a significant step towards the manufacture of high-volume, CFRP intensive lightweight body structures, within the automotive industry. As a result, this research provided a potential solution to a key industrial problem.

1.2. Portfolio and structure of this report

The broad motivation and industrial requirements of this project are discussed within this chapter. Chapter two presents a more detailed explanation of the industrial challenge and the requirements of the automotive industry. A summary of state of the art joining methods is then presented, leading to the identified opportunities for research. Chapter three explores surface pre-treatment for CFRP surfaces, particularly atmospheric plasma treatment. The advantages and disadvantages of the process with respect to alternative surface pre-treatment methods are evaluated and discussed. Chapter four evaluates the use of electromagnetic induction heating for the generation of rapid adhesive handling strength. Factors such as the maximum achievable adhesive handling strength following specified heating cycles, for various adhesive products were evaluated as well as the evaluation of adhesive cure process. Chapter five presents component level evaluation of the techniques developed throughout this research project upon a full sized CFRP sub assembly. The cost implications of the proposed technique vs. existing technology are also presented. Finally, chapter six summarises the main conclusions of the work. The portfolio submissions produced as part of this project are detailed in Table 1.

Submission no.	Submission title	Relevant to chapter
1	*Development of innovative composite joining technologies for high-volume automotive body in white structures.*	2
2	*Atmospheric plasma surface treatment for high-volume, composite intensive automotive body structures.*	3
3	*A review of the specification, tender and commissioning activities for an induction heating facility within WMG.*	4
4	*Rapid adhesive curing technologies using electromagnetic induction heating.*	4
5	*EngD International placement to Lohmann Tapes GmbH.*	4
6	*Optimisation of rapid adhesive curing technologies using electromagnetic induction heating.*	4
7	*Kinetic analysis of structural adhesives and prediction of induction cured adhesive joint strength.*	4

Table 1 EngD Portfolio structure

2. Chapter two - Literature review

A review of state of the art joining technologies was prepared at the start of this project and forms portfolio submission one. This review included an assessment of structural automotive joint requirements, joining methods used within production and experimental research as well as joint durability and performance considerations in service. A primary consideration was given to the automotive industry, however techniques used within other industries were also considered. The available technology was then critically evaluated with respect to the present multi-material automotive joining challenge leading to the opportunities for future work presented within this document. A summary of the state of the art review and more recent research updates is presented in section 2.1.

2.1. The driving force – emissions regulations

Automotive manufacturers across the globe are under intense governmental pressure to reduce their fleet emissions of greenhouse gases, which it is widely claimed contribute towards climate change. The 2008 climate change act set a long term legally binding framework for the UK government to reduce greenhouse gas emissions by at least 34 % by 2020 and 80 % by 2050 compared to 1990 levels (1). Transport has come under significant focus as a target industry for achieving these targets, contributing 23 % of UK total greenhouse gas emissions in 2014 (2). By 2021 UK automotive manufacturers and all vehicles registered within the EU must reach the target of 95 g CO_2/km on a fleet average basis. The European Union will set harsh financial penalties to manufacturers if these targets are exceeded (3). Limits have also been placed upon the emissions of CO (carbon monoxide), NO_x (Nitrogen dioxide NO_2 and nitrogen oxide NO), particulate matter and HC (hydrocarbons) to which manufactures must adhere under the European Union Air Quality Directive (1). In order to achieve these targets automotive manufacturers are considering a variety of techniques, generally falling into three categories (4);

1. Propulsion, including alternative fuels, hybrid powertrains and powertrain efficiency gains.
2. Weight reduction throughout the vehicle, with a multiplier effect with respect to propulsion.
3. Parasitic improvement in aerodynamics, rolling resistance and vehicle energy systems.

As a result, it is of critical importance that automotive manufacturers focus significant research efforts upon methods to increase efficiency in these target areas. In particular this project focuses on weight reduction of the vehicle via the use of alternative, lighter materials for automotive body construction.

2.2. Multi-material body structures

Multi-material body structures were recently identified as a significant enabler towards achieving a reduction in the weight of the automotive structure, in particular the body in white. This was recently highlighted in an UK automotive technology road mapping exercise (5). The body in white (BIW) is defined as the main structure of the vehicle body, less doors and bolt on or skin assemblies (6). The BIW, which was the focus of this work generally consists of the floor and main cage containing “A” “B/C” and “D” pillars, roof surround and various closed sections such as cross members (6). A typical aluminium intensive BIW for a Jaguar Land Rover vehicle can be seen in Figure 1.

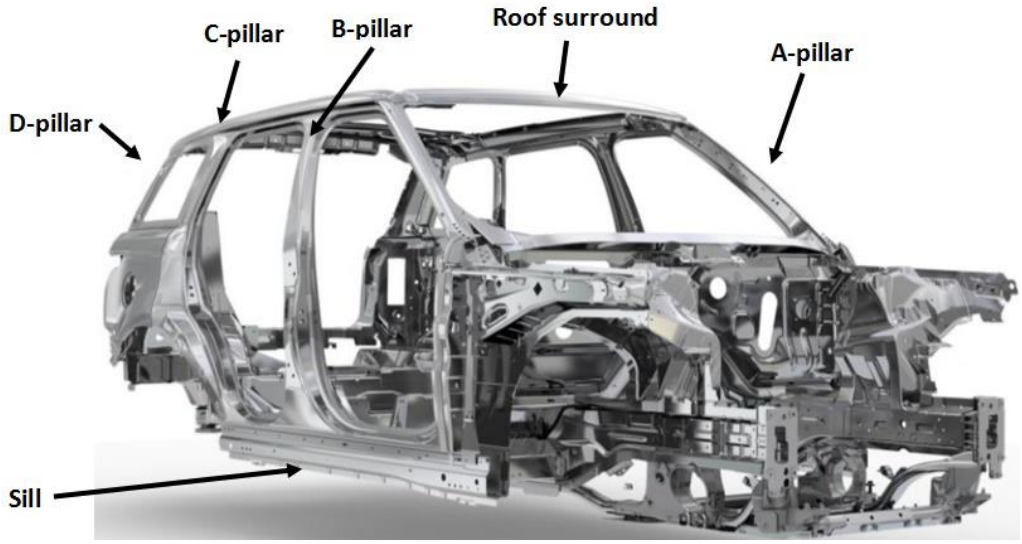

Figure 1 Aluminium intensive body in white (7)

Traditionally low carbon steels were the material of choice for BIW construction. This is due to relatively low cost in comparison to more exotic metals and established manufacturing techniques, with a gauge thickness of structural components ranging from 0.7 to 2.0 mm. More advanced steels offer increasing opportunities to down gauge, saving weight whilst maintaining stiffness. Aluminium body in white structures have become increasingly prevalent over recent years, offering a weight saving over a steel baseline of up to 41 % (4, 8). The move from a steel intensive BIW to aluminium brought with it a shift in production methodology, extending to areas such as forming and joining methods. Audi were one of the

pioneers of this change with the Audi A2, one of the first high-volume predominantly aluminium body structures manufactured between 1999 and 2005 (9).

Alongside the introduction of alternative metals to the BIW, manufacturers have for many years explored the potential of fibre reinforced polymer (FRP) composite materials. A composite material can be defined as "*a material with at least two elements which work together, resulting in a material with improved properties to those elements on their own"* (10). FRP composites consist of a bulk polymer matrix reinforced with fibres, predominantly glass or carbon, adding strength and stiffness to the matrix. As early as 1972 Ford commissioned research demonstrating that the replacement of a steel BIW with a carbon fibre reinforced polymer BIW (CFRP) could deliver a weight saving of 62.2 % (11) compared to a low carbon steel design. In 2002 it was demonstrated (12) that a CFRP BIW could deliver 60 % weight reduction compared to a steel equivalent whilst maintaining stiffness targets. More recently, figures of up to 70 % weight reduction have been quoted as achievable from a CFRP intensive automotive structure (4, 13). The BMW I3 "life pod" was one of the first high-volume CFRP intensive body structures, produced using a high pressure resin transfer moulding (HP-RTM) method (14).

Whilst there are significant weight save advantages to be gained within the BIW from the substitution of traditional steels with high strength steels, aluminium and FRP, cost implications of many of these material choices can be high. As such the trend in recent years has been towards designing with the "right material in the right place" rather than using a single class of material for the whole structure. This approach uses lightweight materials in a systematic way to produce both a weight and cost saving benefit (15, 16). For example, the BMW 7 series is considered an industry flagship BIW at approximately 130 kg lighter than its predecessor and closest competitor. However only 3 % by weight of the BIW, equating to 13 kg, is CFRP (17) combined with steels and aluminium. The BMW 7 series BIW is shown in Figure 2.

Automotive composites can be produced from either thermoset or thermoplastic polymer resins. Thermoset (TS) composites at high-volume are generally produced by HP-RTM moulding or compression moulding processes with a cure cycle time in the order of several minutes. Thermoset resins used within the automotive industry are generally either epoxy, vinyl ester, polyester or polyurethane (18, 19). Structural applications of thermoplastic (TP)

composites lags behind that of thermosets (20). However, research efforts are underway to improve processing technology and reduce manufacturing cycle times, through processes such as stamp forming (21). Lower cost thermoplastics such as polypropylene and polyamide matrices are generally used for composite applications within the automotive industry although higher performance polymers can be used (20). Current applications of thermoplastic composites within the automotive-industry are generally non-structural or semi-structural with random, short fibre, glass reinforcement (22). This produces lower strength parts compared to long , continuous fibre reinforcements, primarily used within structural applications (10).

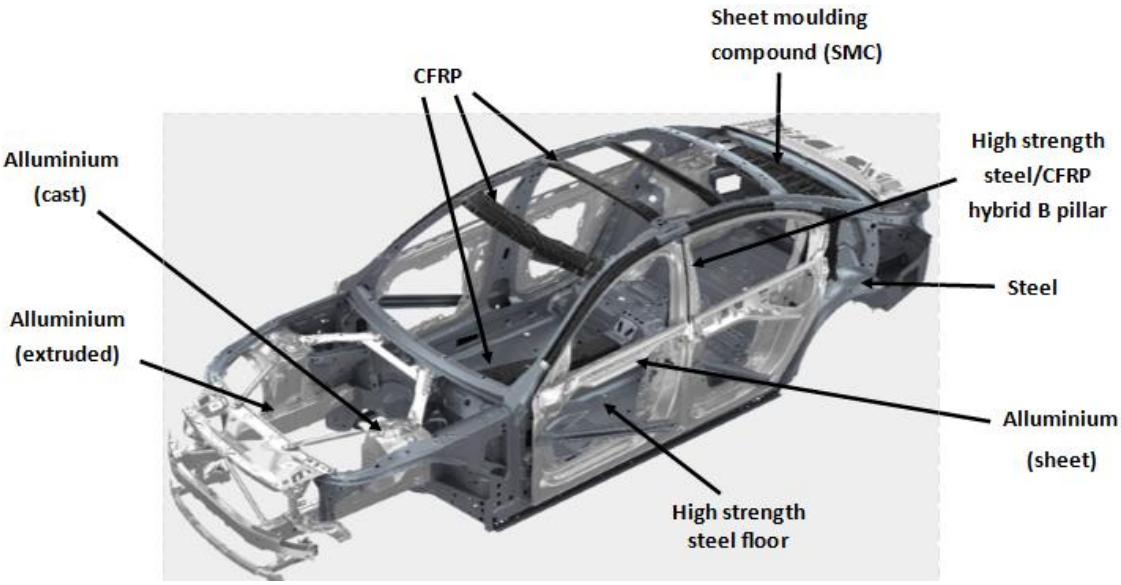

Figure 2 BWM 7 Series multi-material BIW (23) annotated (24, 25)

It is apparent within the automotive industry that the future trend is looking towards multi-material body structures, with the incorporation of proportions of FRP composites. As such there is a need within the industry for joining methods to meet high-volume manufacturing requirements of these material combinations. Overcoming this multi-material joining challenge is key in enabling the adoption of lightweight material combinations.

2.3. Automotive body joining

It has been identified that a prerequisite to unlocking the benefits of mixed material lightweight structures is suitable joining technology (16, 26). Whilst traditionally metals have been resistance spot welded within an automotive assembly, this approach becomes increasingly difficult with mixed material structures. As such alternative technologies are required to meet the needs of future body structures (16).

Design for joining is becoming increasingly important within automotive manufacture. This is a complex area with many considerations such as; energy absorption, fatigue, structural integrity, surface quality as well as noise vibration and harshness (NVH) reduction (27). Further considerations such as structure repair and end-of-life recyclability are becoming increasingly prevalent. Effective joining solutions for multi-material body construction, must be reliable, cost effective and durable through the lifetime of the vehicle as well as meeting manufacturing constraints. With all of these considerations in mind, finding suitable techniques is a significant challenge. Further, the requirement of high-volume manufacture adds greater complexity and cycle time implications. Multi-material joining also provides significant challenges over and above the joining of monolithic material structures. This includes factors such as cost effectiveness, differential thermal expansion, corrosion, durability and process compatibility.

2.4. Joining methods for FRP intensive joints – a review

This section reviews state of the art technologies with respect to multi-material joining. A particular emphasis is placed upon the joining of CFRP intensive automotive structures.

2.4.1. Welding methods

Welding, or fusion techniques have attracted much attention within literature. With reference to the present application of CFRP intensive body structures, the techniques considered have emerged primarily from the TP polymer industry (28). More recently research efforts have focused upon the welding of reinforced TP-FRP's. Fusion welding occurs when similar interfaces are brought together in the molten state. Subsequently the surfaces undergo molecular diffusion and chain entanglement forming a welded joint.

High joint performance can be achieved with fusion welded TP joints compared to adhesive bonding techniques, with joint quality comparable to autoclaved consolidated polymer parts (29). This high joint performance combined with a reduction in assembly costs compared to mechanical fasters and adhesive methods contributes to much of the research in this area being performed with reference to the aviation industry (28, 29). Over the past decade, TP welding techniques for FRP's have begun to emerge within the automotive industry as a result of ongoing research (30).

High joint strength aside, additional advantages of TP welding processes include short processing times compared to adhesives (31), since no curing reaction is required. Generally, less surface preparation is required compared with adhesive bonding since the interface becomes molten during the process. Ease of disassembly is also a significant attraction, the joint can be easily reheated and separated.

Providing a TP polymer is present, FRP's can be fusion bonded to dissimilar materials. There are a number of research efforts addressing metallic/CFRP fusion welding (32), with promising results. One of the concerns of this technique for an automotive application is the difference in thermal expansion of the dissimilar materials which are in intimate contact. TS matrices, which cannot be melted once the curing process is complete, require an additional compatible TP polymer layer to enable TP welding (33). This adds additional complexity and cost to automotive manufacturing applications.

A number of heating mechanisms used for fusion welding of polymers are possible, enabling fusion welding to be performed upon various TP substrates. The most relevant techniques for the present application are presented in section 2.4.1.1 to 2.4.1.3. One of the limiting factors with a CFRP joining process is that generally the polymer layer transfers the load across the joint rather than the load carrying fibres themselves. As a result the reinforcement polymer strength may dominate the resultant joint strength (32).

2.4.1.1. Induction heating and welding

Induction heating is a process used to heat electrically conductive and ferromagnetic materials. The materials are placed in a time varying electromagnetic field (EMF), generally operating in the kilohertz to megahertz range for metallic and composite applications (34). The process is based upon the principle that when an alternating voltage is placed across a conductive coil a resulting alternating current is generated within the coil. As a result of the alternating current an alternating EMF is generated surrounding the coil. This EMF can be used to induce a current in a nearby conductive material, perpendicular to the applied EMF, up to a depth known as the *skin depth* (35). The principles of the induction heating process can be visualised in Figure 3, for a multi-material joint. Since carbon fibres are conductive, CFRP networks can be induction heated, making the process suitable for heating and consequentially welding of TP-CFRP. Induction heating has been identified by many as one of the most promising heating methods for induction welding of TP-CFRP, particularly within the

aerospace industry. Heat can be induced within the laminate, contact free and high heating rates can be achieved (36).

Circular loops of conductive material are required to generate induced currents. As such the process is affected significantly by fibre architecture when heating CFRP. Coil geometry is also critical to effective heating, often an empirical approach is used which is limited compared to a simulation based approach to coil design (36). One of the significant problems with induction heating of CFRP is the low thermal conductivity compared to metallic materials, resulting in high thermal gradients within the material. This usually results in a need for cooling near to the induction coil during welding processes, to avoid degradation of the polymer (36).

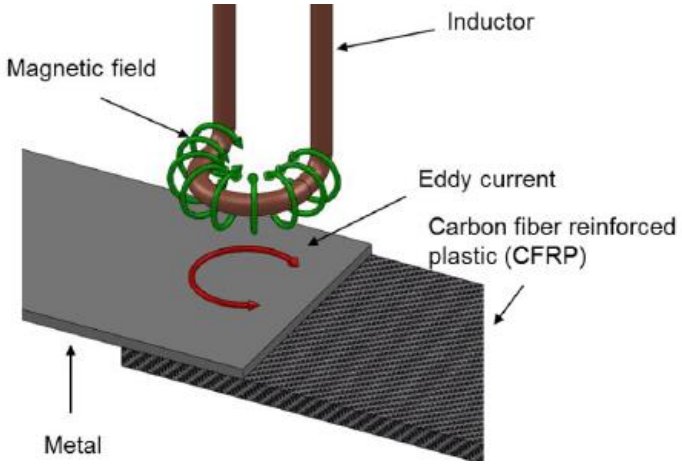

Figure 3 Principles of induction heating (37)

Three different heating effects are considered to be responsible for induction heating of CFRP. The first of these includes fibre heating due to joule losses along the fibres (38). The second method is due to contact resistance at fibre junctions, where layers of fabric, known as plies (10), are present at higher volume fractions this method may start to dominate (38). A final heating effect discussed in literature applicable to CFRP induction heating is dielectric losses within the polymer layer between fibre junctions (34), these effects are illustrated within Figure 4.

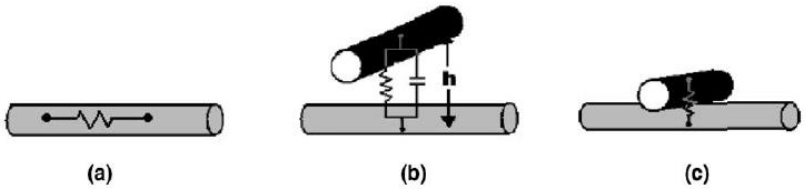

Figure 4 Induction heating mechanisms, (a) fibre heating, (b) dielectric hysteresis and (c) contact resistance (38)

In some cases where ferromagnetic particles have been added to the polymer, or adhesive in some applications, heat is generated by the magnetisation and demagnetisation of these particles during exposure to an EMF (39). This is a combination of heating effects due to eddy current losses and hysteresis losses. This method has the advantage that the heating becomes self-temperature regulating by selection of particles with appropriate Currie temperatures (34). The disadvantage is that to achieve a significant heating effect by this method alone, in non-conductive polymers, up to 74 % weight of particles may be required, reducing any light weighting benefit (34). In some cases in literature, especially where a non-conductive FRP is heated, a susceptor is added to the joint. This is usually a mesh of conductive material, which through the effects discussed above generates heat. The susceptor can also be a metal substrate which is preferentially induction heated. An additional susceptor between substrates however introduces the potential for stress concentrations, corrosion and extra cost as such is undesirable for the present work.

An example of a continuous induction welding setup is seen in Figure 5, where the induction coil and consolidation roller move along the joint forming a continuous weld. This setup can be mounted on an industrial robot for larger three-dimensional applications. Spot welds can also be produced in a discontinuous process. The process has been demonstrated for a glass fibre (GF) polyamide 6 (PA6) automotive bumper application with a secondary roller introduced where the components are unsupported (30).

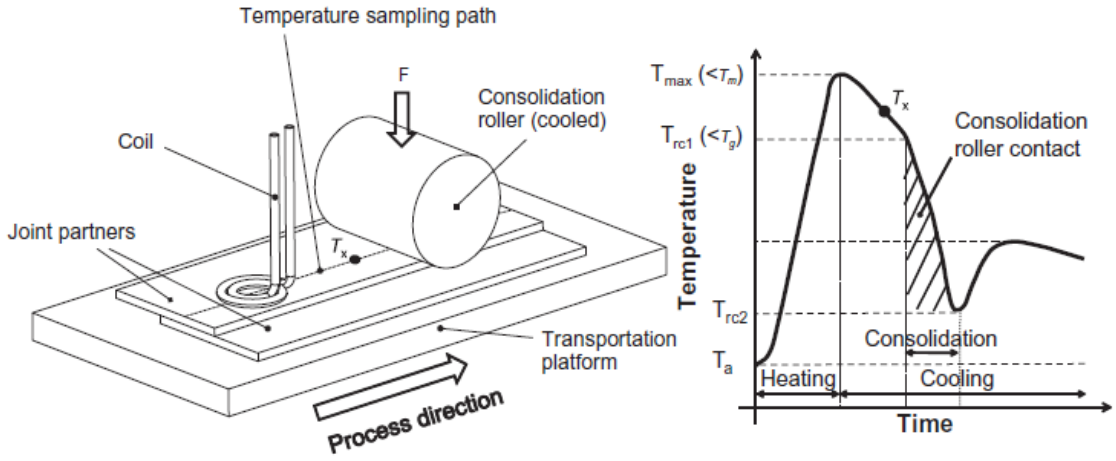

Figure 5 Continuous induction welding setup (34), graph showing temperature vs. time at monitoring point T_s

Lap shear strengths using TP-CFRP substrates and induction welding have been achieved between 18 - 48 MPa (38), which compares well to structural adhesive bonding. Multi-

material metal / TP-CFRP induction welded joints have also been produced with reported lap shear strength of 4 - 25 MPa. It has been identified that metal surface pre-treatments are important in maximising joint strength within fusion welded multi-material joints (40).

2.4.1.2. Ultrasonic heating and welding

Ultrasonic heating is an alternative method to induction heating which has attracted attention relating to CFRP welding in both TP-CFRP / TP-CFRP and TP-CFRP / metal joints. The substrates are held under pressure and ultrasonic vibrations are applied perpendicular to the area of contact (41). The heating effect varies with the nature of the material being welded and the design of equipment. The surface of the polymer can be modified to maximise the heating effect (35), although surface asperities can result in hot spots. Fast weld times can be achieved, in the order of seconds and often below the cycle time of alternative processes (42). The weld length is restricted to a maximum length of approximately 250 mm (41) due to process constraints. The horn, which transmits the ultrasonic vibrations, must be in contact with the substrate. The equipment required is relatively inexpensive and easily automated (43). Demonstrator aerospace applications of ultrasonic composite welding have been produced by ACS Australia (44, 45) with high joint performance demonstrated, similar to that of induction fusion bonding. The ACS process relied upon a TP surface layer upon a TS matrix, an area of much research (33, 46) enabling the ultrasonic welding of TS-CFRP. The substrate sensitivity and restriction in weld length due to horn design issues is a limiting factor for this method in respect of high-volume automotive manufacture. A trial of ultrasonic aluminium welding by Jaguar Land Rover identified process consistency issues and significant variability in joint strength (47).

2.4.1.3. Vibration heating and welding

Vibration heating is a process used to weld unfilled, filled and short fibre reinforced TP composites (48), with a number of applications within automotive manufacture (49). Substrates are held under pressure and a vibration applied. Consequently frequency, time, pressure and amplitude are the important process parameters (48). Vibration welding operates under higher clamping pressure and lower frequency when compared to ultrasonic welding. Components vibrate horizontally with respect to one another compared to vertically in the ultrasonic welding process (50). High weld strengths can be achieved with TP applications of vibration welding (51), relative to the bulk material strength and in comparison to ultrasonic welding. One of the greatest limitations comes with respect to flat geometries being most applicable to the process. It becomes increasingly complex to vibration weld more

complex geometries, as may be found in future automotive structures leading to difficulties applying this technique to the present application.

2.4.2. Mechanical fasteners

Mechanical joining methods are well established and rely on mechanical force, interlocking or physical interference to transfer load. There is no requirement for any atomic, ionic or molecular forces between substrates, where these interactions occur corrosion issues may become a concern (52). It is partly for this reason that mechanical joints are often combined with adhesives to provide a sealing and insulating later between dissimilar materials. Some of the advantages of mechanical joints include increased ease of disassembly and some free movement of the joint to assist with assembly and deviations in part tolerances. Further, little surface preparation is required, a major advantage over adhesive and fusion techniques.

One of the major disadvantages of mechanical fasteners for the joining of FRP is the generation of stress concentrations at the fastener. For example, where holes are required for fastener insertion the hole acts as a stress concentration. Within fatigue critical structures this stress raiser is a critical concern (52). The stress concentrations prove a particularly limiting factor with respect to composite materials which are anisotropic (material properties vary with direction), where mechanical joints can result in fastener pull out and other undesirable failure modes depending on the laminate properties (53). The fastener generally acts directly upon the FRP polymer matrix, often causing damage, further the introduction of a mechanical fastener can cause fibres to break and delamination of the laminate (54). An illustration of failure modes caused as a result of mechanical fasteners in FRP is seen in Figure 6.

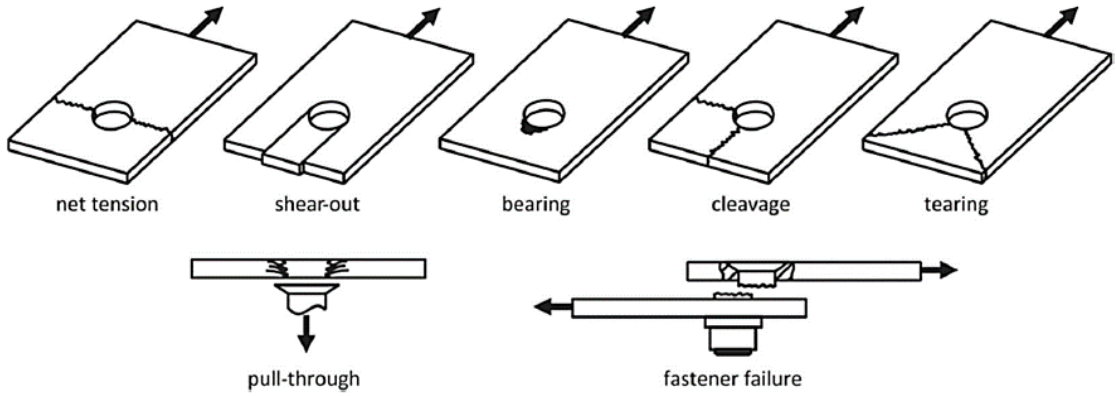

Figure 6 Mechanical fastener induced failure modes in FRP (55)

2.4.2.1. Self-piercing rivet (SPR)

The self-piercing rivet (SPR) technique is one of the preferred techniques at present for mechanical fastening of aluminium within the automotive industry and widely used within Jaguar Land Rover. It is a well suited method for joining metals which exhibit a degree of ductility (56) compared to CFRP's. One of its greatest advantages is the speed of insertion, which is generally in the order of a few seconds per rivet. Other advantages include avoidance of pre drilled holes, ease of automation and relatively low cost compared to other joining methods (57). One of the drawbacks is that two-sided access to the joint is essential for installation and rivet removal is difficult. Four steps are involved with insertion of SPR's, shown in Figure 7 (57) .

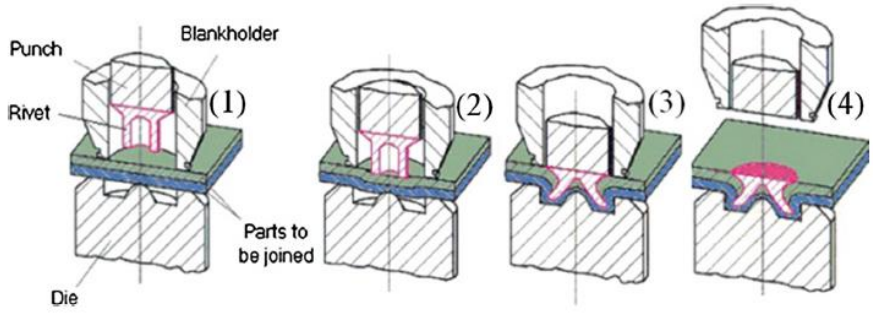

Figure 7 Self piercing rivet process (57), substrate clamping *(1),* rivet forced into substrates *(2)*, rivet flares during insertion (3), punch and die removed *(4)*

Generally, the rivet is then forced through from the thinner substrate (above) into the thicker substrate (below). Upon insertion the rivet flares, providing a mechanical interlock. During the flaring stage the substrates undergo significant plastic deformation, when inserted into CFRP this often results in cracks (58) and delamination (59). This is shown in Figure 8 where fibre fracture, inter fibre fracture and damage to the laminate structure is observed (56).

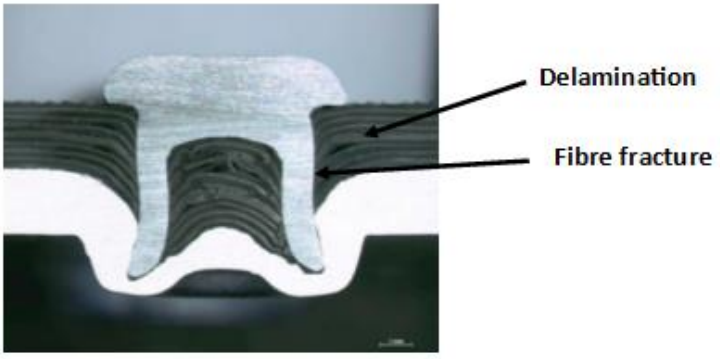

Figure 8 Delamination and fibre damage as a result of SPR insertion, CFRP/aluminium joint (56)

Failure of CFRP SPR joints generally consists of flexural deformation followed by significant localised damage of the CFRP around the rivet hole, finally complete withdrawal of the rivet occurs (58). An example of an SPR inserted into a TS-CFRP to aluminium joint can be seen in Figure 9 and failed in Figure 10. It was observed that joints with a cross ply CFRP layup failed with approximal double the extension of the angle ply joint with similar maximum load (57). As such fibre architecture heavily influences joint performance for a mechanically fastened CFRP joint. Delamination and fibre tearing can be observed in both cases, as well as fastener pull through with the angle ply.

Figure 9 TS-CFRP to aluminium SPR lap joint (57)

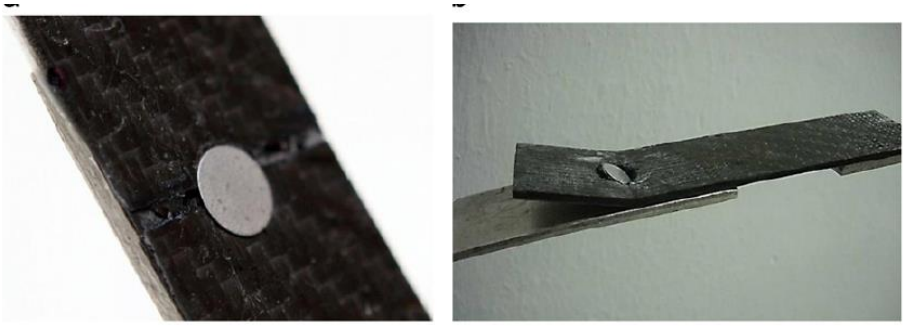

Figure 10 TS-CFRP to aluminium failed SPR lap joint (57), CFRP cross ply (left) and angle ply (right)

Combination of CFRP and mixed material mechanical joints with adhesives can increase maximum joint load transfer by up to 23 %, although maximum energy absorption is dominated by the SPR rather than adhesive. It has been shown within literature that a 25 x 50 mm overlap lap shear joint of CFRP/AL substrates can deliver higher strength and stiffness when adhesively bonded, compared to when an SPR is used. However the addition of the SPR contributes to over a tenfold increase in energy absorption (57).

The combination of SPR's with adhesives is known as *riv-bonding.* This is the current preferred strategy for aluminium body structure manufacture within Jaguar Land Rover. The adhesive helps to provide sealing and NVH benefits to the joint with the rivet providing instant geometry fixture, known as *geo-pinning* or *geo-fixing*. Modifications to the process have been

considered for the joining of CFRP/CFRP intensive structures (59). Improvements in delamination suppression and joint stiffness were achieved, however stress concentrations remained. This was inevitable considering the point loading created by a mechanical fastener, with a bearing failure mode produced. Whilst the SPR strategy is well suited to the joining of metallic structures the technique appeared less desirable for FRP intensive structures.

2.4.2.2. FricRiveting

More recently alternative mechanical fastening techniques have been developed, tailored to FRP joining. One example of this is the FricRiveting technique, essentially a combination of mechanical fastening and fusion welding. A rotating cylindrical rivet is forced into a polymeric substrate under high pressure and rotational speed, seen in Figure 11. The high speed and pressure causes the polymer to melt around the tip of the rivet. Pressure is increased and the rivet is forced into the substrate plasticising the tip of the rivet and causing it to expand. The process however is limited to TP polymer applications. Mechanical performance in some cases exceeds that of bolted joints (60).

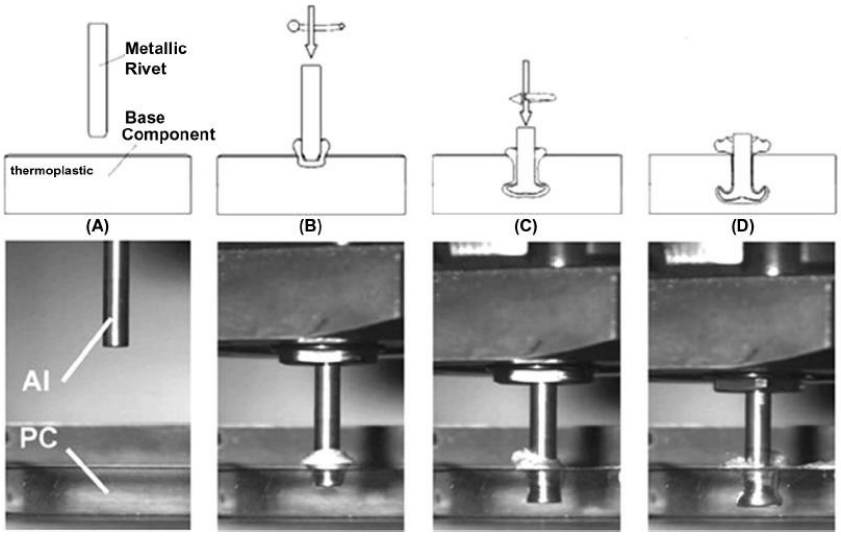

Figure 11 FricRiveting technique (60), rivet inserted (A), rotated and forced into substrate (B), resulting in flaring of rivet (B & C)

2.4.2.3. Flow forming screws

A similar method, known as flow forming screws has emerged within the automotive industry for CFRP / metal and CFRP / CFRP joints. The screw is driven into the workpiece, again under high pressure and high rotational speed. Plasticisation of the substrate occurs and a thread is formed as the screw is driven in. As the materials cools it contracts around the screw forming a strong, removable joint. Generally, the CFRP is the upper of the two substrates, with a more

ductile substrate being placed below. Examples of the process are shown in Figure 12. The choice of optimised screw variants can significantly improve load capacity. The process is well suited to TP-FRP substrates but TS-FRP substrates often demonstrate significant delamination upon screw insertion (61).

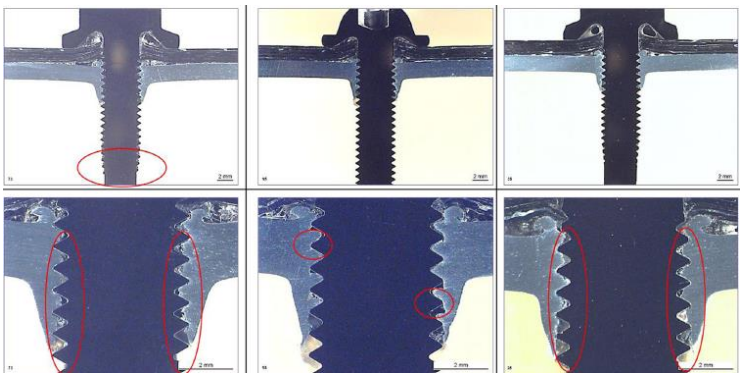

Figure 12 Flow forming screws (61), example of joint formation around screw

2.4.3. Adhesive bonding techniques

Adhesive bonding is a technique where two components are bound together using a suitable binder known as an adhesive. Adhesive bonding is one of the most commonly used joining methods within automotive, aviation and building industries for joining multi-material substrates (58). In fact most products in the home, industry or transportation make use of adhesives in some way (62). The method of adhesive bonding is also one of the most commonly used for the joining of CFRP (58). Adhesive joining is generally considered to be irreversible, once adhesives have cured they are not easily separated although there are some exceptions to this and much ongoing research (63). Some of the advantages of adhesive joints include; sealing of the bondline where the adhesive is placed, galvanic corrosion barriers, improved stress distribution over the loading area with respect to mechanical fasteners, ability to join thin material sheets and applicability to a wide range of substrates (58, 64). The polymeric nature of adhesives results in advantageous damping properties, aiding in automotive NVH requirements and as a result improving fatigue performance (62).

Disadvantages of adhesive joints include; reduced resistance to peeling and cleavage stresses compared to mechanical fasteners in some applications, requirement for suitable surface pre-treatment and a lack of dependable methods for quality control and non-destructive joint testing (58). Design criteria for adhesive joints is less established than for other joining methods, with fewer design guidelines. As such, building confidence for adhesive only

(primary bonded) joints within industry is challenging. One of the greatest disadvantages for high-volume manufacture is that adhesive bonding is usually non-instantaneous. In many cases cure cycles of TS structural adhesives are in the region of 30 minutes or more, requiring fixtures to hold components in place while the adhesive generates strength. This poses a significant problem for high-volume manufacture.

A structural adhesive is one which can resist substantial loads and is responsible for the strength and stiffness of a structure, with shear strength ranging from 5 MPa (polyurethane) to 50 MPa (epoxy) (62). For this work a minimum of 12 MPa is determined as acceptable structural strength (65), based on aluminium joints. For multi-material structural bonding applications an applicable Jaguar Land Rover standard is not available, as such the primary aim is to approach 12 MPa where possible. The materials to be bonded are defined as substrates, or sometimes adherents after bonding. Adhesion is defined as *"the attraction between two substances resulting from intermolecular forces that establish between them (62)*", and cohesion as "involving intermolecular forces inside one substance (62)". Failure of adhesive joints is either by adhesion (adhesive failure) where the adhesive separates cleanly from the substrate, or by cohesion (cohesive failure) where the adhesive fails within itself. Material failure, or cohesive failure in the adhered, can also occur where the substrate fails in itself within a region near to the adhesive. The interphase is defined as the region between the adhesive and substrate, within it lies the interface which is the plane of contact of the two materials (62). An illustration of these adhesive joint failure modes is seen in Figure 13.

One of the important factors of a strong adhesive joint is that the adhesive must have good wettability with respect to the joining substrates. This enables adhesives to achieve intimate contact with the substrates and contributes to a strong adhesive bond (58). To achieve this the surface tension of the liquid adhesive must be lower than the surface free energy (SFE) of the substrate (66). Consequentially the evaluation of surface energy can assist in the selection of suitable adhesives to achieve acceptable wetting behaviour. As adhesive viscosity increases, achieving suitable wetting becomes challenging, similarly surface roughness can directly affect wetting.

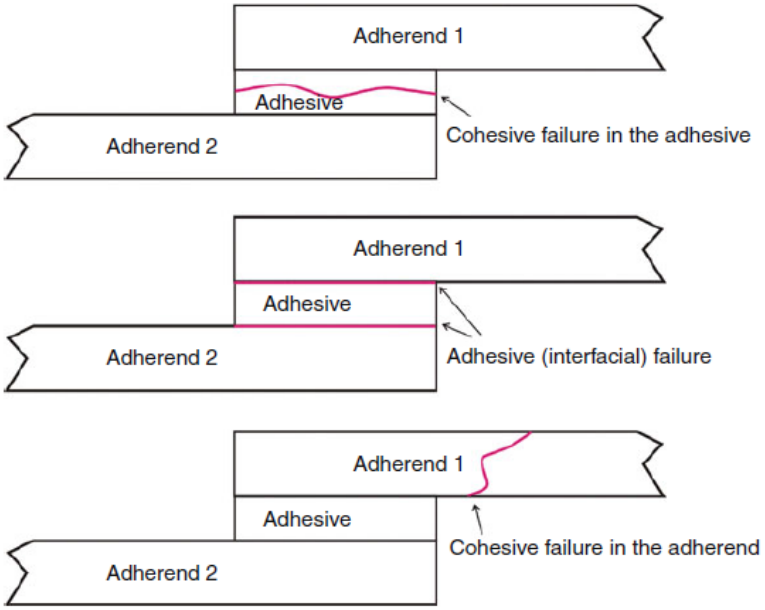

Figure 13 Adhesive failure modes (62), cohesive failure (top), adhesive failure (centre) and material failure (below)

The surface energy of a solid, or surface tension of a liquid, is generated as a result of differential attraction of surface molecules (64) and can be thought of as the work which has to be expended in order to increase the size of the surface (67). The surface tension of liquid adhesives and surface energy of solids can be evaluated using a tensiometer and the contact angle method. Alternatively, an approximation of surface energy can be made using dyne pens.

The contact angle method relates interfacial surface tensions designated γ of the solid (s), liquid (L) and vapour (V) phase to the contact angle θ and is expressed by Young's equation; $\gamma_{SV} = \gamma_{LV}\, cos\theta + \gamma_{SL}$ (62) . The relationship shown is shown diagrammatically in Figure 14. A number of methods can then be used to perform the calculation of the solid SFE from contact angle data, generally using a secondary expression of the general form; $\gamma_{SL} = \gamma_L + \gamma_S - (interaction\ between\ phases)$. One method for the calculation of SFE and the unknown value, γ_{SL}, is the Owens Wendt and Kaelble method (OWRK) which enables total SFE to be separated into polar SFE (γ_s^p) and dispersive SFE (γ_s^d) attributable to differing mechanisms of surface interaction. By using at least two test liquids with known polar and dispersive components of surface tension γ_{LV}, it can be shown that it is possible to evaluate at the two unknowns, the polar and dispersive SFE of the solid surface (62, 67).

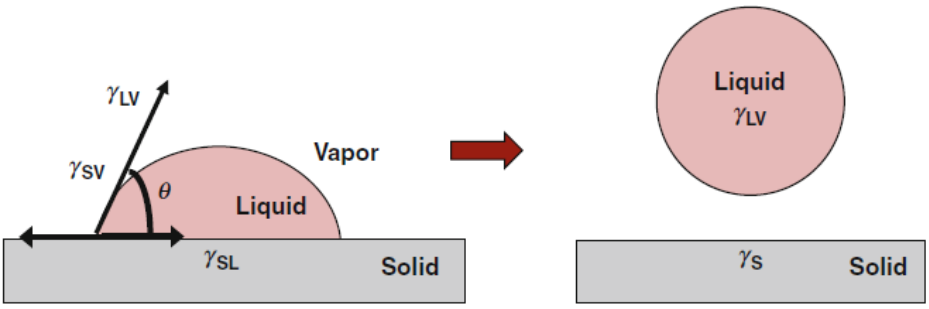

Figure 14 Contact angle measurement using sessile drop (62)

The contact angle, θ, is essentially a measure of a liquids ability to bond with itself compared with the solid surface. A low contact angle indicates good wetting and a hydrophilic surface, and a high contact angle represents poor wetting and a hydrophobic surface (62). Once wetting is complete the adhesive must harden, developing structural strength to support loads in service. This is completed through the curing or crosslinking process for a TS adhesive. TS adhesives are generally preferred to TP adhesives for structural bonding (58), due to improved surface wetting properties, increased strength and improved high temperature strength retention. Various mechanisms are attributed to the creation of adhesive bond strength. It is assumed that adhesion is generally a produced due to a combination of these methods.

A few of the most universally accepted methods are presented;

- Adsorption – it is proposed within this theory that intimate contact between adhesives and substrates creates inter-atomic and inter-molecular forces at the interface. The interfacial forces are generated primarily through secondary Van der Waals interactions (64). In some cases it has been proven that primary covalent bonds are formed within adhesive joints (62). These are up to ten times stronger than secondary Van der Waals interactions, sometimes this is defined as chemical adhesion. Whilst secondary forces may often produce a satisfactory bond, this bond may not be stable in service when exposed to hot wet environments for example (62). Thus the creation of stronger bonds, less susceptible to environmental attack such as hydrolysis may be vital to produce a durable adhesive bond (62). To fracture a joint energy must be supplied to break these bonds, creating new surfaces. This is known as the work of adhesion, W_A. This can be expressed by $W_A = \gamma_1 + \gamma_2 - \gamma_{12}$ where γ_1 and γ_2 are the surface energies are materials one and two respectively and γ_{12}, the interfacial energy between phases (62). As such, it can be seen that the surface energy is fundamentally linked to the work

of adhesion and resultant joint strength. Surface energy measurements can be used to compare surfaces, as well as to assess the contribution to adhesion of different bonding types. As a result, surface energy measurement can be a valuable tool providing greater understanding of observed changes in adhesive bonding behaviour as well as identify the effectiveness of surface treatment methods and differences between materials.

- Diffusion – an alternative proposal is that adhesion strength is associated with the diffusion of molecules through the interface. This was proposed based on early investigations of the self-adhesion of rubber (62). For this to occur macro-molecular chains must be present which are mobile and mutually soluble at the interface. However this method attracts much doubt if the substrates and adhesive are not mutually compatible as is often the case (62).
- Mechanical interlocking - this is the proposal that adhesives wet out pores and cavities within substrate surfaces developing joint strength upon adhesive curing. However the fact that strong bonds can be produced on smooth surfaces largely discounts this theory (58). Any increase in strength may largely be attributable to increased contact surface area for other mechanisms to act upon. It is important to ensure a suitable surface roughness so as not to create air filled voids at the interface whilst maximising the effective surface area (62).

Difference in thermal expansion coefficients (CTE) within multi-material adhesive joints is an important consideration relating to adhesive selection. A similar effect is produced during the curing cycle, where residual stresses can be introduced within the joint (58). Suitable selection of adhesives can help to compensate for this difference (62). Environmental factors can also significantly influence adhesive joint strength. Temperature is known to effect adhesive properties with a dramatic change being identified approaching the adhesive glass transition temperature (Tg) (58). The Tg is defined as the temperature at which polymer chains begin to achieve molecular mobility, although is not normally a unique temperature value (64).

2.4.3.1. Surface pre-treatment for adhesive bonding

A prerequisite to successful adhesive bonding is suitable surface pre-treatment. One of the primary reasons for surface pre-treatment is to remove surface contamination which can reduce the performance of an adhesive joint. This occurs due to various reasons; firstly the formation a weak boundary layer between the adhesive and substrate (62). This is a region of weak cohesive strength between the adhesive and substrate, forming a weak link in the joint.

The surface contaminant can also result in a reduced SFE (62), resulting in reduced wetting by the adhesive and lower joint strength as discussed in section 2.4.3. Contaminants can also disrupt the formation of interfacial interactions reducing the bond strength. Further, surface contamination can migrate into the adhesive itself. This reduces the consequences of the contaminant at the interface but can reduce the bulk cohesive strength of the adhesive itself leading to reduced joint strength (68).

Contaminants are inevitable within a manufacturing environment and are also attracted to high energy surfaces. For example, within FRP manufacture mould release agents and processing aids are used and for metals waxes to aid stamping processes. Solvent cleaning and abrasion are frequently used methods to remove such contamination. Some adhesives, particularly metal bonding adhesives, are designed to bond to surfaces with certain contamination, such as those contaminated with waxes to aid stamping (27). This is the present approach of Jaguar Land Rover for structural aluminium bonding applications. Aluminium alloys are coated with lubricants at the supplier to aid stamping, with structural adhesives being engineered to bond to such surfaces without removing the contaminant.

Solvent based techniques are often effective at contamination removal. The part is dipped in uncontaminated solvent, contaminants are dissolved and then drip off the part. Solvents however are generally toxic and often highly flammable. Chlorinated solvents are also becoming almost unusable due to legislation in many manufacturing environments. As such solvent based pre-treatment processes in industry are generally considered highly undesirable with the exception of some specific applications. Scrubbing with water based surfactants is an alternative solution, effective at the removal of some contaminants (62). Abrasion of the substrate surface can be effective at removing surface contamination. One of the drawbacks however is that the process is dirty, time consuming and undesirable in an automotive manufacturing environment.

Often degreasing and abrasion alone are sufficient to produce strong adhesive bonds, however in some cases, chemical treatments are required. Chemical exposure time is critical to achieving optimal treatment efficiency, some treatments can be highly environmentally undesirable. Chemical treatments for metals to promote adhesive bonding are generally well understood. Material can often be supplied pre-treated and treatments are generally based upon modification of the oxide layer. An example of this is aluminium alloys which if

untreated form oxide films. This results in poor wetting and requires chemical treatment to provide a more suitable surface for adhesive bonding.

Chemical pre-treatment methods help to produce strong covalent bonds between surface oxides and the cured adhesive, or they produce functional surfaces with tailored structures in the oxide film to enable increased wetting (58). Polymeric materials however, require an entirely different surface pre-treatment method which alter their surface chemistry to promote adhesion (69). Polymers have inherently lower surface energy than uncontaminated metals and have a tendency to form low strength bonds without additional surface pre-treatment. This is particularly important for many TP materials, TS polymers are generally less challenging to bond (62). Thus, for adhesive bonding of FRP surfaces, pre-treatment may be a prerequisite prior to adhesive bonding. One option is chemical treatment methods, such as etching or acid induced oxidation, however as discussed this is environmentally undesirable. Another option, as discussed, is physical methods such as flame, corona or plasma treatment. These methods are often attributed to cause ablation where loose organic material is broken down into volatile species and removed from the surface. This can assist in the removal of a weak boundary layer prior to bonding.

Plasma treatment has been considered by many as one of the most versatile surface pre-treatment techniques (62). This can be performed at low pressure (vacuum plasma) which is ideal for small, intricate components at the cost of expensive capital investment. Or, alternatively in air at atmospheric pressure, known as atmospheric pressure plasma treatment (APPT), bringing greater flexibility. Plasma is produced by exciting a working gas with electrical energy producing a collection of charged particles with positive and negative ions. Other particles such as free radicals, atoms and molecules may also be present. Varying gases can be used to achieve differing surface effects with the level of surface modification generally confined to tens of nanometres. Plasma induces surface reactions between the gas phase, surface molecules and chemical groups as well as reactions amongst surface species to produce functional groups and surface crosslinking. Once treated the surface of a polymer may change over time, as a result the treatment is most effective performed immediately prior to bonding (62, 70).

Oxygen and nitrogen containing plasmas are widely used to modify polymer surfaces to increase adhesion. APPT systems aim to create a uniform plasma cloud, completely

surrounding small objects on a surface. Detailed analysis of plasma jet architecture is presented within literature (71). Generally power requirements are low, in the order of a few hundred watts. APPT has been identified in a number of studies to be effective in increasing the SFE of surfaces (62). Various literature investigations have found that APPT can yield effective increase in adhesive bond strength and SFE upon polymer surfaces. For example, one investigation (72) analysed plasma pre-treatment of polypropylene (PP) TP substrates prior to bonding with polyurethane adhesives. A variety of differing surface pre-treatments were applied, including abrasion, chemical primer and application of atmospheric pressure air plasma torch (APPT). It was shown that the APPT process appeared the most suitable method to enhance adhesion to PP with mechanical abrasion performing poorly. Total SFE and the polar component of SFE increased from 23.01 to 50.29 and 0.19 to 29.05 mJ/m^2 respectively as a result of APPT.

The use of APPT to activate various TP other thermoplastic polymer surfaces was also investigated (73). Substrate contact angles were measured and SFE calculated according to the OWRK method. It was concluded that nearly every polymer type can be activated with the plasma gun, although PTFE (Teflon) showed negligible change in SFE, Figure 15. Other authors (74) demonstrated that APPT could be effectively applied to polyimide TS sheet to increase adhesive bond strength. Up to 60 s treatment time SFE and single lap shear (SLS) strength increased, above this a decrease in both was observed. A fourfold increase in SLS strength was noted as a result of APPT. The increase in SFE was attributed largely to an increase in the polar characteristics of the surface.

Some evidence was also identified within literature of the effectiveness of APPT at removing surface contamination from polymer surfaces. For example in one investigation (75) APPT appeared to remove solvent based mould release from a CFRP surface. A change was produced from adhesive failure upon the contaminated surface before plasma to a material failure with optimised APPT parameters upon the contaminated surface following treatment. This effect was thought to be a result of breaking down the siloxane chain allowing silicon contaminant to be removed by gas pressure, this produced an apparent 7 % adhesion improvement compared to a grit blasting technique. A similar contamination removal effect was however noted using a methanol wipe treatment.

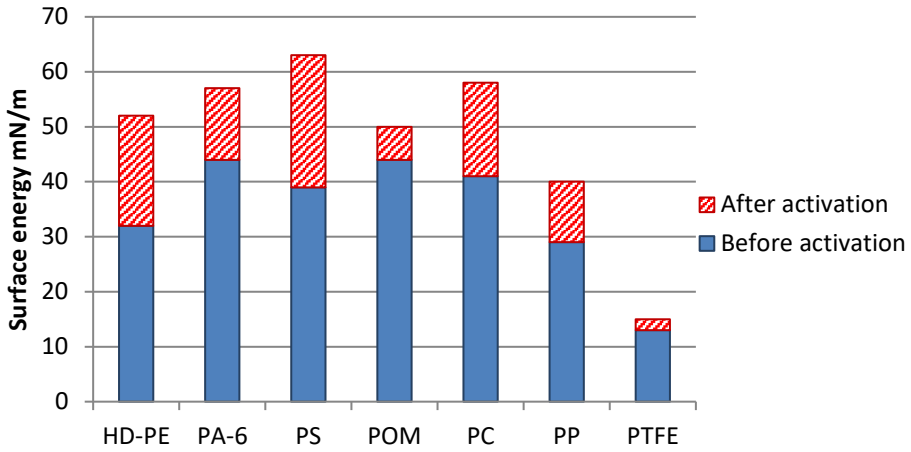

Figure 15 Surface activation using the plasma gun for various TP polymers (73)

2.4.3.2. The adhesive cure process

One of the limiting factors of adhesive use within high-volume manufacture is the slow rates of cure, and consequently strength development of many structural TS adhesives (27). This, amongst other factors, has led to the requirement for hybrid joining techniques. For example, where a mechanical fastener such as the self-piercing rivet is combined with the adhesive to provide immediate handling strength upon insertion. Without the rivet, a fixture would be required to hold the geometry in position whilst the adhesive cures. Within a modern high-volume manufacturing operation a joining cycle time of one minute or less is generally considered acceptable (27). This was considered as a suitable to target for the present work, agreed in conjunction with Jaguar Land Rover. As such, the fixture would need to be removed within this time. In order to achieve sufficient strength to remove the fixture without a mechanical faster acceleration of the adhesive cure process is required.

TS adhesives are cured by the process of chemical reaction, with the rate of reaction often being highly dependent upon temperature. As the degree of reaction increases, the rate of reaction generally decreases. A consequence of this is that viscosity increases as the degree of reaction progresses and the polymer crosslinks. The result of this is competition between the requirement for adhesion and polymerisation as generally the adhesive begins to cure before it has reached the substrate. Or in manufacturing terms, competition between open time and close time. Where the open time is the time available to apply the adhesive and close the joint, once mixed, and the close time the time taken for the cure process to complete once the joint has been closed. This whole process dictates the processing window of the adhesive. If the degree of adhesive cure is too great upon initial contact and joint closure, the

adhesive wetting will be poor (62) and the joint strength low. This has implications for adhesive application. A potential solution to this is the concept of *cure on demand*, the adhesive applied in a low viscosity state to achieve effective wetting and then cure initiated when required.

To compensate for the slowing rate of reaction during the final stages of cure and the rapidly increasing viscosity of fast curing adhesives, the automotive industry often uses slower curing adhesives and post cure thermal cycles to accelerate the rate of reaction in later stages of production. Within Jaguar Land Rover this often occurs through the e-coat process or through a paint bake cycle (76) which can take up to 30 minutes or longer. Most structural adhesives are either one-component (1K) where an atmospheric condition initiates the reaction or where the reactant is hidden in some way. Alternatively, two-component (2K) adhesives can be used where two separate parts must be mixed to initiate the curing reaction. Following application and substrate wetting, the temperature is then raised to accelerate the cure of the adhesive joint. In doing this however, care must be taken not to distort the substrate material.

The most common method for analysing polymer and consequently adhesive cure is using differential scanning calorimetry (DSC) evaluation (77). Using this method, the heat flow to and from the polymer is monitored at an isothermal temperature or at a constant heating rate (dynamic). The cure of thermoset adhesive is exothermic, as such by monitoring the exothermic heat generation during cure, the degree of cure can be calculated from the difference between heat at a given time and the total heat output of the reaction. Various parameters can be found from DSC analysis, to include onset, midpoint and endset of glass transition temperature (Tg), degree of cure, rate of cure and cure onset temperature. The Tg being the temperature at which the polymer transitions to a rubbery state, above which temperature the polymer chains gain increased molecular mobility (64). The Tg is usually identified over a temperature range, rather than a unique value although the midpoint is often used to define the Tg. Consequently, approaching Tg thermosetting adhesives show distinct changes in mechanical properties. Recent work has been performed in fitting thermo-kinetic models to curing reactions (77). This enables features of the curing system to be investigated for a given time – temperature profile, optimising the curing processing parameters for a given requirement. A curve fitting approach can be performed, establishing the relationship between a theoretical model and a measured DSC curve.

Epoxy TS adhesives, based on epoxide chemistry, are one of the most preferred products for manufacture of structural automotive joints. This is due to the epoxy chemistry offering high strength compared to alternative chemistries with the possibility to increase elongation at break when required for crash critical applications. This relationship between elongation and break and joint strength is shown in Figure 16 for a variety of chemistries.

Epoxy adhesives can be either single part, cured at elevated temperature or two-part adhesives. Another common automotive structural adhesive chemistry is that of TS polyurethanes. These are based on urethane chemistry and can also be formulated into one or two-part adhesive products. Higher modulus polyurethane adhesives are frequently used with multi-material structural bonding applications, with the lower modulus helping to reduce residual stresses generated as a result of substrate differential thermal expansion. Lower modulus polyurethane products are predominantly used for glazing bonding and sealing applications within the automotive industry.

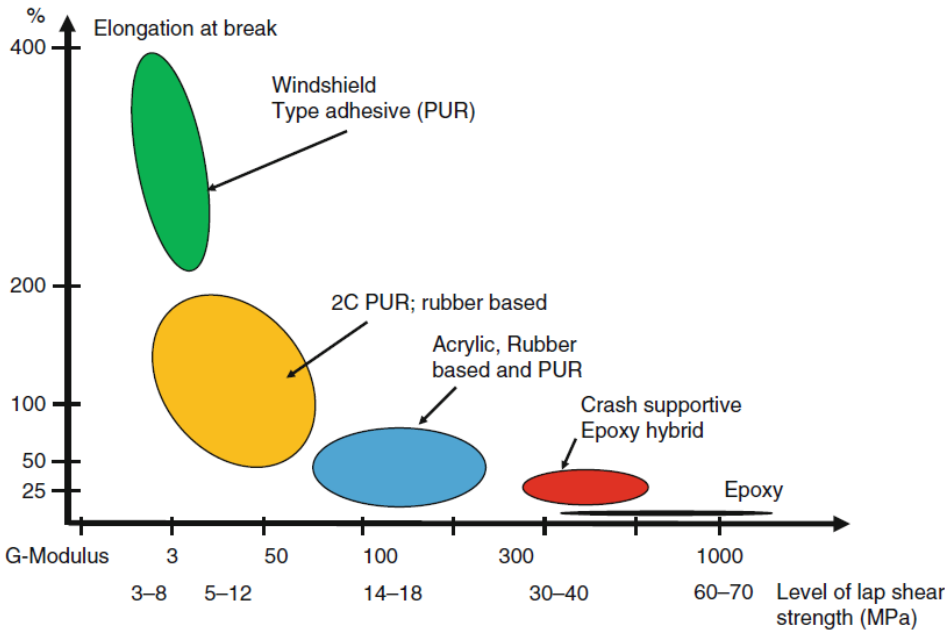

Figure 16 Adhesive categories frequently used for automotive bonding applications (62)

2.5. Joint test methods

One of the final important considerations relating to the analysis of joining methods is the choice of test method. The range of tests which could be performed upon a joint is extensive, extending to mechanical, thermal, optical and chemical analysis methods. Mechanical testing is one of the fundamental ways of testing the strength of a joint, with the joint usually being loaded until failure to equate the ultimate joint failure strength. Shear tests are one of the most common adhesive tests, used to compare and quality control adhesives. The lap shear test gemoetry is shown in Figure 17 with test parameters detailed by BS EN 1465:2009 (78). An improvement upon this method is the thick adherend shear test. This aims to eliminate one of the biggest problems with the standard single lap shear test which is a complex state of stess. Load misalignment in the single lap shear test can lead to to non uniform shear, stress concentrations and peel stresses. The joint fillet shape can also effect the joint strength (79), seen in Figure 17. As a result it is important to produce a consistent joint fillet between comparative joints. An alternative method to the single lap shear joint test is the double lap shear joint. The limitations of the single lap shear test method must be concidered when interpreting the results. The single overlap however does relate to one of the most common joint configurations used within automotive body construction.

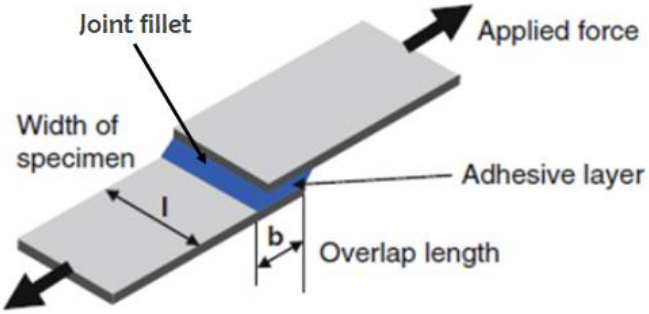

Figure 17 Single lap shear test method (62)

Peel tests measure the force per unit width of joint to separate the joint shown in Figure 18. The peel test result is very dependent upon test geometry and geometry independent peel analysis using fracture mechanics and energy balance is an area of much research (62). Various fixed geometry peel test methods are available with dedicated standards. Alternative test methods include joint testing in pure tension, often performed using butt joint method as described by BS EN 15870:2009 (80). Fracture tests of varying configurations are also performed widely upon adhesives to determine fracture toughness K_{IC} or fracture energy $G_{IC,}$.

These tests aim to characterise the fracture resistance of the joint as a system in one or more loading conditions. An example of this is the double cantilever beam test (DCB).

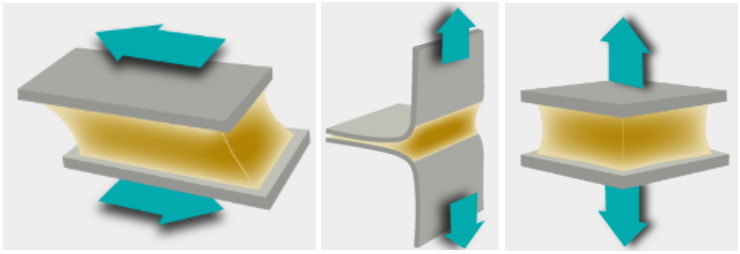

Figure 18 Standard joint testing methods, shear (left), peel (centre) and tension (right) (81)

2.6. Joining methods – conclusions

Section 2.4 summarised much of the state of the art within automotive joining technology, a particular emphasis being placed upon multi-material and CFRP intensive structures. The reviewed technologies extended to the use of fusion, mechanical and adhesive techniques as well as hybrid techniques combining more than one method. It was shown that there are a variety of techniques available to the automotive industry for addressing different joining problems. It was apparent however that the joining of FRP's bring additional challenges compared to the joining of traditional metallic materials.

Fusion welding techniques were shown to offer the potential for rapid joining of TP-FRP, with excellent joint strength and the absence of additional materials such as adhesive or fasteners to the joint saving weight and cost. However, extending these techniques to the joining of TS-FRP brought the requirement for an additional compatible thermoplastic layer, creating extra cost and an undesirable step in an automotive manufacturing environment. Further, extending the technique to dissimilar material joints brings concerns over differing CTE and durability performance. As such, whilst these techniques hold great potential for similar TP material joining, they did not appear suitable for the present multi-material application within the high-volume automotive industry.

Mechanical fasteners have been a key component in automotive assembly for decades, however they were identified as unsuited to the joining of FRP. They generally result in fibre breakage, delamination and poor joint stress distributions compared to when used with more ductile metals. This results in undesirable joint failure modes. An improvement was identified

when TP-FRP substrates are used compared to TS-FRP, the fastener being inserted into molten polymer thus redistributing the reinforcement fibres rather than fracturing them. Similarly, when used in combination with adhesives such as in the *riv-bonding* technique load transfer across the joint is improved. For the present multi-material challenge mechanical fasteners appeared an unattractive option and certainly would be a poor choice of joining method for FRP joints in isolation.

Adhesive bonding techniques offer an attractive solution to multi-material joining applications. A wide variety of adhesives are commercially available, suitable for bonding a variety of different substrates. Further adhesives are able to tolerate a range of differing CTE's with appropriate joint design. Structural adhesives, if applied correctly, produce very strong joints with a much more desirable stress distribution using FRP substrates compared to mechanical fasteners. Further, to deliver sealing and meet NVH requirements adhesives or sealants were likely to be present in many joints anyway. The application of structural adhesives thus creating no extra step in joint production. Adhesive technologies are also familiar to the automotive industry. Two main disadvantages of this technique with respect to the present application were identified. These included the requirement for surface preparation to deliver acceptable structural adhesive bond strength upon FRP's, as well as frequently lengthy cure cycles for many FRP bonding adhesives. Without addressing these disadvantages primary bonded (adhesive-only) joints are unlikely to meet high-volume cycle time requirements.

2.7. Opportunities identified

Chapter two identified that adhesive bonding appeared the most appropriate method for the joining of FRP intensive automotive structures compared to fusion welding or mechanical joining techniques. Adhesive bonding was shown to be a flexible technique, applicable to many different substrates and able to perform under a variety of environmental conditions. The ideal adhesive bonding technique for high-volume FRP and multi-material structures would require no surface preparation in order to achieve a reliable cohesive failure mode upon FRP and metallic substrates. The adhesive would also possess a suitably long open time for application and re-alignment of components if required and then fully cure instantaneously on demand. The adhesive would also meet various engineering requirements. However, such a product does not exist at present. Thus, an alternative approach to implement a high-volume, FRP intensive, adhesive bonding technique may be to

combine a reliable surface pre-treatment method with a means of accelerating the adhesive cure cycle on demand.

It was identified that the requirement for substrate surface preparation prior to adhesive bonding exists for two main reasons, the first being to remove surface contamination and the formation of a weak boundary layer. The second reason being to activate the surface to maximise the formation of strong chemical bonds between the adhesive and substrate. This requirement appeared particularly prevalent with low surface energy polymer surfaces such as many engineering thermoplastics. Of the various methods that were identified for performing the required surface preparation the most promising for a high-volume manufacturing environment appeared to be APPT. This process was shown to be effective at activating polymer surfaces prior to adhesive bonding and some evidence exists to suggest the process can remove some industrial surface contamination. Thus, the research questions identified were;

- Could APPT alone deliver suitable surface activation and acceptable joint failure modes upon TS and TP-FRP within a high-volume manufacturing environment?
- Would this surface pre-treatment method prove reliable for the manufacture of high-volume structural adhesive joints including upon contaminated surfaces?
- Further, would the process produce a durable adhesive bond suitable for an automotive structure?

With CFRP intensive structural bonding applications becoming increasingly prevalent within the high volume automotive industry the focus for surface preparation techniques was placed upon the CFRP surface, within chapter three. Structural metallic bonding is much more established within the automotive industry and already performed within Jaguar Land Rover, resulting in less requirement for development of metallic surface pre-treatments. As such, bonding to metallic surfaces was not investigated further in chapter three.

The second area of research that was identified relates to the requirement of sub one-minute cycle times for high-volume automotive manufacture. With full cure of many structural FRP bonding adhesives in the region of 30 minutes or more the following research question was identified;

- Could a primary bonded, FRP intensive, multi-material structure, consisting of adhesive only (primary bonded) joints meet the required manufacturing cycle time?

Whilst full cure was not necessarily required to generate sufficient handling strength for fixture removal, could sufficient handling strength be generated in under one minute? Answering this question required rapid curing TS adhesives for which the epoxy and polyurethane families were identified as suitable candidates. It was known that by increasing temperature, curing rates could be increased. It was also established within section 2.4.1 that various methods existed to rapidly heat FRP developed for fusion bonding technologies. Thus, the opportunity was identified for these rapid heating technologies be used to meet structural, primary bonded, requirements of multi-material structures. Induction heating appeared to be one of the most promising rapid heating methods, discussed in section 2.4.1.1 and was already used for aluminium non-structural hem flange adhesive curing within the automotive industry. It was proposed that the process could be adapted to heat CFRP and multi-material adhesive joints. The heating cycle could be used to accelerate the cure and strength development of structural adhesives. As a result, this may enable joint handling strength requirements of the high-volume automotive industry to be met, as well as the requirements of the final fully-cured structural adhesive joint.

These two opportunities formed the primary areas of research for this project;

1. The first area being analysis of APPT for the surface pre-treatment of FRP prior to structural adhesive bonding. This area is explored within chapter 3.
2. The second is the development of electromagnetic induction curing technologies for FRP intensive and multi-material structures. Primarily to identify whether a primary bonded structural adhesive joint is achievable within an acceptable high-volume manufacturing cycle time. This area is explored within chapter 4.

3. Chapter three - Atmospheric pressure plasma treatment

Atmospheric pressure plasma treatment (APPT) is an established method for promoting adhesion upon polymer surfaces, some of the results presented in literature were discussed within section 2.4.3.1. A further, more detailed, analysis of the literature was also produced in submission one to this EngD portfolio (82). It was reported that the APPT process can produce significant adhesion improvements upon TS and TP surfaces, with the latter being particularly effective. It was also identified that the process may be effective at removing some surface contamination.

The available literature however, made very little reference to the high-volume manufacturing environment, where cycle time limitations are much more critical than in other manufacturing and research areas. Thus, the research question was raised whether APPT alone could provide a suitable surface pre-treatment for FRP polymers, both TS and TP, when used within a high-volume automotive manufacturing environment. This raised several research questions, of key interest to Jaguar Land Rover.

The first area for research was whether APPT could maximise adhesive joint strength and minimise undesirable adhesive failure modes upon TS and TP substrates, at the treatment speeds required for high-volume manufacture. To investigate this an extensive parameter optimisation was required, identifying optimal treatment parameters and the trade-off between joint performance and APPT treatment parameters. Throughout this the APPT process was compared to benchmark alternative treatments including; a dry cloth wipe (DW), a solvent wipe with isopropanol (IPA) as well as a grit blast abrasion (ABR) and solvent cleaning combination (IPA + ABR).

A second question which needed to be investigated was whether APPT alone could remove typical FRP surface contamination, which may be detrimental to adhesive joint performance. At the time of project commencement this possibility had been suggested by Jaguar Land Rover, however there was little literature to support the effectiveness of APPT regarding surface contamination removal, particularly FRP mould release agents at high-volume APPT treatment speeds.

Finally, it was important to identify whether APPT could enhance the durability of an FRP adhesive joint under aggressive environmental conditions, compared to alternative pre-treatment methods. This could severely affect the process suitability for an automotive application. An emphasis was primarily placed upon the surface pre-treatment of FRP surfaces within this work. This is due to this area being less developed for high-volume structural adhesive bonding than the pre-treatment of metallic surfaces.

3.1. Investigation methodology

A Diener Electronic Atmospheric PlasmaBeam Duo system was specified and purchased for use with this project, seen in Figure 19. This twin head system utilised dry compressed air to generate the plasma jet and had a plasma generator power of 600 W. Only one plasma head was used for this investigation. The movement of the plasma heads was controlled by a Janome three axis programmable robotic stage.

The Jamome robotic stage enabled controllable and repeatable positioning of the plasma heads in relation to the substrate. One of the key process parameters is defined as the working distance (WD), the distance between the tip of the plasma torch and the substrate. The other key parameter being the treatment speed (V), the speed at which the plasma head moves along the substrate. Alignment fixtures were placed upon the robotic stage to ensure samples were positioned in a repeatable manor with respect to the plasma treatment head. Machined PTFE spacers were used to set the WD relative to the substrate.

Figure 19 Diener Electronic plasma treatment system coupled to Janome 3 axis robotic stage

Single lap shear (SLS) adhesive testing was determined as the most appropriate test method for this work, in line with other related work and the recommendations of Jaguar Land Rover. Specimen preparation was performed to BS EN 1465:2009 (78), utilising a 12.5 mm overlap, 0.3 mm glass beads within the adhesive and a 25 mm specimen width. Samples were tested on a 30 kN Instron 3367 universal testing machine at 13 mm/minute (65), with 100 mm gauge length. Tabs equal to the specimen width were placed within the self-aligning grips of the tensile test machine to compensate for the joint offset.

A two-component epoxy structural adhesive was used, Sika 490c manufactured by Sika Automotive AG. This product had been identified by Jaguar Land Rover as a high performing structural adhesive for the bonding of composite substrates within previous work. Oven curing was performed at 85 °c for a total of 30 minutes as per the manufacturers recommendations (83). The oven was preheated to 85 °c before loading samples, consistent with the advice of Jaguar Land Rover. This cure cycle produced an adhesive Tg of approximately 95 °c (83). Glass beads were supplied pre-mixed within the adhesive. Adhesive was applied to one specimen using a spatula and the substrates brought together. Excess adhesive spew was then removed to achieve a relatively controlled fillet prior to spring clips being applied to the joint to hold geometry during cure. The target fillet shape and overlap geometry can be seen in Figure 20. Samples were left for a minimum of 24 hrs at room temperature between oven curing and tensile testing.

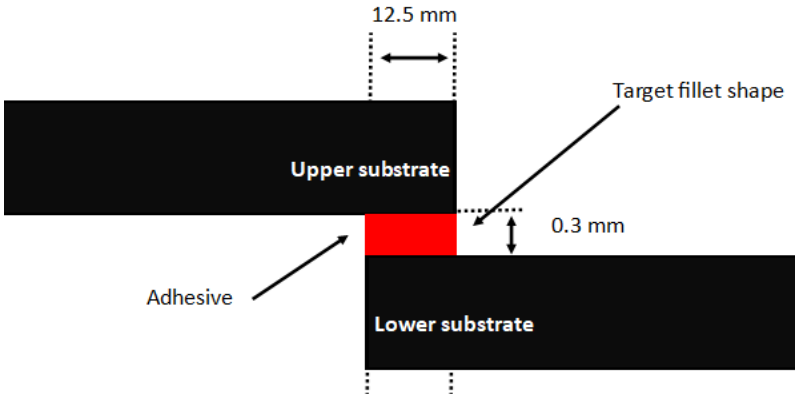

Figure 20 Target fillet shape and overlap dimensions

Two materials were used for the APPT investigation as specified by Jaguar Land Rover, the first being a biaxial CFRP non-crimp fabric (NCF) impregnated with MTM710 epoxy TS resin produced by Cytec Industrial Materials. The 400 gsm material was laid up to $[-45,+45]_{3s}$ and cured at approximately 140 °c using a compression moulding process. A force of 1800 kN was applied to the $250x10^3$ mm^2 flat plaque tool for which the cavity was held under vacuum

during moulding. A cycle time of under five minutes was performed, shown in previous work to achieve full cure by DSC analysis. This processed produced a laminate of approximate 2.5 mm thickness. A water-based mould release, Marbocote W1141 was applied by hand using a spray application to the mould tool, being reapplied approximately every 5 plaques.

An alternative TP-FRP material was produced using a unidirectional carbon reinforcement and a BASF Ultramid B3 polyamide 6 (PA6) matrix, supplied by Jonam Composites Ltd. This material was processed using a vacuum bag upon a polished aluminium sheet. The sheet was coated with Marbocote 227CEE mould release, applied using a cloth wipe. The mould release was cured upon the sheet for 30 minutes at 140 °c prior to processing the composite laminate. The laminate was placed over the mould released aluminium sheet and a peel ply, followed by PA66 bagging material placed over the top, sealed with high tack composite moulding tape. The composite was then held under vacuum for 10 minutes at 245 °c, prior to cooling and subsequently releasing the vacuum. The layup used for Carbon PA6 was $[0/0/90/0/90/0/90]_S$ producing an approximate laminate thickness of 1.8 mm. In all cases the direction of surface fibre orientation was aligned with the direction of applied load during the tensile test to avoid undesirable fibre pull out. Adhesive SLS specimens were cut using an automated water-cooled diamond blade and bonding performed only on the side of the specimen in contact with the aluminium sheet during moulding.

The maximum load was recorded by the Instron tensile test machine during the SLS test. The failure shear strength was then calculated based on the measured joint overlap. This was measured using a ruler following each test to ensure it did not deviate by more than ± 0.5 mm from specification and the overlap area calculated. Once measured, the calculation was performed according to the relationship; SLS joint strength (MPa) =(load (N) / joint overlap area (m^2)) / 1000000.

It was predicted that effective treatment width would vary according to the WD. An understanding of the effective treatment width is vital in a manufacturing environment, dictating the number of APPT torch passes required to treat the entire bondline width. Some overlap may also be desirable in a manufacturing environment to ensure full coverage, however the exact width of treatment was used for this study to reduce the number of variable factors. An initial study was performed to evaluate the width of APPT treatment (W) at differing WD, detailed in section 3.1.1. Once treatment width was established this data was

then used to perform the parameter optimisation and further studies. In many cases multiple passes of the plasma torch where required to treat test the bonded area of test coupons, spaced at a distance equal to the width of treatment. Coupons were subsequently treated at varying working distances and treatment speeds as stated in the experimental results.

Alternative surface pre-treatments were also applied to the specimens to compare the joint performance with and without APPT. These included the DW, IPA and ABR as previously discussed. Combinations of these methods were also included in some cases, when detailed within the experimental results. Following surface pre-treatment and immediately prior to adhesive bonding SFE evaluation was performed upon all treated surfaces using the sessile drop contact angle method. The SFE analysis was performed for the following reasons;

1. SFE analysis provided an alternative method to destructive joint testing for the comparison of surfaces following different surface pre-treatments. This lead to an identification of the most effective surface pre-treatment processes and an understanding of their effects upon SFE.
2. The collection of SFE data enabled a greater understanding to be developed of the link between surface energy and bonding characteristics for the selected substrate, adhesive and pre-treatment combinations.
3. An understanding could be developed of the achievable surface energy following differing pre-treatments, this could then be used to assist with adhesive selection in later work, the methodology is discussed further in section 2.4.3.
4. The SFE analysis enabled comparison between the treated SFE of the candidate materials and materials used in literature bonding studies with alternative materials and pre-treatment processes. This would not be possible where adhesive dependent bonding studies were used alone due to the critical dependence of bond strength upon the adhesive itself.

To perform the SFE analysis 2 µl droplets of de-mineralised water, ethylene glycol and diodomethane were applied to the CFRP surface and contact angle analysed with a One-Attension tensiometer. The frame rate was set to 7 Hz with a 10 s record duration and automatic trigger. Once recorded the mean left and right contact angles were calculated over the final ten recorded frames to give an average contact angle for each drop. This was performed three times for each of the three test liquids. Subsequently, the OWRK method

used to calculate the polar, dispersive and total components of SFE. The corresponding average SFE value was then plotted for each set of treatment conditions with error bars of +/- 2σ , σ representing the estimated standard deviation of the population calculated using the (n-1) method. The error bars were chosen in this way due the maximum and minimum sample values providing a poor representation of a population with a small sample size. The SFE analysis was performed on a treated region of the bondline, behind the area where adhesive was subsequently applied. Once tensile testing had been completed SLS strength data for each batch of samples, consisting of five repeats in each case were plotted. With error bars again corresponding to +/- 2σ using the (n-1) method.

3.1.1. Treatment width assessment

Various methods were used to evaluate the plasma treatment width. The first method consisted of plasma treating single lines at varying WD across a TS-CFRP plaque at a slow speed of 30 mm/s. The plasma treatment was performed parallel to the plaque edges. Following treatment, lines of sessile droplets of water and ethylene glycol were placed perpendicular to the treatment lines, placed at 5 mm increments. The contact angle was recorded for each droplet using the method described in section 3.1. A subsequent row of droplets was then placed at an offset of 1 mm to the previous row, and this repeated until droplets were recorded at effectively 1 mm increments across the plaque, perpendicular to the treated lines. The data was then used to express the variation in liquid contract angle and surface free energy across the treated lines at differing WD. The process is illustrated in Figure 21.

An example of the results produced is shown in Figure 22. It became apparent that a plasma treatment width of approximately 8 - 10 mm is achievable at working distances of up to 10 mm. At greater WD water contact angle begins to increase although there is considerable scatter in the data. Result scatter this is often the case with contact angle measurement due to small variations in surface conditions across the surface. It was also observed in early investigations that there is a notable difference in SFE between compression moulded TS-CFRP and autoclaved TS-CFRP. The untreated autoclaved material had an average water contact angle of approximately 90 ° whereas the same material compression moulded around 80 °. The industrial implication of this was that FRP processing method may have an influence upon adhesion to FRP surfaces and that development work should be performed on representative material wherever possible. An inverse Gaussian fit was fitted to the data in

Figure 22 and the full width half maximum used to approximate an “effective treatment width”.

One of the concerns that was identified with this method of treatment width evaluation was the tendency for liquid droplets to shift upon the surface once deposited. Droplets placed near to the edge of the APPT treated region are attracted to the higher SFE region and shift, thus the drop measurement location may differ slightly from the deposition location. Likewise, the width of the 2 µl drop limits the resolution of the technique. The effect of this may be an overestimate of the treated area.

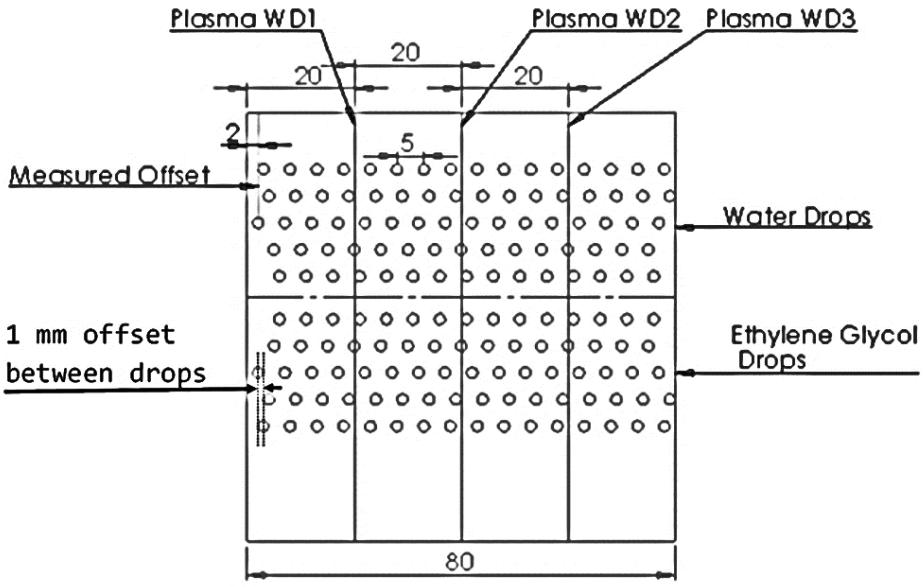

Figure 21 Treatment width assessment multiple drop method

An alternative method was used, in this case a plaque of TS-CFRP was APPT treated in the same way at differing WD values. Calibrated dyne pens, supplied by Dyne Technology Ltd were then applied perpendicular to the treated lines. The wet-out area was then measured using a calibrated optical microscope. The wet-out treatment width for the 60 dyne (60 mN/m) pen was then taken as an alternative treatment width assessment, being the highest dyne value pen available. Treatment widths were then rounded to the nearest one decimal place.

The data presented for both width evaluations is presented in Figure 23 with estimated error in both WD and treatment width calculation for both measurement techniques. The relationship was approximated to be linear with the same gradient for both techniques. By

calculating the difference in line intercepts the contact angle measurement method appeared overestimate the treatment width by approximately 3.2 mm. The linear trend using the dyne pen method was carried forwards to calculate the required width between APPT treatment passes upon test substrates. An APPT treatment overlap was considered preferable to an untreated region, which was observed upon early substrate investigations using the contact angle method of width approximation.

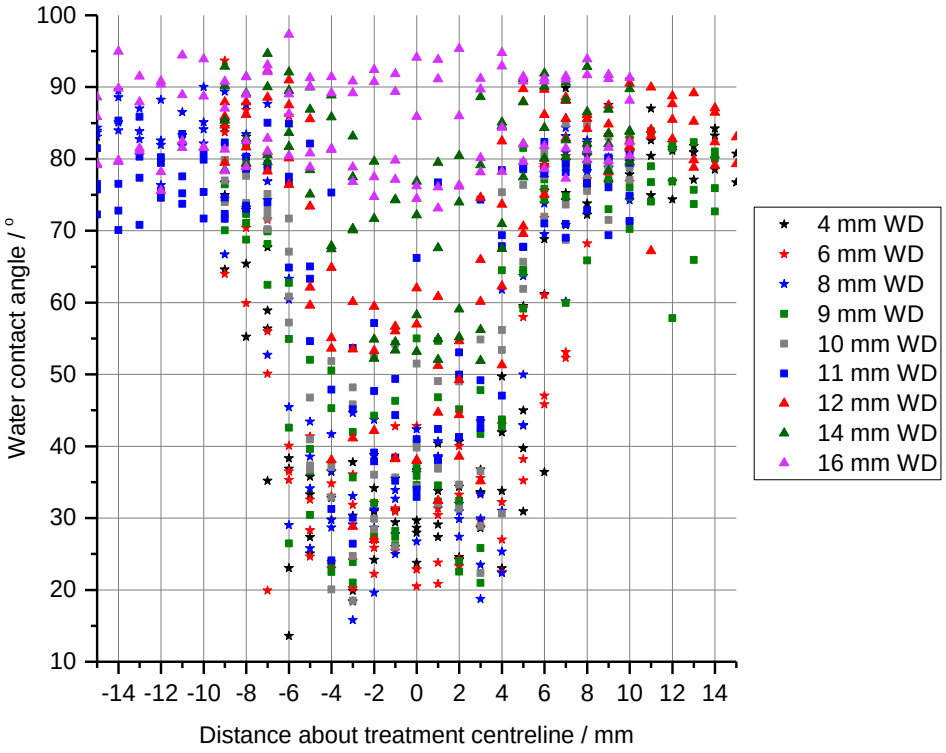

Figure 22 Treatment width data water contact angle

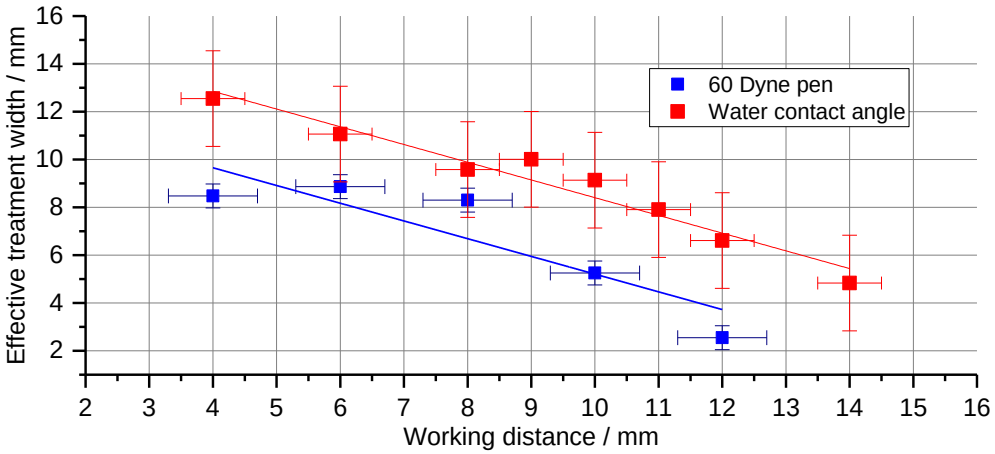

Figure 23 Treatment width assessment contact angle and dyne pen method

3.1.2. Surface scanning electron microscopy

To gain a greater understanding of the physical surface effect of APPT upon the surface of a TS-CFRP, both treated and untreated plaques were analysed using a Zeiss Scanning Electron Microscope (SEM). Figure 24 shows the effect of APPT when treated at 4 mm WD and 30 mm/s compared to the untreated surface. It appears there is some surface ablation, with the surface appearing etched. This suggested some ability of the process to remove surface contamination through removal of some surface material.

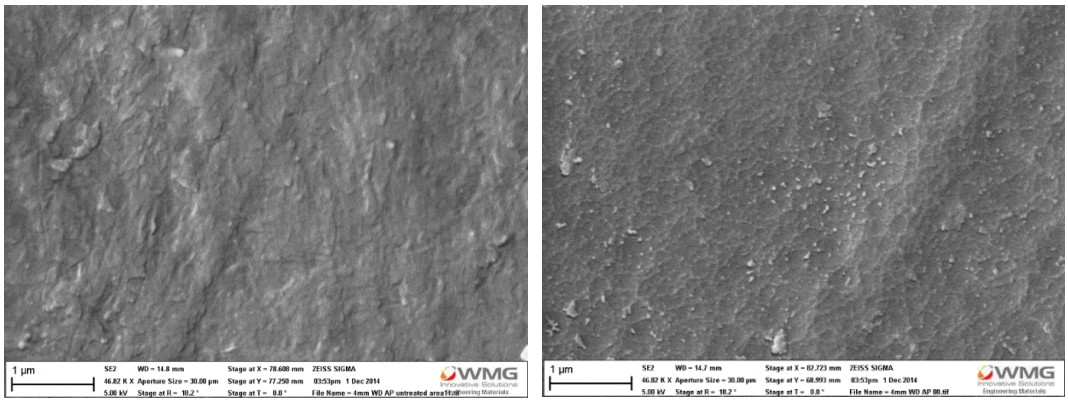

Figure 24 TS-CFRP untreated (left) and plasma treated 30 mm/s, 4 mm WD (right), both images to the same scale

As the WD increased the ablation effect became less notable with appearance approaching that of the untreated surface. It was also observed following APPT at 4 mm WD that the TP polyester stitching in the NCF appears much more prominent. With further SEM analysis, this was attributed to an expansion and blistering of the TP stitching, through the cured TS-CFRP surface seen in Figure 25. This blistering would suggest that the temperature in the region of treatment exceeds approximately 295 °c, the melting temperature of polyester causing it to blister through onto the surface.

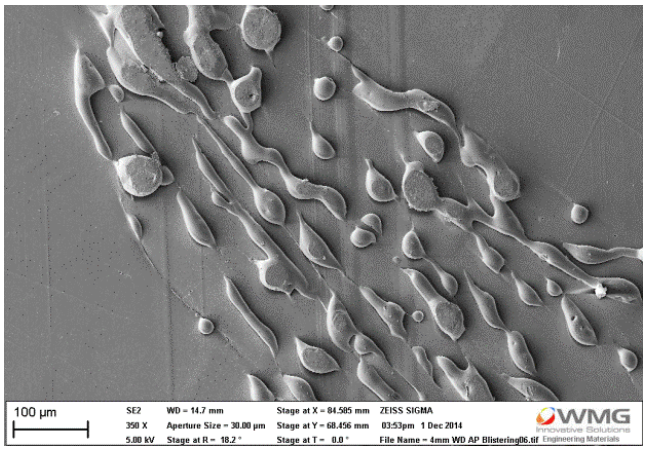

Figure 25 Blistering observed at 4 mm WD

3.2. Epoxy thermoset CFRP APPT

This section addresses APPT when applied to thermoset (TS) CFRP substrates, a subsequent analysis of thermoplastic (TP) substrates is presented in section 3.3. It was initially required to identify the optimal speed and WD for promoting structural adhesive bonding upon TS-CFRP surfaces. A preliminary set of data was collected investigating APPT treatment speeds of 25 – 200 mm/s and WD of 4 – 12 mm and is detailed in portfolio submission two (84). The treatment parameters were within the range suggested by the equipment supplier, Henniker Scientific.

The conclusions from the first set of data were;

- APPT did not appear to yield a stronger joint compared to IPA wipe only or abrasion, with an optimal SLS strength of 30 – 31 MPa in all cases.
- There was evidence to suggest surface contamination may be responsible for reduced SFE and SLS strength following APPT, leading to a change in joint failure mode from cohesive to adhesive. This was evaluated further in section 3.2.1 with similar results found. As such ensuring consistent plaque surface condition and rigorous control over FRP plaque production methods was considered highly important for future data collection and optimal adhesive bonding.
- Where multiple FRP plaques were used within a data set consisting of multiple sample batches, the plaques must be randomised to prevent one individual batch of samples being adversely affected by a change in plaque surface condition. It was not possible in many cases to produce a full set of comparable samples from a single plaque due to the quantity of material required.

A repeat set of data was produced. In this case APPT working distances of 4, 8, 10 and 12 mm were used with treatment speeds of 10, 30, 60 & 120 mm/s in a fully factorial experimental design. This enabled the most influential parameters of the APPT process to be identified in relation to both SLS strength and SFE. Multiple APPT passes were applied to the bond area spaced according to the dyne pen relationship, in section 3.1.1 TS-CFRP substrates were randomised from a number of plaques to produce the material required for investigation.

The collected SLS and average SFE data is shown in Figure 26. It was immediately apparent in this case that a mean SLS strength of approximately 30 MPa was achieved in all cases

regardless of the surface pre-treatment applied. There was only evidence of a small improvement in SLS strength from the introduction of APPT with the present adhesive and substrate combination compared to an untreated (DW) surface, however given the variation in the data set this was largely insignificant.

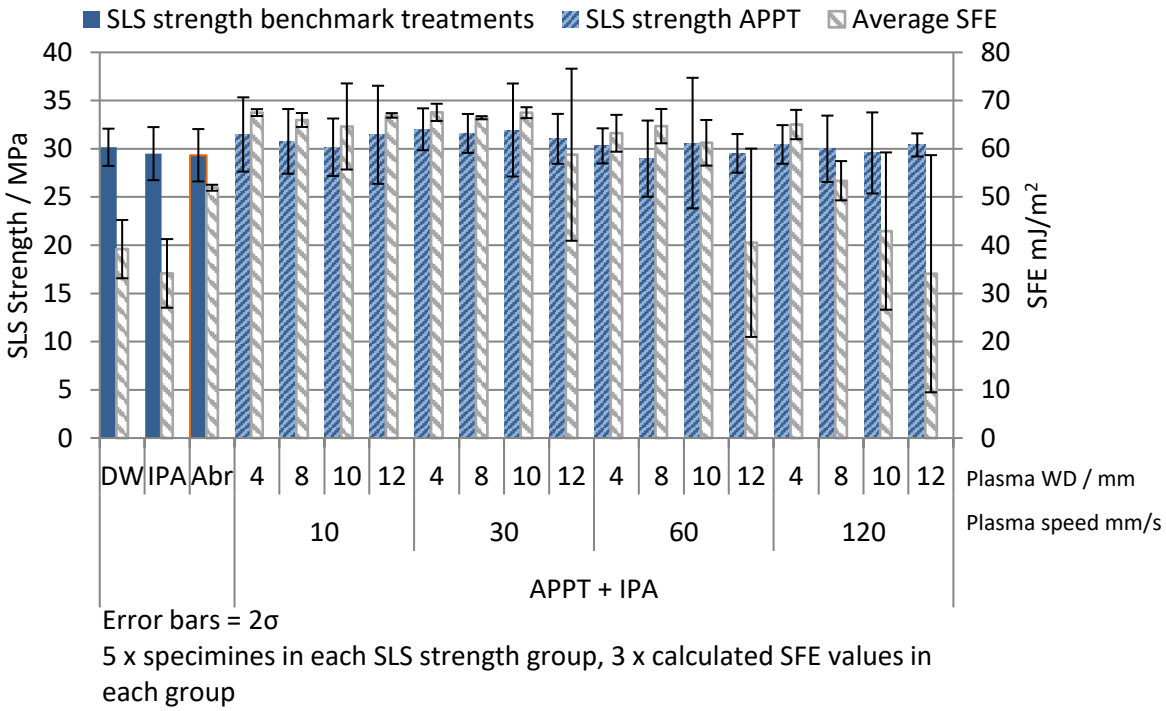

Figure 26 TS-CFRP repeated plasma data

As discussed in section 2.4.3.1 a high surface energy can assist in promoting adhesion and increased joint strength. It can be seen that a mean SFE of 39 mJ/m^2 was achieved with only a DW surface pre-treatment. This was slightly reduced when an IPA wipe was applied, down to 34 mJ/m^2. To identify whether this difference was statistically significant a paired sample t-test was used to the 95 % significance level. The paired t-test was used due to the only significant change between sample batches being the surface pre-treatment. A calculated probability, or P value, of 0.028 was calculated, indicating with 95 % confidence that the mean SFE of IPA is lower than that of DW. This may have indicated some surface contamination was removed by the IPA wipe. It was predicted that this contamination may have either caused a small increase in SFE or effected the contact angle measurement such to reduce the liquid contact angle. This would have resulted in lower measured contact angles and a lower calculated SFE, although this would require further investigation.

Abrading the surface resulted in an increase in the mean SFE to 52 mJ/m^2 attributable largely to an approximate 20 mJ/m^2 increase in the dispersive component of SFE. This difference in means between the ABR samples and IPA cleaned samples was identified also as statistically significant with the paired t-test, P=0.011. The introduction of plasma treatment caused a much smaller increase in the dispersive component of SFE compared to abrasion however a large increase in the polar component of SFE. Polar SFE increased from a mean of 5 mJ/m^2 with a DW to 25-30 mJ/m^2 with optimal APPT, attributable to the significant increase in total SFE. It was found using a two-sample t-test, due to different sample sizes that there was a statistically significant difference between the mean SFE of the abraded samples and the sum of APPT treated samples at 10 mm/s, with P<0.001, indicating with greater than 99 % certainty that plasma treatment is more effective at increasing the SFE of TS-CFRP than abrasion.

An analysis of variance (ANOVA) statistical analysis was performed upon the APPT treated SLS strength results in the data set. The ANOVA analysis splits variability within a data set into two parts, systematic factors and random factors (85). The analysis can be used identify whether the effect of changing independent variables, in this case WD and treatment speed, has a statistically significant influence upon the output of the system, or whether the effect is purely random. As a result, the method can be used to identify the important APPT process parameters with a specified certainty. The analysis can be performed with one independent variable (one-way ANOVA), or with two independent variables (two-way ANOVA). Interaction effects between two factors (two-way ANOVA with interaction) can also be identified with the analysis techniques. If required, the analysis can also be extended to a greater number of independent variables.

A two-way ANOVA with interaction was performed to identify whether treatment speed or WD significantly affected SLS strength to the 95 % confidence level, results are shown in Table 2. It was found that treatment speed was the only statistically significant parameter that effected SLS strength, with a calculated probability P = 0.008 lower than the P=0.05, 95 % significance level. As such a one-way ANOVA analysis was performed, also shown in Table 2. This highlighted that the residual error in the system was σ = 1.713 MPa, this is random variability in the system not effected by the independent variables. A linear regression model was fitted to the collected plasma treatment data over a range of treatment speeds to the 95 % significance level. Error bounds equal to ± 2σ were also added, seen in Figure 27. The regression model enabled a prediction to be made of the SLS strength for a specified plasma

treatment speed within a stated confidence level. Over the range of treatment parameters investigated the joint failure mode was predominantly cohesive. Small amounts of material failure were observed at the higher WD and treatment speed combinations.

Two-way ANOVA					
Source	DoF	SS	MS	F	P
Speed	3	40.758	13.586	4.28	0.008
WD	3	5.583	1.861	0.59	0.627
Speed x WD	9	14.025	1.558	0.49	0.876
Error	64	203.367	3.178		
Total	79	263.733			

One-way ANOVA				
DoF	SS	MS	F	P
3	40.758	13.586	4.63	0.005
76	222.975	2.934		
79	263.733			

Table 2 TS-CFRP SLS strength, two-way ANOVA with interaction and one-way ANOVA

It was observed within the regression analysis, Table 3, and the regression plot Figure 27, that the standard error inherent in the system contributes 93.21 % of variation. This is a much larger variation in SLS strength than can be attributed to varying plasma treatment speed over the range investigated, equal to 6.79 %. An F-test indicated that the coefficient of speed in the regression model is statistically significant, P = 0.02 however the difference in SLS strength of the joints over the range investigated is largely insignificant in a practical engineering context compared to the residual variation. This was highlighted by the wide prediction interval, representing where a single response may fall. The high standard error was attributed to small variations between samples, including joint spew, overlap, adhesive mix state, surface condition etc. Whilst these parameters were controlled as closely as reasonably possible, some additional variation is inevitable in the manual production of adhesive joints.

Source	DoF	SS	MS	Contribution / %	F value	P value
Due to regression	1	17.92	17.96	6.79	5.68	0.020
About regression	78	245.82	3.15	93.21		
Total	79	263.73		100		

Table 3 TS-CFRP SLS data regression analysis of variance

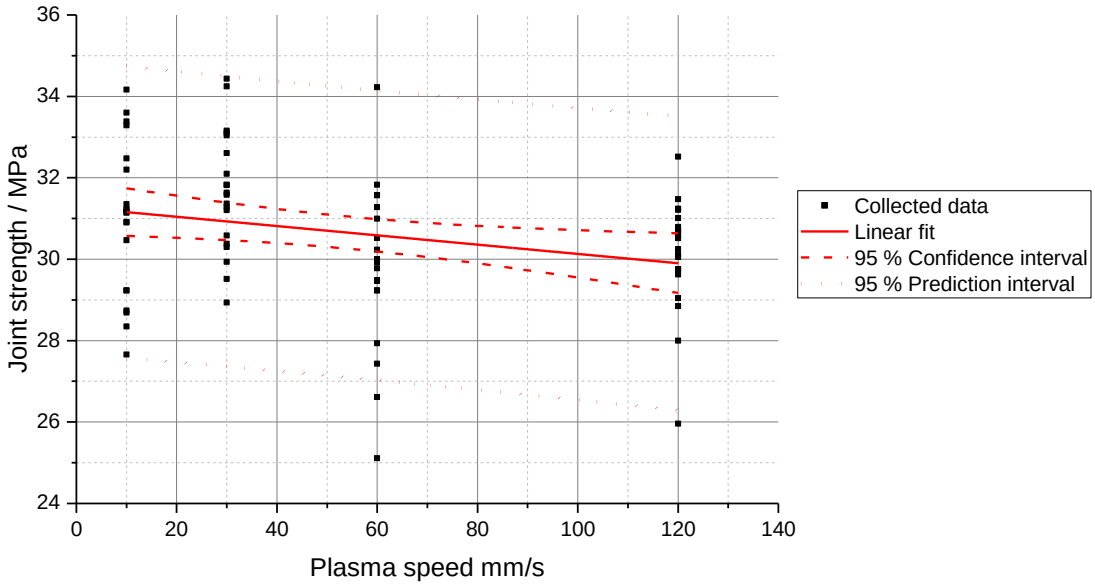

Figure 27 Regression model TS plasma speed vs SLS strength

A further statistical analysis was also performed upon the total SFE data to the 95 % significance level. Initially a two-way ANOVA identified that both the WD, Speed and WD speed interaction produce a statistically significant change in total SFE. This is shown in the ANOVA results, Table 4. A mean residual error standard deviation of $\sigma = 5.20$ mJ/m^2 was calculated, equal to the error of SFE measurement and inherent variability within the samples.

Two-way ANOVA					
Source	DoF	SS	MS	F	P
Speed	3	2330.59	776.86	28.68	0.000
WD	3	1665.74	555.25	20.50	0.000
Speed x WD	9	1276.44	141.83	5.24	0.000
Error	64	866.86	27.09		
Total	79	6139.63			

Table 4 TS-CFRP total SFE two-way ANOVA with interaction

A linear regression model was fitted to the SFE data, presented in Figure 28, along with regression confidence intervals and collected data for the 4 and 12 mm WD. The confidence intervals represent with 95 % confidence where the mean response may fall. The regression analysis of variance is seen in Table 5, where the speed x WD interaction had the most significant effect upon the regression model. The effect of WD and speed on their own was not found to be statistically significant, with a P value of greater than the 95 % significance level criteria of 0.05 in both cases.

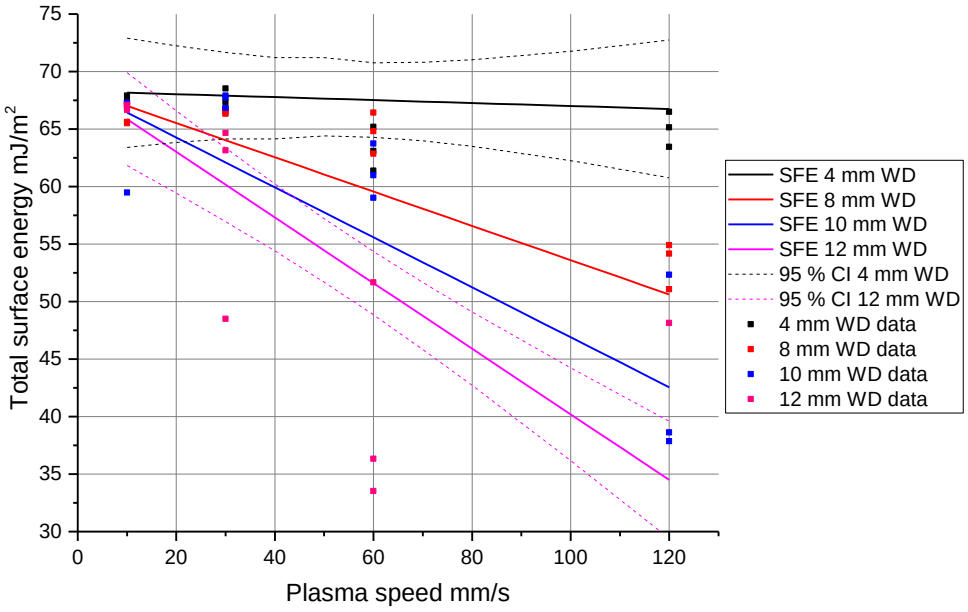

Figure 28 Total SFE variation of TS–CFRP with varying APPT treatment parameters

Source	DF	DoF	SS	MS	F	P value
Due to regression		3	4511.34	1503.78	40.64	0.000
	WD	1	0.43	0.43	0.01	0.915
	Speed	1	136.01	136.01	3.68	0.062
	WD x Speed	1	839.41	839.41	22.68	0.000
About regression		44	1629.28	37.01		
Total		47	6139.63			

Table 5 Regression analysis of variance TS-CFRP total SFE

Figure 28 highlights that with a TS-CFRP, APPT treatment speeds of up to 120 mm/s could achieve a mean SFE of approximately 61 - 73 mJ/m^2 providing WD does not increase above 4 mm. This compares to a mean SFE of 39 mJ/m^2 without APPT. With an increase in WD at higher treatment speeds a rapid reduction in achievable SFE was observed compared to the maximum values at the lower treatment speeds. The residual error of measurement would also combine with the standard error of the regression model should a prediction interval be required for a given combination of APPT parameters.

3.2.1. Surface contamination removal

Based upon the unexplained variation observed in preliminary data collection and sponsor company concerns regarding surface contamination upon bonding surfaces, it was required to identify the ability of APPT to remove expected surface contamination upon FRP surfaces. The available literature, as well as expectations from equipment suppliers, had suggested APPT may be able to remove some surface contamination. However, this effect had not been

proven for the expected contaminants and for a range of APPT treatment parameters. Contaminants thought likely to be present are presented in Table 6. To investigate the effect of APPT upon surface contamination removal these contaminants were forcibly applied to fully cured TS-FRP plaques, prior to surface pre-treatment, SFE and SLS testing. Surface pre-treatments were applied individually in this case, and not in combination. This was to identify the effectiveness of a single method alone at surface contamination removal. APPT S (slow) refers to a treatment at 4 mm WD, 10 mm/s and APPT F (fast) refers to a plasma treatment at 4 mm WD 120 mm/s. These parameters were used based on optimal surface free energy data available at the time of investigation.

To simulate the curing process of the mould release onto the TS-FRP surface, as predicted to occur during the moulding process the plaques were heated to the application temperature of the mould release prior to surface pre-treatment. Once contaminants were cured the surfaces were cooled and surface pre-treatment applied. The application method and curing cycle is also detailed in Table 6. It should be noted that the level of contamination represents a worst-case scenario, it is very unlikely that a transferred contaminant would have a layer thickness as great as that directly applied to the tooling. The collected data thus provides some insight into the ability of surface pre-treatment methods to remove specific surface contamination in the worst case. It should be considered that smaller levels of contamination may be more easily removed.

Once contaminated, and cured in the case of the mould release, surface pre-treatments were performed, SFE recorded of the contaminated surfaces and SLS joints produced. An uncontaminated batch of samples were also included, as-received straight from the press. The collected data is shown in Figure 29. The as-received specimens performed consistently with those presented within Figure 26, with similar SLS strength SFE values. This provided confidence to the previous data set and suggested a reliable set of benchmark data to compare the contaminated and pre-treated surfaces to.

Contaminant number / designation	Contaminant name	Description	Application method
1 / WMR	Marbocote W1141 **water-based mould release**	Spray applied to the compression moulding tool prior to TS-FRP moulding.	Pre-cleaning of FRP using IPA wipe. W1141 spray applied to FRP plaques oven cured for 15 minutes at 90 °c.
2 / SMR	Marbocote 227CEE **solvent-based mould release**	Applied using a wetted cloth to the TP vacuum bag moulding sheet.	Pre-cleaning of FRP using IPA wipe. Contaminant applied with a cloth wipe and oven cured for 15 minutes at 90 °c.
3 / VG	Dow Corning **high vacuum silicone grease**	Applied to aid TS-FRP mould tool sealing. During moulding a vacuum is applied to the compression moulding tool to remove air pockets from the laminate. The grease improves the performance of the vacuum seals.	Pre-cleaning of FRP using IPA wipe. Smeared initially onto an aluminium sheet and then transferred using a cloth to the FRP surface. Visible upon surface.

Table 6 Applied surface contaminants

The water-based mould release (WMR) contaminant interestingly resulted in little observable change to SFE regardless of the surface pre-treatment method applied compared to the as-received samples. This was validated with a two-way ANOVA analysis, results are shown in Table 7. A contamination calculated probability of P=0.854 and a contamination/surface pre-treatment interaction value of P=0.539 was significantly higher than the P=0.05, 95 % significance level, thus the introduction of WMR contamination did not statistically affect the SFE observed by the sessile drop method.

There was however a substantial change in SLS strength between the as received and water-based mould release contaminated samples. The mean of dry wipe samples reduced by 5.20 MPa and σ increased by 1.80 MPa as a result of the introduction of water-based mould release. The mean of the APPT slow and fast samples reduced by 15.1 and 14.9 MPa respectively. This was approximately 50 % of the mean as-received SLS strength with the same pre-treatment and approximately three times greater reduction in SLS strength compared to the same contaminant on a dry wiped surface.

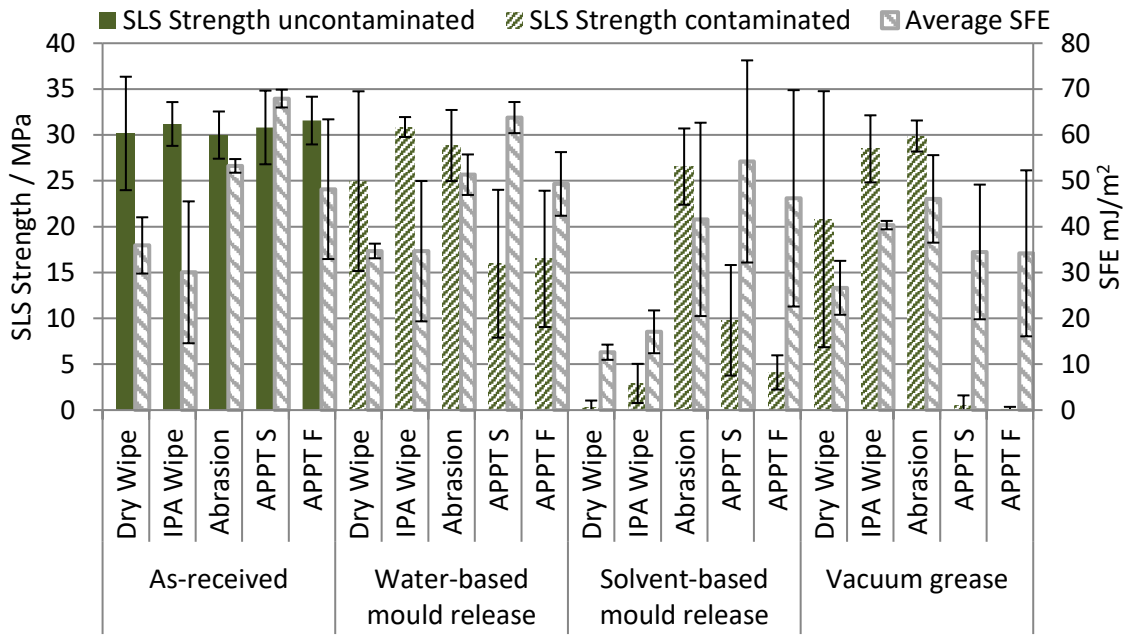

Error bars = 2σ
5 x specimines in each SLS strength group, 3 x calculated SFE values in each

Figure 29 Contaminated surfaces data TS-CFRP with various pre-treatments

Two sample paired t-tests were performed to identify if there was a statistically significant change in the mean SLS strength between the corresponding as-received, and contaminated data sets. The P statistics are shown in Table 8. Where P <0.05, it was concluded with 95 % confidence that there is a significant difference between the sample means based on the collected data sample size and standard error of the mean. It can be seen that with a water-based mould release contaminant, the reduction in mean strength was statistically significant when a dry wipe and APPT were applied whereas this is not the case when IPA wipe an abrasion method were applied. Thus, these appear the only methods which satisfactorily remove water-based mould release contamination.

Two-way ANOVA					
Source	DoF	SS	MS	F	P
Contaminant	1	0.70	0.70	0.03	0.856
Treatment	4	4428.40	1107.10	53.30	0.000
Contaminant x treatment	4	66.56	16.64	0.80	0.539
Error	20	415.44	20.77		
Total	29	4911.10			

Table 7 ANOVA analysis TS-CFRP Total SFE with and without WMR contamination with various pre-treatments

It was identified within Figure 29 that solvent-based mould release does reduce SFE with a dry wipe and IPA treatment, resulting in approximately half the as-received SFE and no

overlap in the error bars of 2σ. A small mean reduction in SFE however was observed with abrasion. Inspecting the raw data with abrasion and solvent-based mould release contaminant two SFE values of approximately 35 mJ/m^2 and one of approximately 54 mJ/m^2 contribute to the wide error bars. Thus, it is likely from this uncertainty and the two substantially lower values of SFE that there is some reduction in SFE upon the abraded surface with solvent-based mould release present. APPT fast with solvent-based mould release present resulted in an almost identical average SFE to the as-received surfaces with values of 46.2 and 48.2 mJ/m^2 with and without solvent-based mould release respectively, together with an increase in σ to 11.8 from 7.62 mj/m^2. This highlights that once APPT treated SFE is a poor indicator of solvent based mould release surface contamination. APPT slow resulted in a mean SFE reduction of 13.7 mJ/m^2 with the introduction of solvent-based mould release compared to the as-received surface. An increase in σ also occurred to 11.02 mJ/m^2 with APPT slow and solvent based mould release from 0.971 mJ/m^2 as-received with APPT slow. It was concluded that whilst SFE analysis can indicate the presence of solvent-based mould release upon a dry wiped, IPA wiped and abraded samples, it was challenging to observe any significant change upon APPT treated surfaces with the sample sizes available.

The SLS strength of the solvent-based mould release contaminated surfaces is vastly lower than that of the uncontaminated surfaces except for the case of the abraded surface. The paired t-test, Table 8, highlights that all samples contaminated with solvent-based mould release have a statistically significant difference in means compared to the as-received specimens with the same pre-treatment parameters. It is clear however that the mean SLS strength reduction is much smaller with an abrasion process at 3.45 MPa compared to 21.03 MPa with APPT slow, compared to the as-received samples. Thus, abrasion appeared the most effective method to remove solvent-based mould release contamination, with all other methods tested being largely ineffective. The solvent-based mould release was clearly highly detrimental to adhesive bond strength with the given experimental conditions. Whilst the mean SFE of the APPT treated solvent-based mould release samples appeared similar to the as received, the resultant SLS strength was substantially lower.

The SFE of the vacuum grease contaminated samples showed a much smaller drop in the case of dry wipe and IPA wipe compared to the solvent-based mould release contaminant. A difference was observed in mean SFE following a dry wipe of 9.24 mJ/m^2, between the as-received and vacuum grease contaminated samples with σ of 2.50 and 2.40 mJ/m^2

respectively. The average SFE of the IPA wiped samples increased by 10.29 mJ/m^2 with the addition of vacuum grease and σ of 6.31 mJ/m^2 as received to 0.376 mJ/m^2 with vacuum grease. Abrasion appeared to restore mean SFE to within 7.20 mJ/m^2 of the as received samples however with a notable increase in σ from 0.744 to 4.77 mJ/m^2 without and with vacuum grease contamination respectively. Thus, the change in SFE as a result of the vacuum grease contamination was relatively small compared to the as-received substrates. The mean SFE upon APPT treated vacuum grease contaminated samples compared to the as-received and other contaminated samples is notably smaller, appearing to reach a maximum of 34.5 mJ/m^2 with APPT slow. A standard deviation σ, of 7.34 and 9.04 mJ/m^2 for APPT slow and APPT fast upon vacuum grease contaminated samples was calculated respectively, slightly lower than with a solvent based mould release contaminant. Thus, the presence of vacuum grease would appear identifiable through SFE analysis following APPT treatment.

Average SLS strength of the IPA wiped and abraded vacuum grease contaminated samples appeared similar to that of the uncontaminated surfaces, with the difference in means being statistically insignificant, see Table 8. As such an IPA wipe or abrasion is sufficient to remove vacuum grease contamination. The DW surfaces show significant average drop of SLS strength of 9.35 MPa compared to the AR sample with similar variation. However, plasma treatment of vacuum grease contamination produced a highly significant change in SLS strength, down to negligible values, which was found to be a statistically significant change in means with 95 % confidence. Thus, plasma treatment of vacuum grease can be catastrophic to joint strength, whereas a dry wipe resulted in a much smaller strength loss.

An F-test was also performed to identify whether there was a significance difference in variance between the as received samples to the 95 % significance level. However, with the given sample size it was not possible to identify a significant difference in variation except where SLS strength was negligible. A greater number of samples would be required to identify a smaller significance difference in variance between samples.

It was concluded with each of the contaminants investigated, that APPT is an unreliable surface pre-treatment method for removing surface contamination compared to abrasion, and in some case an IPA wipe. Whilst some evidence of an abrasion effect was observed as a result of APPT in Figure 24, section 3.1.2, the effect was shown not to be significant enough to remove surface contaminants, prior to bonding. Further, in the case of water-based mould

release and vacuum grease contaminants plasma treatment can result in a reduced bond strength compared to bonding to the dry wiped contaminated surface. This was predicted to be a result of the APPT process creating a stronger interaction between the surface and the contaminant. Further this may have reduced the mobility of the contaminant into the bulk adhesive, discussed further in section 2.4.3 resulting in an increased amount of residual contaminant to disrupt the interface bond. Where water-based mould release and vacuum grease contaminants were present SFE analysis appeared poor indicator of surface condition following APPT. The method often failed to indicate that a reduced bond strength is likely due to surface contamination. This is also the case with solvent-based mould release contamination that has been plasma treated, although a small increase in SLS strength could be achieved using APPT compared to a dry wipe surface with solvent-based mould release contamination.

Contaminant	WMR	SMR	VG	WMR	SMR	VG
	Difference in means / MPa			2 sample paired t-test P statistic (equal means). P crit = 0.05		
DW	5.20	29.9	9.35	0.006	0.000	0.043
IPA	0.333	28.3	2.71	0.589	0.000	0.083
ABR	0.960	3.45	0.101	0.391	0.027	0.905
APPT F	15.1	27.5	31.45	0.001	0.000	0.000
APPT S	14.9	21.0	30.3	0.001	0.000	0.000

Table 8 Evaluation of SLS strength differing means and paired t-test between AR samples and contaminated samples

3.2.2. Cataplasma durability testing

To assess whether surface pre-treatment methods of TS-FRP prior to adhesive bonding effected the joint strength, following exposure to aggressive environmental conditions a series of specimens with different surface pre-treatments were produced. Five specimens from each batch underwent the cataplasma aging cycle, and five identical specimens were stored at room temperature and standard humidity as a benchmark. Abrasion in this case involved a 3M Scotch Brite abrasive wheel mounted to a drill, due to the grit blast system being unavailable. APPT parameters were the same as those in section 3.2.1. The cataplasma test, used by many automotive manufacturers including Jaguar Land Rover, involves wrapping sets of five samples up in cotton wool and filling the cotton wool with 10 times its mass of water. The water-soaked cotton wool is then sealed in sample bags and wrapped in aluminium foil. The specimens were then placed in the oven at 80 °c for seven days before rapid relocation to -30 °c for one day. Following this the samples were removed and located

at room temperature and humidity for 48 hours before tensile testing. This test is often performed within the automotive industry for assessing the durability of an adhesive joint within hot-wet environments. SLS results are shown in Figure 30.

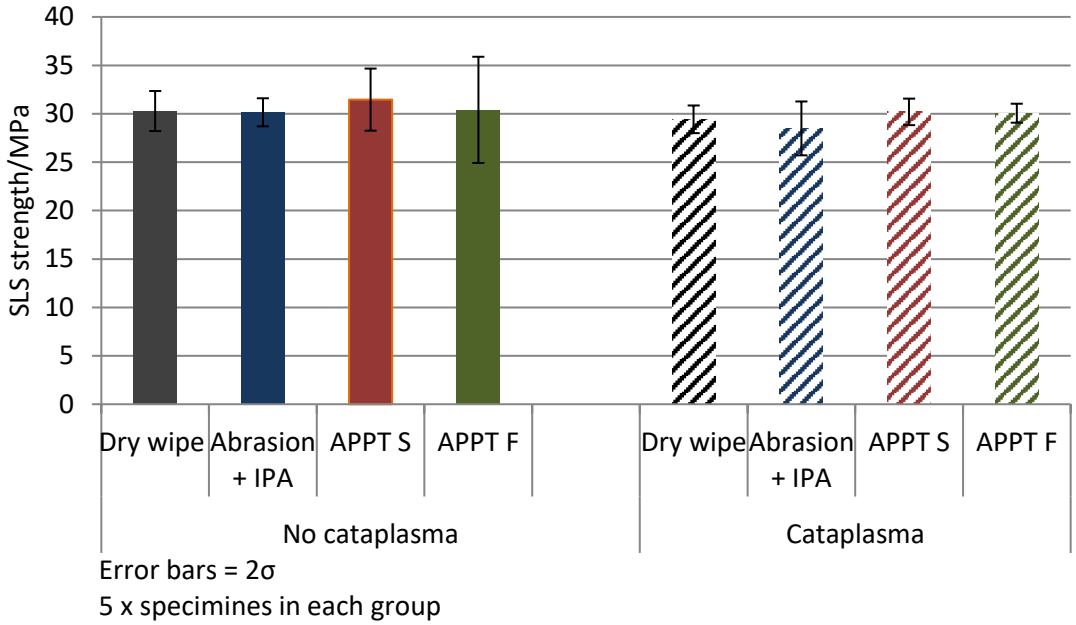

Figure 30 TS-CFRP cataplasma testing

After performing paired t-tests between the non-cataplasma and corresponding cataplasma samples it was concluded, to the 95 % significance level, that the abraded samples were the only specimens which showed a small mean strength loss. This was shown through a confidence interval, highlighting the reduction in means of between 0.313 and 3.013 MPa following cataplasma aging. This equates to a strength loss of between 1 and 10 % which is relatively small in a practical context and within specification, where a maximum of 30 % strength loss after ageing is acceptable (65). With the present adhesive and TS-CFRP combination it was concluded that the cataplasma ageing process did not significantly reduce the mean bond strength with any of the other surface pre-treatments applied. This was attributed to be a result of the initially strong interface, regardless of surface pre-treatment applied. Thus, the interface was not broken down by environmental factors during the aging process. This would highlight that with suitable selection of adhesives, which achieve a cohesive failure mode prior to ageing, there is unlikely to be degradation of the interface as a result of the cataplasma cycle upon a TS-CFRP substrate. Further evaluation would be required to identify whether this is the case when joints are loaded during ageing. As well as the effect of test methods such as cyclic fatigue, however this was outside the scope for the present work.

Pre-treatment	Mean difference, 95 % CI lower (AR - Cataplasma) / MPa	Mean difference 95 % CI upper (AR - Cataplasma) / MPa	P value
DW	-1.298	3.007	0.332
ABR	0.313	3.013	0.027
APPT - S	-0.866	3.989	0.149
APPT - F	-2.80	3.50	0.775

Table 9 Cataplasma testing of TS-CFRP, paired t-test results, SLS strength

3.3. PA6 Thermoplastic APPT

Using a similar procedure to that in section 3.2 APPT was performed upon PA6 TP substrates. This investigation aimed to identify the significant and optimal APPT process parameters, as well as achievable joint strength compared to alternative pre-treatment methods. PA6 TP-CFRP material properties and processing methods were detailed within section 3.1, using the same epoxy adhesive as in section 3.2. Effective treatment width was assumed to be the same as that estimated in section 3.1.1 using the dyne pen method. A full parameter optimisation was performed with IPA + APPT, WD of 4, 8, 10 & 12 mm were used with treatment speeds of 10, 30, 60 & 120 mm/s. Benchmark treatments including DW, IPA and also abrasion + IPA were used. Total SFE following treatment and SLS strength is presented in Figure 31.

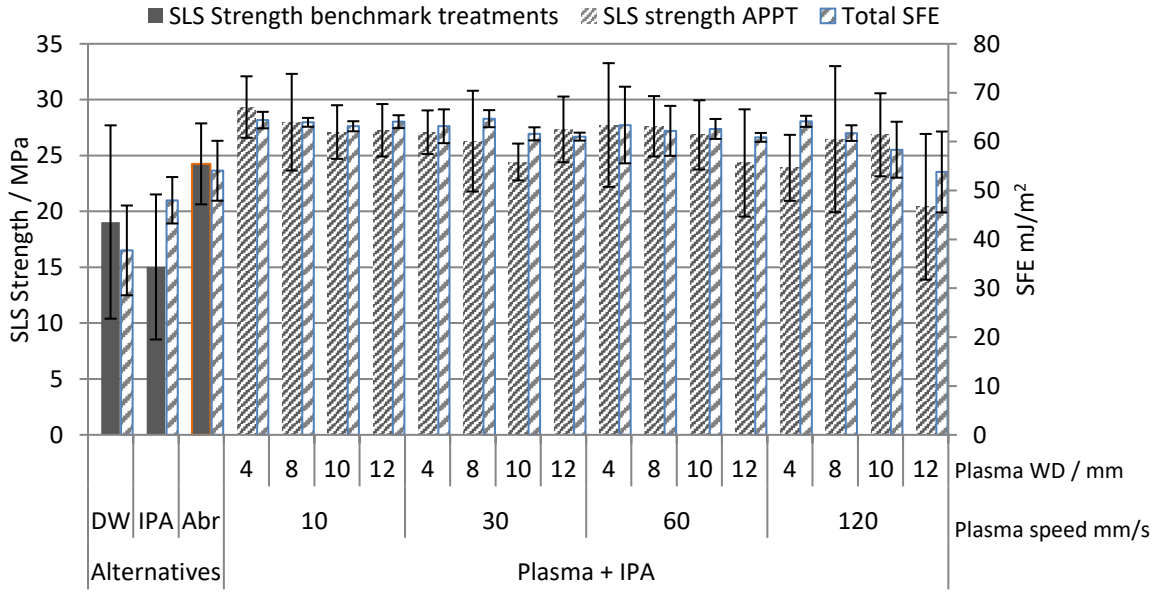

Error bars = 2σ

5 x specimines in each SLS strength group, 3 x calculated SFE values in each group

Figure 31 PA6 CFRP, APPT treatment optimisation and total SFE data

Upon first inspection of Figure 31, there was a substantial increase in SFE as a result of APPT, above the benchmark treatments. On average, this was up to approximately 10 mJ/m^2 higher than abrasion with optimal APPT parameters and 23 mJ/m^2 higher than an IPA wipe. Minitab software was used to perform a balanced two-way ANOVA analysis with interaction upon the APPT treated samples alone to identify the significant factors effecting the variation in SFE. It was identified to the 95 % significance level that treatment speed, WD and the WD x speed interaction all significantly affected the total SFE of the PA6 substrate with P values below the 0.05, 95 % significance level. This is shown in the ANOVA results in Table 10.

Two-way ANOVA					
Source	DoF	SS	MS	F	P
Speed	3	122.630	40.877	11.81	0.000
WD	3	108.207	36.069	10.42	0.000
Speed x WD	9	110.881	12.320	3.56	0.004
Error	32	110.754	3.461		
Total	47	452.472			

Table 10 ANOVA table APPT treated PA6, SFE data

A linear regression model was subsequently produced to the 95 % significance level to model the change in total SFE with APPT speed and WD. Both the coefficients of APPT speed, and WD x speed interaction were found to be significant to the 95 % confidence interval, shown in Table 11.

Source	DF	DoF	SS	MS	F value	P value
Due to regression		3	291.345	97.115	26.52	0.000
	Speed	1	22.647	22.647	6.18	0.017
	WD	1	1.385	22.647	0.38	0.542
	WD x Speed	1	77.940	77.940	21.28	0.000
About regression	Error		161.127	3.662		
Total			452.475			

Table 11 Regression analysis PA6 SFE data

The fitted model is shown in Figure 32, with an r^2 value of 64.39 %. The confidence limits of the regression model are also plotted. The residual standard deviation which must be considered in making an SFE prediction equates to $\sigma = 1.86$ mJ/m^2. The residual variation however may have been reduced by various measures such as a more homogenous FRP material, potentially using an alternative processing technique, greater environmental control of the SFE measurement environment and SFE correction for surface roughness. It was again identified that providing WD remains close to 4 mm optimal levels of SFE can be produced at treatment speeds of up to 120 mm/s, Figure 32. A similar procedure was performed with the

SLS joint strength for the APPT treated samples. A two-way with interaction ANOVA analysis demonstrated that both speed, WD and speed x WD interaction produced a significant effect upon SLS strength as seen in Table 12.

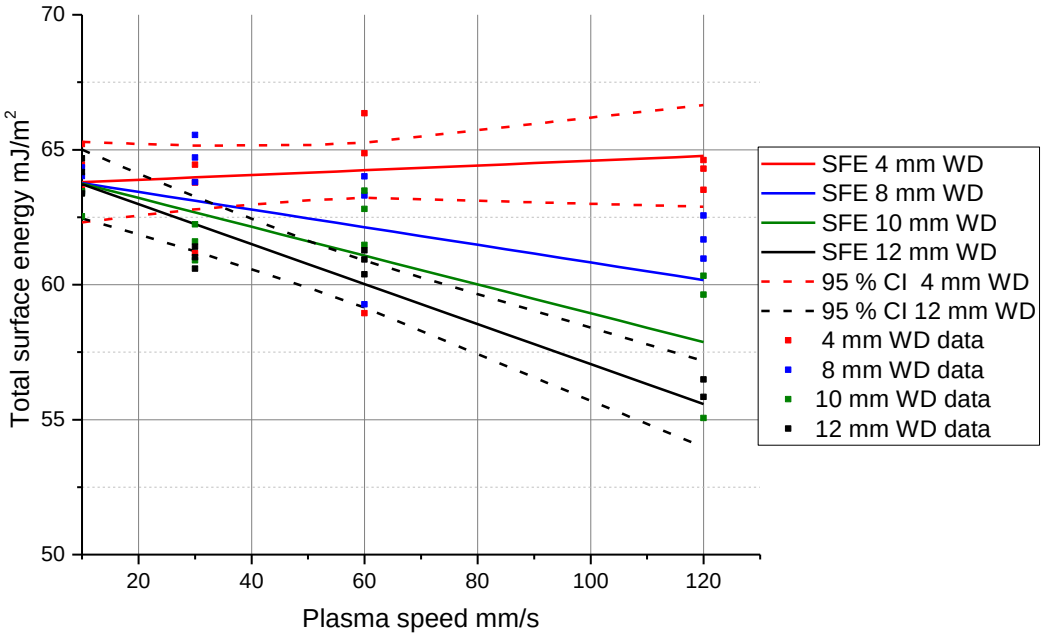

Figure 32 TP-CFRP SFE regression plot with varying APPT parameters

Two-way ANOVA					
Source	DoF	SS	MS	F	P
Speed	3	126.411	42.137	11.04	0.000
WD	3	65.571	21.857	5.73	0.002
Speed x WD	9	146.149	16.239	4.26	0.000
Error	64	224.243	3.816		
Total	79	582.374			

Table 12 ANOVA results PA6 APPT treated SLS strength

A residual error standard deviation of σ = 1.95 MPa was identified from the ANOVA results in Table 12. This residual error is relatively large in comparison to the range of SLS strength. A linear regression model was produced in Figure 33 to the 95 % significance level although the fitted regression model only explained r^2=26.25 % of the variation in SLS strength, which given the residual error was unsurprising. The regression analysis is presented in Table 13, the coefficients of speed, WD and speed x WD interaction are all below the 95 % confidence level, thus the model poorly fits the collected data. This may be due to large residual variation, relatively small sample sizes and the possibility of a non-linear relationship between APPT parameters and SLS strength. The model however gives some indication of how mean SLS strength may vary with APPT parameters within the stated confidence levels.

Source	DF	DoF	SS	MS	F value	P value
Due to regression		3	152.851	50.9504	9.02	0.000
	WD	1	12.049	12.0492	2.13	0.148
	Speed	1	8.030	8.030	1.42	0.237
	WD x Speed	1	0.399	0.3991	0.07	0.791
About regression	Error	76	429.522	5.6516		
Total		79	582.374			

Table 13 Regression analysis PA6 APPT treated SLS strength

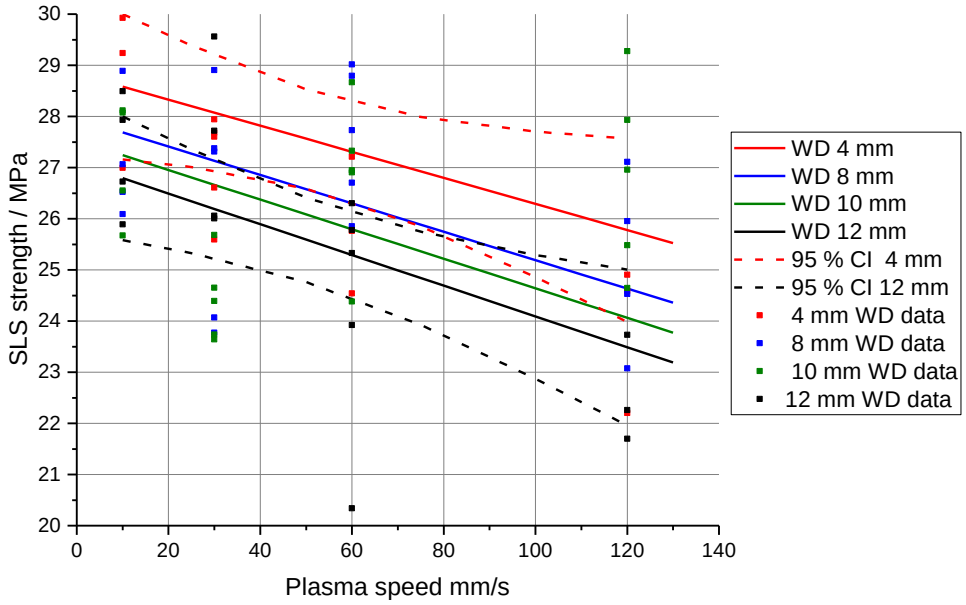

Figure 33 Regression model SLS strength PA6 at various APPT parameters

Figure 33 suggested that the greatest improvement to SLS strength was achieved at the lowest tested WD of 4 mm, consistent with the SFE analysis in Figure 32. Based on the complete APPT treated data set at 4 mm WD it was found using a two-sample t-test to the 95 % significance level that there was no significant difference in sample mean at 4 mm APPT, compared to the abraded samples where P=0.423. If the 120 mm/s APPT treated samples at 4 mm WD are excluded from the data set the mean increase in bond strength of 3.8 MPa is statistically significant with 95 % confidence, P=0.04. However, there was a statistically significant increase between the mean SLS strength of the IPA and DW samples compared to the 4 mm APPT treated specimens with a P value of <0.001 and 0.017 respectively. This demonstrated that APPT treatment, with appropriate treatment parameters, could produce a mean increase in bond strength greater than an abrasion process with a PA6 substrate.

A further conclusion came from the analysis of joint failure modes, with reference to the definitions in Figure 13, secion 2.4.3. Each joint failure surface was visulally categorised into its percentage of each failure mode, either adhesive faliure (where adhesive is removed cleanly from the substrate), material faliure (cohesive failure in the adherend) or cohesive failure (cohesive failure of the adhesive). An example of this for a characteristic SLS joint failure surrface is seen in Figure 34. Mean failure mode propotions for each batch of five samples were plotted as a proportion of total SLS strength within Figure 35. It was seen that both DW and IPA samples exhibit 100 % adhesive failure. Introducing abrasion brings a small increase in the mean proprtion of material faliure, however generally adhesive failure dominates, see Figure 36 for an example of an adhesive failiure mode.

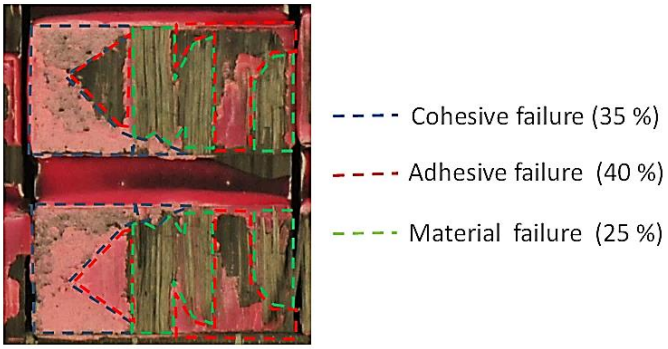

Figure 34 Example of failure surface visual characterisation by proportion of failure mode

Upon the application of APPT a vast change from predominantly adhesive failure with the benchmark treatments to a mix of material and adhesive faliure is observed, see Figure 37. The proportion of adhesive failure begins to increase at the higher treatment speeds and WD. It is clear from Figure 35 that APPT can effectively influence the faliure mode with PA6 substrates and the specified adhesive system.

In order to determine optimal surface pre-treatment parameters for a high-volume automotive application it was necessary to define which failure mode would be acceptable for a high-volume automotive application. It was determined that the avoidance of adhesive failure is the most appropriate priority, as specified by the most relevant Jaguar Land Rover standards for this application (65). The adhesive failure mode is attributed to weak adhesion forces at the interface, these weaker adhesive bonds are more easily displaced by presence of aggressive mediums such as water, leading to failure of the bond (86). This is investigated further in section 3.3.1. The surface pre-treatment can be effective in establishing resistance

to hydration of the interface, through the development of stronger interfacial forces. As such it was valuable to understand how APPT could affect the mean joint failure mode proportion.

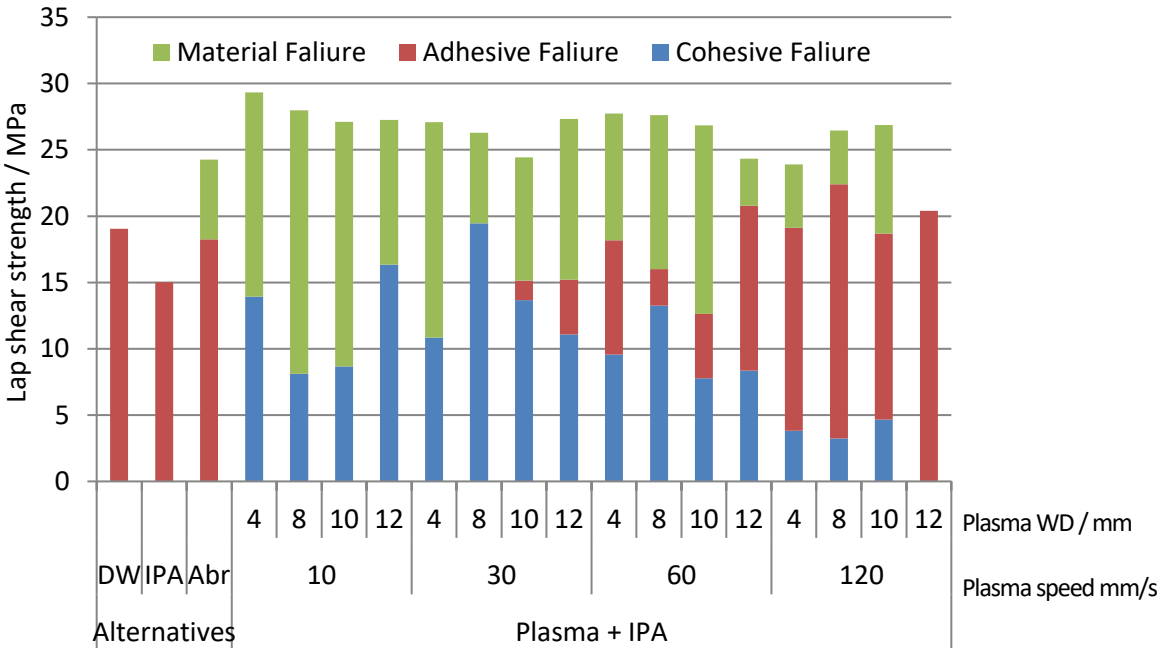

Figure 35 PA6 SLS strength data categorised by failure mode type. Bar height representing average SLS strength, colours representing the mean proportion of each failure mode within each batch

Figure 36 100 % Adhesive failure as observed on PA6 DW surface

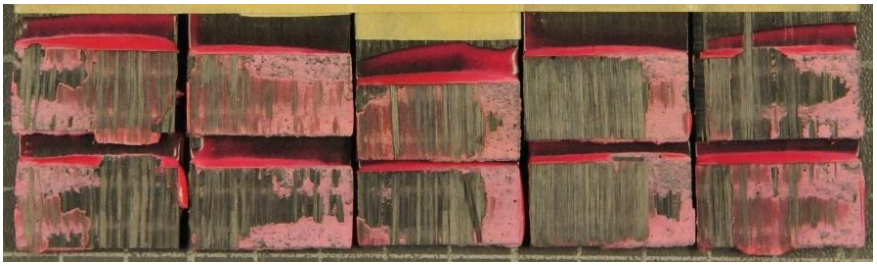

Figure 37 Mix of material and cohesive failure with APPT upon PA6 surface

To the 95 % significance level using an ANOVA analysis treatment speed was found to be the statistically significant parameter to minimise the proportion of adhesive failure, see results in Table 14. APPT WD was found to be just outside the same 95 % confidence interval, thus

the one-way ANOVA analysis was performed with a residual standard deviation of σ = 0.243 = 24.3 %, the residual uncertainty of the system. A linear regression model based on speed alone was produced with r^2=59.44, presented in Figure 38. The prediction interval is also included and represents the likely range of values a single observation will fall rather than the mean response represented by the confidence interval. It can be seen that there was significant uncertainty in the prediction interval due to the large residual error. As plasma speed increases the probability of resultant proportion adhesive failure increases. The coefficient of speed in the linear regression model was found to be statistically significant with P = 0.000. It was concluded that the APPT process can effectively influence joint failure mode, which when used to minimise adhesive failure may lead to an improvement in long term joint durability.

Two-way ANOVA					
Source	DoF	SS	MS	F	P
Speed	3	7.358	2.453	45.71	0.000
WD	3	0.438	0.146	2.72	0.052
Speed x WD	9	0.623	0.0692	1.29	0.260
Error	64	3.434	0.0537		
Total	79	11.853			

One-way ANOVA				
DoF	SS	MS	F	P
3	7.358	2.4526	41.47	0.000
76	4.495	0.0591		
79	11.853			

Table 14 ANOVA results PA6 combined cohesive + material failure %

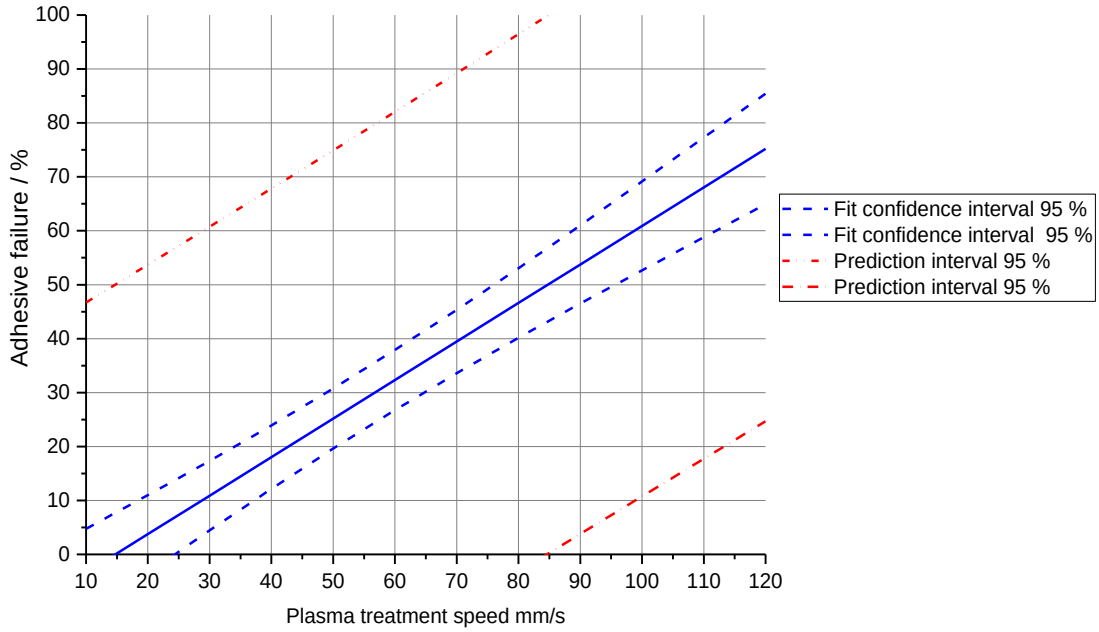

Figure 38 Plasma speed and adhesive failure regression model, PA6 TP-CFRP

3.3.1. Durability assessment

In order to validate whether, with a PA6 TP-CFRP substrate, the use of APPT to alter the joint failure mode would provide a durability improvement compared to benchmark pre-treatments cataplasma testing was performed. The cataplasma testing provided a high humidly environment to encourage hydrolysation of the adhesive / substrate interface. The cataplasma procedure was broadly the same as that presented in section 3.2.2, the only difference being SLS testing of the sample immediately after defrosting without an opportunity for the sample to dry and the freeze step performed for 24 hrs at -20 °c. The testing of a damp sample was performed to avoid any reversible effect upon sample drying and regaining strength, thus representing the worst-case joint strength. The higher temperature freeze step was performed due equipment availability. Un-aged control samples were also produced and tested. Two APPT parameters were considered, both 8 mm WD at 10 and 60 mm/s. These provided a comparison between an optimal APPT treatment, where minimal adhesive failure would be expected and a faster APPT treatment where some adhesive failure may be expected. The results are presented in Figure 39.

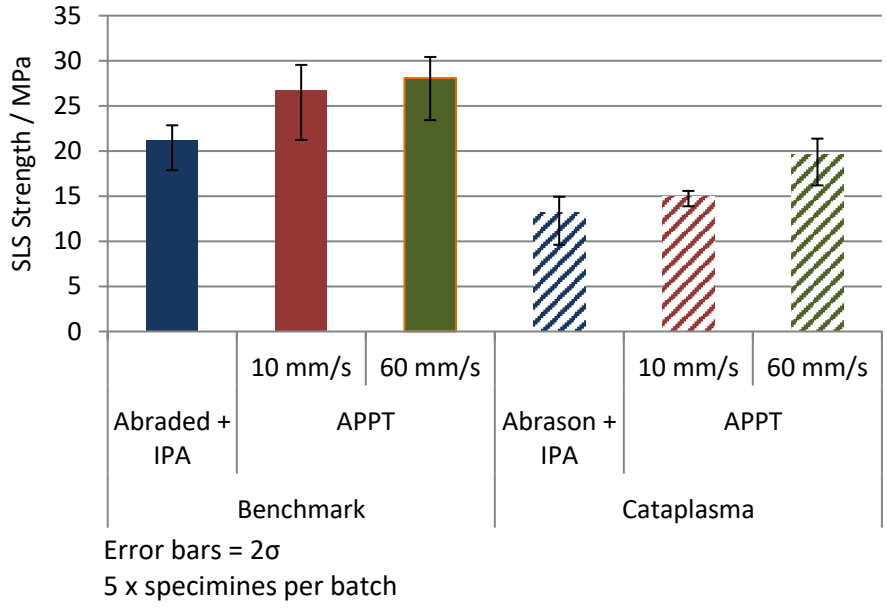

Figure 39 PA6 TP-CFRP SLS samples abraded and plasma treated with cataplasma exposure

It was observed upon first inspection of Figure 39 that the cataplasma ageing resulted in a significant strength loss compared to the benchmark (non-cataplasma) samples in all cases. This drop off must be accounted for in the assembly design phase. This was confirmed using two sample paired t-tests in all cases that the strength loss before and after cataplasma was

statistically significant, see Table 15. The faster APPT at 60 mm/s (APPT F) yielded the lowest mean strength loss at 28 % of the unaged control samples. A slower APPT at 10 mm/s (APPT S) yielded a greater mean percentage strength loss than abrasion despite the inherently higher SFE, although an increase in sample minimum strength compared to abrasion reflected through the 95 % confidence interval of sample mean difference. This suggested that there were durability benefits from APPT treatment on PA6 substrates compared to abrasion. However, an over treatment of APPT appeared to reduce environmental resistance more significantly than an abrasion treatment in respect of both in sample mean and minimum SLS strength.

	No cataplasma			Cataplasma			
	Sample min	Mean	St. Dev	Sample min	Mean	St. Dev	Units
Abr + IPA	19.49	21.19	1.66	10.41	13.16	1.78	MPa
APPT S	22.73	26.77	2.77	14.36	15.01	0.57	MPa
APPT F	24.67	28.09	2.33	18.33	19.64	1.73	MPa

Comparative calculations / Paired T test				
Treatment	Mean difference / %	Mean difference (95 % CI) L / %	Mean difference (95 % CI) U / %	P value
Abr + IPA	37.9	28.8	47.1	0.000
APPT S	44.5	33.0	55.7	0.000
APPT F	28.9	12.0	45.9	0.009

Table 15 SLS joint strength loss as a result of surface pre-treatment after cataplasma ageing

Abraded surfaces appeared very similar with the naked eye before and after APPT. Upon closer inspection with 3D optical microsopy, Figure 40, there appeared to be regions of adhesive failure (pink) with other regions of transferred PA6 matrix (dark). Following ageing the propotion of adhesive failure appeared to increase, although the surfaces were broadly similar.

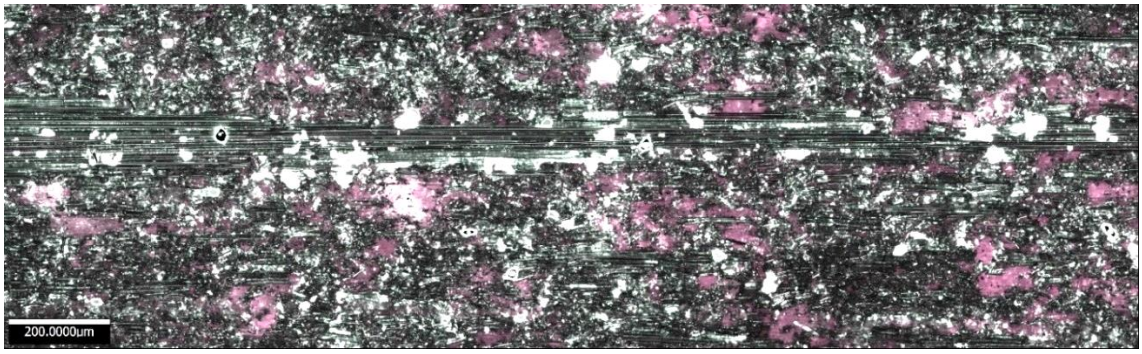

Figure 40 PA6 Abraded surface unaged PA6 TP-CFRP substrate

The APPT treated surfaces showed predominantly cohesive and material failure at 10 mm/s, at 60 mm/s an average of 26 % adhesive failure was observed pre-cataplasma. Post cataplasma, average adhesive failure proportion increased to 56 % for the APPT samples treated at 10 mm/s and 27 % for those treated at 60 mm/s contributing to the reduction in SLS strength compared to the slower APPT treatment.

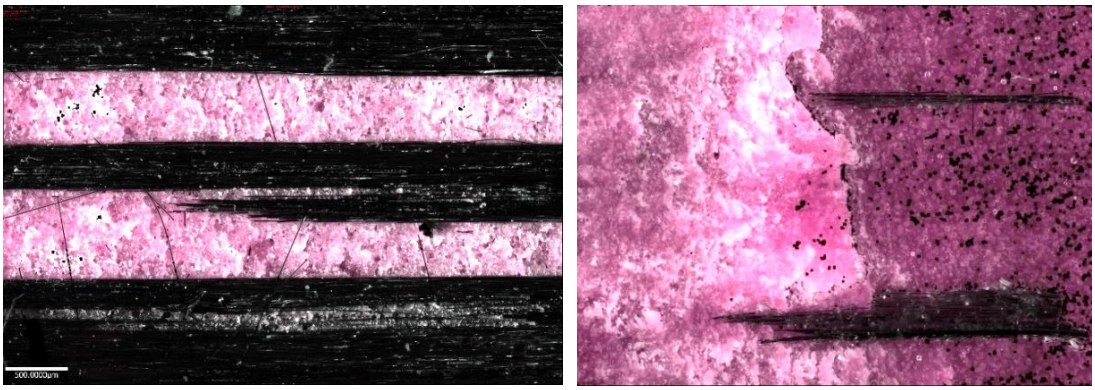

Figure 41 APPT TP-PA6 failure surface cohesive/material without cataplasma (left), mix of adhesive and cohesive failure following cataplasma (right)

It was concluded that the avoidance of adhesive failure mode is influential in reducing the strength loss of PA6 adhesive joints and that the proportion of adhesive failure can effectively be influenced through optimisation of the APPT process.

3.3.2. Treatment standoff

To investigate the possible decay of the APPT treatment effect an investigation was performed to analyse how SFE and SLS bond strength falls with delay time following APPT treatment, upon PA6 CFRP substrates. Substrates were left at room temperature for a given delay time following APPT, up to seven days post treatment. SFE analysis then took place after the defined delay time followed by bonding and tensile testing following cure. Two different APPT parameters were used, preceded initially by an IPA wipe; 10 mm/s at 8 mm WD and 50 mm/s at 8 mm WD. Results are shown in Figure 42. The significance of treatment delay time has profound manufacturing implications within industry, dictating whether APPT must occur immediately prior to adhesive application or whether it could occur at a supplier where a delay would occur before components are assembled during production. This was an industrial concern that was raised during discussions with Jaguar Land Rover.

It was observed that total SFE is approximately 45 mJ/m^2 on the untreated surface prior to APPT. Applying APPT at 50 mm/s increases total SFE to approximately 54 mJ/m^2 which

changes very little up to 48 hours after APPT. After seven days the mean value is 57 mJ/m^2 highlighting that there was very little drop in total SFE following 50 mm/s APPT on a PA6 surface. At 10 mm/s treatment a mean total SFE of 65 mJ/m^2 is produced two hours following APPT. This value begins to fall above approximately 24 h to a mean of 61.5 mJ/m^2, after seven days this reduces very little to 60.8 mJ/m^2. This suggested that as SFE begins to reach the maximum achievable values with APPT some reduction may be observed in the time following treatment upon a PA6 substrate. At 10 mm/s this is largely a result of a fall in polar SFE from an average of 27 mJ/m^2 to 25 mJ/m^2 after seven days, although there is considerable scatter as has been previously observed with SFE analysis. The polar SFE seven days after a 10 mm/s APPT remains a considerable improvement from the untreated of mean 8.83 mJ/m^2 to 25 mJ/m^2. This highlights the retained effectiveness of the APPT process up to seven days after treatment.

At 50 mm/s APPT treatment speed the increase in polar SFE is much lower compared to 10 mm/s treatment speed. A mean 14 mJ/m^2 two hours following treatment. After seven days the mean polar SFE is still 14 mJ/m^2 highlighting little change in polar SFE following APPT at 50 mm/s. It is difficult to identify any significant trends in SLS strength particularly at 50 mm/s treatment speed. This is partly due to data in section 3.3 identifying that a SLS strength of can be achieved without APPT at the consequence of a less desirable failure mode. At 10 mm/s a small drop in average SLS strength is observed from 24 MPa, two hours following treatment to 23 MPa after seven days. Given the residual error in the data set, it is very unlikely this difference would be statistically significant.

It was concluded that there is likely to be a small drop in SFE when APPT is applied to PA6 at 10 mm/s which is most observable between 6 and 24 hrs after APPT. This decrease is less observable at a faster treatment speed of 50 mm/s. However, seven days following treatment the SFE is still significantly greater than that of the untreated surface. This highlights that if required APPT could be applied to PA6 components at a supplier, prior to shipping in order to raise the SFE of the substrate, reducing the number of steps in assembly. Further, if APPT was applied on the assembly line, should the line be stopped for a period of hours post APPT treatment there would be no apparent reason to repeat the treatment prior to bonding. These conclusions were significantly important consideration for Jaguar Land Rover, should an APPT process be introduced.

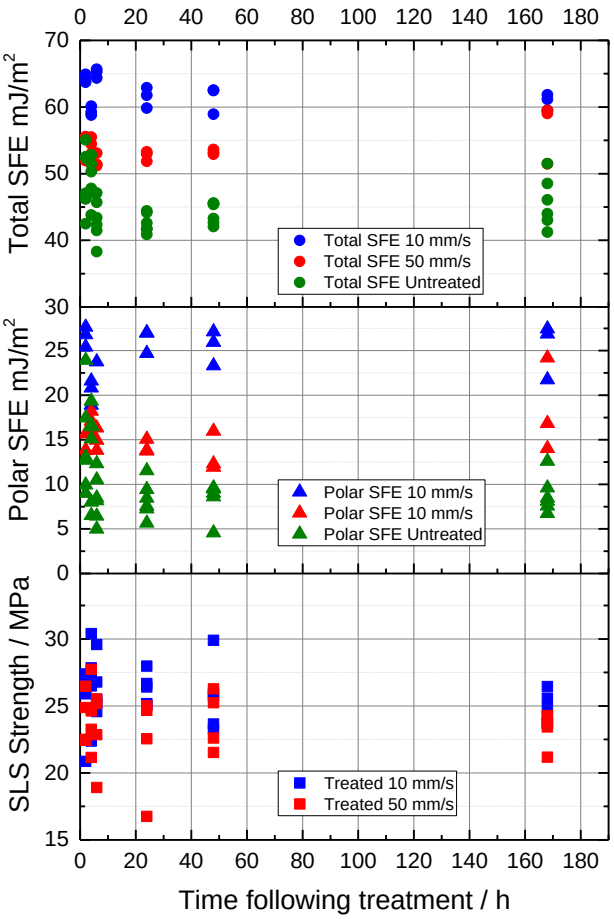

Figure 42 Relationship between total SFE, polar SFE and PA6 TP-CFRP bond strength with time delay following APPT

3.4. APPT XPS Thermoplastic and thermoset substrates

In order to gain a greater understanding of the surface chemistry effects as a result of APPT and benchmark treatments, x-ray photo electron spectroscopy (XPS) was performed upon TS and TP surfaces. The XPS method uses x-rays, to excite the state of atoms up to 10 nm below the sample surface (87). Electrons are then ejected from the surface atoms with specific energy levels which allow identification of element identity, quantity and chemical state.

Substrates were plasma treated at 4 mm WD and a speed of 25 mm/s. Samples were pre-treated within an ultrasonic bath of isopropanol (IPA) prior to APPT treatment and XPS analysis, handled using IPA cleaned tweezers and stored in clean glass jars. Initial XPS relative atomic concentrations are presented in Figure 43 for both substrates with and without APPT. Initial observations were that the most significant change as a result of APPT is the increase in surface oxygen atomic percentage (at.%), from 20.9 - 29.0 at.% with TS-CFRP and 12.5 - 24.5 at.% with TP-CFRP before and after APPT respectively. A resolution of approximately one

decimal place can be achieved when calculating at.% (88). The increase in oxygen containing surface groups is thought to largely contribute to the change in failure mode upon TP-CFRP surfaces as a result of a stronger adhesive to substrate bond and increased surface free energy leading to improved adhesion (89).

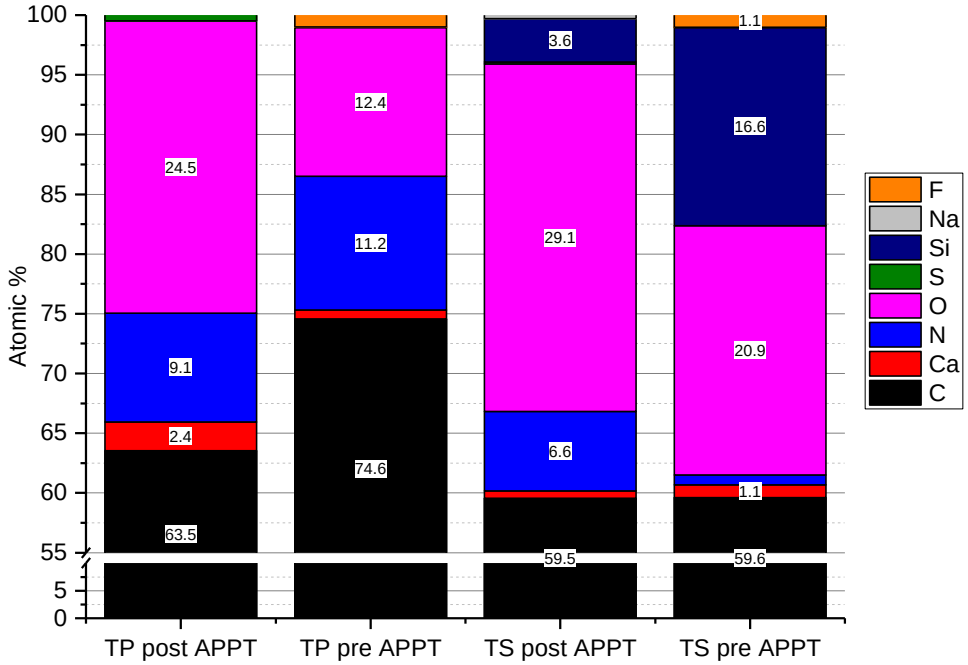

Atomic % values < 1 %, numerical labels hidden for clarity.

Figure 43 XPS Relative concentration TS & TP-CFRP

A further explanation of the chemical changes as a result of APPT is seen within Table 16 for TS-CFRP where a substantial increase in the number of oxygen containing groups appears post APPT. The greatest proportional percentage increase being in C-O-C, C-OH, O=C-OH and C=O groups, contributing towards increased polar SFE. This increase was however not required to generate a cohesive failure with the specified epoxy adhesive and TS substrate combination used within this work. This was believed to be due to –OH groups being present in the untreated TS surface aiding in the generation of a cohesive failure mode (89). Oxygen containing groups are exceedingly challenging to identify exactly using XPS because of their close binding energy, as such the data provides a best estimate of those present (88). Aside from the increase in surface oxygen containing groups post APPT, a substantial change was observed in the surface nitrogen concentration increasing from 0.8 to 6.6 at.%. This related to the increase in the number of nitrogen containing groups such as N-(C=O)-C. The increase in oxygen and nitrogen containing groups would be logical from an air-based plasma. A reduction in the at.% of silicon and fluorine was observed post APPT from 16.6 and 1.1 at.%

pre APPT to 3.6 and 0 at.% post APPT respectively. It was predicted that this may be due to transferred contamination from mould release which is partially removed by APPT.

	IPA Only		IPA + APPT		
Bonding group	Binding energy (BE) / eV	Relative surface concentration / %	Binding energy (BE) / eV	Relative surface concentration / %	Surface concentration change / Δ%
C-O-C / Imidazole		0.0	286.7	19.2	19.2
C-OH/C-NH2	286.1	6.6	285.9	15.5	9.0
O=C-OH / O=C-NH		0.0	289.1	7.2	7.2
C=O	288.5	1.4	287.9	6.6	5.2
N-(C=O)-C	399.8	0.6	400.2	5.0	4.4
SiO2 (2p3/2) & (2p1/2)	103.3 & 103.9	1.0	103.7	4.6	3.5
C=N-C	398.2	0.4	398.9	2.4	2.0
N-(C=O)-O	401.6	0.1	401.7	1.9	1.8
O-CO-O		0.0	290.4	1.2	1.2
NaF	1071.7 & 684.7	0.6	1071.8	0.6	0.0
Sulfate S (2p 3/2) & (2p 1/2)		0.0	168.8 & 170.0	0.1	0.1
Si 2p		0.0			0.0
CaCO3 Ca (2p 3/2) & (2p 1/2)	347.5 & 351.0	1.4	347.8 & 351.3	0.8	-0.5
Si3N4 / SiOx (2p3/2) & (2p1/2)	101.8 & 102.4	19.9	102.3 & 102.9	0.5	-19.4
C-C/C-H	284.6	67.4	284.6	34.2	-33.1

Table 16 TS-CFRP XPS data with and without APPT – bonding environments

The data for TP-CFRP is given in Table 17, again a substantial increase in other oxygen containing groups was observed particularly O=C-OH of 9.8 % compared to pre-APPT. There also appears to be an increase in other groups such as $CaCO_3$ and N-(C=O)-O. A notable change was the removal of fluorine post APPT, from 1 at.% prior to APPT, further evidence that APPT may remove some mould release contamination.

A further evaluation was performed upon a range of PA6 TP-CFRP samples with different pre-treatment parameters, at.% data presented in Figure 44. It was observed that the greatest change over the range of APPT parameters investigated is in the surface content of oxygen and nitrogen, which can be seen to vary over the range of parameters investigated. Again, as expected from the use of an air-based plasma. For example surface oxygen content is approximately 10.2 at% with an IPA wipe, abrading the surface increases this to 16.3 at.%

which is similar to that with IPA + APPT at 12 mm WD and 120 mm/s. With an APPT at 10 mm/s and 8 mm WD a surface oxygen content of 29.7 at.% can be achieved the greatest observed, nearly three times greater than following an IPA treatment only.

	IPA Only		IPA + APPT		
Bonding group	Binding energy (BE) / eV	Relative surface concentration / %	BE	Relative surface concentration / %	Surface concentration change / Δ%
O=C-OH / O=C-NH			288.5	9.76	9.76
CaCO3 Ca (2p 3/2) & (2p 1/2)	347.2 & 350.7	0.912	347.2 & 350.7	3.18	2.27
N-(C=O)-O	400.5	0.728	400.6	1.46	0.730
Sulfate S (2p 3/2 & (2p 1/2)	167.8 & 169.0	0.114	168.5 & 169.7	0.662	0.548
C=N-C	397.8	0.358	397.9	0.470	0.112
C=O	287.6	12.9	287.5	12.9	-0.0603
N-(C=O)-C	399.4	11.7	399.5	10.1	-1.56
C-OH/C-NH2	285.6	16.8	285.9	15.2	-1.62
C-C/C-H	284.6	55.4	284.6	46.3	-9.11

Table 17 TP-CFRP XPS data with and without APPT – bonding environments

The surface at.% of nitrogen showed a similar relationship, although with a smaller at.% change. For example at.% nitrogen following IPA treatment is 1.1 at.% , increasing to 7.8 at.% with IPA and abrasion. With an APPT at 12 mm WD and 120 mm/s this increases to 10.0 at.% and as high as 13.7 at.% at 4 mm WD and 30 mm/s. The change in concentration of other elements is less significant, for example the silicon content is shows some evidence of reducing at slower APPT parameters although there is considerable scatter and greater data collection would be required to reduce this uncertainty. The highest proportion of silicon, 1.76 at.% appeared after ABR, potentially indicating a contaminant from the grit blast media, as previous data had suggested abrasion the most appropriate way to remove mould release contamination. Further investigation revealed the grit blast media was produced from silicate mineral deposit (90) adding confidence to this conclusion.

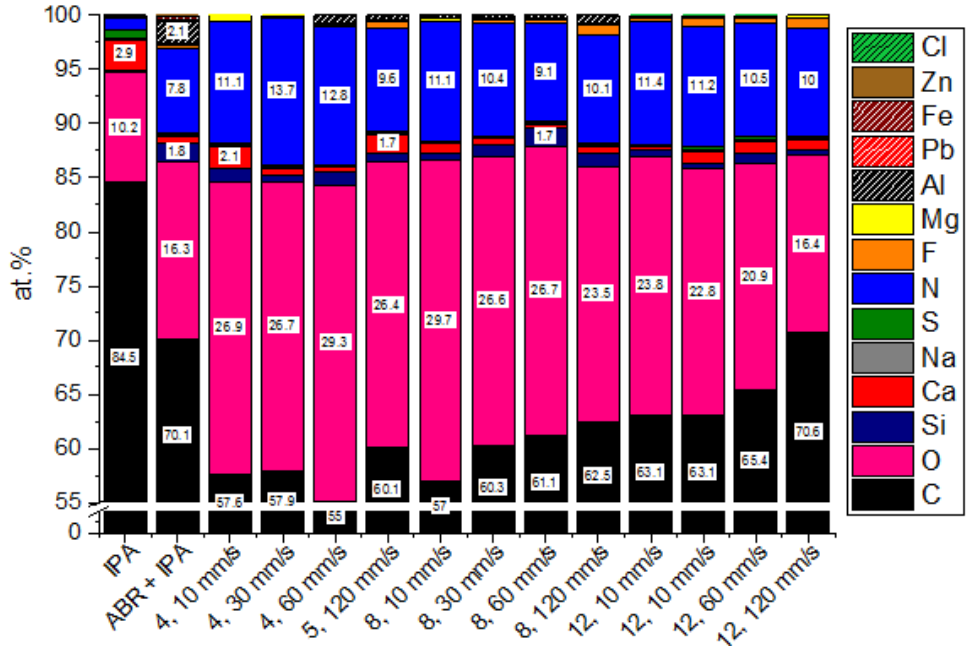

Atomic % values < 1 %, numerical labels hidden for clarity.

Figure 44 TP-CFRP XPS at.% vs various APPT pre-treatment parameters and benchmark

Figure 45 draws the XPS investigation to a conclusion and highlights the relationship between SFE and the surface at.% oxygen for PA6 TS-CFRP. It is highlighted how the incorporation of polar, oxygen containing groups in the polymer surfaces as a result of APPT can increase the SFE of the TP-CFRP with both sets of data showing remarkably similar trends.

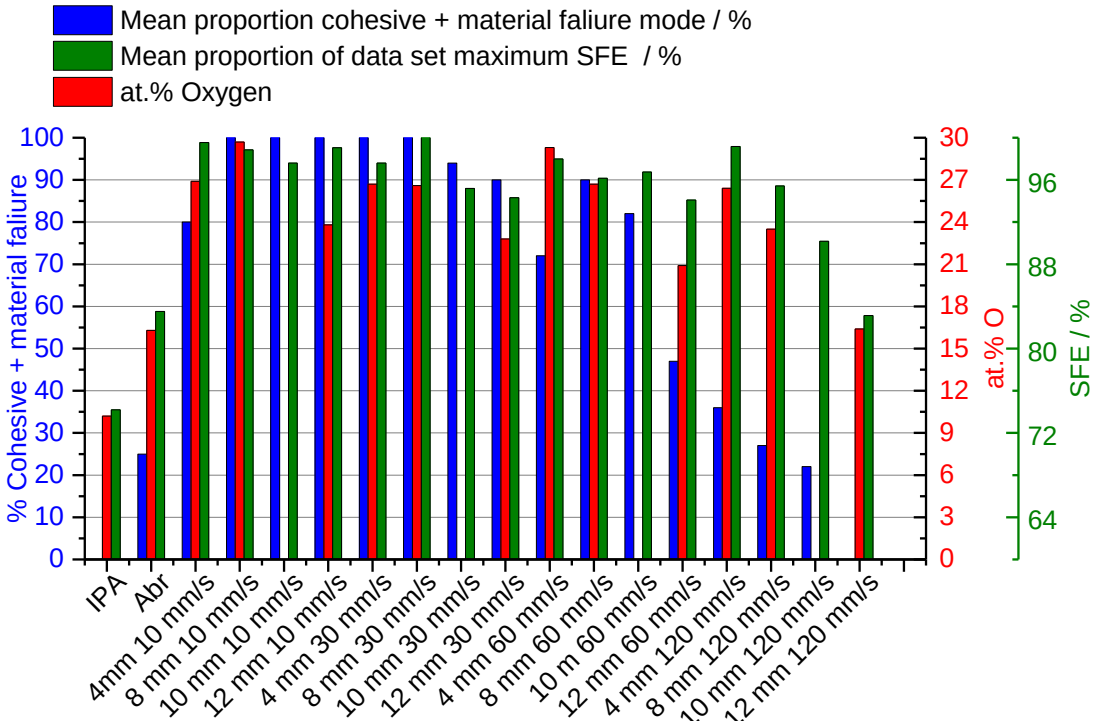

Figure 45 TP-CFRP relative comparison between failure mode, at.% oxygen and SFE

The data in Figure 45 is all based upon the mean sample values observed and SFE expressed proportionally as the percentage of the maximum sample SFE from the whole data set, being 64.7 mj/m^2 following APPT at 30 mm/s, 8 mm WD. The mean proportion of combined material and cohesive failure was also included, which again shows a striking relationship to SFE and at.% oxygen. There is a significantly more rapid reduction in failure mode proportion at the higher APPT speeds and WD compared to SFE. This highlights the value to industry of knowledge of the required APPT treatment parameters and SFE in order to minimise undesirable adhesive failure modes. To conclude, the XPS analysis provided valuable further understanding relating the surface chemistry changes to the observed changes in failure mode and SFE.

3.5. APPT conclusions

The APPT surface pre-treatment analysis highlighted a number of considerations of particular importance to the present, multi-material adhesive bonding application and the high-volume automotive industry. With a TS-CFRP and the specified epoxy adhesive, it was observed that where significant surface contamination was not present the APPT process yielded a relatively insignificant change in SLS strength compared to benchmark treatments such as a dry wipe, IPA wipe or abrasion. The introduction of APPT however, can achieve substantial increases in SFE compared to the benchmark treatments. For example, increasing from from 39 mJ/m^2 with a dry wipe to 68 mJ/m^2 with APPT. This is valuable information to support adhesive selection in later work. The knowledge of achievable SFE can be used to help identify adhesives which may provide suitable wetting characteristics upon the APPT treated surface. Further, knowledge of the polar and dispersive SFE components can assist adhesive manufacturers in making product recommendations, compatible with both the TS-CFRP surface and other manufacturing constraints. The current study has shown there to be no link between the total SFE and joint failure mode with an epoxy TS-CFRP substrate and the candidate epoxy adhesive. An understating of the relationship between APPT parameters and SFE for both TS and TP-CFRP has been identified.

APPT was also demonstrated to yield a small increase in SLS strength with a PA6 TP-CFRP substrate and epoxy adhesive with much uncertainty. However, it was identified that the APPT process can significantly influence the joint failure mode, from predominantly adhesive failure with the benchmark treatments to proportions of material and cohesive failure with optimised APPT parameters. Knowledge of the relationship between SFE and TP-CFRP joint

failure mode also provided valuable information in the case where the pre-treatment system were to be changed in later work. This is a result of understanding the required SFE to generate a proportion of acceptable failure mode, thus requiring only limited comparable tests with a new system to achieve this level of SFE. The observed change in failure mode posed the question of; what is an acceptable proportion of adhesive failure for an automotive FRP joint in respect to available cycle time and treatment parameters? Evidence was produced which showed that a sub-optimal surface pre-treatment upon PA6 TP substrates can result in a greater strength loss under cataplasma aging compared to where an optimal APPT process was performed. Reducing the proportion of unaged adhesive failure mode upon a joint failure surface appeared to enhance the durability of the joint when exposed to hot / wet environments.

Surface contamination from mould release and vacuum grease was identified to be a significant concern with the APPT process. Prior understanding within literature and Jaguar Land Rover had suggested that the APPT process could be used to clean the FRP surface, however the experimental data suggested otherwise. Contamination was manually applied to surfaces, forcibly contaminating them and the contaminated surface APPT treated. In many cases the contaminated surfaces resulted in a negligible difference in SFE compared to the uncontaminated reference sample. However, the resultant bond strength can be catastrophically reduced as a result of the surface contamination. With contaminants such as water-based mould release and vacuum grease the mean strength loss after exposure to APPT was much greater than the mean strength loss when bonding directly to the contaminated surface. This is a significant finding, disproving previous theories. Further it brings significant financial and performance implications for industry should APPT be used in an attempt to remove surface contamination upon bonded structures. Potentially resulting in reduced joint performance and premature joint failure.

The following conclusions were made;

- APPT yields no bond strength improvement upon a TS-CFRP surface however can effectively increase the SFE. With the epoxy adhesive system used this was not required to generate a cohesive failure mode. This is however valuable knowledge to assist in the selection of alternative adhesives in later work.

- APPT can effectively increase the proportion of cohesive failure upon a TP-CFRP substrate, this was shown to be a result of the incorporation of oxygen containing functional groups within the surface increasing the SFE of the substrate. This can also result in improved joint durability. Understanding the relationship between SFE and joint failure mode provided valuable information if an alternative pre-treatment system was to be used in later work.

- Abrasion was identified as the most failsafe method of surface contamination removal. To optimise joint strength and failure mode it may be necessary to adopt a failsafe contamination removal process such as abrasion, combined with APPT, if required. Alternatively, it may be preferable to control surface contamination levels much more closely through the FRP production process.

- The use of APPT to remove surface contamination appeared ineffective, in many cases resulting in a reduction in bond strength compared to bonding directly to the contaminated surface.

4. Chapter 4 - Rapidly cured primary bonded structures

Chapter 2 identified that one of the greatest limitations towards the use of primary bonded, adhesive only, structural joints within high-volume automotive structures was the long cure times of many structural adhesive products. The ability to reduce adhesive cure time and generate handling strength in a shorter cycle time was identified as critical to meeting high-volume cycle time requirements for primary bonded structures. Whilst there were industrial automotive applications of rapid adhesive curing applications within metallic structures few applications existed with FRP intensive and multi-material structures. The adhesive handling strength may be generated at a degree of partial cure as discussed further within chapter two. It was envisaged that the partial degree of cure could be achieved through a rapid thermal cycle, with a subsequent cycle, such as an oven cure, fully curing the adhesive joint.

An induction heating method was used to rapidly heat adhesive joints. This process was identified as a rapid and efficient method for heating FRP and metallic substrates in section 2.4.1.1. Extensive investigation was performed to identify the achievable adhesive handling strength following a defined thermal cycle. Targets were initially defined as one minute from adhesive application to achieve a target handling strength of 8 MPa SLS. This was based on the hem flange induction cure handling strength targets within Jaguar Land Rover. This was the closest relevant target at the time of investigation (91), with a primary bonded structure handling strength target not yet developed. Subsequently it became apparent that this may be a higher strength than required for a BIW application and that in many cases the handling strength would be dependent upon the component, its location on the BIW and many other factors. As such, a focus was subsequently placed on the identification of achievable handling strength given optimal curing schedule with a number of commercially available structural adhesives. This would provide Jaguar Land Rover with knowledge of the thermal cycle that would be required to achieve a specified handling strength.

The main aims of this chapter were to identify;

- Suitable rapid curing adhesives for a primary bonded FRP intensive structure.
- Suitable induction heating parameters to maximise the rate of handling strength development, including parameters such as heating rate, dwell time and dwell temperature.
- The dependence of other considerations upon handling strength, such as joint temperature.
- The effect upon final, fully cured, joint strength following an initial induction heating step.

Establishing knowledge of these factors provided Jaguar Land Rover with a greater understanding of the feasibility of producing a CFRP intensive, high-volume, primary bonded body structure. This was a primary aim of this work. Further, a successful feasibility study in chapter five, showed how on demand induction curing can be applied to CFRP intensive structures, combining rapid curing adhesives and induction heating technologies to a challenging area in high-volume automotive manufacture.

4.1. Experimental methodology

It was identified that TS structural adhesives, such as the epoxy and polyurethane families are familiar with the automotive industry, as discussed in section 2.4.3.2. These adhesives develop strength through the curing process, which can generally be accelerated by the application of heat. A number of leading adhesive manufacturers were engaged during this research, resulting in a range of potentially suitable structural adhesives based on the application requirements. In particular rapid strength development for multi-material structural automotive bonding. Further details of the selected adhesives are presented in section 4.1.3. Various heating methods are suitable for the curing of adhesives upon multi-material structures. These include infra-red, convection oven and microwave, however for the present application electromagnetic induction heating was selected based on the theory discussed in section 2.4.1.1.

The primary method of investigation used was SLS testing. SLS specimens with a 12.5 mm overlap were cured with a specified induction heating profile and then tensile tested at a rate of 13 mm/minute on a 30 kN Instron 3367 universal test machine. Bondline thickness in all

cases, unless otherwise stated, was 0.3 mm and regulated by the use of glass beads added to the adhesive in the same way as chapter 3. A target fillet shape was used as shown in Figure 20. Surface treatment upon all TS-CFRP consisted of an IPA wipe, based on the data in section 3.2. This data showed that an IPA wipe sufficient to remove water-based mould release and vacuum grease, the contaminants that may be present upon the TS-CFRP substrates used for this investigation. Induction curing profiles follow that shown in Figure 46. This profile was based upon discussions with adhesive manufacturers. The dwell time and temperature were varied depending on the adhesive product used. The ramp was set at 20 s from ambient temperature to isothermal dwell temperature in preliminary testing. In later work a cooling phase was incorporated varying the temperature the joint SLS test was performed (T_{test}) between the dwell temperature (T_{dwell}) and ambient temperature ($T_{ambient}$).

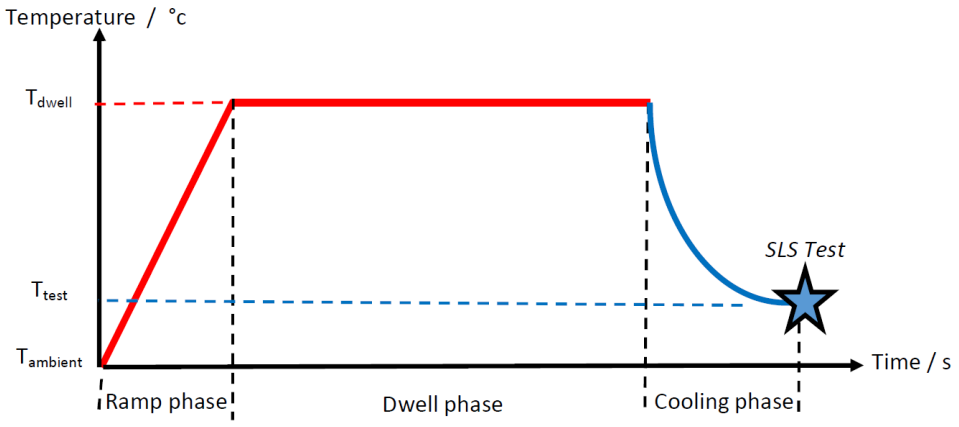

Figure 46 Adhesive cure thermal cycle

In all cases joint temperature was monitored using an in bondline k-type thin thermocouple of 0.13 mm wire diameter. The thermocouple was coupled to a PID controller which controlled the output power of the induction generator. In a manufacturing environment, such as detailed within chapter five, a PID control loop would not be used. Instead, the induction generator would be programmed with a specified output profile to achieve the required heating profile. However, for joint development work the PID control method provided a rapid method for altering the heating profile as required and ensure the target heating profile was achieved.

4.1.1. Initial testing methodology

Initial testing used a 180 mm single sided induction coil which was specified during the purchase of induction heating equipment for this work, further details are presented within portfolio submission three. Five SLS adhesive samples were produced in each batch of

specimens, initially these were produced in the form of large 150 x 100 mm plaques with a 12.5 mm overlap. The arrangement can be seen in Figure 47. The coupons were then cut to 25 mm width following the induction cycle on a water-cooled diamond blade saw. This enabled more accurate and efficient sample positioning under the induction coil and more efficient sample heating. To prevent excessive loading during the cutting process tabs of the same material were bonded with a polyurethane structural adhesive to the sample plaques prior to the induction cycle. This also helped to provide sample support during the curing process. PTFE adhesive tape was used to ensure joint overlap did not exceed 12.5 mm. The thermocouple was initially placed just outside the bondline centre although this highlighted other concerns as detailed in section 4.2.1.

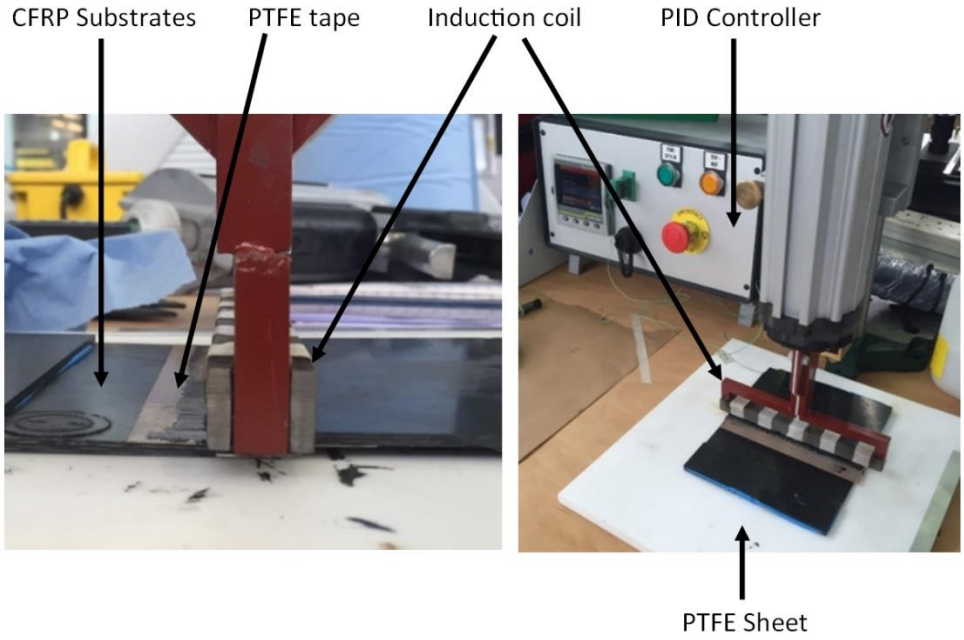

Figure 47 Experimental set up initial rapid curing investigation

TS-CFRP material was used, the same as that detailed in section 3.1. The TS material being of greater significance to Jaguar Land Rover at the time of investigation compared to TP material. Initial testing was performed on CFRP/CFRP joints. During the curing cycle the induction coil and transformer unit were rested on the joints, with a weight of approximately 10-15 kg ensuring joint consolidation. All joints were tested at ambient temperature, shown by $T_{ambient}$ in Figure 46. This followed quenching joints in water immediately after the cure cycle, it was estimated that joints were produced, cut to size and tensile tested within 1 hour. The quenching step was designed to prevent additional cure during the cooling stage. This would not be a feasible step in a manufacturing process, however the step was designed to reduce the additional cure generated during cooling. In the case of a slower cool it is likely the

resulting joint strength upon returning to ambient temperature would be higher due to the additional cure generated over the cooling phase. Varying isothermal cure temperatures of three levels 100, 150 and 175 °c were established for each adhesive product after discussions with adhesive manufacturers. Similarly, three dwell times of 30, 60 and 100 s. The ramp stage to isothermal temperature was set to 20 s in all cases.

4.1.2. Available induction heating equipment

A Minac 18/25 SH, 100 kHz induction generator was available which provides up to 18 kW output power, supplied by EFD Induction Ltd. The system was water cooled, with a chiller which provided cooling water to the induction coils. The system can be controlled manually, using set induction programmes based on percentage power output. Alternatively, the system can be controlled using a Eurotherm PID controller based on thermocouple temperature monitoring. This enables the programming of a set temperature profile and output power is adjusted to meet the required temperature profile. This approach was used for all of the coupon level validation work in this chapter.

4.1.3. Adhesive selection

A number of leading adhesive manufacturers were engaged in the search for structural adhesive products for the present work, key requirements being;

1. Suitable bonding performance upon FRP intensive and multi-material substrates.
2. Ability to rapid cure at elevated temperature.
3. 12 MPa SLS strength fully cured to meet structural specification (65).
4. Suitability to meet a minimum bondline thickness of 0.3 mm.

The adhesives which were initially selected are presented within Table 18. Due to the relative immaturity of high-volume, composite-intensive, BIW adhesive joining, many of these products form a compromise between rapid curing products designed for metallic applications as well as composite bonding products designed for a slower cure cycles. For reference, Table 19 presents the SLS strengths achieved with the candidate adhesives following an oven cure only, upon different substrate combinations with an approximate thickness of 2.5 mm. It is most notable that the substrate combination in SLS testing significantly effects the SLS strength. A drying process was used to optimise the performance of 10400 SBF at increased bondline thickness, this is discussed more within portfolio submissions five and six. Substrate combinations differ due to the collection of benchmark

data at differing stages during the experimental work, requiring differing comparable data. 3M™ SA9820 and SBF 10630 were not continued into the later stages with TS-CFRP/AL substrates.

Supplier & Product	Chemistry	Data sheet description	Form
3M™ SA9816 Two Part Epoxy Adhesive	Epoxy	Formulated for galvanised steel or aluminium hem flange bonding. Good induction reactivity, quick lock-up and low activation temperatures. (92)	2K (two component) 4:1 mix
3M™ SA9820 Two Part Epoxy Adhesive	Epoxy	Crash resistant adhesive for composite and aluminium bonding. Wide process window, can be applied under body-in-white (BIW) conditions. Can be induction heated at low temperatures. Room temperature curing provides excellent performance. (93)	2K (two component) 4:1 mix
Henkel PU 1510	PU	Used for bonding of primed or painted metal parts and FRP in the automotive or commercial vehicle industry. Suitable for various curing methods between 90 and 170 °c. (94)	1K (one component)
Lohmann DuploTEC® 10400 SBF	Epoxy	Heat sealable film for special labels and bonding of metals, fabrics, glass and ceramics. High shear strength. Induction cure between 130 and 200 °c. (95)	Film 0.04 mm
Lohmann DuploTEC® 10630 SBF & 10625 SBF	Epoxy	Typical application bonding of glass and metals within automotive applications. Induction curable and greater thickness availability compared to 10400 SBF.	Film 0.6 & 0.3 mm
Sika 7666/522	PU	2K Polyurethane development product designed for TS-CFRP/Aluminium bonding with accelerated cure.	2K (1:1 mix)

Table 18 Candidate adhesives

Substrate		3M™ SA9816	3M™ SA9820	PU 1510	10400 SBF 0.3 mm, dried with beads	10630 SBF 0.3 beads	10625 SBF	7666/ 522
TS-CFRP/ TS-CFRP	Mean SLS strength / MPa	23.8	27.2	11.3		16.5		5.8
	TS-CFRP/Al σ (n-1)/ MPa	0.989	0.894	0.363		1.09		1.93
TS-CFRP	Mean SLS strength / MPa	16.1		12.9	13.0		14.0	11.0
	σ (n-1)/ MPa	1.26		0.449	1.36		2.34	1.01

Table 19 Optimal oven cured SLS strength of candidate adhesives. Standard deviation calculation uses the (n-1) method to estimate the population standard deviation based on the sample data

4.1.4. Material considerations

Initial in plane shear (IPS) testing was performed upon the TS-CFRP substrate material to identify the maximum temperature at which the matrix to fibre interface breaks down. This is of key importance because if the bulk laminate properties are reduced the mechanical performance of laminate will consequentially fall, potentially leading to failure to meet engineering requirements. Further, the load transfer through the joint is likely to be reduced as a result. IPS testing was performed according to ASTM D3519 (96) with three coupons in each batch. The IPS coupons were induction heated centrally to 175, 200 and 225 °c, for 20 s and compared to an unheated benchmark. A control thermocouple was placed on the underside of the central coupon. Coupons were cooled to room temperature before IPS testing. The orientation of the IPS coupons relative to the induction coil during heating can be seen in Figure 48.

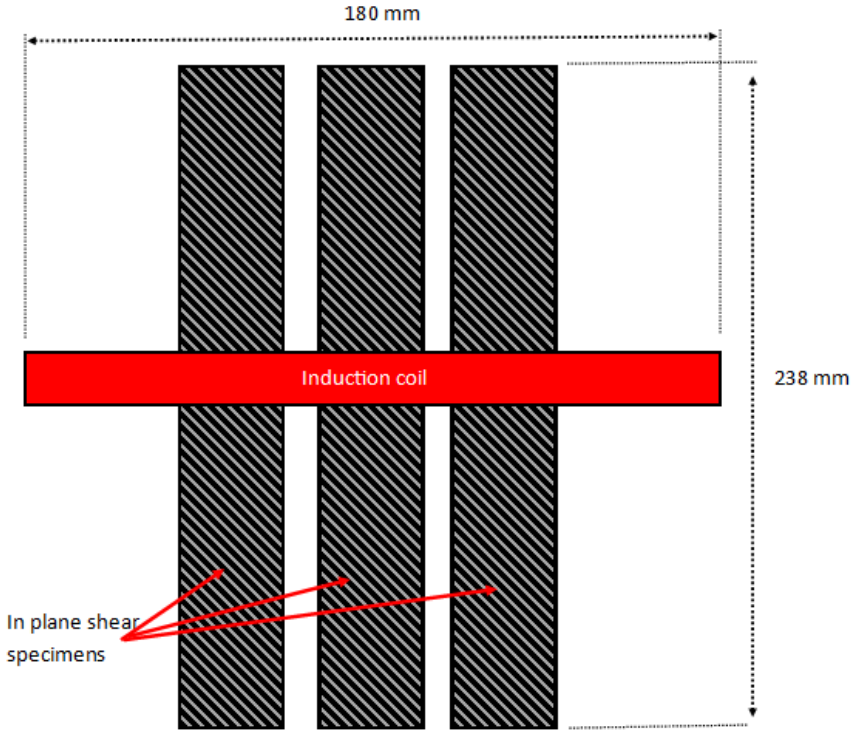

Figure 48 In plane shear test specimen production

It was identified that following heating to 175 °c, no change in mean IPS was observed with a mean IPS strength of 68.6 MPa for both unheated coupons and coupons heated to 175 °c. A standard deviation of σ=0.97 and 2.66 MPa was calculated respectively. Upon heating to 200 °c mean IPS strength dropped by 14.8 % to 59.3 MPa with a standard deviation of 2.05 MPa. An even greater drop in IPS strength was observed upon heating to 225 °c of 26.6 %, compared to unheated coupons with a mean of 51 MPa and σ=1.07 MPa. The drop in

IPS strength correlated with a visible delamination of the FRP seen in Figure 49. As such 175 °c was determined as the maximum induction curable temperature for the specified TS-CFRP based on the range of temperatures investigated.

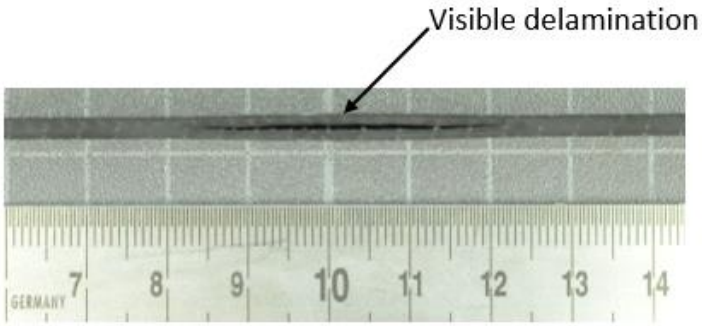

Figure 49 TS-CFRP Induction heated IPS coupon (side view) to 200 °c, visible delamination

4.2. Initial rapid curing data collection – TS-CFRP to TS-CFRP

Data was collected according to the methodology in section 4.1.1 . Table 20 shows the mean SLS strength achieved ($\bar{x}$) in MPa, and estimated population standard deviation (σ) based on the samples using the (n-1) method. It was immediately apparent that the standard deviation in many cases was exceedingly large compared to the mean SLS strength. This shows the high variability within each set of data.

Dwell temp /°c	Dwell time /s	3M™ SA9816		3M™ SA9820		PU 1510		Sika 7666/522		10630 SBF		10400 SBF	
		$\bar{x}$	σ	$\bar{x}$	σ	$\bar{x}$	σ	$\bar{x}$	σ	$\bar{x}$	σ	$\bar{x}$	σ
175	30	3.0	0.9			2.5	3.1	0.2	0.2			1.6	1.8
150	100	0.6	0.2	1.0	0.4	7.7	1.3	4.0	1.6	0.0	0.0		
150	30	1.5	0.5			6.4	1.0	4.7	2.8				
150	60	2.0	1.1			7.7	1.8	0.6	0.9				
100	30	0.0	0.0			4.6	1.1	2.5	1.6				
175	100	2.6	0.3	0.0	0.0	0.6	0.4	0.9	0.7	2.9	2.7	8.4	5.8
100	60	1.8	1.2			4.5	3.2						
100	100	2.1	1.2	1.4	0.8	4.6	3.6	4.8	1.9	0.0	0.0		
175	60	2.0	0.7			0.7	0.6	0.1	0.1				

Table 20 Initial induction cured data set, all adhesives showing sample mean ($\bar{x}$ / MPa) and standard deviation (σ / MPa), TS-CFRP/TS-CFRP.

Upon further inspection of the joint failure surfaces it was apparent that within each batch of samples a vast difference in failure mode could be observed. For example, with the epoxy adhesives, samples located towards the outside of the coil often appeared less cured and

tacky, whereas those towards the inside samples were often porous and overbaked. With PU 1510 adhesive, samples towards the outside of the coil often had regions apparently uncured with remaining liquid adhesive and samples towards the centre showing regions of apparent adhesive failure at the higher target cure temperatures. Examples of this can be seen in Figure 50.

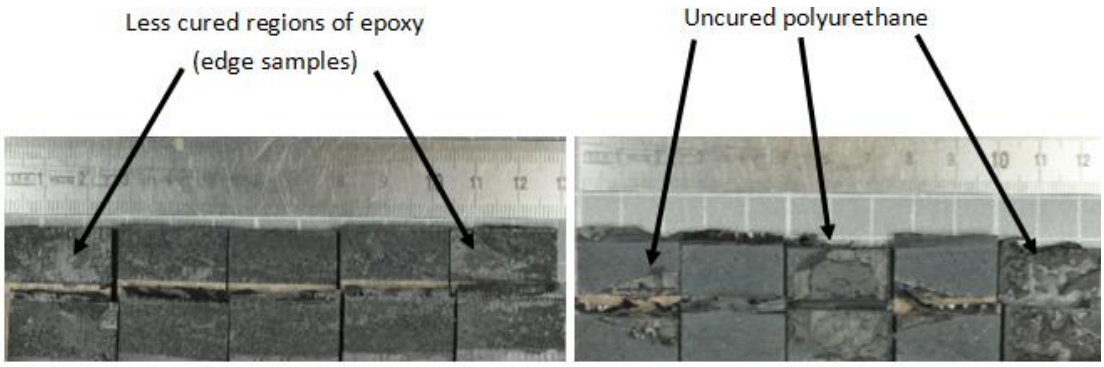

Figure 50 3M™ SA9816 150 °c 30 s (left image), PU 1510 100 °c 100 s dwell (right image), variation in failure mode visible following induction cure

This highlighted that there would appear to be considerable variation in temperature distribution along the adhesive bondline leading to the variation in adhesive appearance and joint strength within each batch of samples. This is evaluated further in section 4.2.1. There appeared to be a direct correlation between the amount of porosity present and reduction of SLS strength compared to low porosity samples in a number of cases. This was evaluated further within portfolio submission six. The variation in temperature distribution within batches however yielded an indication of the maximum joint strength which may be achievable with further optimisation of heating parameters, further it proved the concept that a CFRP/CFRP induction heated joint is achievable. Maximum batch SLS strength is shown in Table 21. Whilst the target temperature may deviate significantly from the actual cure temperature of the joint, it is observed that over 3 MPa can be achieved in 60 s or less with 3M™ SA9816 and over 8 MPa with PU 1510 or Sika 7666/522.

It was identified that although over 2 MPa was achieved with 3M™ SA9820, the adhesive outgasses significantly upon induction curing with the parameters investigated, leaving an exceptionally porous joint. The temperature of outgassing onset was identified through TGA analysis in section 4.2.2 and it was suggested the outgassing is a result of volatilisation of components within the adhesive. Outgassing was later shown as highly detrimental to resultant joint strength upon full cure. As such, the product was not continued for use with this work. It was identified that 10400 SBF exhibited significant outgassing, which was later

attributed to solvent evaporation during cure. A drying process was implemented in later work, improving joint strength. Lohmann 10630 SBF yielded a maximum SLS strength of 6.5 MPa however this was achieved in the central region of the induction coil where it was identified that cure temperature was highest. A thinner version of the film, 10625 SBF (0.3 mm) was used in later work with the aim of reducing the heat required to cure the adhesive. PU 1510 was found to achieve in excess of 10 MPa with a 60s dwell and 8 MPa in 30s dwell, appearing a highly suitable adhesive product for the present application. Sika 7666/522 also produced over 8 MPa SLS strength within a 30 s dwell. 3M™ SA9816 also showed promising maximum SLS strength, with up to 4 MPa being achieved in 30 s and over 3 MPa in many cases at lower temperature.

		3M™ SA9816	3M™ SA9820	PU 1510	7666/ 522	10630 SBF	10400 SBF
T / °c	**Time / s**	*SLS Strength / MPa*					
175	30	4.14		6.82	0.35		0.00
150	100	0.80	1.46	8.78	6.03		
150	30	2.09		8.00	8.24		
150	60	2.88		10.72	2.04		
100	30	0.00		5.93	5.03		
175	100	3.07	0.00	1.22	1.70	6.53	2.97
100	60	3.26		7.96	0.00		
100	100	3.12	2.23	8.60	6.65		
175	60	3.20		1.74	0.35		

Table 21 Maximum SLS strength reached initial data collection TS-CFRP / TS-CFRP, following induction cycle only

4.2.1. Bondline temperature distribution

A series of investigations were performed to identify the variation in temperature along the adhesive bondline that was used within the methodology in section 4.2 upon TS-CFRP substrates. The requirement for this work was based upon the observed variability in previous SLS data as well as variation between failure surfaces of samples produced within the same batch. K-type thermocouples of 0.3 mm wire diameter were placed symmetrically within the bondline area, at 10, 37.5 and 75 mm from the plaque edges and data recorded using a Pico-logger TC-10. The set-up is shown in Figure 51. A Flir infrared camera was also used to monitor the bondline temperature along the external edge of the joint overlap. The temperature was monitored over a range of heating cycles, with the control thermocouples placed in differing positions within the plaque overlap and outside the overlap.

Figure 52 shows the temperature profile at various locations along the bondline at intervals throughout the heating cycle. The heating cycle shown followed a target 20 s ramp to 150 °c and a 30 s isothermal dwell, the same profile as used in a number of cases within the previous data set. It can be seen that where the control thermocouple located just outside the bondline in the plaque centre a peak bondline temperature is experienced of 188 °c, measured within the bondline, significantly in excess of the target temperature. Near the edges of the bondline, the temperature is much reduced, nearer 113 °c following the ramp phase. Thus, considerable variation from the 150 °c target existed. The thermal camera line plot along the edge of the bondline shows a similar trend, although the temperature is lower due to thermal conduction within the plaque and cooling of the exposed edges.

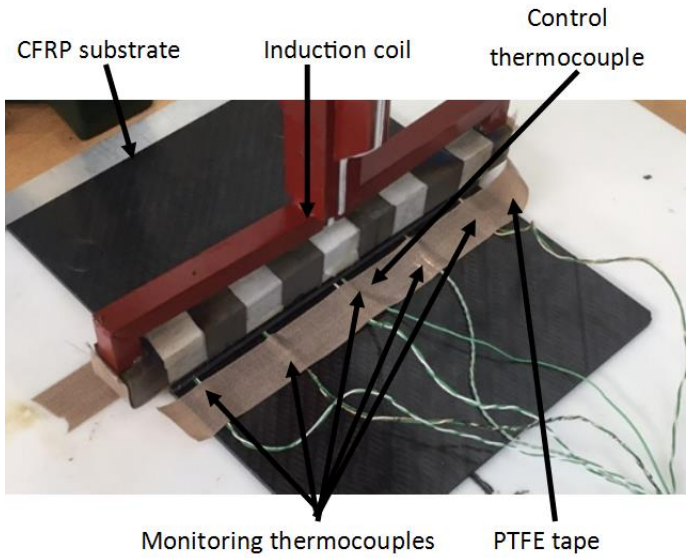

Figure 51 Bondline temperature monitoring initial data collection

Locating the thermocouple within the centre of the bond area reduced the peak temperature to approximately the 150 °c target, however the edges of the plaque reached only 97 °c following the 20 s ramp phase. Locating the control thermocouple in differing positions within the bondline yielded a similar temperature distribution profile, shifting the point of control to approximately the target temperature with a temperature peak in the centre and cool spots at the edges. As such, the temperature variation explained the significant scatter in previous data using this coil and TS-CFRP substrates. Figure 53 highlights this temperature variation as seen from the rear of the upper substrate with the induction coil in the same position as that during the test, the set up being rotated by 90 ° and camera repositioned. Of interest is that the uneven temperature gradient did not notably reduce after the 30 s dwell, due to the low thermal conductivity of the TS-CFRP.

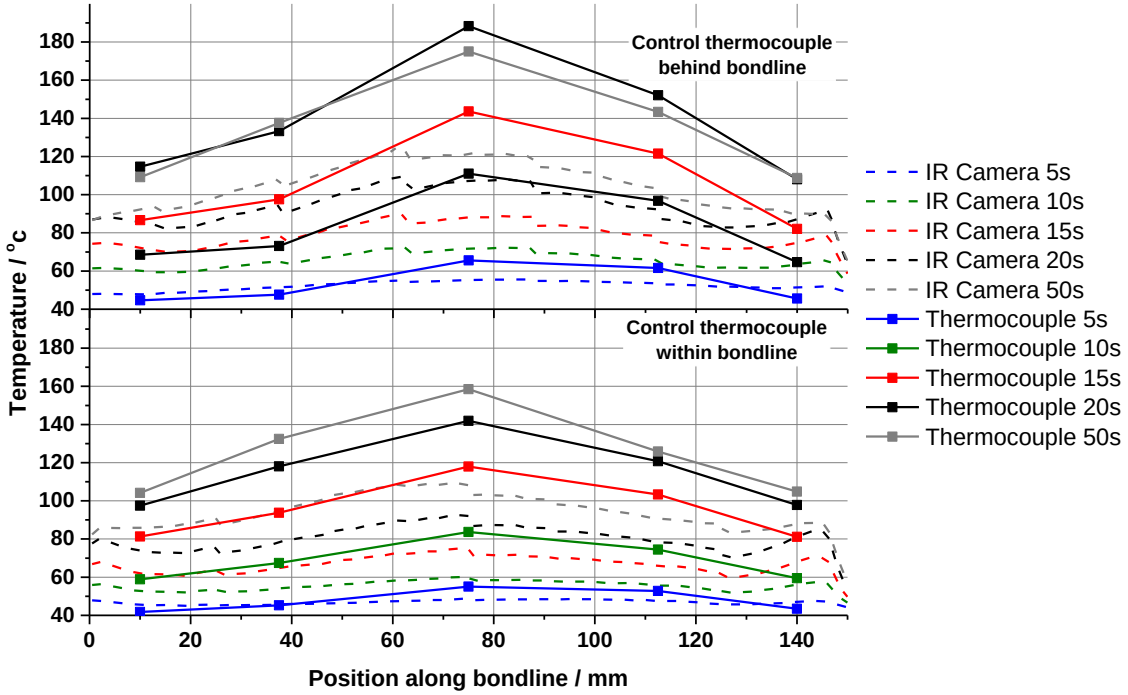

Figure 52 TS-CFRP joint temperature distribution along bondline with control thermocouple centrally located, 150 °c target following 20 s ramp. Measurements plotted at intervals though the heating profile. Top plot control thermocouple located outside of bondline in centre, lower plot thermocouple located centrally within bondline

A further investigation was performed upon a TS-CFRP 25 x 100 mm^2 coupon, 2.5 mm thick, with the induction coil aligned with the short side of the plaque in the same orientation as Figure 51. It was observed that as the TS-CFRP component geometry became smaller the temperature distribution became increasingly non-uniform compared to a benchmark aluminium coupon of 2mm thickness, seen in Figure 54.

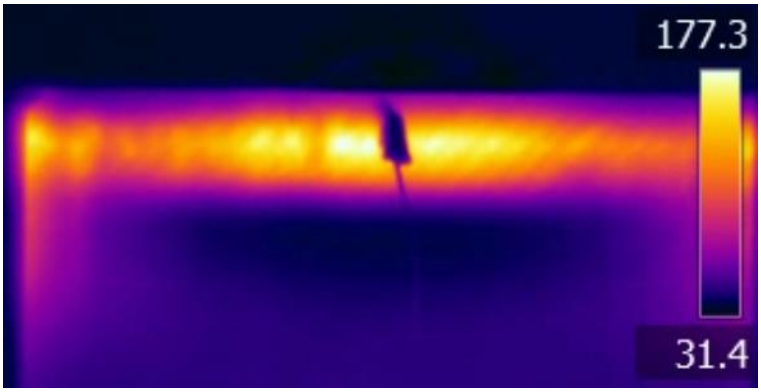

Figure 53 Temperature distribution profile seen from the rear of 150 x 100 mm^2 TS-CFRP plaque

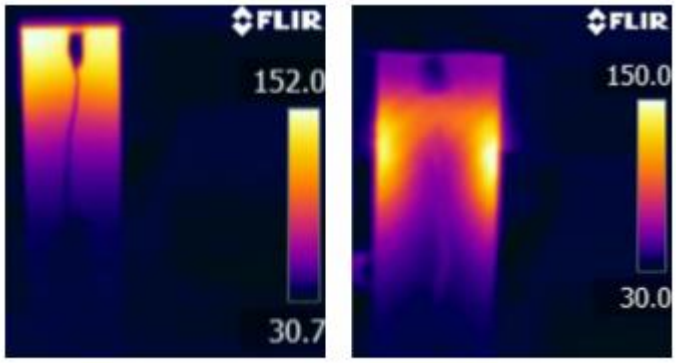

Figure 54 Temperature distribution when induction heating 25 mm wide coupon TS-CFRP (right) and aluminium comparison (left)

It was concluded that the initial experimental methodology yielded a highly non-uniform temperature distribution when induction heating TS-CFRP plaques. Further, as TS-CFRP component geometry became smaller the temperature distribution became increasingly non-uniform, in comparison to an aluminium substrate. For further adhesive analysis a revised methodology was required that resulted in a more uniform temperature distribution within adhesive specimens, in order to optimise adhesive cure profiles. As an aside, it was also identified that induction coil design for CFRP heating requires considerably more development than for the heating of metallic materials.

4.2.2. Thermogravimetric adhesive analysis

Previous data had highlighted the variation in bondline temperature distribution which was attributed to cause the change in failure surfaces within sample sets. Many of these specimens showed porosity within the failed adhesive, which may be indicative of volatilisation of components within the adhesive. This was not raised as a potential issue during initial discussions with adhesive manufacturers. It was expected that the porosity could significantly reduce the fully cured adhesive strength. In order to identify the temperature at which volatilisation occurs thermogravimetric analysis (TGA) was used. This technique was used to measure the change in sample mass with temperature at a defined heating rate. The 2K adhesive components were analysed separately, preventing cure from occurring which would restrict any outgassing. The TGA analysis was performed upon the adhesives which showed the most significant volatilisation, Lohmann products were excluded. This was due to no porosity being observed with 10630 SBF and the outgassing of 10400 SBF being attributed to solvent evaporation, discussed in detail within portfolio submission five.

TGA data is presented in Figure 55, it is seen that the rate of mass loss with 3M™ SA9820 component A is greater than with any of the other products tested, increasing at a relatively linear rate until 160 °c where the rate increases dramatically. This helps to explain the significant outgassing and porosity observed during accelerated induction cure. A similar trend was observed with 7666/522 component A although at approximately half the mass loss rate of 3M™ SA9820. Upon reaching approximately 130 °c the rate of mass loss rate of 7666/522 increased dramatically. 3M™ SA9816 shows a slower rate of mass loss compared to 7666/522 which is approximately linear until 140 °c, losing just 2 % mass. Above 140 °c at the mass loss rate of 3M™ SA9816 increases dramatically. Negligible mass loss was observed with PU 1510 below 200 °c. This was possibly attributed to the product curing rapidly, rather than outgassing, upon reaching 100 °c in the TGA chamber, identified in later work presented within section 4.4.

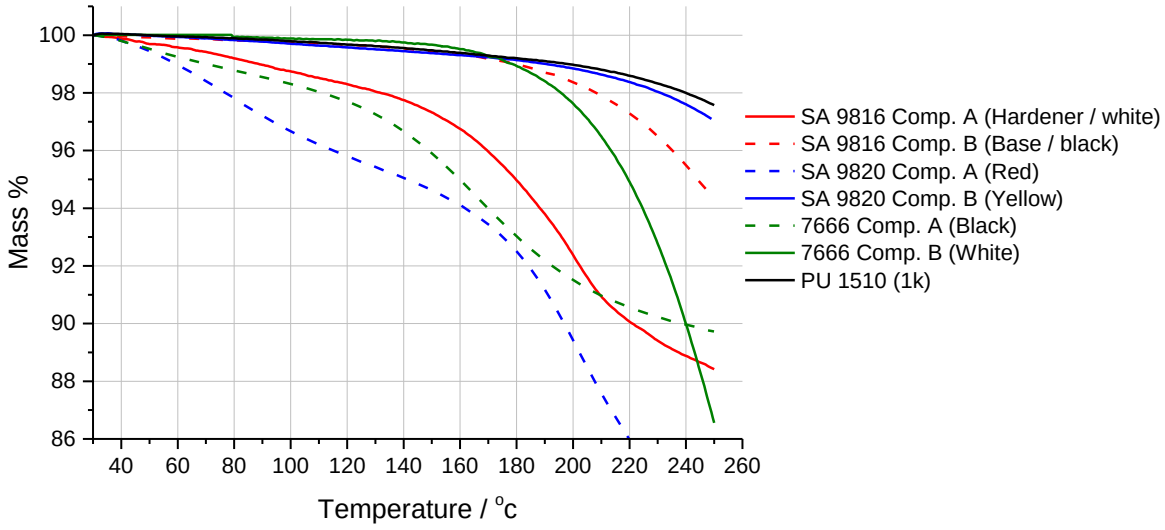

Figure 55 TGA data for 3M™ SA9816 , 3M™ SA9820, 7666/522 and PU 1510 at 30 °c/minute ramp rate

The TGA data helped to identify maximum cure temperatures to be used in subsequent adhesive trials. It also helped to explain the significant outgassing observed in some of the previous data sets, especially when combined with an overheating of the joint due to uneven temperature distribution detailed in section 4.2.1. Since no significant lass loss was observed in Figure 55 around 100 °c, the mass loss was not attributed to water evaporation, instead attributed to the volatilisation of adhesive components during heating.

4.3. Multi-material joint investigation – Aluminium to TS-CFRP

Section 4.2 highlighted that the available induction heating equipment and experimental methodology used for initial testing produced significant temperature variation within batches of samples. This lead to exceptionally high failure load standard deviation, variation in joint failure mode and variable amounts of adhesive porosity within each sample batch. The data collected however showed the maximum joint strength that may be achievable with each adhesive in a given cycle time, although the actual temperature profile of each joint was variable according to sample position within the original, larger plaque. A more reliable test method was required to optimise adhesive handling strength performance. Alongside this it was desired to perform the SLS test immediately after the cure cycle, the specimen geometry thus being limited by the grip size upon the available equipment. The requirement to test immediately after the induction trial relates directly to an automotive manufacturing application. Following initial curing it would be required to remove fixtures from the assembly before moving along the production line. Thus, immediately upon future removal the joint would experience a load. The adhesive handling strength must be able to sustain this load without failure of the assembly immediately upon fixture removal. The immediate test following the induction cycle simulates the immediate application of load following fixture removal.

4.3.1. Second phase testing methodology

The second phase testing was designed to improve upon initial methodology presented in section 4.1. Primarily by addressing three considerations;

1. The time delay in section 4.2 between joint cure and joint testing of approximately 1 hour poorly represented the removal of fixtures and load application immediately after the cure cycle as in a production scenario. To address this the curing and test phase were combined and performed within the test machine, enabling an immediate tensile test following the curing cycle.

2. Single sided TS-CFRP induction heating yielded high variability in bondline temperature distribution in previous work, detailed in section 4.2.1. It was identified that this was a more significant problem with smaller geometry TS-CFRP coupons. To address this problem aluminium (AL)/TS-CFRP joints were used for subsequent coupon level development. The high thermal conductivity of the aluminium was

aimed to reduce the temperature variation within the joint. The specimen width was also increased from 25 mm to 50 mm to assist in TS-CFRP heating efficiency. The aluminium and TS-CFRP substrates had a thickness of approximately 2.5 mm. TS-CFRP substrates were the same as that used in section 4.2 unless otherwise stated. Aluminium substrates were 5754 grade unless otherwise stated, initial development work used some 6000 series aluminium due to material availability.

3. The bondline temperature at the point of starting the tensile test, T_{test}, was identified as highly influential to joint SLS strength in discussions with adhesive manufacturers. With joint cooling initially limited by natural cooling processes a forced air jet was added to accelerate the cooling profile, thus reducing total cycle time. The quench method used in the initial data collection was unsuitable compared to an air jet for use within a manufacturing environment. Further, the quench method was unsuitable for use in conjunction with the tensile test machine without removing the sample first, introducing undesirable delays into the test method.

An in-situ test method was developed to perform the investigation requirements based on the above consideration, the equipment set up is shown in in Figure 56. This utilised a two-sided induction coil which was developed through collaboration with the induction equipment supplier, EFD Induction. This coil was mounted horizontally between the grips of the tensile test machine. The same Instron universal test machine was used as detailed in section 4.2. A modified drill press stand was used enabling the coil to be slid into position around the SLS coupon for the curing stage and retracted immediately prior to tensile test. The air cooling jet was developed for the investigation and used to cool the joint to T_{test}, as detailed in the experimental results. The cooling jet is shown in Figure 57, with a typical cooling profile in Figure 58. Following a substrate isopropanol wipe, adhesive was applied to the AL and CFRP substrates prior to loading in the tensile test machine.

As in previous work tabs were inserted into the grips to compensate for the offset geometry of the SLS test. A centrally embedded K-type thermocouple of 0.1 mm wire diameter was inserted into the adhesive joint, connected to the PID feedback controller used to control the heating process. 0.3 mm glass beads were added to the adhesive prior to application, unless otherwise stated, to control bond thickness. The control thermocouple and feedback loop was not used in later component level testing, however provided a convenient way to control

joint heating profiles for coupon level development. Joint overlap was measured using a Vernier calliper and adjusted to 12.5 mm prior to curing using the crosshead adjustment on the tensile test machine. Adhesive spew was removed from the joint prior to cure with a target spew shape as shown in Figure 20. An inconsistent spew shape was identified as a cause of joint variability within literature. The induction coil was placed around the sample, with non-conductive tabs placed either side of the specimen inside the grips. A spring clamp was then added to help control bondline thickness during cure. This applied some consolidation pressure ensuring the joint was closed until the glass beads were contacted at 0.3 mm bond gap, unless otherwise stated. The experimental set up can be seen in Figure 56.

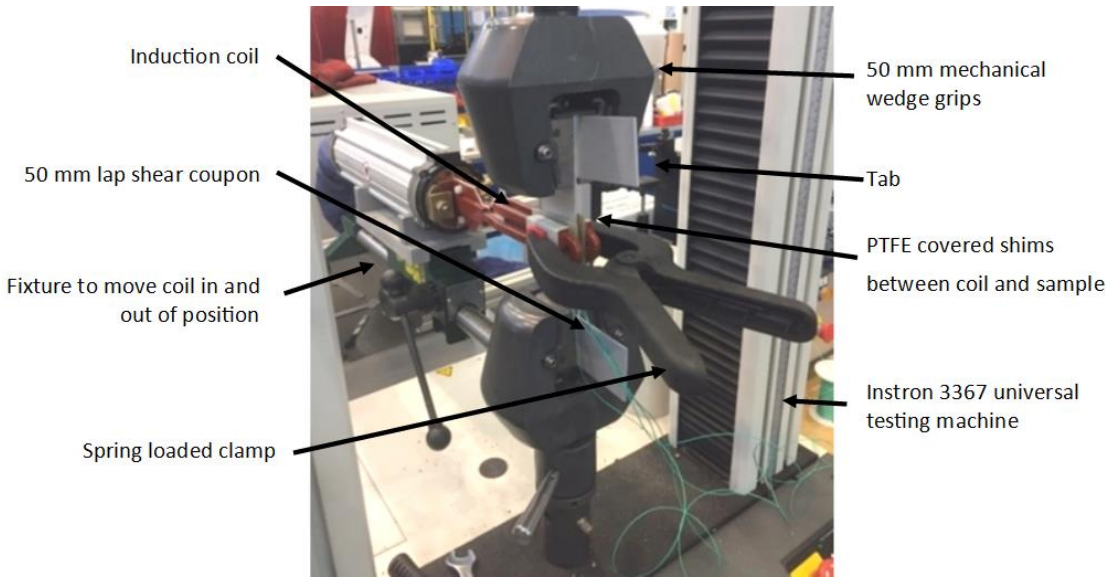

Figure 56 Second phase testing methodology rapid cured adhesive joints

The cure cycle followed a ramp at constant heating rate to an isothermal dwell temperature, where an isothermal dwell period took place. The heating profile parameters are specified within experimental results for each investigation. Following the specified dwell, the coil was removed and cooling air jet applied. Upon the joint reaching the desired T_{test} the SLS tensile test would be immediately started at 13 mm/minute until joint failure. A minimum of three repeat coupons were produced for each set of test parameters. Adhesive choices were the same as those discussed within section 4.1.3 . A silane primer, 3M P592, was identified as required to produce a cohesive failure mode with Henkel PU 1510 upon untreated aluminium substrates. This was identified as an effective aluminium pre-treatment in preliminary trials, detailed further within portfolio submission six. This primer was applied following IPA wipe in all subsequent bonding of PU 1510 adhesive to aluminium. At partial cure 3M™ SA9816 was identified as not producing a cohesive failure upon aluminium substrates, although PT3

coating was recommended by 3M as the most suitable aluminium surface treatment (97). PT3 coated aluminium, grade 5754, was sourced and used with the 3M™ SA9816, 7666/522 and Lohmann adhesives in later work presented in this report, unless otherwise stated.

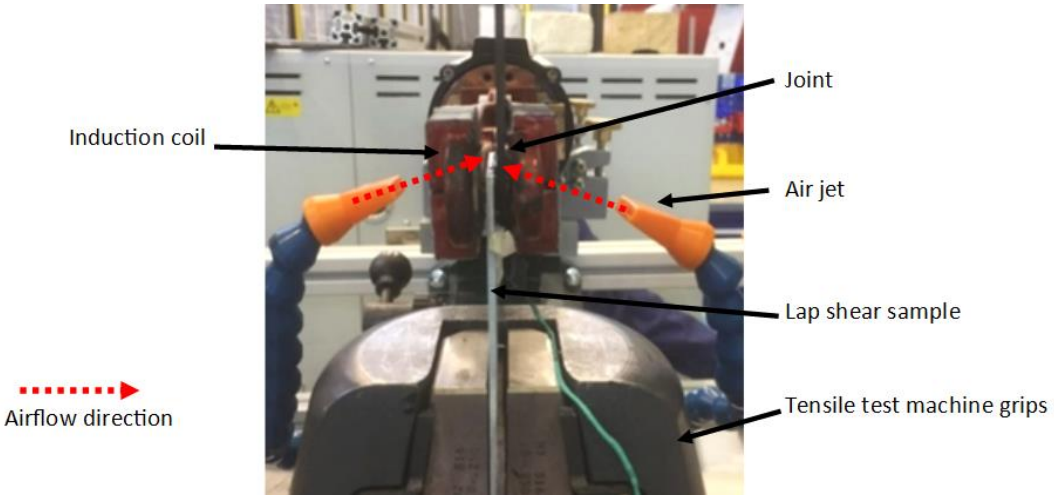

Figure 57 Cooling airflow jet image with annotations

The representative joint temperature distribution of the improved CFRP/AL experimental methodology is seen in Figure 59 with thermocouples located at 5, 25 (centre) and 45 mm through the 50 mm wide SLS joint overlap, inside of the adhesive joint. The in-joint temperature distribution with the double-sided coil and multi-material substrates is a considerable improvement upon the previous single sided coil with TS-CFRP substrates which can be seen for reference in Figure 52.

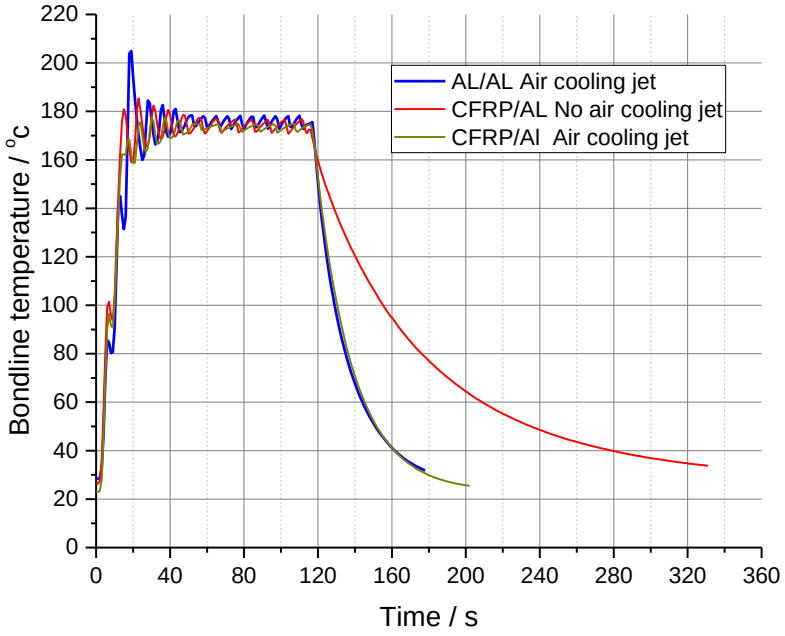

Figure 58 Cooling profile with and without air jet for various substrates

With the multi-material joint and double sided coil the temperature differential within the joint was approximately +/- 5°c, compared to +/- 38°c in some cases with the TS-CFRP / TS-CFRP single sided arrangement. This enabled more accurate identification of achievable handling strength following heating cycles, with less variability. Optimisation of induction heating coils to provide a more uniform temperature distribution with CFRP/CFRP substrates remained an area for future work.

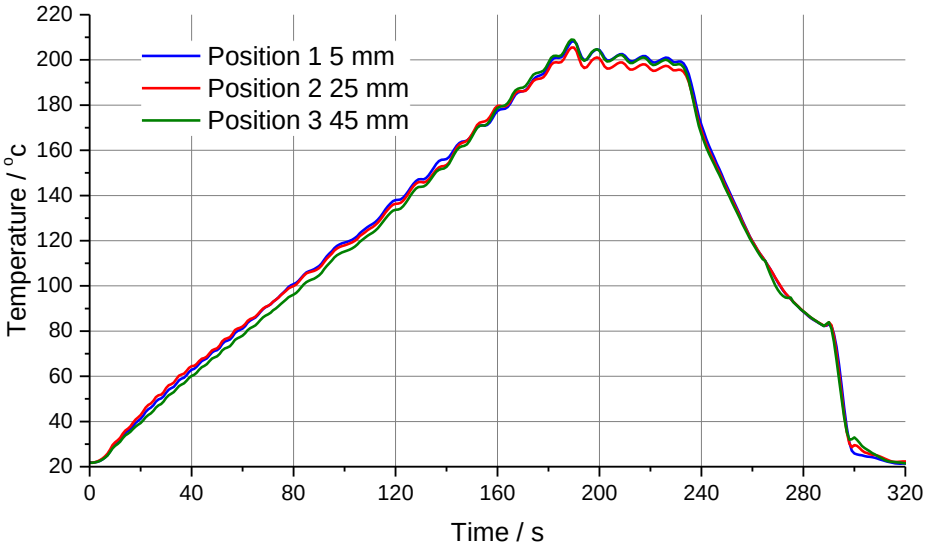

Figure 59 Temperature distribution AL/TS-CFRP coupon, 50 mm wide, 12.5 mm overlap with adhesive, 0.3 mm bond thickness

4.3.2. Henkel PU 1510

Initial testing upon TS-CFRP/P592 treated AL substrates using PU 1510 adhesive generally yielded a fully cohesive failure mode following an oven cure cycle, indicating suitable substrate surface preparation. In some cases, small amounts of adhesive failure were observed upon the TS-CFRP interface, which it was believed to be caused by surface contamination not removed by the IPA wipe. To identify the significant process parameters during induction cure of PU 1510 initially a partially factorial Taguchi experimental design was performed, to identify the significant parameters that effect SLS strength. In this case three levels and three factors were used. This included dwell temperatures of 130, 150 and 170 °c, dwell times of 30, 45 and 60 s as well as ramp rates of 100, 250 and 500 °c/minute. Performing a general linear model analysis of variance, it was highlighted that the isothermal dwell temperature was the only factor investigated that significantly affected SLS strength, see Table 22. A residual error standard deviation σ = 1.48 MPa was calculated.

It was identified that at 170 °c dwell temperature the failure surface of PU 1510 showed a thin layer of adhesive on the substrate surface, defined as special cohesive failure. This was notably different to that at 150 °c where the failure was generally fully cohesive with equal amounts of adhesive on both substrates. The SLS strength correlated well to a quadratic fit, applied to the main effect parameter of dwell temperature. However, a low r^2 = 26.2 % was obtained, this was considerably higher than an alternative linear model, a notable trend was observed with an SLS strength peak at 150 °c seen in Figure 60. As such, from the main effect plot data 150 °c appeared the most beneficial isothermal dwell temperature to maximise SLS strength, from the range of values investigated. A dwell temperature of 170 °c was identified as leading to adhesive degradation and a reduction in SLS strength.

Source	DF	DoF	SS	MS	F value	P value
Source	Temp (dwell)	2	23.4943	11.7471	5.59	0.012
	Time (dwell)	2	0.0581	0.0291	0.01	0.986
	Ramp	2	8.0923	4.0461	1.93	0.172
Error		20	42.0020	2.1001		
Lack of fit		2	2.7295	1.3647	0.63	0.546
Pure error		18	39.2725	2.1818		
Total		26	73.6467			

Table 22 Analysis of variance PU 1510 initial data collection TS-CFRP/AL

Due to the effect of ramp rate appearing insignificant over the range investigated, the highest ramp rate of 500 °c/minute was used in all subsequent testing with PU1510. Based on dwell time appearing insignificant with respect to SLS strength in the range 30– 60 s an investigation was performed to establish the relationship between dwell time and SLS strength, increasing dwell time from 0-30 s at 150 °c dwell. All joints were tested upon reaching 50 °c using an air jet cool. The results are presented in Figure 61. It was observed that a number of failure surfaces showed in excess of 30 % adhesive failure upon the TS-CFRP surface. These specimens were excluded from the analysis, attributed to excess mould release contamination on the CFRP surface.

It was concluded from the gradient of the linear fit in Figure 61 (-0.000015) and associated confidence intervals, that there was virtually no relationship between dwell time and SLS strength with PU 1510 adhesive at 150 °c dwell. Thus, once the adhesive reached the 150 °c dwell temperature at 500 °c/minute its maximum SLS strength had been reached. This relates to the encapsulated isocyanate technology attributed to this product where a rapid reaction is initiated upon reaching the activation temperature (94). Further evidence to support this

can be seen in section 4.4. One of the drawbacks however with this product is that if the activation temperature was not reached the reaction will not be initiated, resulting in negligible joint strength.

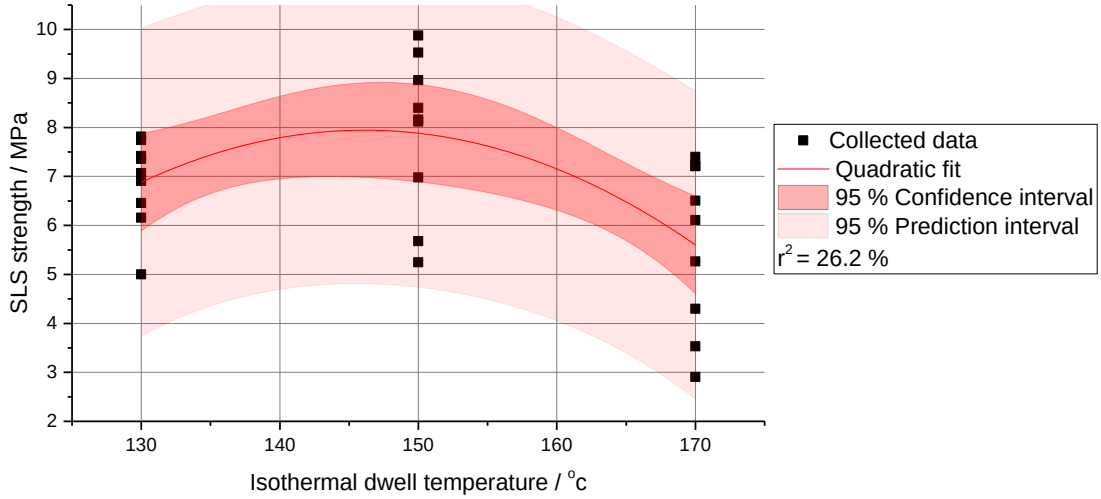

Figure 60 Main effect plot PU 1510 dwell temperature vs SLS strength, TS-CFRP/AL, tested at 50 °c

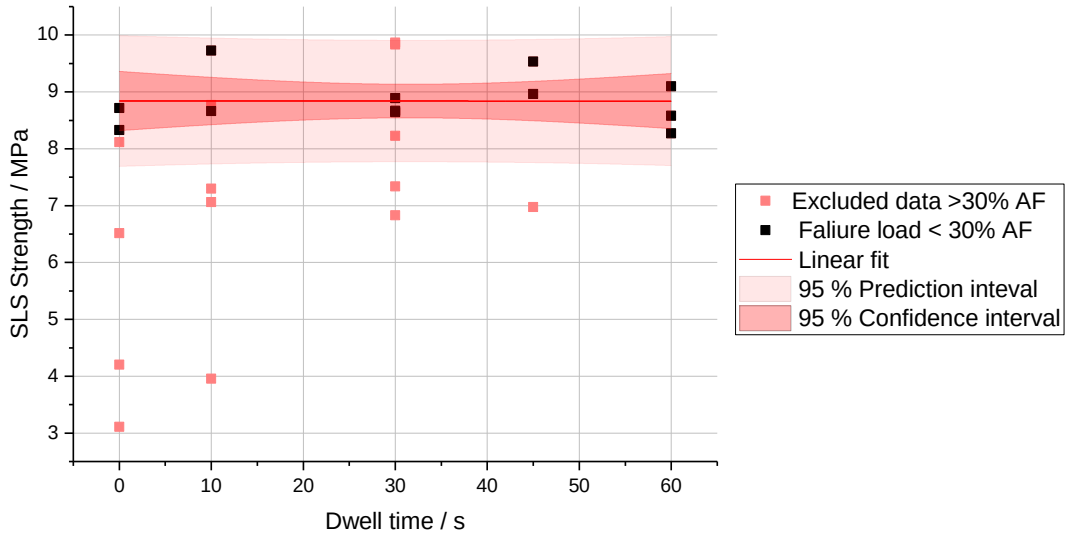

Figure 61 Dwell time vs SLS strength PU 1510 TS-CFRP/AL tested at 50 °c

Once the relationship between dwell time and SLS strength had been understood it was required to evaluate the importance of tensile test temperature upon SLS strength. TS-CFRP/AL coupons were induction cured for 10 s at 150 °c, cooled using the air jet to a range of tensile test temperatures. Results shown in Figure 62, a linear fit was found to most accurately represent the trend in data. Samples were excluded which showed greater than 30 % adhesive failure with r^2=74.0 %. The strong negative correlation, within 95 % confidence

levels shows the confidence in the relationship. Approximately 50 % strength loss was observed between 25 °c and 150 °c tensile test. This is an important industrial consideration, in that as the bonded assembly moves through the production line the joint strength will vary. Should the joint strength reduce excessively the primary bonded structure may distort or in the worst case fall apart, for example when moving through the paint oven. No relevant standard existed at the time of writing specifying an acceptable strength loss for a partially cured joint in a handling strength application. The most relevant standard available (65) specified no greater than 30 % strength loss between 20 and 80 °c however this is considering a fully cured joint. As a result, it is important to understand the strength loss which may be expected for a partially cured joint, over a range of temperatures to design a primary bonded assembly process. The cooling process using an air jet could, in theory, be scaled to any length joint providing sufficient compressed air capacity is available.

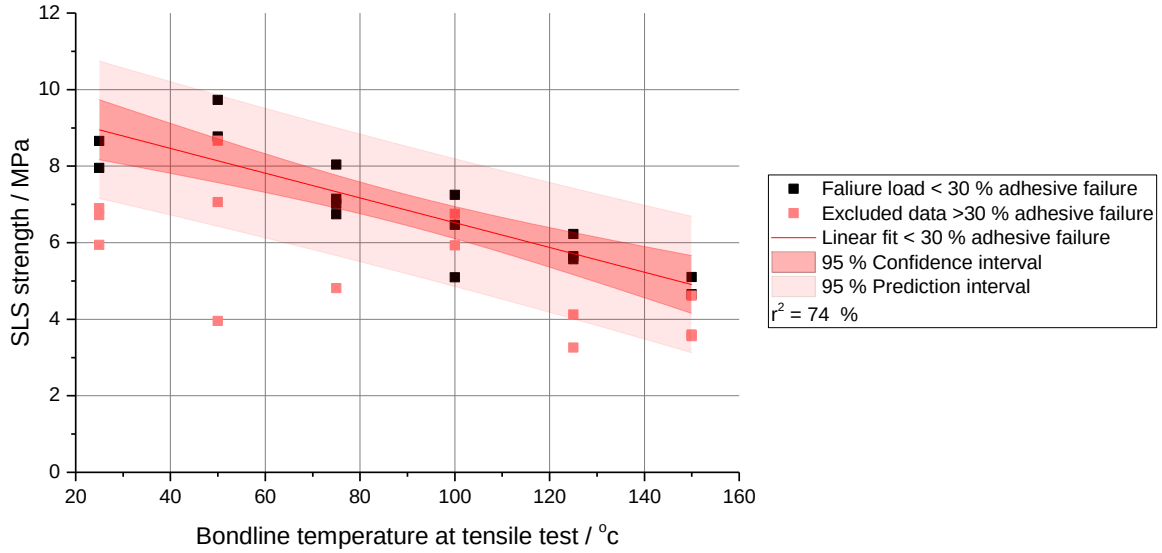

Figure 62 Variation in SLS strength with bondline temperature TS-CFRP/AL, following induction cure for 10 s at 150 °c

Finally, it was investigated whether SLS strength was affected by an induction cure cycle prior to a subsequent oven cure reduced the final joint strength. TS-CFRP/AL specimens were induction cured for 10 s at 150 °c prior to being placed in a pre-heated oven at 100 °c for one hour. Identical comparative specimens were cured in the oven only at 100 °c for one hour. Results are shown in Table 23, using the paired t-test to identify whether there is a significant difference between the sample mean SLS strengths to the 95 % confidence level.

Test no	Cure condition	Sample mean μ / MPa	Sample standard deviation σ / MPa	Paired – T Δμ (1-2)/ MPa	Paired – T 95 % CI, Δμ Upper / MPa	Paired – T 95 % CI, Δμ Lower / MPa	P value
1	Oven only	12.87	0.449	1.11	0.14	2.09	0.034
2	150 °c, 10 s + oven	11.76	0.707				

Table 23 Paired t test comparison of SLS strength with PU 1510 with and without prior induction cure TS-CFRP/Al, tested at room temperature

It was observed using a paired t-test that there is a statistically significant mean reduction in SLS strength between the oven cured only samples and induction plus oven of 1.11 MPa, approximately 8.6 % of the maximum mean oven cured strength. This may increase to 2.09 MPa within 95 % confidence interval, equating to 16 % of mean oven cured strength respectively. This has important implications for Jaguar Land Rover in that the reduction in strength as a result of the initial induction cure must be considered in the design of the structure and the adhesive joint.

4.3.3. 3M™ SA9816

Second phase testing with 3M™ SA9816 initially identified significant porosity at 140 °c dwell temperature upon failure surfaces, this was consistent with TGA data in section 4.2.2. Thus, three levels of dwell temperature were analysed further; 110, 120 and 130 °c. Second phase testing with other adhesives identified the ramp phase as a less significant variable, as such the ramp rate levels were reduced to 250 and 500 °c/minute to reduce the quantity of data collection required. Three isothermal dwell time levels were also investigated of 30, 45 and 60 s. A fully factorial two factor, three level Taguchi design of experiments was used and repeated for both ramp rates, enabling the identification of significant main and interaction effects. An air jet cool was applied with samples tested upon cooling to 50 °c. A three-way ANOVA analysis using a general linear model was performed upon the SLS strength data. It was identified that dwell temperature, dwell time and ramp rate all statistically effected SLS strength to the 95 % confidence level. The results seen in Table 24 with a residual error standard deviation of σ=0.100 MPa.

It can be seen in Table 24 that the main effect of ramp rate contributed a small proportion to the total sum of squares, compared to the dwell temperature and time terms. As such the ramp rate is considered the least significant main variable. Time, temperature and their respective interactions appeared much more significant. The significance of the time and

ramp interaction was thought to be a result of the increase in total cycle time thus increasing the total cure time in a similar way to the main effect of time.

Three-way ANOVA with interaction						
Source	DoF	SS	SS contribution / %	MS	F	P
Temp (dwell)	2	2.890	35.843	1.445	143.29	0.000
Time (dwell)	2	3.513	43.559	1.756	174.13	0.000
Ramp	1	0.191	2.366	0.191	18.91	0.000
Temp x time	4	0.422	5.238	0.106	10.47	0.000
Temp x ramp	2	0.160	1.979	0.080	7.91	0.001
Time x ramp	2	0.390	4.832	0.195	19.32	0.000
Temp x time x ramp	4	0.135	1.680	0.034	3.36	0.02
Error	36	0.363	4.507	0.010		
Total	53	8.064				

Table 24 3M™ SA9816 partially factorial experimental SLS strength data following induction cure

Performing a linear regression model upon the ramp rate alone highlighted to the 95 % confidence interval that ramp rate does not contribute a statistically significant change in SLS strength. It was predicted that the marginal drop in strength with an increase in ramp rate may be due to increased temperature variation at higher heating rates and a shorter ramp phase, reducing the degree of product cure and consequentially strength development. Due to the marginal effect observed the higher heating rate of 500 °c/minute was used to reduce total cycle time in later testing.

It was observed after performing linear regression analysis upon the time and temperature variables with r^2=82.17 %, excluding the effect of ramp rate, that the time and temperature interaction contributed the greatest sum of squares, Table 25. As such this interaction provides the greatest contribution to the model. A positive coefficient of the time and temperature interaction was identified, statistically significant to the 95 % confidence interval. Thus, the higher dwell temperature and time of the range tested would appear to maximise the rate of SLS strength development.

Source	DF	DoF	SS	MS	F value	P
Regression		3	6.62628	2.20876	76.81	0.000
	Temp (dwell)	1	0.01156	0.01156	0.40	0.529
	Time (dwell)	1	0.19416	0.19416	6.75	0.012
	Time x temp	1	0.32332	0.32332	11.24	0.002
About regression		50	1.43774	0.02875		
Total		53	8.06402			
Coefficients						
Term	Coefficient	SE Coef	T-value	P-value		
Constant		1.29	0.27	0.787		
Temp	-0.0068	0.0108	-0.63	0.529		
Time	-0.0721	0.0278	-2.60	0.012		
Time x temp	0.000774	0.000231	3.35	0.02		

Table 25 Linear regression analysis 3M™ SA9816 TS-CFRP/AL initial SLS strength data following induction cure

Following on from the initial set of data, further investigation was performed upon the rate of 3M™ SA9816 SLS strength development at 130 °c. This temperature was identified from failure surfaces as the highest acceptable dwell temperature without excessive porosity generation. Dwell time was varied over a range between 20 and 130 s, cooled using an air jet and tested immediately upon reaching 50 °c. The data is presented in Figure 63. It became apparent that up to 60 s dwell the rate of SLS strength development appears linear, over 60 s dwell the rate shows much greater variation and a lower mean increase in SLS strength.

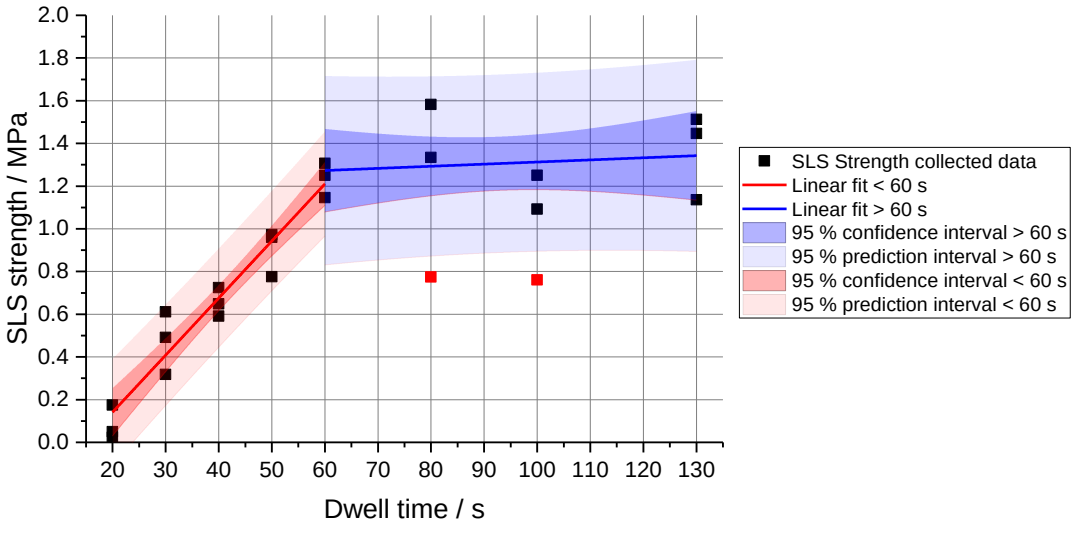

Figure 63 3M™ SA9816 dwell time at 130 °c vs partial cure SLS strength, 50 °c tensile test TS-CFRP/AL

A linear fit was applied to both regions shown in Figure 63, sub 60 s dwell an r^2 value of 93 % was produced and a residual error standard deviation of σ = 0.105 MPa. Above 60 s a much lower r^2 value of 3.13 % and residual error of σ = 0.172^2. Thus, the linear model fits well up to

60 s dwell, however the mean rate of strength increase above 60 s appeared much slower over the range of dwell times investigated. This is consistent with the two stage cure of the product, previously discussed with the manufacturer (97). It is shown within the DSC cure analysis in section 4.4.1 that the secondary cure stage of the product is much slower at 130 °c with an initial step designed to generate handling strength.

Once the rate of SLS strength development at isothermal dwell temperature was understood it was important to understand the variation in SLS strength at different test temperatures. A variation in test temperature was investigated between the 130 °c cure temperature and 30 °c following a 60 s cure at 130 °c, 500 °c/minute ramp and air jet cool. The results are presented in Figure 64. It can be seen that a substantial drop in mean SLS strength is observed between 100 °c and 30 °c of approximately 0.3 to 1.9 MPa, this highlighted the importance of bondline temperature upon SLS strength with partially cured 3M™ SA9816. An exponential decay fit produced an r^2 of 94 % and residual error σ of 0.158 MPa.

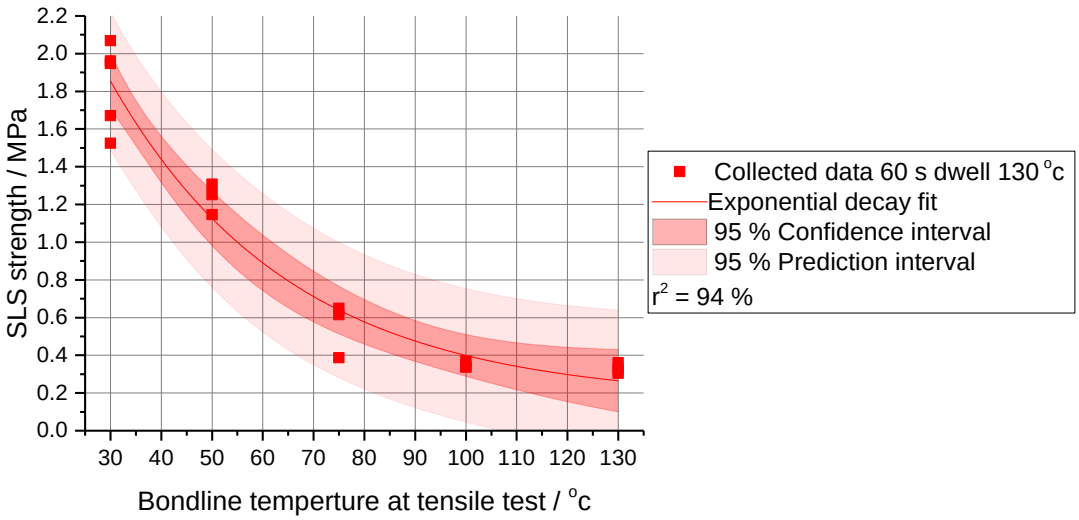

Figure 64 3M™ SA9816 relationship between bondline temperature and SLS strength following partial cure at 130 °c for 60 s, TS-CFRP/AL

As a final investigation with 3M™ SA9816 it was important to understand whether the initial induction cure of 60 s at 130 °c with a 500 °c/minute ramp to achieve SLS strength would reduce the final, fully cured, properties of the joint. Induction curing was also performed for 60 s dwell at 110 °c, 130 °c and 140 °c. The range was used to highlight the effect of joint induction cure temperatures upon fully cured SLS strength. Following induction cure specimens were fully cured at 130 °c for 1 hour in the oven as per the manufactures recommendations, alongside a batch of identical oven cured only specimens. The paired t-

test was used to analyse the data, comparing the induction heated specimens to the oven only cured benchmark. This was performed to identify whether there was a statistically significant mean change in joint strength.

Table 26 shows using the paired t-test to 95 % confidence interval that following induction cure at 130 °c or lower temperature and a subsequent oven cure cycle, there is no apparent loss of SLS strength when fully cured compared to benchmark samples without a prior induction cycle. The oven cured benchmark samples were loaded into a preheated oven for one hour at 130 °c, following recommendations from the adhesive manufacturer (98). Following induction cure with a 140 °c dwell a statistically significant mean reduction in sample means of 3.35 MPa was observed increasing to 6.35 MPa at the extreme of the 95 % confidence interval following an oven cure cycle compared to the benchmark samples only cured with an oven cycle. This was attributed to outgassing of the adhesive, resulting in porosity and low joint strength.

Test no	Cure condition	Sample mean μ/ MPa	Sample standard deviation σ / MPa	Paired – T Δμ / MPa	Paired – T 95 % CI, Δμ Upper / MPa	Paired – T 95 % CI, Δμ Lower / MPa	P value
1	Oven only	16.06	1.26				
2	110 °c, 60 s + oven	16.85	1.06	0.787 (2-1)	2.27	-0.70	0.214
3	130 °c, 60 s + oven	16.49	1.49	0.427 (3-1)	-1.78	2.64	0.620
4	140 °c, 60 s + oven	12.71	3.00	-3.35 (4-1)	-0.35	-6.35	0.036

Table 26 Paired t-test SLS strength comparison of oven cured and induction + oven cured 3M™ SA9816, TS-CFRP/AL

The adhesive outgassing created at the higher dwell temperature can be seen by comparing Figure 65 and Figure 66. In Figure 66 large proportions of material failure were observed following 130 °c or lower temperature induction cure with a subsequent oven cure. Sample 1 and 2 in Figure 66 show some porosity, thought to be a result of slight variations in thermocouple position and some overheating of the joint from target during the ramp phase. Contrastingly in Figure 65 a porous failure surface can be seen following 140 °c induction cure and subsequent oven cure. Clearly the generation of a porous failure surface can result in a much reduced fully cured joint strength.

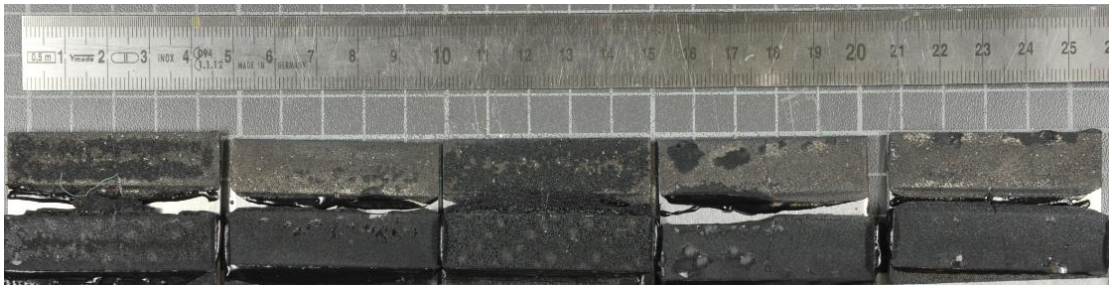

Figure 65 Failure surface 3M™ SA9816, 140 °c induction cure plus oven, TS-CFRP/AL

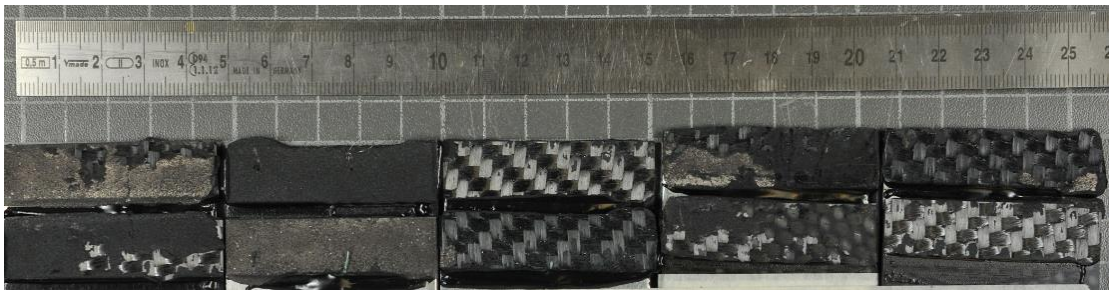

Figure 66 Failure surface 3M™ SA9816, 130 °c induction cure plus oven, TS-CFRP/AL

4.3.4. Sika 7666/522

Using a similar procedure to that in section 4.3.2 and 4.3.3 a three level, three factor, partially factorial Taguchi design of experiments was produced to identify the main effects of dwell temperature, time and ramp rate for Sika 7666/522 adhesive. Dwell temperatures of 100, 110 and 120 °c were used based on the previous investigations, TGA data and discussions with the adhesive manufacturer. Dwell times of 30, 45 and 60 s were used with three ramp rates 100, 250 and 500 °c/minute. Main effect plots highlighted the high degree of SLS strength variablity with this product, a linear model was applied to analyse the variance with respect to the three experimental levels and factors. To the 95 % confidence level no factor was identified as statistically significant within the range of parameters investigated. However, with approximately 90 % confidence dwell temperature appeared to significantly affect SLS strength as seen in the analysis of variance calculations, Table 27.

Whilst the apparent main effect plot for dwell temperature, Figure 67, showed that the mean trend is for an increase in SLS strength to be attributed to an increase in dwell temperature the joint failure modes at 120 °c were undesirable, with high porosity. As shown in section 4.3.3, a porous failure surface was known to correlate with a reduced fully cured joint strength. Thus, for further work 110 °c was the maximum dwell temperature investigated, showing significantly lower porosity. The wide prediction interval highlights the great

uncertainty in making predictions based on this preliminary data alone. Dwell time in the region 30 – 60 s appeared statistically insignificant in influencing SLS strength to the 80 % confidence interval, shown in Table 27.

Source	DF	DoF	SS	MS	F value	P value
Source	Temp (dwell)	2	10.5221	5.2611	2.58	0.101
	Time (dwell)	2	0.9525	0.4763	0.23	0.794
	Ramp	2	1.9145	0.9572	0.47	0.632
Error		20	40.7591	2.0380		
Lack of fit		2	3.4785	1.7392	0.84	0.448
Pure error		18	37.2806	2.0711		
Total		26	54.1482			

Table 27 Analysis of variance 7666/522 initial SLS strength data at partial cure TS-CFRP/AL

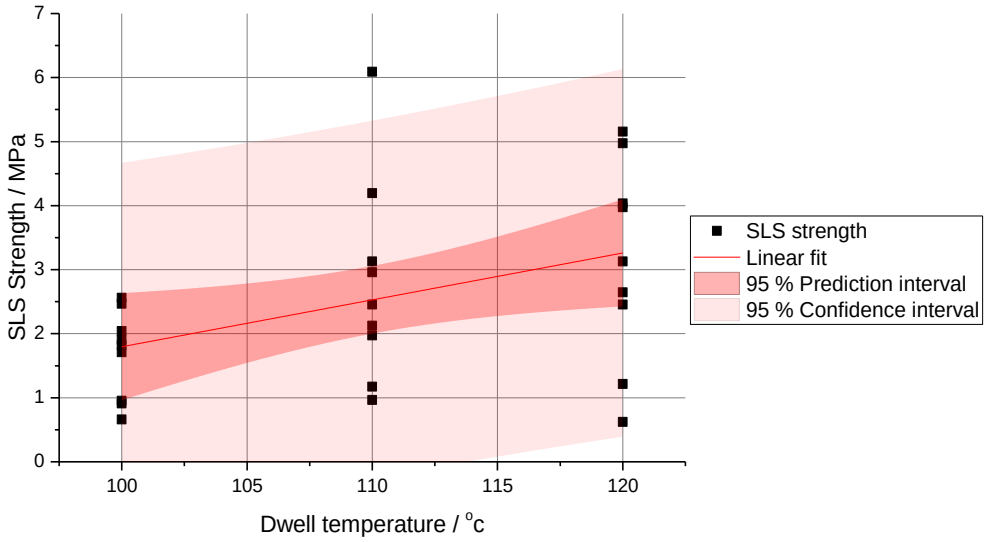

Figure 67 Main effect plot 7666/522 dwell temperature vs SLS strength at partial cure, AL/TS-CFRP, 50 °c tensile test

Further data was collected at the 110 °c dwell temperature between 0 and 90 s dwell time, presented in Figure 68. Two data sets are combined due to uncertainty in the initial data sets and a delay whilst new adhesive was formulated. Consequentially a change in aluminium surface treatment from PT3 to P592 primer occurred combined with a change in TS-CFRP from compression moulded epoxy to an equivalent HP-RTM epoxy resin due to material availability in the later stages of the project. The change in substrate combination was not found to significantly affect the resultant SLS strength to the 95 % confidence level performing an analysis of variance with a calculated probability of P=0.192.

To the 95 % confidence interval Figure 68 highlights the positive relationship between dwell time and SLS strength, however the wide prediction interval highlights the significant uncertainty with this adhesive and experimental methodology, residual error σ=1.62 MPa. This may be related to a large variation in failure mode, generally characteristic of adhesive failure appearing on both the TS-CFRP and AL interface. More extensive surface preparation may be required with this product to reduce the residual error and proportion of adhesive failure mode. This effect was also observed upon oven only cured specimens. The residual error may also be attributed to rapid increases in viscosity of the product during application, increasing viscosity and reducing wetting.

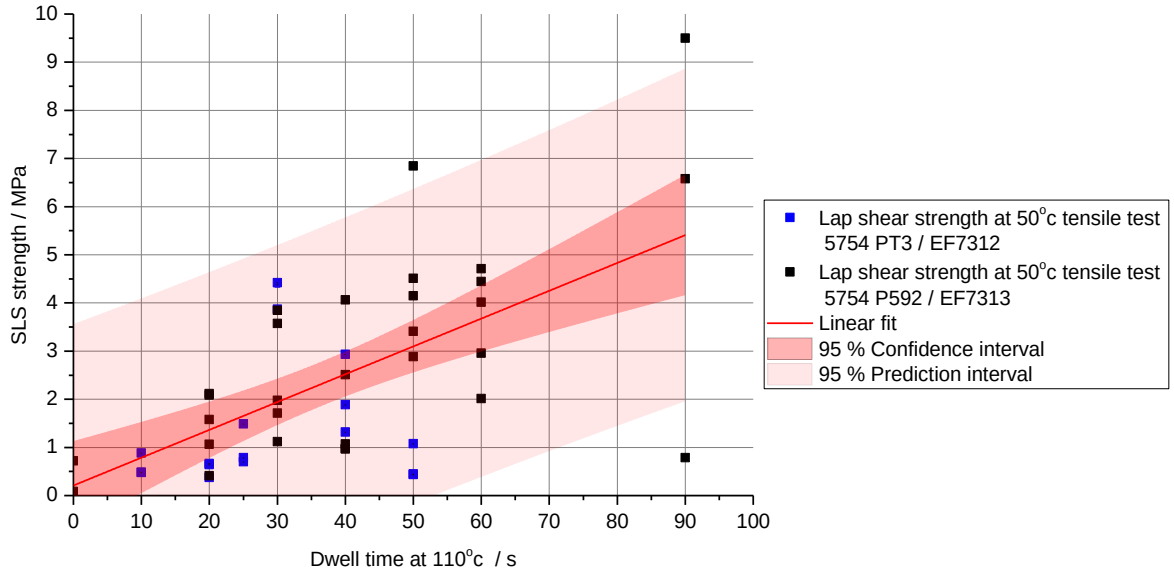

Figure 68 7666/522 dwell time at 110 °c vs partial cure SLS strength, TS-CFRP / AL 50 °c tensile test

Finally, the effect of full oven cured SLS strength following an initial induction cure was investigated. Five specimens were oven cured in a pre-heated oven for one hour at 100 °c as well as batches of pre-induction cured specimens cured for 30 s at 100, 110 and 120 °c respectively. Results analysis using the paired t-test to the 95 % confidence level are shown in Table 28.

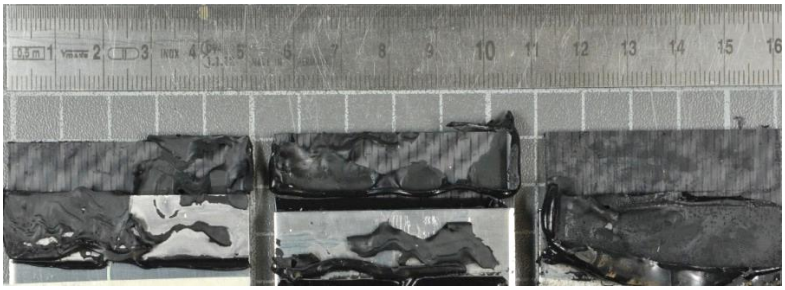

Figure 69 Failure surface EF7313 / P592 5754 AL, predominantly adhesive failure switching between TS-CFRP and AL interface following induction cure

It was observed that a 120 °c induction cure temperate results in a significant reduction in mean SLS strength compared to oven only cured samples, consistent with a change in failure surface observed and increased porosity. Heating to 110 °c caused no statistically significant reduction in mean SLS strength with a mean reduction of -4.39 MPa compared to the oven cured specimens increasing to a maximum of -6.19 MPa following a 100 °c induction cure. The reduction at a lower cure temperature was surprising, combined with reduced porosity on the failure surface and highlights the great uncertainty with this product requiring further development. Due to the significant SLS strength uncertainty with this product the significance of the cooling step was not analysed. It should be noted that this adhesive product was under development at the time of investigation and did not represent a commercially available product.

Test no	Cure condition	Sample mean μ / MPa	Sample standard deviation σ / MPa	Paired – T Δμ / MPa	Paired – T 95 % CI , Δμ Upper/ MPa	Paired – T 95 % CI , Δμ Lower / MPa	P value
1	Oven only	11.03	1.01				
2	110 °c, 60s + oven	9.83	3.30	-1.20	1.90	-4.31	0.343
3	120 °c, 60s + oven	6.64	4.07	-4.39	0.18	-8.96	0.056
4	100 °c, 60s + oven	4.84	1.579	-6.19	-4.055	-8.33	0.001

Table 28 Paired t-test SLS strength comparison of oven cured and induction + oven cured 7666/522

4.3.5. Lohmann DuploTEC® 10400 SBF

Initial investigations using Lohman DuploTEC® 10400 SBF film identified that when the standard 0.04 mm thickness film is laminated to 0.3 mm bond thickness a drying step is required to reduce film solvent content and consequential dispersion of the adhesive within the bondline. This is further discussed within portfolio submission five. To address this

problem, 10400 SBF film laminated to 0.3 mm with embedded glass beads was dried for 1:30 h at 80 °c prior to application in the present work. This temperature is below the product cure onset temperature and the step was assumed to result in negligible increase in the degree of cure, based on discussions with the manufacturer (99). The drying step combined with an oven cure at 140 °c resulted in predominantly cohesive failure with some TS-CFRP material failure upon TS-CFRP/AL substrates. Preliminary investigations suggested that the highest dwell temperature of 175 °c would be most appropriate to maximise SLS strength in under one-minute cycle time. Similarly, ramp rate had previously been identified as insignificant so the fastest rate of 500 °c/minute was used to minimise cycle time. An investigation was performed to identify the rate of SLS strength development following a 175 °c dwell with results plotted in Figure 70, a quadratic fit was identified as the best fit to the experimental data r^2= 87.1 % . A residual error was calculated with σ = 1.38 MPa. Due to the increased amount of data collected below 100 s more certainty can be attributed to this region of data.

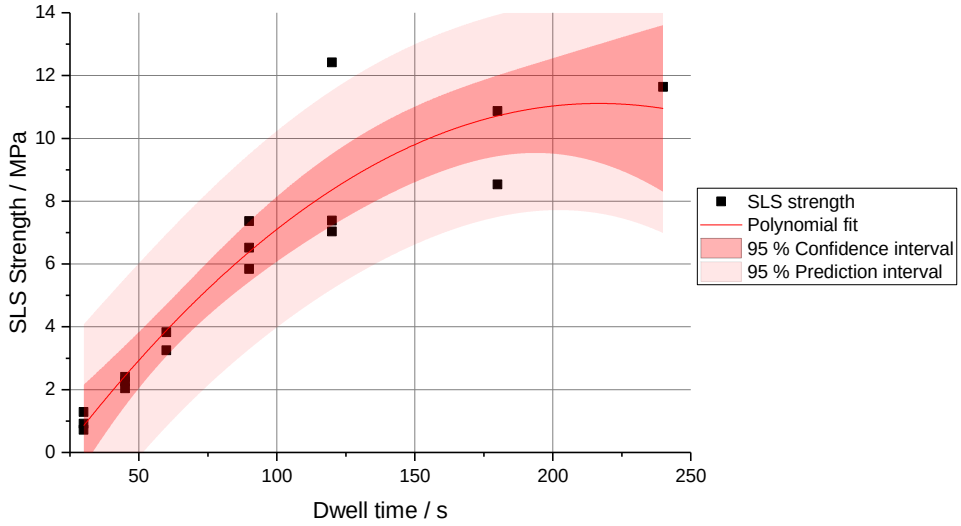

Figure 70 Lohmann 10400 SBF dwell time vs SLS strength at partial cure, TS-CFRP/AL, 50 °c tensile test

Subsequently the relationship between SLS strength and bondline temperature at the point of tensile test was evaluated, this used 5754 AL/5754 AL, PT3 coated substrates due to material avaliability. The bondline temperature at tensile test was varied between 30 °c and the isothermal dwell temperature of 175 °c. Two dwell cycles were investigated, 90 and 45 s at 175 °c, the air jet cool being used to reach the desired tensile test temperature. It was observed within the results in Figure 71 that both the bondline temperature and degree of cure (achieved as a result of increasing dwell time) significantly influences SLS strength over

the range investigated. For example, an approximate 50 % reduction in mean strength is observed between approximately 30 and 75 °c following a 90 s dwell at 175 °c. An exponential decay model was fitted, with residual error σ=0.487 and 1.11 MPa for 45 s dwell and 90 s respectively.

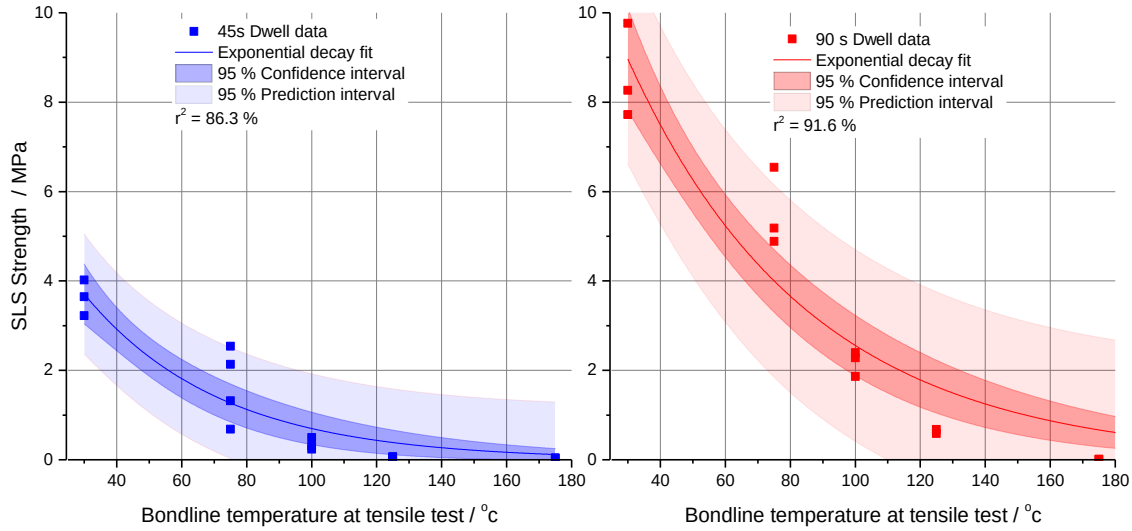

Figure 71 10400 SBF SLS strength at partial cure vs bondline temperate 5754 AL substrates

Finally, the effect of an initial induction cure step upon 10400 SBF with TS-CFRP/AL substrates prior to an oven cure cycle was compared to oven cured only samples in the same way as previous adhesive products. An oven cure of 1 hour at 140 °c was performed, with induction cure performed for 60 s at 175 °c. The paired t-test to the 95 % confidence interval was used to analyse the results, shown in Table 29. The difference in sample means was not found to be statistically significant however this may be a result of a significant increase in the standard deviation as a result of the initial induction heating stage. The difference in sample means was substantial following an initial induction cycle, increasing by up to 7.28 MPa. At the extremes of the 95 % confidence interval the reduction in strength may be as great as 88 % of the mean SLS strength only cured with an oven cycle. This was thought to be a result of residual solvent evaporation during cure and the rapid induction cure altering the distribution and characteristic size of the porous regions of the bondline. This can be seen in the failure surface images in Figure 72 and Figure 73, where a change in failure mode from cohesive and material with an oven cure only to porous cohesive failure with the addition of induction cure.

	Cure condition	Sample mean μ / MPa	Sample standard deviation σ / MPa	Paired – T Δμ (1-2) / MPa	Paired – T 95 % CI, Δμ Upper / MPa	Paired – T 95 % CI, Δμ Lower / MPa	P value
1	Oven only	20.84	2.17	7.28	18.32	-3.75	0.141
2	175 °c, 60 s + oven	13.55	7.11				

Table 29 10400 SBF Paired t-test SLS strength comparison of oven cured and induction + oven cured 10400 SBF TS-CFRP/AL

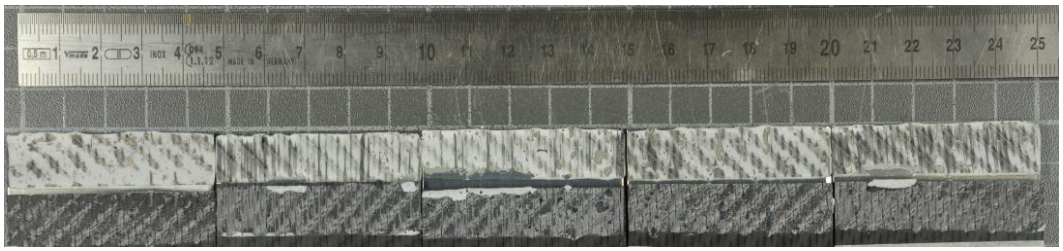

Figure 72 Failure surface Lohmann 10400 SBF oven cure only TS-CFRP/AL

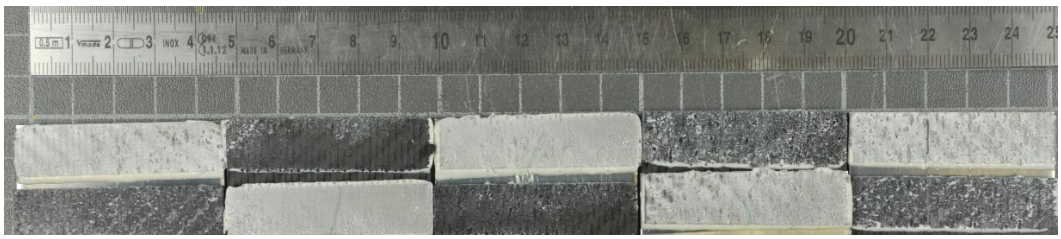

Figure 73 Failure surface Lohmann 10400 SBF induction cycle plus oven cure TS-CFRP/AL

4.3.6. Lohmann DuploTEC® 10625 SBF

A similar investigation was performed using 0.3 mm Lohmann DuploTEC® 10625 SBF film, initially investigating the development of SLS strength at 175 °c between 60 and 300 s dwell time. Previous data collected with DuploTEC® 10630 SBF film had suggested with a 60 s dwell minimal SLS strength would be achieved at dwell temperatures below 175 °c. Glass beads were not added based on previous work and discussions with Lohmann (99). Results are plotted in Figure 74, a linear and quadratic fit were investigated, both achieving an r^2 value of 74 % as such the linear fit was used for simplicity. A residual error of σ=1.09 MPa was calculated. It was observed that the rate of SLS strength development of 10625 SBF is considerably slower than 10400 SBF, seen by comparison in Figure 70.

The effect of bondline temperature upon SLS strength following a 100 and 200 s dwell at 175 °c upon 5754/ 5754 PT3 coated substrates was investigated. A similar trend was observed with 10625 SBF as with 10400 SBF with SLS strength being highly dependent upon bondline temperature and degree of cure. An exponential decay function provided the most accurate

fit to the data with an r^2 value of 95.9 % and 97.8 % after 100 and 200 s dwell respectively. A non-linear regression analysis calculated a residual error σ=0.708 and 0.748 MPa respectively. It was observed with 10625 SBF that the experimental methodology resulted in insufficient application pressure. This had the effect of some regions of adhesive appeared to lack contact with the substrates. This can be seen in Figure 76. As a consequence, additional error was introduced within the experimental results.

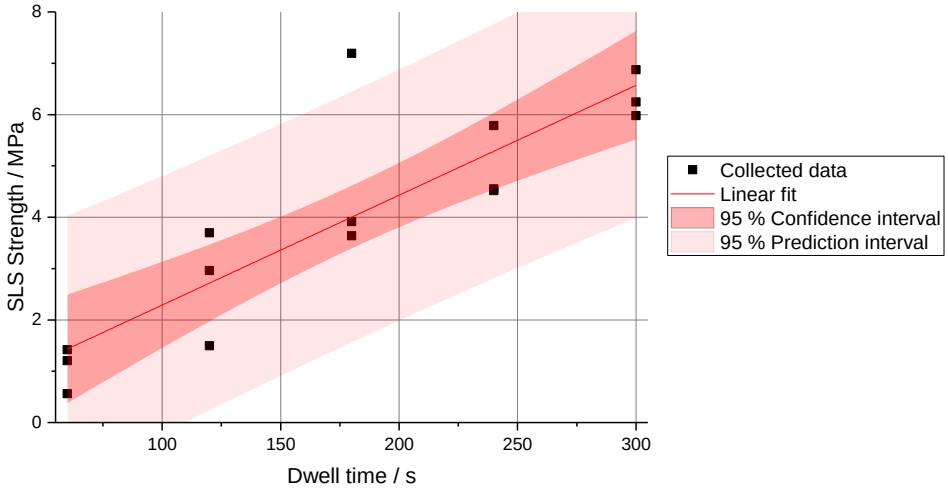

Figure 74 Lohmann 10625 SBF variation in SLS strength at partial cure with dwell time at 175 °c, TS-CFRP/AL, 50 °c tensile test

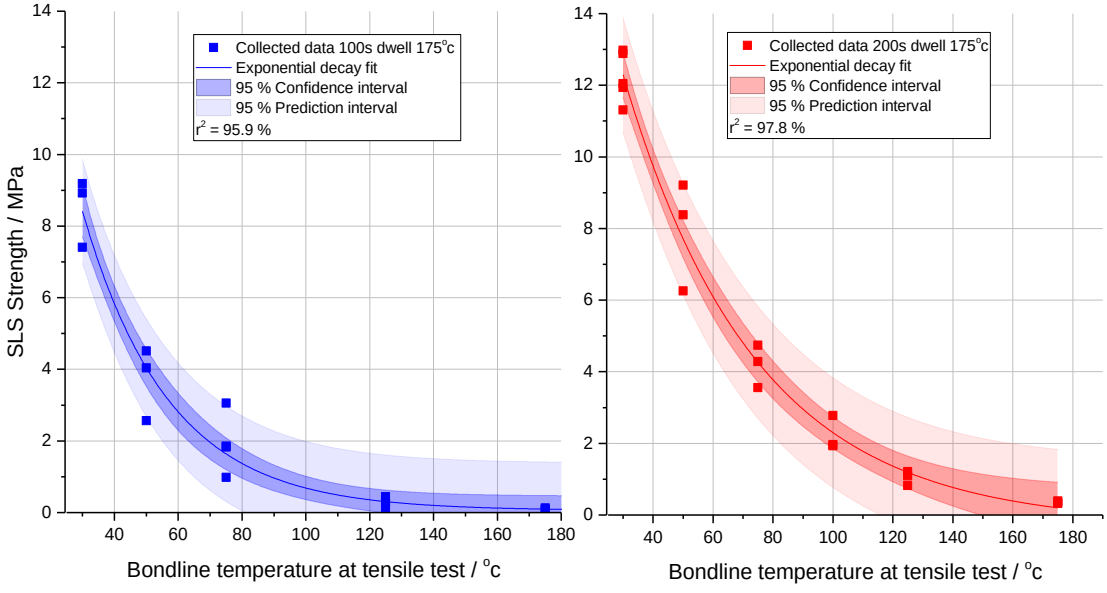

Figure 75 Lohmann 10625 SBF, SLS strength at partial cure vs bondline temperate, 5754 AL substrates

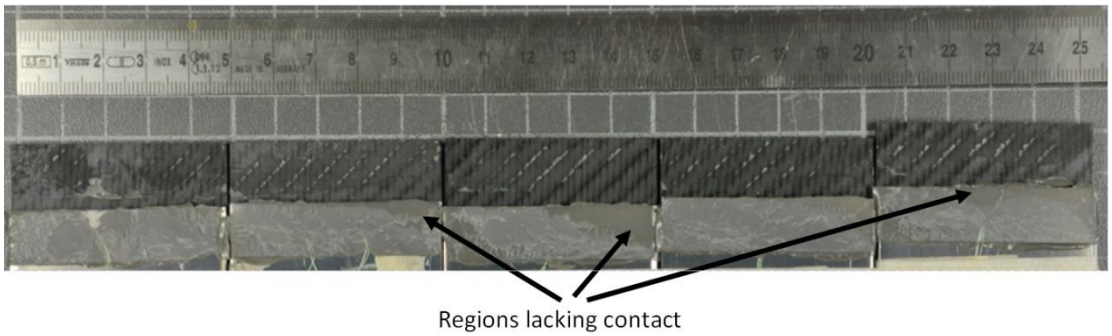

Figure 76 Lohmann 10625 SBF failure surface, 175 °c, 100 s plus oven cure AL/TS-CFRP

10625 SBF adhesive using TS-CFRP/AL specimens was subsequently prepared into lap shear coupons. These were induction cured for 100 s at 175 °c and then oven cured for 1 hour at 140 °c. These were compared to identical specimens which had only been oven cured. Results are presented in Table 30 with the paired t-test used to compare the difference in sample means. The overlap area was corrected for the approximate proportion of adhesive to substrate contact calculated by a visual approximation due to the previously identified issue of lacking adhesive contact within the joint. A mean SLS strength increase of 1.93 MPa was identified with the pre-induction cured specimens compared to the oven cured only specimens. This difference was not found to be statistically significant to the 95 % confidence interval, with the calculated error in mean difference being between -4.11 and 0.26 MPa. It was concluded there is not statistical evidence to suggest the induction cure step reduces the fully cured strength with 10625 SBF adhesive film.

	Cure condition	Sample mean μ / MPa	Sample standard deviation σ / MPa	Paired – T Δμ (1-2) / MPa	Paired – T 95 % CI , Δμ Upper / MPa	Paired – T 95 % CI, Δμ Lower / MPa	P value
1	Oven only	18.26	0.67	-1.93	0.26	-4.11	0.070
2	175 °c, 100 s + oven	20.18	2.23				

Table 30 Paired t-test SLS strength comparison of oven cured and induction + oven cured 10625 SBF, AL/TS-CFRP

4.4. Differential scanning calorimetry (DSC) based cure analysis

In order to gain a greater understanding of the curing behaviour of the adhesive products evaluated within this chapter differential scanning calorimetry (DSC) analysis was performed. The DSC analysis provided information to aid the initial design of optimal cure profiles as well as assist in interpreting the experimental SLS strength results. A further explanation of the process was discussed within section 2.4.3.2. In this case isothermal DSC measurements

followed BS EN ISO 11357-5:2014 performed on a Mettler Toledo HP DSC using aluminium crucibles with a pierced lid. The primary goal was to understand the relationship between cure temperature, time and degree of conversion of the adhesive products to fully cured adhesive. An adhesive mass of approximately 5–10 mg was used in each investigation weighed using a Mettler precision balance. A summary of a selection of the results is presented in this section, with a more detailed analysis presented in portfolio submissions four and seven.

4.4.1. Isothermal methods

Initially isothermal DSC measurements were used to investigate the relationship between degree of cure and time at isothermal temperature. In this case the specimens were loaded into the DSC at 30 °c, the temperature of DSC then ramped up to the specified isothermal dwell temperature at the fastest achievable rate and held for a specified period of time according to earlier results. A second identical run was then performed upon the same sample and the raw data subtracted to correct for calorimeter perturbation caused by the rapid heating process (100). The degree of conversion was then calculated according to the formula; $\alpha = {\Delta H_j}/{\Delta H_{tot,T}} \times 100,$ where α = degree of conversion in % , ΔH_j the part enthalpy of reaction calculated by the area between time = 0 and *j* in j/g . $\Delta H_{tot,T}$ is the total enthalpy of reaction which was calculated by a dynamic DSC scan also in j/g. The dynamic DSC scan was performed from 30 °c until the end of the curing reaction at a rate of 10 °c/minute for a separate uncured sample of the same adhesive. If $\Delta H_{tot,T}$ was less than the total enthalpy calculated at the end of the isothermal run this value was substituted by that from the isothermal technique. In all cases mass normalised heat flow values were used for ease of comparison between samples. The dynamic scan also provides important information on the cure onset and endset temperatures which is advantageous for cure cycle design. Dynamic DSC scan data for each candidate adhesive is presented in Figure 77.

Figure 77 highlights some of the striking differences in cure behaviours between the adhesive products. For example, Sika 7666/522 begins to cure at room temperature with a peak at approximately 55 °c explaining the rapid change in viscosity during application and variability noted in section 4.3.4. Contrastingly PU 1510, Lohmann DuploTEC® 10400 SBF and DuploTEC® 10600 SBF cure much more slowly until reaching an onset temperature of approximately 90, 115 and 145 °c respectably. DuploTEC® 10600 SBF being the 0.6 mm thickness version of DuploTEC® 10625 SBF. Generally only one peak was observed in the dynamic scan with the

exception of 3M™ SA9816 which has two peaks at approximately 85 and 115 °c and two higher peaks at 250 and 280 °c, these were believed to be due to a dual stage cure of the product which is identifiable with the distinct two steps observed in section 4.3.3 Figure 64.

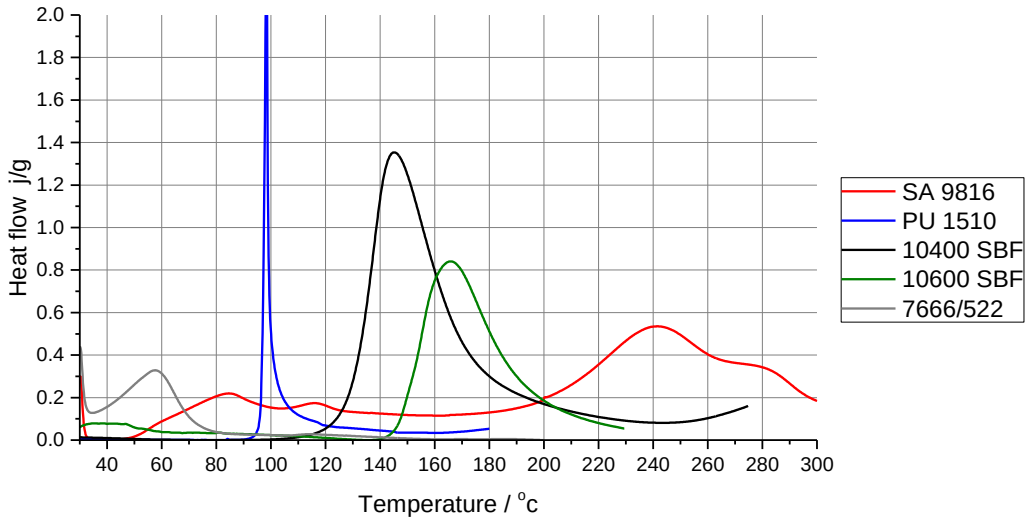

Figure 77 Dynamic DSC scans at 10 °c/minute for candidate adhesives linear baseline subtracted

Degree of conversion vs isothermal temperature plots are shown in Figure 78. Upon first inspection it appeared that PU 1510 has by far the fastest rate of cure, followed by 10400 SBF, 10600 SBF and finally 7666/522. However, several concerns were identified with this method of data colelction. Firstly, for rapid curing products such as 7666/522 a substantial proportion of the reaction may have occurred in the time taken to prepare, weigh, load the sample and start the test. Thus, the loss of exotherm data during this time results in an apparent reduction in degree of cure. It was identified that the sampling rate of 1 sample/s may not be great enough to record all of the data with the fast reacting PU 1510 (101) as such data may be lost resulting in an apparent reduction in final degree of cure. Another consideration is that during the sample ramp to isothermal temperature cure will occur at non-isothermal temperature. For rapid curing products this could result in unreliable data. An alternative method is to load the specimen at the isothermal test temperature and start the analysis immediately after loading. However, this method introduces noise during loading especially using the available HP-DSC with a more complex chamber closing procedure, DSC systems with an automatic sample loader may be beneficial for this approach.

As a final conclusion of the isothermal DSC degree of conversion method, neglecting the considerations previously mentioned, the data is only relevant for the temperature profile

investigated. For example, in a manufacturing environment where there may be a requirement to change the cure temperature or profile, it would be required to repeat the DSC data for an identical thermal profile to establish the exact relationship between degree of cure and the thermal profile. Due to these drawbacks of isothermal DSC data for evaluating degree of cure vs time it was determined than an alternative approach to degree of cure evaluation would be beneficial. As a result, it was identified that model fit approaches may be of much greater benefit to industry than isothermal methods, avoiding these limitations.

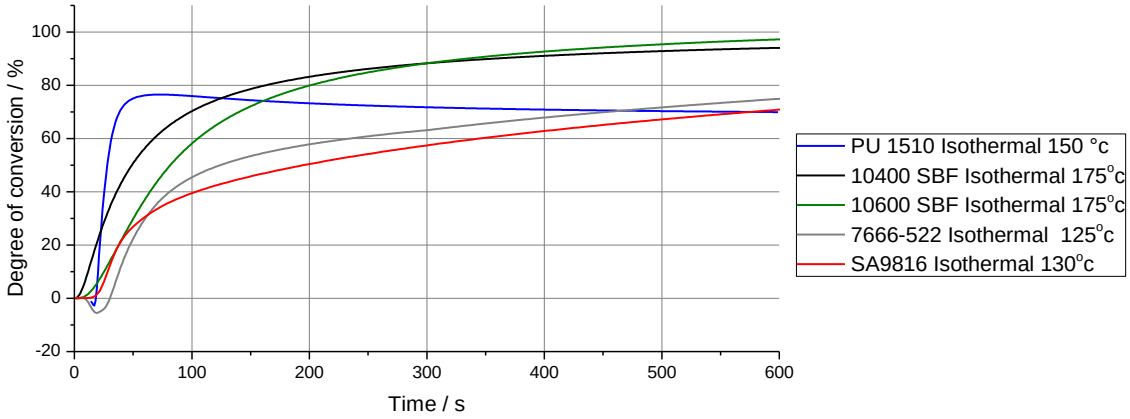

Figure 78 Degree of conversion vs time at isothermal temperature, isothermal DSC method

4.4.2. Model fit methods

The fundamental theory of thermokinetic cure modelling was presented in detail within submission seven. The aim of thermokinetic cure modelling for the present application was to fit a mathematical model to the adhesive reaction rate experimental data that can then be used to predict curing rate for a given thermal profile. The advantage of this process is that should the thermal cure profile change, it is only necessary to re-apply the model, rather than repeat all of the experimental data. Further, using the model, a thermal profile could be designed to provide a specified joint degree of cure during manufacture based on the thermal history of the assembly within the manufacturing process. If the relationship between degree of cure and mechanical properties can be established the required degree of cure for a specified mechanical property can be identified. Thus, the cure model can be used to minimise cure thermal cycle times to achieve the minimum required handling strength and mechanical properties required during manufacture, contributing to manufacturing efficiency gains.

Netzsch Thermokinetcs software was used to perform the cure modelling, benefiting from a library of different model types and the ability to fit and optimise multiple steps for a given reaction of differing configurations. The process fundamentals build on the assumption that the reaction rate $\left(\frac{da}{dt}\right)$ is described by two separate variables; $\frac{da}{dt} = k(T).f(a)$ where $k(T)$ is a temperature dependant rate constant given by Arrhenius relationship and $f(a)$ a reaction model which expresses the rate of a reaction as a function of the extent of the reaction (77). Arrhenius's relationship is expressed by; $k(T) = Ae^{-\frac{E_A}{RT}}$, where k = reaction rate, A a pre-exponential factor, R the universal gas constant, T temperature and E_A activation energy. DSC data was collected for each adhesive model produced using a dynamic scanning method of at least four heating rates, for example 2.5, 5, 10 & 20 °c/minute. Data was normalized by sample mass and a linear baseline subtracted.

Initially model free analysis using the Friedman method (102) was applied to the DSC data to identify the fundamental Arrhenius constants E_A and A, providing starting parameters for the model fitting. In the majority of cases multi step models were identified as the most appropriate fit for the adhesives investigated. The Netzch software uses a 6th degree Range Kutta method to optimise the model parameters for each step and model selection (102). The deviation of model response to the collected DSC data was compared and the most accurate fit selected. A summarised example of the model fitting to Lohmann 10400 SBF film is presented, with the process being similar when applied to other products. A more detailed process description of the process is presented within portfolio submission seven.

A model free Friedman analysis was initially applied to 10400 SBF film, identifying start parameters for E_A and A. Subsequently a nonlinear multiple regression was used to fit various models and step combinations to the experimental data. The optimum model fit was found to be a two-step process, with first step modelled by a Prout-Tompkins autocatalytic reaction of the form; $\frac{da}{dt} = Ae^{-\frac{E_A}{RT}} \times E^n \times P^a$ where E = concentration of educt and P = concentration of product the optimised model parameters are presented in Table 31. The second step which followed the first was modelled by an nth order step of the form; $Ae^{-\frac{E_A}{RT}} \times E^n$.

Step	Parameter	Optimum value
1	$\log A$	9.47
1	E_A	87.29
1	Reaction order, n	1.07
1	Exponent, a	0.62
2	$\log A$	2.95
2	E_A	39.94
2	Reaction order, n	1.52
1	Foll Reaction.1	0.34

Table 31 Optimised parameters two-step model fit 10400 SBF

The fitted two-step model along with collected DSC data is shown in Figure 79 it can be seen that there is a high degree of correlation between the experimental data and the fitted model. To validate the model, the degree of conversion vs isothermal temperature data was compared to Isothermal DSC measurements of the same adhesive shown in Figure 80, collected using the method discussed in section 4.4.1.

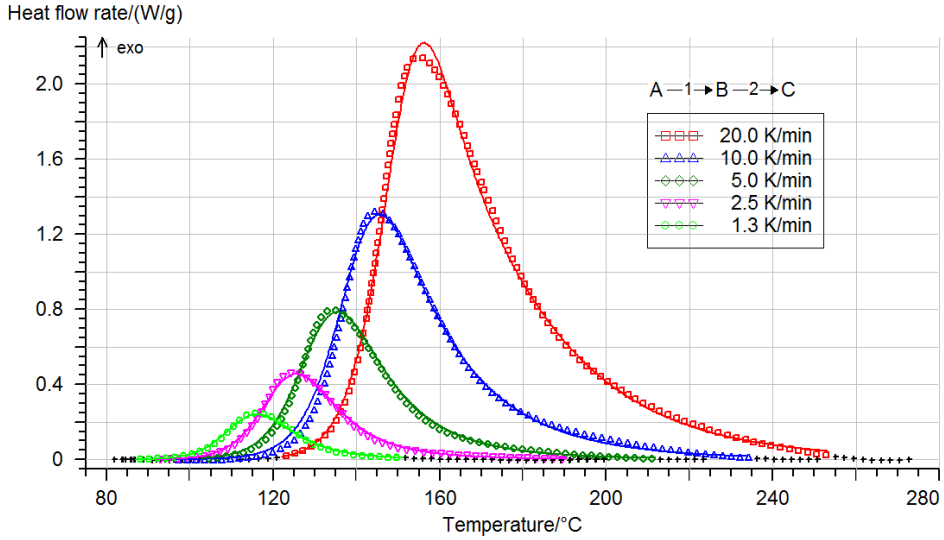

Figure 79 Netzch Thermokinetics model fit 10400 SBF two-step model. Step 1 Prout-Tomkins autocatalytic, step two nth order. Solid lines represent model, symbols experimental data.

It can be seen in Figure 80 that a very similar profile is produced between the model fit data and the isothermal calculated data. There is however a significant time lag between the model data and collected data. This was attributed to the ramp rate of the DSC deviating from the manufacturers stated value of 300 °c/minute and thermal conduction within the crucible and adhesive, although this would require further work to validate this conclusion. Based on the high degree of curve correlation the model was accepted as accurately representing the curing process. Finally, the model was used to predict the evolution of cure over the induction

cycle used within section 4.3.5, Figure 70. Following a 500 °c/minute ramp to 175 °c followed by an isothermal dwell. This enabled the relationship to be identified between the SLS strength upon CFRP/AL substrates at 50 °c test temperature with degree of conversion as shown in Figure 81.

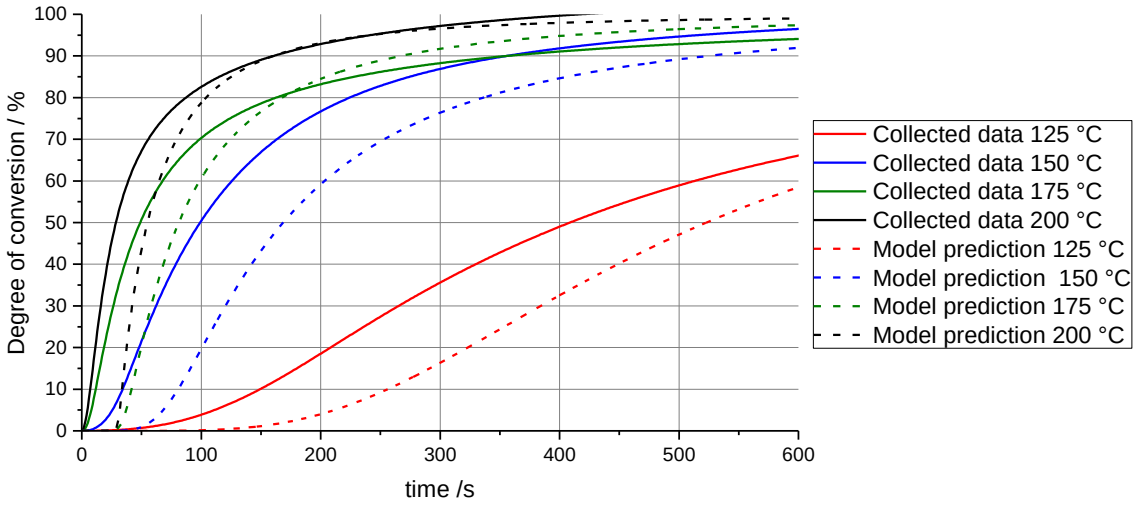

Figure 80 Comparison between collected isothermal DSC data and model fit data for 10400 SBF adhesive

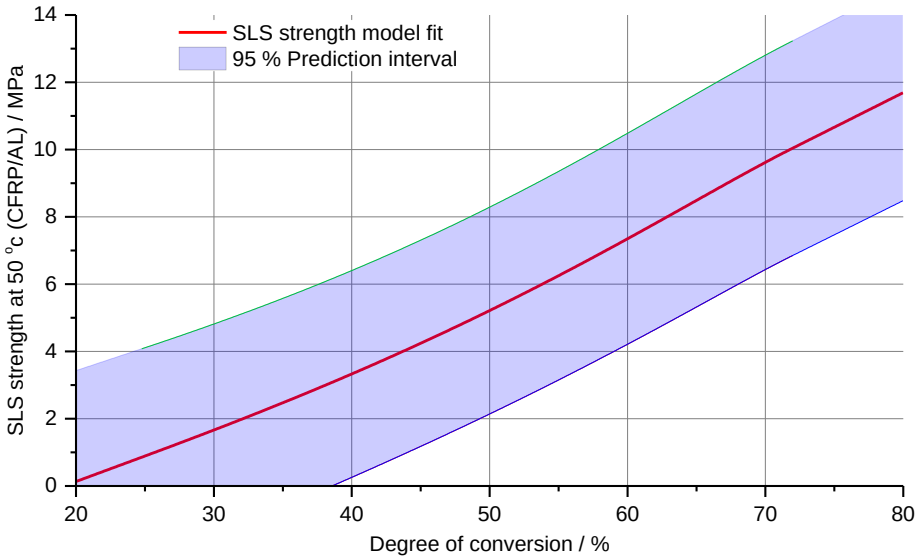

Figure 81 Relationship between 10400 SBF SLS strength and degree of conversion

Relationships such as Figure 81 could be used to enable optimal thermal cycle times to be designed, in order to generate a specified component handling SLS strength or other mechanical properties such as peel strength or creep behaviour. Extension could also be made to encompass consideration relating to substrate combinations and test temperatures. Thus, manufacturing cycle time can be reduced as well as the required energy input during a pre-

cure stage. Further evaluation of the manufacturing thermal cycle could be performed to ensure sufficient joint strength is achieved through later heating cycles such as a paint oven bake to meet the product service requirements. As such, cure cycles could be reduced to the minimal required to save manufacturing time and cost. Should the joint requirements change, a rapid model re-application would be able to identify the change in cure cycle required to meet the specification, avoiding repeated mechanical testing and extensive DSC evaluation.

4.5. Adhesive evaluation conclusions

Section 4.2 and 4.3 provided valuable information for a number of selected adhesives, from leading manufacturers, relating achievable SLS strength to thermal cure profiles. Knowledge of these relationships is a vital predecessor towards the manufacture of high-volume, primary bonded multi-material joints and a number of key considerations were highlighted to Jaguar Land Rover. Considerations such as the relationship between SLS strength and optimal dwell time at isothermal temperature, bondline temperature at the point of tensile test and the retention of full cured strength following full cure were also evaluated. Table 32 highlights some of the key differences between the products investigated.

Preliminary data showed that electromagnetic induction heating can be successfully applied to CFRP/CFRP substrates to accelerate adhesive cure based on the results shown in section 4.2. It was identified however, that uneven temperature distribution within the adhesive bondline led to significant variability in experimental joint strength results. This became especially apparent when induction heating smaller sized CFRP coupons with the available single sided coil, where significant hot spots were identified around the coupon edges. For the present work a supplier had been used to design and manufacture induction heating coils, however the supplier's primary experience was with metallic heating rather than CFRP.

To mitigate against the effect of uneven temperature distribution when heating CFRP with the available coils, later development work at coupon level focused on multi-material bonding with CFRP/AL substrates. The improved bondline temperature distribution when heating the multi-material joint enabled more accurate optimisation of adhesive cure parameters for handling strength development. The implication is however, that with further optimisation of induction coil design CFRP/CFRP induction heating for accelerated adhesive cure would be equally feasible upon larger geometry CFRP components. It was identified that for further

work, it would be necessary to apply a more rigorous approach to the design of CFRP induction heating coils, compared to that used for metallic coils. This may involve multi-physics simulation packages and consider the CFRP fibre architecture and component geometry surrounding the joint.

It can be seen in Table 32 that following a 30 s dwell the greatest mean SLS strength is achieved by PU 1510 of 8.84 MPa followed in the order of 7666/522, 10400 SBF and 3M™ SA9816. However, both 7666/522 and 10400 SBF have a 95 % prediction interval of zero SLS strength after 30s dwell indicating there is considerable uncertainty whether any handling strength will be achieved. The smaller prediction interval of 3M™ SA9816 compared to these alternative products is an advantage in terms of joint strength prediction resulting in a non-zero 95 % prediction interval after 30 s, however the mean and maximum strength identified of 0.41 and 0.65 MPa is lower after a 30 s dwell compared to 10400 SBF, 7666/522 and PU 1510. Further, both PU 1510 and 3M™ SA9816 had the lowest residual error values of all the adhesive products tested. It was concluded that for an automotive manufacturing application repeatability and confidence may be more important than maximum possible joint strength in the introduction of primary bonded structures. With the possibility to some extent to design the joint around the suitable adhesive to compensate for lower ultimate mechanical performance.

Following a 60 s dwell 10400 SBF showed the second greatest mean of 3.89 MPa SLS strength behind PU 1510 at 8.84 MPa, however the loss of strength as a result of induction cure with 10400 SBF needed to be resolved before further work was completed and the residual error reduced. Subsequently to commencing this investigation Lohmann DuploTEC® 10400 SBF was replaced with an improved formulation DuploTEC® 10410 SBF, however the original version was used within the experimental work for continuity. The SLS strength of 10625 SBF was greater than 3M™ SA9816 at 1.43 compared to 1.21 MPa however the greater residual error of 10625 SBF resulted in a zero 95 % prediction interval after 60 s dwell. The factor of reduced bondline contact discussed in section 4.3.6 is likely to significantly contribute to this error as a result of inadequate pressure application, resolving this requires further work. Sika 7666/522 demonstrated the highest residual error of all of the products investigated, however the maximum 95 % prediction interval of 6.97 MPa indicates the products potential if the residual error can be reduced, possibly through failure mode optimisation. For the present work, manual application to a long bondline would become challenging due to the

limited open time of the product. This factor combined with the high variability in SLS strength observed in section 4.3.4, resulted in the product not being taken through to further work.

PU 1510 and 3M™ SA9816 were taken forward for further, component level work. This was due to their low residual error as well as 3M™ SA9816 showing no statistical strength loss as a result of induction cure and rapid strength generation. PU 1510 showed a relatively small strength reduction as a result of induction cure, approximately 8.6 % on average, combined with exceptionally fast strength development. Whilst the polyurethane products have an oven cured SLS strength close to, or in some cases below the 12.5 MPa Jaguar Land Rover specification (65) there rapid cure properties and low residual error in the case of PU 1510 may provide a greater advantage, aiding in the justification of a product with a lower ultimate joint strength for improved repeatability and manufacturing benefits.

Product	**30 s dwell, tested at 50 °c**		**60 s dwell, tested at 50 °c**		Residual error, σ / MPa	Strength reduction with induction?
	Mean SLS strength / MPa	95 % PI / MPa	Mean SLS strength / MPa	95 % PI / MPa		
3M™ SA9816 130 °c dwell	0.41	0.17 – 0.65	1.21	0.97 – 1.46	0.105	No
PU 1510 150 °c dwell	8.84	7.77-9.90	8.84	7.70 - 9.97	0.460	Yes 8.6 % – 16 %
10400 SBF 175 °c dwell	0.86	0.00 - 4.08	3.89	0.83 – 6.96	1.38	Yes 0 % – 88 %
10625 SBF 175 °c dwell	0	0	1.43	0 – 4.02	1.09	No
766-522 110 °c dwell	1.94	0 – 5.20	3.67	0 .38–6.97	1.6	Yes at 110°c , 0 % - 81 %

Table 32 Adhesive SLS strength generation evaluation based on regression models following induction cure only when tested at 50 °c, TS-CFRP/AL

It was identified that with partially cured epoxy adhesives that bondline temperature is significantly influential upon handling strength. This is highly important for primary bonded vehicles within production scenarios. For example, when a vehicle entered the paint oven adhesive strength could drop significantly, until degree of cure increased resulting in structure distortion under load. To validate the significance of this further information of the production cycle would be required, including the complete production temperature cycle and loading requirements during that cycle. Due to the immaturity of high-volume primary bonded structures within Jaguar Land Rover this information was not available at the time of

investigation. Knowledge of the bondline temperature and SLS strength relationship, however, has highlighted to Jaguar Land Rover that this is an important consideration in the design of primary bonded structures.

Another consideration is the relatively small temperature processing window with a number of adhesives between maximal cure development and excessive porosity, reducing final strength. Where bondline temperature distribution is known to vary during the heating phase this is an important consideration if fully cured strength is not to be lost. Thus, for any production requirement the development of heating coils which achieve near uniform temperature distribution is important if adhesive performance and cure cycle times are to be optimised.

In summary, the following were concluded;

- The maximum SLS strength of all the products investigated was 8.84 MPa after a 30s dwell at 150 °c with PU 1510 although a shorter dwell time is possible. This highlights the rapid cure cycle which can be applied to a primary bonded structure within industry.

- Whilst a number of products can deliver high mean SLS strength, adhesive products and methods which can assist in reducing residual error may be of greater importance than maximum joint strength alone. This is important to improve confidence in primary bonded structure manufacturing methodology and enable an accurate prediction of joint strength. This is vital if primary bonded structures are to be adopted within the high-volume automotive industry.

- Ensuring the initial induction heating step does not compromise the final joint strength following a secondary curing cycle is an important consideration. Reduction in full cure strength was observed with a number of candidate adhesives, highlighting this conclusion. Control over the heating phase and temperature deviation from the target was shown to be important to avoid this strength reduction.

- Bondline temperature was identified to significantly affect joint handling strength for a primary bonded, partially cured structure. This is an important consideration for industry. As the temperature of the structure changes through the production cycle the joint handling strength may also vary possibly leading to structure deformation or in the

worst-case failure. It is important that this strength loss is accounted for in the manufacturing process design for a primary bonded structure.

- Improving the joint temperature distribution when induction heating CFRP/CFRP components is critical in reducing joint strength variability. This remains an area for further work.

Chapter five carried forward the work developed within this chapter with two adhesive products, 3M™ SA9816 and Henkel PU 1510. The aim was to demonstrate how the developed knowledge of rapid adhesive cure, using electromagnetic induction heating for handling strength generation, could be applied to a full-sized demonstrator assembly.

5. Chapter five – Demonstrator component

A full scale automotive sub-assembly was selected in conjunction with Jaguar Land Rover, to demonstrate the application of the induction curing technologies presented in chapter four to a full-sized CFRP automotive joint. The work primarily aimed to highlight the achievable cycle time and rate of handling strength development for a primary bonded automotive joint, proving the validity of the joining technique developed throughout this project. The sub-assembly consisted of a sill to floor joint from a demonstrator Jaguar vehicle and is shown in Figure 82. Previous developmental adhesive bonding of the same components within Jaguar Land Rover had been performed using the much slower curing Sika 490c adhesive used within chapter three. This adhesive was designed for a minimum cure cycle time of 30 minutes at 85 °c (83), as such this assembly method was not suited to high-volume manufacture. The work presented within this chapter provides an alternative assembly technique suitable for high-volume manufacture, with a target of under 1-minute cycle time for handling strength development. Following the component level testing the business case for the proposed joining technique was explored, presented in section 5.5. This work illustrated how a production scale assembly line may look and compared the costs of the proposed technique to an existing assembly technique used by Jaguar Land Rover.

Two adhesives, 3M™ SA9816 and PU 1510 adhesives were used within this chapter for the demonstrator component testing. Both adhesives were induction cured to generate handling strength within the floor to sill joint, based on the adhesive evaluation conclusions in section 4.5. The induction cure step was designed to provide a degree of initial adhesive cure, in order to generate the handling strength required during manufacture. Full cure would be expected to take place at a later stage of manufacture such as a paint oven bake, this is already an established process for many automotive hem flange adhesive bonding applications (103). Additionally, many 2K adhesives will cure at ambient temperature with time. As such, it may also be feasible for any remaining cure, not generated during the induction cycle, to be developed over time at ambient temperature before the vehicle is put into service. Once the adhesive had been induction cured, according to a specified heating profile for each adhesive, a bespoke test method was applied. A predominantly shear load was applied to the floor to sill joint using a servo-hydraulic test machine and a custom designed fixture. This aimed to test the developed joint handling strength following the induction cure cycle, simulating a load being applied to the assembly during the manufacturing process.

Throughout the component level testing 3D digital image correlation (DIC) was used to track the joint movement during load application. This validated whether the adhesive joint was able to resist the applied load without excessive deformation. Significant deformation would have indicated the joining method unsuitable for high volume manufacture, resulting in assembly tolerance issues or in the worst case, total failure of the joint.

Figure 82 CFRP Floor / sill demonstrator component shown assembled

It should be considered in a manufacturing environment, that the load cases applied to any joint are often highly complex and unlikely to be represented by a shear loading alone. Other load cases which may apply include peel and tension which can be visualised in section 2.3, Figure 18. In order to demonstrate the application of induction cured, primary bonded joints, within this chapter the load case was restricted to predominantly shear loading. This enabled a direct compaction to the work performed in chapter 4, where shear loads were primarily considered. Other load cases were considered outside the scope of this work. Before implementing a primary bonded joining technique into a production environment, the load cases applied to specific component geometry must be considered. Subsequently, further analysis would be required to ensure sufficient strength is developed during the induction heating phase to avoid structure distortion due to the increased complexity of load cases.

5.1. Demonstrator component test methodology

A handling strength test was designed to apply a shear load to the joint between the floor and sill component. The test primarily aimed to validate whether sufficient handling strength could be generated using the induction curing process to maintain the geometry of the sub-assembly during manufacture, without additional fixtures to support the assembly. The geometry of the overlap joint between the floor and sill is show in Figure 83.

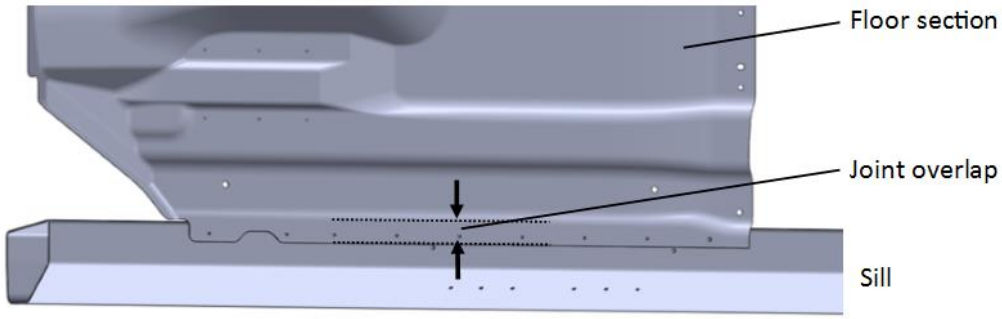

Figure 83 Demonstrator component CAD overlap joint geometry. Orientated as viewed from below the BIW

A bespoke test fixture was designed to apply the shear load to the joint. A detailed description of this test fixture and its design methodology is given in section 5.1.3, with a brief description presented within this section. An illustration of the test fixture can be seen in Figure 84. The floor section shown in Figure 82 was sectioned to fit within the tensile test machine, the complete assembly being too large. The sill was fixed to the steel I beam using two 50 mm ratchet straps, placed at either end of the sill. In later tests the sill was also bolted to the fixture, more details on the sill attachment to the fixture are provided in section 5.1.3. During the test load was applied through the tensile test machine grips to the pull plate. The pull plate was bolted through to the mounting plate which was bolted through bonded tabs to the floor component. The mounting plate aimed to distribute the applied load across the floor section, preventing undesirable CFRP failure modes associated with mechanically fastened joints.

A loading rate of 20 kN/minute was applied to the joint in all tests. This simulated a load being applied to the assembly in a production situation. For example, when the structure is lifted from one area of the plant to another and a particular joint has to support the weight of the structure. In all tests a Zwick 250 kN servo-hydraulic test machine was used in load control mode with a maximum load applied to the joint in any test of 20 kN. The load control mode

ensured a specified tensile load profile was applied to the joint during the test. The load profiles applied to the joint are presented in detail with the results in section 5.2. Position limits were also applied to prevent excessive movement of the test machine crosshead, should the joint break.

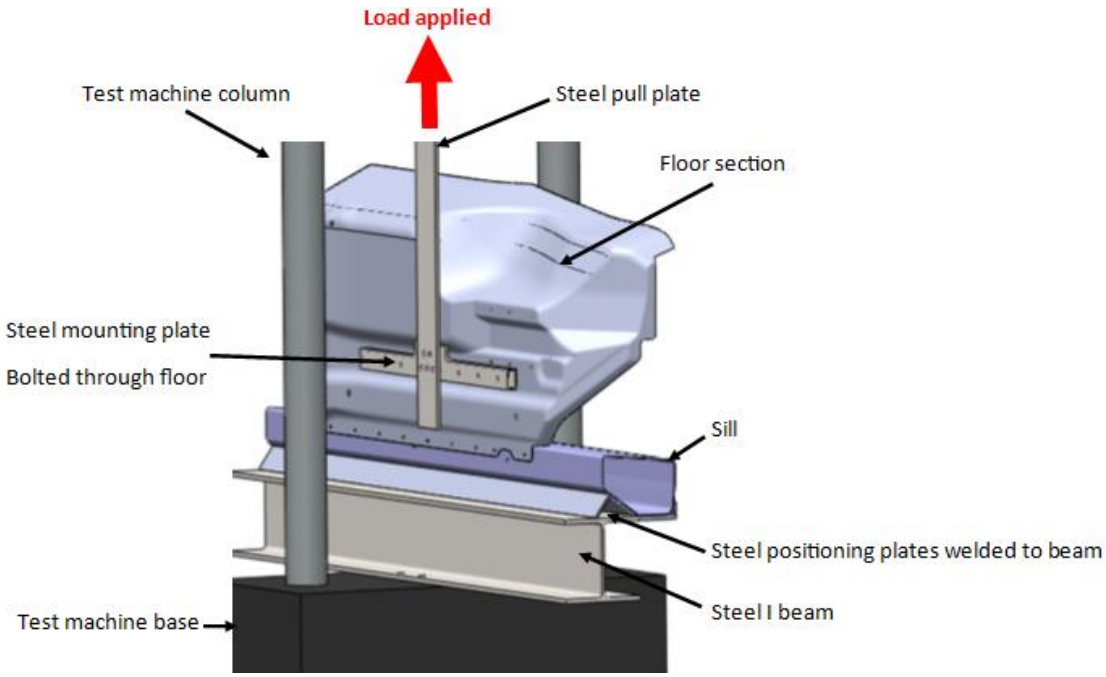

Figure 84 CAD model of experimental fixture

The CFRP floor and sill components were produced from an TS epoxy matrix, reinforced with a NCF carbon fibre similar to that used in section 3.2 and 4. The floor component was produced using a HP-RTM method with Marbocote W1141 mould release applied during moulding. The sill was produced using a pultrusion method. Due to some uncertainty regarding the surface contamination which may be present upon the components, a hand abrasion using a light 3M Scotchbrite pad was applied to the adhesive bondline prior to adhesive application. This combination of pre-treatments was identified as most suited to removing surface contamination based on the surface contamination results from section 3.2.1. This abrasion process was also predicted to reduce the appearance of adhesive failure mode with PU 1510 adhesive as seen on some specimens in section 4.3.2. Following abrasion, an IPA wipe was applied to the bondline in order to remove the abrasion debris and any remaining contamination.

The overlap area of the joint shown in Figure 83. The overlap was reduced to 8 mm from the design overlap of approximately 28 mm, using non-stick PTFE tape to reduce the failure load of the joint, this procedure is detailed further in section 5.1.1. Based on the calculated joint overlap area, the predicted failure load of the sub-assembly joint was calculated in section 5.1.2 for both 3M SA9816 and PU 1510 adhesives. Glass beads of 0.3 mm diameter were mixed into both adhesives prior to the test. The induction heating cycle parameters used to cure the adhesives are also detailed in section 5.1.2. The selection of adhesives and optimal cure parameters were based on the conclusions of chapter four presented in section 4.5.

The TS-CFRP assembly joint was induction heated using the longest available coil, in this case the 180 mm single sided coil used within section 4.1 and seen in Figure 85. The coil was stepped along the bondline performing the cure cycle over a calculated effective length of the coil before being moved to the next region of the bondline. The effective heating length of the coil was calculated in section 5.1.4 at 120 mm, less than the full 180 mm length of the coil. This was due to uneven temperature distribution when heating CFRP with the 180 mm coil. The stepping process is illustrated in Figure 85. An alternating pattern was used to reduce the severity of heat build-up when curing a region adjacent to one previously cured.

The possibility of a coil running the length of the floor to sill joint was investigated, as would be intended in an industrial application. However, this was not possible using the available induction generator. With alternative, larger induction heating equipment this may be possible. Induction coils in the order of several meters are frequently used in hem flange heating applications. In all cases induction heating was performed for the test specimens using a programmed heating profile, without thermocouple feedback control. This represents the way the system would be required to operate within industry. Initial set up using a feedback controller was performed to establish the required heating profiles, this process is detailed further in section 5.1.4. The coil and transformer, approximately 15 kg, rested on the bondline during induction heating to apply moderate application pressure and help ensure a consistent bondline thickness.

Digital image correlation (DIC) was used to track substrate strain and joint displacements during the test, the methodology of this technique is discussed in more detail within section 5.1.5. The primary aim of this analysis method was to identify the specific displacement of the joint during load application. This would not be possible through monitoring crosshead

displacement of the test machine alone, due to rigid body movements and compliance within the test machine and fixture as a whole.

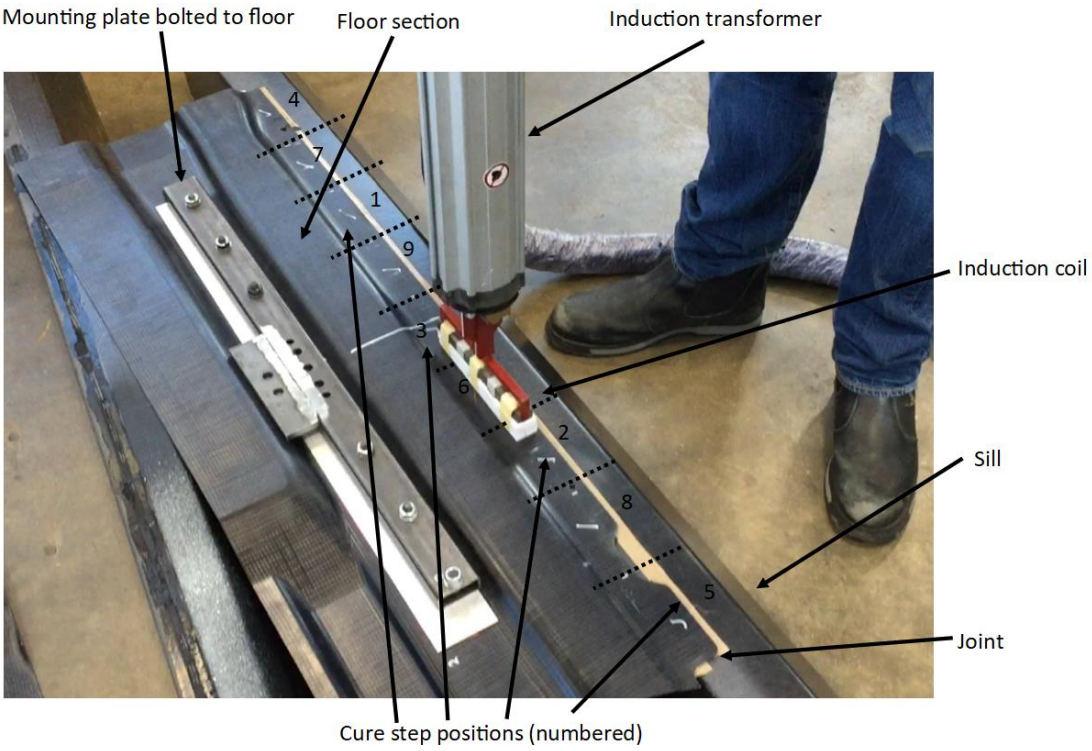

Figure 85 Induction heating of demonstrator sub-assembly joint using a step cure process

Due to space limitations with the addition of the 3D DIC system the assembly was loaded into the test machine following the bonding process. Prior to this, the floor and sill components were loaded into the tensile test machine fixture. Once in the fixture, the joint overlap was aligned using a Vernier calliper, temporarily held into position using large G clamps. The pull plate, which applies load to the floor section was then fixed in the grips whilst bolted to the floor component. See Figure 84 for an illustration of the pull plate mounting. Once the floor and sill were in position, two 8 mm shoulder bolts were then drilled into the CFRP joint to constrain the position of the overlap joint as specified in section 5.1.1. The parts were then relocated and shoulder bolts removed prior to surface preparation and adhesive application.

The joint was then closed and the shoulder bolts re-inserted to preserve the original component alignment during adhesive cure. Induction curing was then performed according to the procedure detailed in section 5.1.4. Once induction cured the shoulder bolts were removed for a final time and the bonded assembly loaded back into the test machine for the experimental test a quickly as possible. The shoulder bolts prevented slipping of the component joint alignment during curing and ensured alignment of the components upon

reloading of the assembly into the test fixture. The bolts were removed prior to the test. In all cases the test was performed within approximately 30 minutes of the induction curing process. As a result, the handling strength produced can be primarily attributed to that developed during the induction cure process.

5.1.1. Joint overlap configuration

Due to the large design overlap between the floor and sill joint, the 20 kN load applied during the handling strength was very unlikely to have been enough to approach the failure strength of the joint with either adhesive used for the investigation. In order to more closely understand the handling strength limitations of a primary bonded joint it was desirable to load the joints to failure. In order to achieve this PTFE tape was used to restrict the joint overlap to 8 mm wide. The joint length between the floor and sill was approximately 1118 mm long with a total design overlap of maximum 28 mm. Restricting the bond width to 8 mm resulted in a total bond area of 7576 mm^2. An illustration of the reduced overlap bond area is shown in Figure 86, where the perimeter represents the total available bond area based on the sub-assembly design. Based on the reduced bondline area and the experimental strength of the candidate adhesives, section 5.1.2 estimates the strength of the joint and the resultant failure load of the assembly.

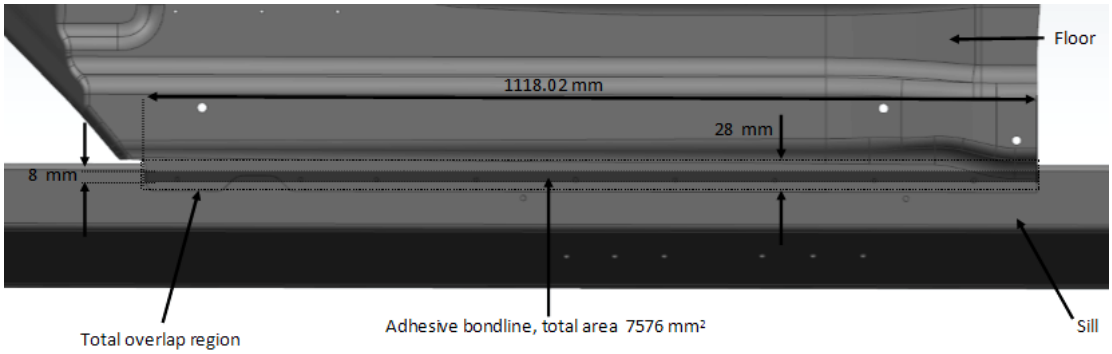

Figure 86 Bond overlap area for demonstrator test geometry, shaded area representing reduced adhesive bond area, dimensions in mm

5.1.2. Adhesive cure parameters and handling strength prediction

Both PU 1510 and 3M™ SA9816 adhesives were used to bond the assembly, with 0.3 mm glass beads mixed in during adhesive dispensing. Based on the data collected in section 4.3, PU 1510 was cured for 10 s at a target dwell temperature of 150 °c and 3M™ SA9816 for 60 s at 130 °c target dwell temperature. A target ramp rate of 500 °c/minute was used in both

cases, the highest ramp rate previously investigated, shown not to significantly effect joint strength. Data collected in section 4.3 was used to estimate the SLS strength which may be achievable following the induction cycle. Due to the substrate combination changing from that of a multi-material combination in later coupon level work, to CFRP/CFRP, as well as a change in test temperature correction factors were applied to coupon level SLS strength to produce an approximate prediction of joint failure strength. This approximation assumes adhesive fails cohesively in all cases. The approximation is seen in Table 33. It should be noted that this approximation ignores many interaction effects which could significantly change the resultant SLS strength and should only be considered as a first approximation. It can be seen that a shear strength of between 2.3 and 3.5 MPa was predicted using 3M™ SA9816 and 9.7 to 12.6 MPa with PU 1510.

	Assumption based on data in;	**3M™ SA9816 60 s, 130 °c**		**PU 1510, 10 s , 150 °c**	
		SLS strength min 95 % PI / MPa	SLS strength max 95 % PI / MPa	SLS strength min 95 % PI / MPa	SLS strength max 95 % PI / MPa
CFRP / AL 50 °c test	Figure 61 & Figure 63	0.97	1.46	7.70	9.97
Change from CFRP / AL to CFRP / CFRP /	Table 19	+ 48 %	+ 48 %	+ 12 %	+ 12 %
Change from 50 °c test to 25 °c test	Figure 62 & Figure 64	+ 60 %	+ 60 %	+ 12.5 %	+ 12.5 %
First estimate of SLS strength CFRP/CFRP, 25 °c test / MPa		2.3	3.5	9.7	12.6

Table 33 First approximation of joint shear strength for induction cured CFRP/CFRP joint upon demonstrator component using PU 1510 and 3M™ SA9816 adhesives

Based on the data in Table 33, the reduced overlap in Figure 86 and assuming predominantly shear loading and uniform degree of cure Table 34 presents an estimate of the predicted failure load of the assembly joint. It can be seen that at 20 kN maximum load, joints bonded with 3M™ SA9816 may be expected to break, whereas PU 1510 would not be expected to break under 20 kN maximum load.

The failure load predictions were used to specify the loading profiles for the test as detailed in the results in section 5.2. Due to the SA9816 adhesive being expected to fail under the maximum applied load, smaller incremental loads were applied up to 20 kN to observe the joint behaviour prior to failure. Whereas with PU 1510 the maximum load of 20 kN was approximately 20–27 % of the predicted failure load in Table 34. As a result, the maximum load was applied to this adhesive for the duration of the test. In later tests the same load profile was applied to both adhesives enabling a direct comparison.

	Units	**3M™ SA9816 60 s, 130 °c**		**PU 1510, 10 s , 150 °c**	
		Min based on 95 % PI corrected	Max based on 95 % PI corrected	Min based on 95 % PI corrected	Max based on 95 % PI corrected
First approximation of SLS strength CFRP / CFRP, 25 °c test	MPa	2.3	3.5	9.7	12.6
First approximation of failure load for demonstrator component	kN	17.4	26.5	73.5	95.5

Table 34 Predicted failure load demonstrator component

5.1.3. Test fixture design

A number of fixture designs and load application methods were considered to constrain the sub-assembly geometry and achieve joint loading primarily in shear. A final fixture design was developed for this work to fit within a Zwick 250 kN servo hydraulic test machine as shown in Figure 84. Finite element analysis (FEA) as well as simply supported beam theory was applied, with the test fixture designed around suitable sized 1.74 m long mild steel I beam. A maximum deflection of 0.4 mm between the central support on the test machine and extreme ends of the beam when loaded to 20 kN was calculated using FEA. The I beam geometry was used due to its high resistance to bending loads and relatively low section weight to lift into the test machine compared to other section geometries.

Maximum beam stress when loaded to 20 kN was calculated using FEA not to exceed 5 % of the beam yield strength. The choice of 20 kN maximum load came from adhesive strength and bondline considerations in section 5.1.2 and a trade-off between fixture size, weight and a relatively safe working load. Further, it was identified that a typical complete Jaguar Land Rover vehicle weighs in the region of two tonnes (4), as a result the load applied to any single

joint during manufacture is very unlikely to exceed this value, equivalent to 20 kN load. Therefore, if the joint can withstand this maximum load case it is likely to meet all handling strength requirements during Jaguar Land Rover during manufacture assuming the same loading conditions and temperature.

The sill was fixed to the beam at each end using 50 mm ratchet straps rated to 50 kN failure load. Plates were welded to the beam to ensure repeatable positioning of the sill and alignment of the central axis of the joint with the central axis of the test machine. The beam was rigidly bolted to pre-tapped holes within the test machine grips using 4 x M16 bolts. Sections of the floor were water jet cut to suitable dimensions to fit within the test machine. A mild steel mounting plate was fabricated to distribute the load through the floor section, this can be seen in Figure 84. FEA analysis and optimisation was performed upon this component to ensure that at a load of 20 kN the yield strength of the mild steel material was not exceeded by more than 70 %.

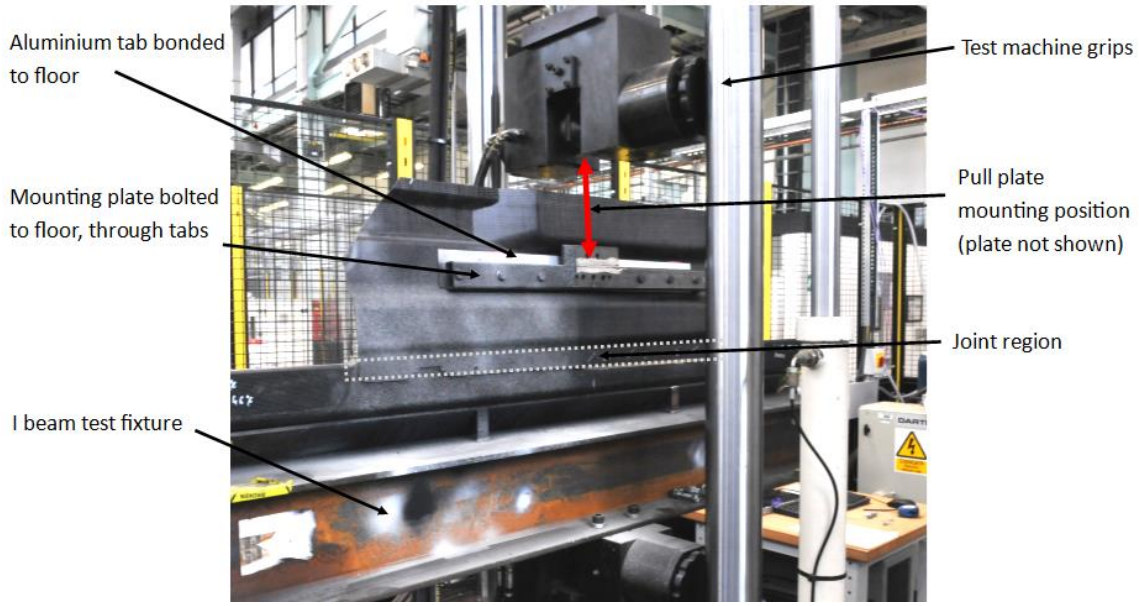

Figure 87 Test fixture design with demonstrator components loaded

The mounting plate was bolted through the floor with 9 x M10 bolts through 2.5 mm aluminium tabs bonded on both sides of the floor section with oven cured Sika 490c adhesive, this is shown in Figure 87. It was calculated that 1.15 x M10 bolts would be required to withstand the shear load applied, highlighting a high factor of safety with the developed test methodology. The area of tabs and shear strength of the 490c adhesive was significantly greater than that of the test joint with either of the adhesives used for the investigation. The

tabs helped distribute the concentrated load around the mounting bolts, reducing the risk of damaging the floor component under load. The mounting plate was bolted to a mild steel pull plate, which fitted within the test machine grips, again shown in Figure 84.

Initial testing identified that despite an additional 40 mm rectangular steel stiffener with 5 mm wall thickness placed above the sill, the straps alone provided insufficient restraint to the sill to prevent rotation and excessive central sill displacement relative to the fixture. This lead to undesirable loading modes and a significant deviation from a shear load to peel in the joint, see Figure 88.

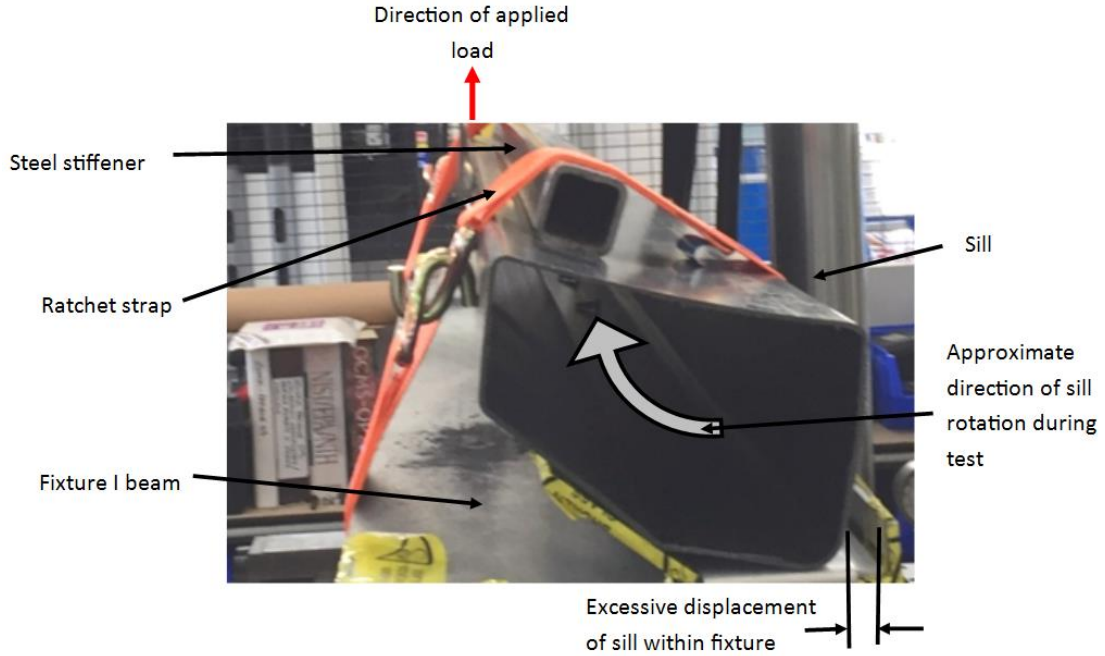

Figure 88 Excessive rotation of the sill with steel stiffener strapped above sill

In later tests, a steel section was bolted through the sill into the steel fixture, preventing this from occurring, shown in Figure 89. The restraint used in each test is detailed within the experimental results.

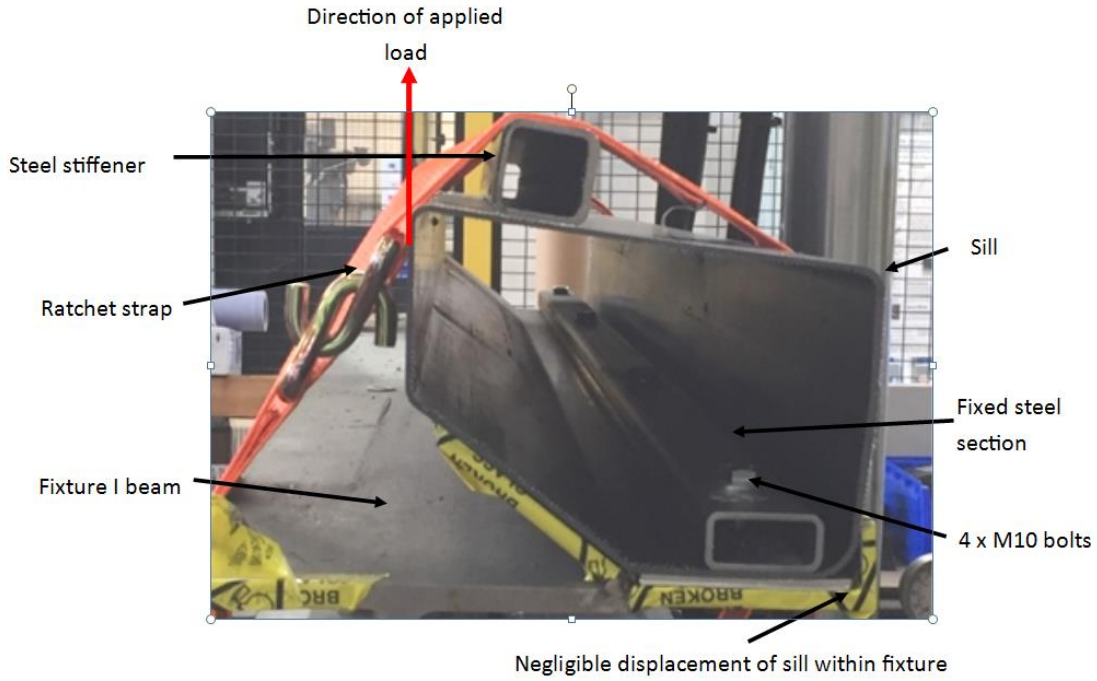

Figure 89 Sill rotation corrected with additional bolted steel restraint inside sill

5.1.4. Induction heating

In order to demonstrate the use of induction curing technologies without a feedback control loop it was required to program the induction generator with a specified AC current (ACC) output profile. This enabled a repeated heating cycle to be performed upon each component as well as each position along the joint. This sub-section details the process of establishing the induction heating cycle parameters used for the scale up testing.

In order to generate an initial heating profile a dry (no adhesive) trial was performed in the centre of the bond length with components orientated as they would be for curing during the testing process, illustrated in Figure 85. This trial used a thermocouple located centrally within the joint connected to the feedback controller, programmed to achieve the desired cure temperature profile with PU 1510 adhesive. The induction coil was rested directly upon the upper surface of the joint immediately above and parallel to the bond length. The controller output profile during the cycle was downloaded and an integration performed of ACC with respect to time over the ramp and dwell phase. Based on this a constant ACC was calculated for both the ramp and dwell phase to deliver the same integral value.

The process was subsequently repeated for the heating profile required with 3M™ SA9816. It was identified that the Minac programming feature required an ACC of minimum 2 % output

(15 A) during the programme. This was greater than the required ACC for the CFRP components to achieve a steady state dwell at 130 and 150 °c. In order to increase the ACC required 25 mm PTFE spacers were included between the coil and CFRP components, thus reducing the electromagnetic field intensity surrounding the CFRP. This process established starting parameters for the induction cure profile. The PTFE spacers can be seen under the induction coil in Figure 85.

A subsequent, dry investigation, was performed to identify whether the location of the coil along the bondline affected the joint heating performance. The coil and a monitoring thermocouple were placed in four differing positions as approximately shown within Figure 90. The feedback controller and induction coil with PTFE spacers were used to identify the required ACC to achieve the required heating rate for both adhesives. The results are shown in Figure 91 for the profile used with PU 1510 adhesive. Of particular interest is the ACC required to meet the temperature profile in position one which peaks at 70 A compared to 63 A in point 3 and point 4. It was predicted this was due to the damage to fibre architecture caused by the cut notch visible in Figure 90, reducing the induction heating efficiency. As such in order to heat this position it was calculated that an increase in steady state ramp current of 6 A would be required, to a first approximation.

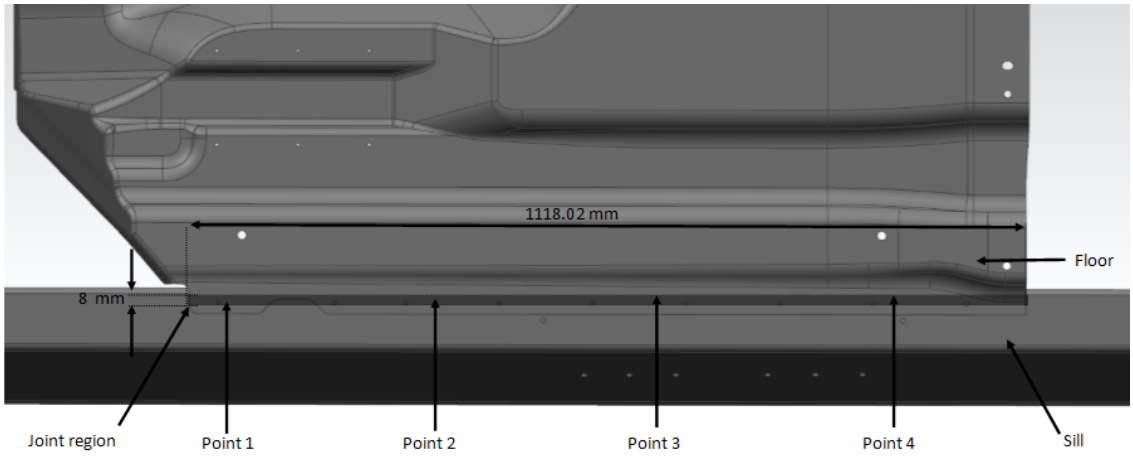

Figure 90 Approximate coil location along adhesive bondline

Required ACC output profiles were calculated for the ramp and dwell stages of both adhesives. Upon initial dry joint trials it was noted that the calculated parameters resulted in some overshoot from the desired dwell temperature. This used a thermocouple mounted centrally within the joint overlap under the centre of the induction coil. A trial and error approach was used, as well as the addition of adhesive to finally optimise the parameters to

achieve the required bondline temperature and reduce overshoot. A compromise was found between a slow rate of cooling in the joint from isothermal temperature, which was preferred, and steady increase in temperature based on the adjustment achievable with the Minac controller.

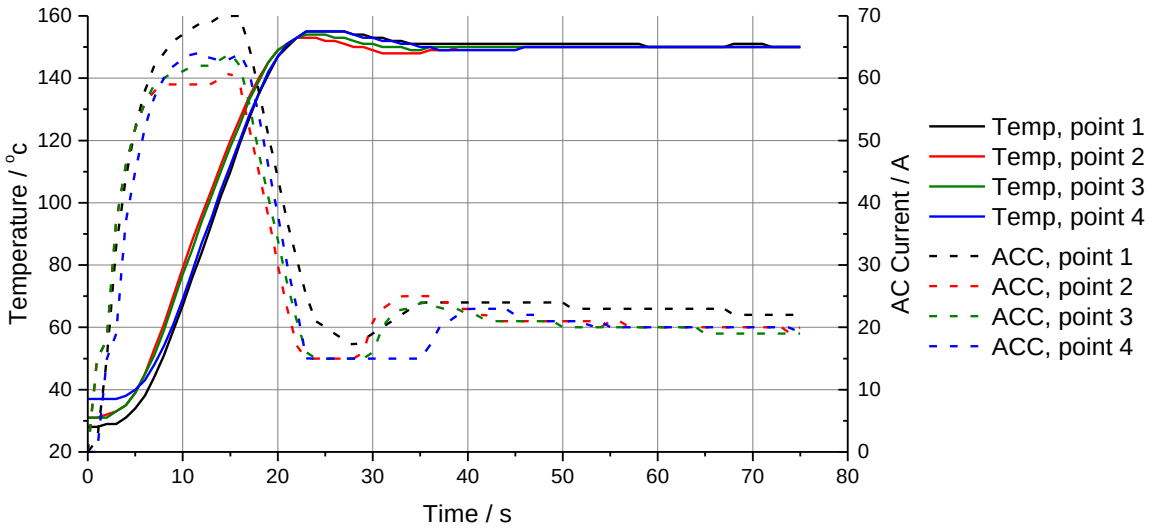

Figure 91 Variation in ACC with coil position upon CFRP demonstrator component joint with a defined temperature profile for use with PU 1510 adhesive. Thermocouple positioned centrally under the induction coil, within the joint

An approximate 68 A ACC (45 % output) was required to achieve a 500 °c/minute ramp in point 2 – 4, Figure 90, increasing to 47 % in point 1. A 13 % power output achieved a relatively constant isothermal temperature at 150 °c and 12 % at 130 °c dwell. It was observed that the addition of adhesive resulted in the requirement to increase the ACC in the ramp by approximately 5 % to achieve the same heating rate as with a dry joint. A subsequent investigation was performed to monitor the temperature distribution along the coil length, when heating the component level CFRP joint. The investigation was performed in the centre of the bondline length. Seven thermocouples were placed within the joint overlap under the induction coil. Two thermocouples were located under the extreme ends of the coil, two 30 mm from the ends symmetrically, two 45 mm from the ends symmetrically and one in the centre. In this case the investigation was performed upon a dry joint with the ACC in ramp reduced to compensate. The temperature distribution over a 150 °c target dwell, 500 °c/minute ramp is shown in Figure 92.

The trend in Figure 92 was remarkably similar to that within section 4.2.1 upon smaller geometry CFRP plaques, this suggested that the coil design is significantly influential upon temperature distribution as well as component size. One of the greatest problems identified

was the large temperature differential between the edges of the coil and the centre, peaking at a difference of approximately 80 °c. Clearly this would cause great variability in adhesive strength along the coil length. The temperature at the edges of the coil would also be too low to activate the PU 1510 adhesive, highlighted in section 4.4. To compromise the usable length of the coil was reduced to 120 mm symmetrically about the centre. With 120 mm effective coil length the minimum temperature reached 122 °c with a temperature differential of 41 °c between maximum and minimum values.

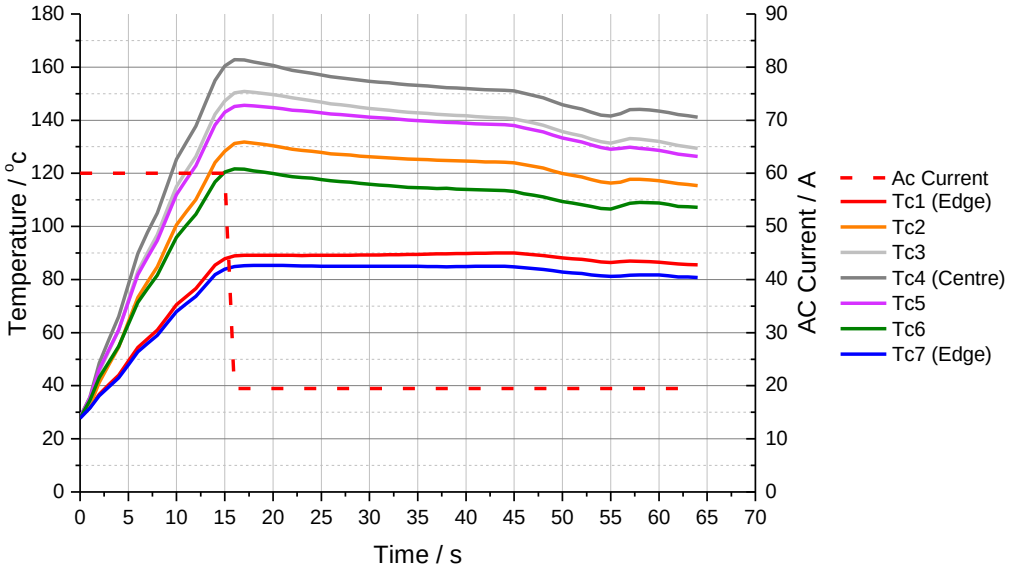

Figure 92 Temperature distribution under coil CFRP/CFRP demonstrator component joint

Whilst this temperature differential was unlikely to be acceptable within a production environment it was determined as suitable for activating the PU1510 adhesive, requiring a minimum temperature of approximately 100 °c. Further, providing the peak temperature does not exceed 130 °c for 3M SA9816 joint porosity was unlikely to be observed as shown in chapter four, avoiding damage to the adhesive. It was not possible to develop a new induction coil within the timescales available for this work, as such the 180 mm coil was used, with a 120 mm effective length, accepting that the temperature variation under the coil will reduce the resultant handling strength achieved in the component level test.

5.1.5. 3D Digital image correlation methodology

3D Digital image correlation was used to track a section of substrate and joint movement throughout the sub-assembly testing process. This optical measurement method compares digital photographs of the test surface recorded a specified frame rate during the test. Photograph image pixels are then tracked with time, this can subsequently be built up into

full 3D deformation vector fields and strain maps (104). The process relies on unique pixel patterns which are generally created up using a spray paint speckle pattern of contrasting colours upon the part surface. The three-dimensional variation of the process uses at least two cameras, in a fixed orientation relative to the observed test. Triangulation methods can then be used to track the location of the surface pixels in 3D. A specific calibration panel is used, positioned through various orientations to calibrate the cameras prior to the test.

The deformation of the surfaces during the testing process is calculated using virtual rectangular regions called facets, of a specified pixel size. The facets are spaced in a repeating pattern over the surface, producing a repeating mesh. Deformation of the mesh is then calculated relative to the centre of each facet (105). Thus, strain and displacement measurements can be calculated by tracking the deformation of the mesh, similar to an FEA approach to deformation calculation. The specific advantage of the 3D DIC technique for tracking the joint displacement is that in plane and out of plane displacements can be calculated, thus enabling rotation of the joint and other out of plane deformations to be analysed which could significantly affect the joint failure. Further, the method can analyse and allow for separation of rigid body movement of the system. This is critical if the separation of the joint alone is to be resolved, rather than the total movement of the system, as would be identified monitoring crosshead displacement of the test machine alone.

A GOM dual 12-megapixel camera setup was used to record images throughout the test, with post processing conducted using GOM Aramis software. The two cameras were set with a 1405 mm measurement distance enabling a measurement volume of 400 x 300 mm over 4096 x 3072 pixels. As such, a reduced section of the floor to sill joint was analysed. The system was calibrated after a minimum 30 minutes warm up time and prior to loading each test, to a maximum acceptable deviation of 0.04 pixels. As such a minimum measurement resolution of + /- 3.91 x 10^{-3} mm could be achieved. Assistance was sought from experienced DIC users within WMG to generate an acceptable speckle pattern upon the test surface. Matt black spray was used to cover the CFRP measurement area and satin white speckles sprayed over the black surface. A DIC sample rate of 2 Hz was used in the ramp phases and 0.2 Hz in the dwell phases. It was predicted that failure was most likely to occur in the ramp phase, as such the faster frame rate was used in the ramp phase. A default, recommended facet size of 19 x 19 $pixels^2$ was used with a 4 pixel overlap between facets (105).

The DIC measurement area depended on whether the floor section was taken from the left or right-handed side of the floor due to its symmetry. The DIC cameras were in the same fixed position for each test. The two orientations are shown in Figure 93, identifiable by the existence of the notch. The locations can be identified approximately in the CAD geometry within Figure 83 relative to the position of the floor edge and notch. The orientation of the part is detailed within the test results, section 5.2.

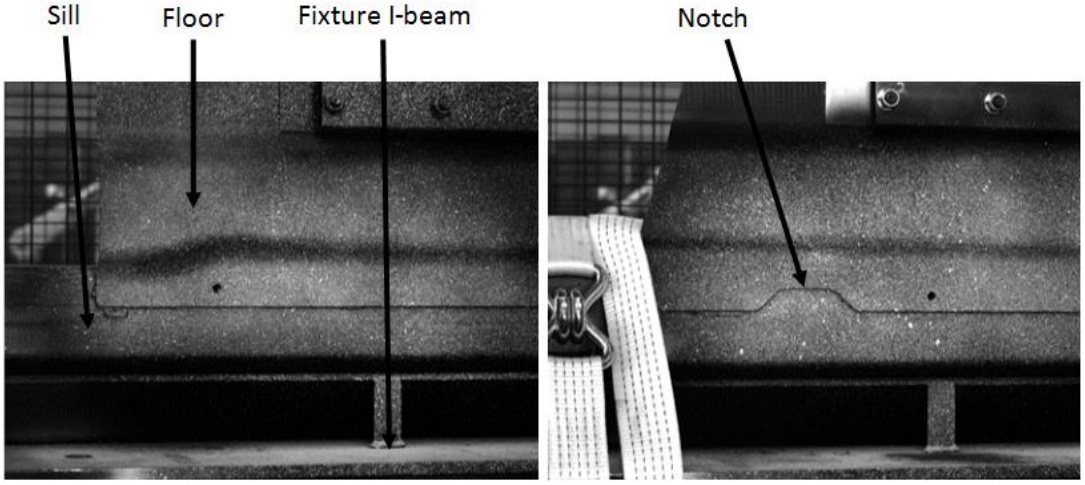

Figure 93 Demonstrator component orientation and DIC view one (left) and two (right)

The 3D mesh was created over the facets generated upon the part surface, an example of the mesh is seen visualised in Figure 94. A variety of virtual measurement points were then used to analyse the DIC data and track joint displacements and substrate strain over the applied mesh. For joint separation two measurement points, one above the other below the joint were placed in various positions over the measurement area as seen in Figure 95. This enabled the joint separation in the direction of loading to be calculated, without the effect of rigid body movement. This joint separation was as such recorded in a fixed position relative to the assembly, rather than the fixture, continuously over the duration of the test cycle.

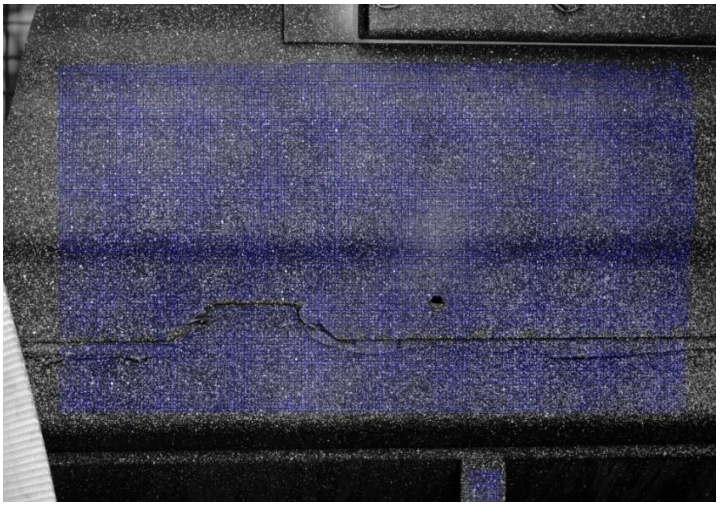

Figure 94 Generated mesh over DIC monitored area

For substrate strain measurement small regions of area statistics within the floor section were analysed. These regions are used to compute average strain over this specific region of the mesh incorporating multiple facets. This method improved the accuracy of the major strain calculation compared to single point measurement alone. The substrate major strain was primarily used for substrate results analysis, acting in the direction of applied load. The major strain also enables a qualitative analysis to be made of joint stress near to the region of substrate major strain analysis. The approximate location of these regions relative to the DIC measurement region is shown in Figure 96. In a similar way to the point to point analysis this method enables substrate major strain to be calculated in specific regions, continuously over the duration of the test.

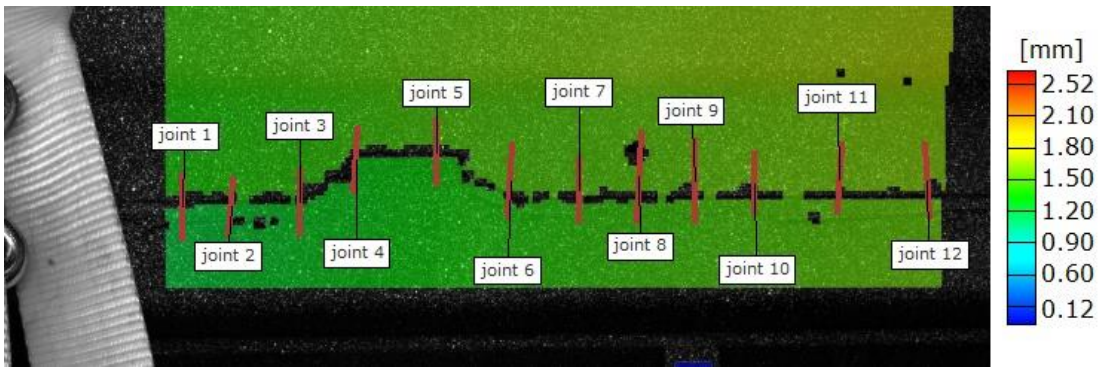

Figure 95 Example of two-point joint separation measurement technique

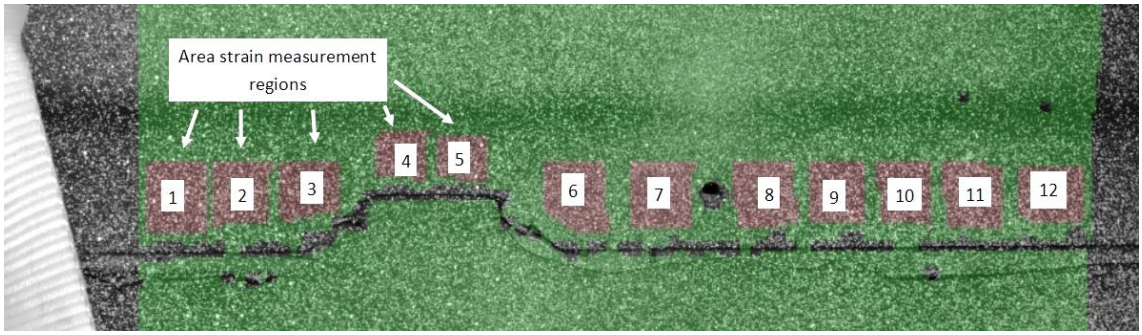

Figure 96 Example of area statistics used to calculate substrate major strain

A final method of tracking joint separation was also used, applying line sections at various points above and below the joint as seen in Figure 97. This method can be used to provide an instantaneous measure of displacement over the continuous region along the line. The separation of the lines immediately above and below the joint correspond to the joint separation continuously along the bondline, eliminating rigid body movement. Further any separation between the lines within either the floor or the sill can be used to show an extension within the substrate under load. This was used to validate the assumption that the strain within the floor and sill is negligible compared to the separation of the joint. This assumption was important in the subsequent calculation of joint shear strain, assuming that shear within the adhesive is the primary source of extension within the joint. This is illustrated in Figure 98. Calculated joint shear strain was used to compare much of the experimental results.

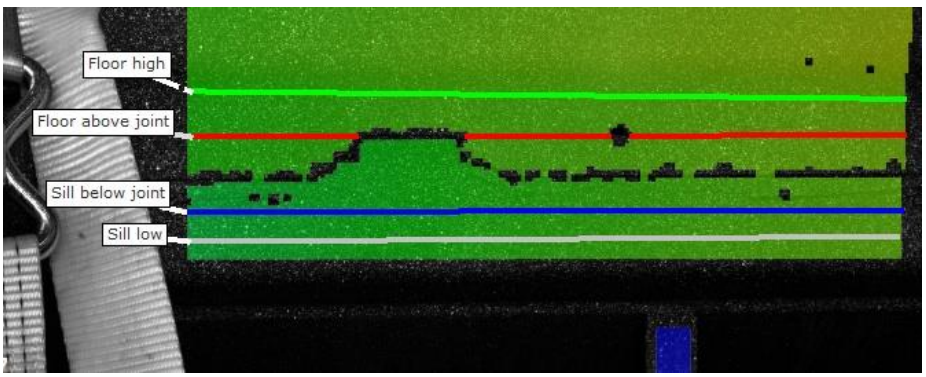

Figure 97 Line statistics used to calculate joint separation

The shear strain calculation relates the joint separation, δ to the shear angle of the joint θ using the principle of conservation of adhesive volume within the joint. This was taken as a first approximation of joint shear strain, sufficient for the present work. Further, it is assumed that the bond cross sectional area also follows the same conservation principle though the

deformation process. The shear angle was calculated using the relationship $\theta = \tan^{-1}\left[\frac{\delta^2+\delta L}{t\,w}\right]$ further the joint shear strain was expressed in percentage by the relationship; $\frac{\theta}{45} \times 100$.

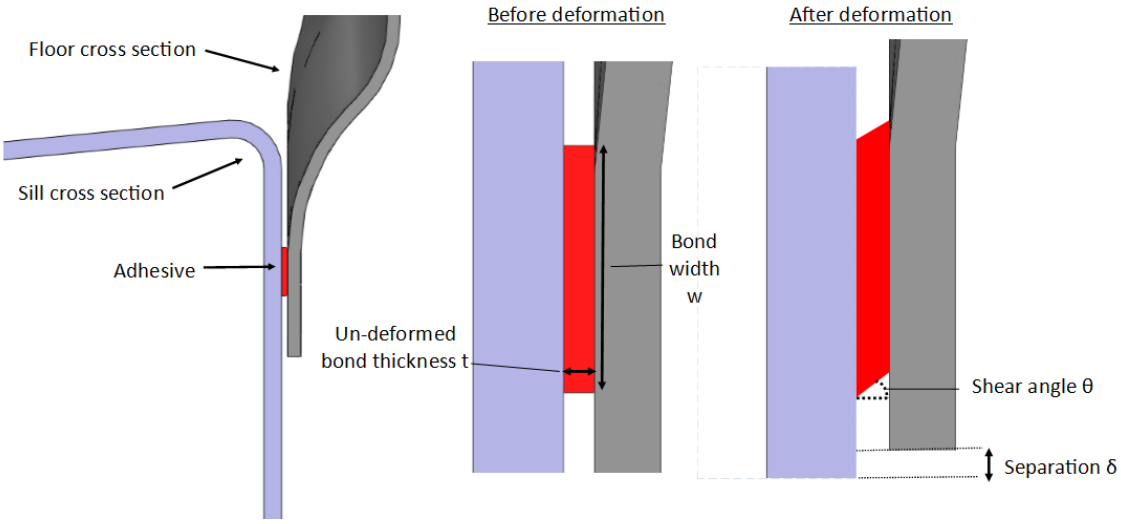

Figure 98 Cross section illustration of joint shear angle following joint deformation

The 3D DIC measurement technique thus provides a rigorous methodology for interpreting the deformation of the assembly during the testing process. This extends to rigid body movement, out of plane displacement identification and substrate major strain and joint shear strain analysis.

5.2. Results and discussion

In total five tests were conducted, due to limitations of available time and components, the summary of tests performed is shown in Table 35. Testing corresponds to the loading profiles shown in Figure 99. It can be seen that over the course of the tests performed changes were made to the restraint of the sill. This relates to the discussion in section 5.1.3 and restraint improvement methods shown in Figure 89. The initial sill restraint methods in test one and two resulted in excessive out of plane displacements, which effected the joint behaviour during the test. This is discussed in more detail within the experimental result sub sections for each test. As a result of the changing restraint, test one and two are considered as preliminary tests with tests three, four and five as final tests with optimised sill restraint.

Test no.	Adhesive	Restraint	Failure load / kN	Orientation	Load profile	Notes
1	PU 1510	Straps only	13.90	1	1	Excessive rotation, bending of sill and lifting of assembly noticed within fixture
2	PU 1510	Straps + steel stiffener above sill	Did not fail at 20.00 kN	2	1	Bending of sill reduced, large rotation and sill lifting remained
3	3M™ SA9816	Straps + steel stiffener above sill+ sill bolted to fixture	15.49	1	2	DIC calibration issues, ran without DIC. Sill remained rigidly fixed to fixture, significantly less rotation.
4	3M™ SA9816	Straps + steel stiffener above sill + sill bolted to fixture	15.24	2	2	As previous test with DIC functioning correctly.
5	PU 1510	Straps + steel stiffener above sill + sill bolted to fixture	Did not fail at 20.00 kN	2	2	DIC power failure mid-way through test.

Table 35 Demonstrator assembly test matrix

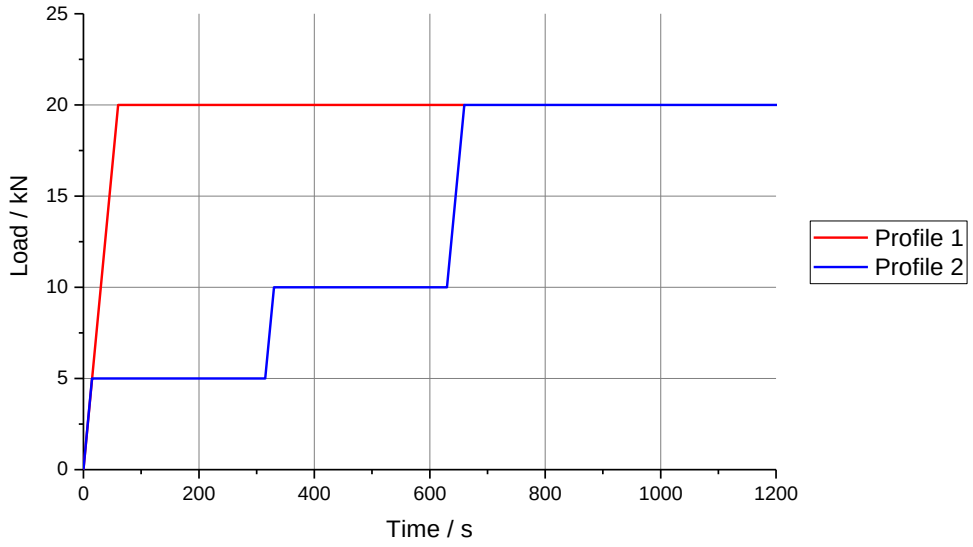

Figure 99 Target loading profiles for demonstrator testing

5.2.1. Preliminary demonstrator test one results

It is seen within Figure 100 that test one, using PU 1510 adhesive, failed at a maximum load of 13.9 kN. This was well below the minimum predicted failure load calculated in Table 34 of 73.5 kN. The substrate major strains however were much greater than test two, which did not fail, despite the lower load applied to test one at the point of failure. Maximum floor substrate

major strains in test one reached 0.12 % at failure whereas approximately 0.03 % in test two. Notably the greatest substrate strain in test one was observed at the edges of the floor near point one. It was predicted that the increase in major strain is a result of significant lifting and rotation of the assembly within the test fixture changing the stress distribution within the assembly, this is highlighted later in Figure 110. Test one did not have the steel stiffener placed above the sill as seen in Figure 89, as a consequence significant bowing of the sill towards the centre of the part was observed as well as out of plane rotation. The joint shear strain shows a similar pattern of shear strain distribution and magnitude compared to test two peaking at approximately 0.12 % nearest to the edge of the assembly.

Joint separation data was also collected by the method shown in Figure 97. The section data was analysed in the frame immediately prior to joint failure thus enabling the y axis (axis of loading) separation of joint to be calculated. For test one results in Figure 101, y-axis displacement in the floor 30 mm above the joint appears much greater than y displacement immediately above the joint, attributed to the sill rotation and deflection out of plane. There also appears to be some extension of the joint, greatest at the edges of the joints compared to the inside, evidence of a joint stress concentration near to the edges. This is identified by the increasing difference in the y axis deflection between the sections immediately above and below the joint. Further the sill sections show virtually identical displacement in the y axis along the measurement area, highlighting the lack of extension within the sill itself. The curvature of the plot also gives an indication of the bowing that was observed within the sill believed to contribute towards the observed joint stress concentration at the edges.

It was observed that the joint failed at the notch end, away from DIC measurement area. The joint was subsequently seen to lever open progressively. Upon inspection of the failure surface there was evidence to suggest insufficient cure at the edge of the part, near to the notch and reduced adhesive contact. This helped to explain the location of failure initiation. Generally, the adhesive in test one failed with a mixture of cohesive and material failure although regions of uncured adhesive were observed. This indicates insufficient bondline temperature to activate the adhesive and may help to explain some of the difference in substrate major strain between test one and test two. A section of the failure surface is seen in Figure 102. The lower failure mode compared to the prediction was attributed to the combination of; regions of uncured adhesive, stress concentrations at the edges of the joint

due to sill bowing and the rotation of the assembly out of plane creating additional joint peel stresses.

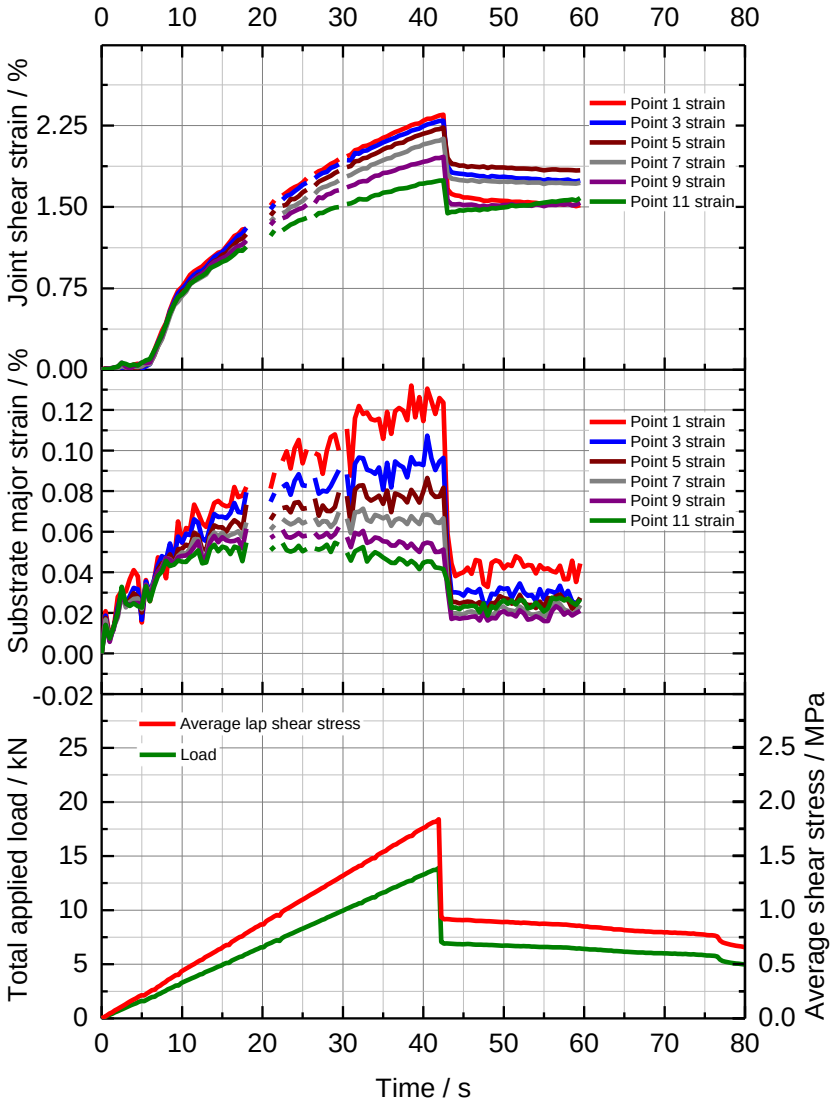

Figure 100 Demonstrator test one results PU 1510 adhesive

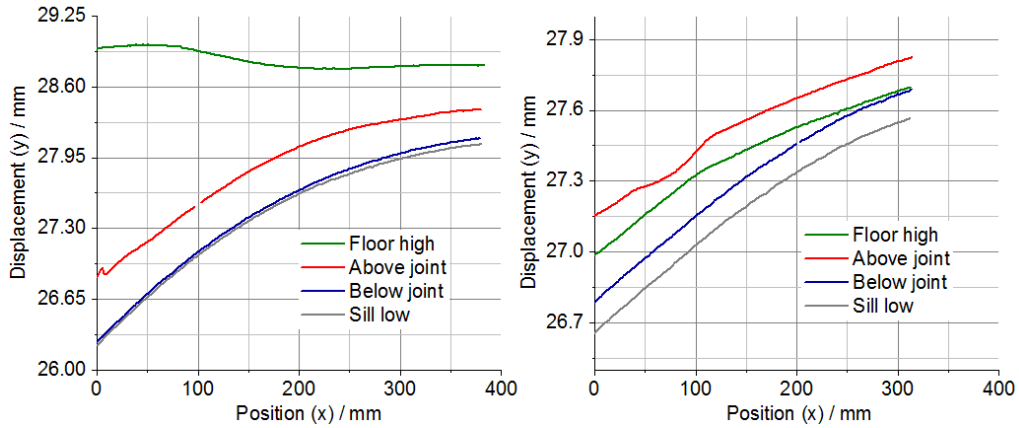

Figure 101 Joint separation immediately prior to failure PU 1510 test one (left) and test two (right)

Figure 102 Section of failure surface in test one

5.2.2. Preliminary demonstrator test two results

Test two results are shown in Figure 103, this test did not fail under the applied load of 20 kN. The stiffener added above the sill reduced the bowing of the sill under load, which appeared to reduce the substrate maximum major strain by approximately 0.09 % despite the increase in applied load. The change in orientation of the part may also account for some of the difference in major strain distribution over the DIC monitored area, with the greatest major strain in the floor around the region of the notch in test two compared to at the edge in test one. This is expected to be due to a redistribution of stress around the notch area where the bond is not present. The joint shear strain appears to decrease progressively from the edge of the floor towards the inside, suggesting a stress concentration is created within the bond nearest to the edge of the part in a similar way to test one. The shear strain within the adhesive also appears to increase as a result of creep throughout the test. This posed the question of whether the creep would continue until failure or reach a steady state over time, later investigated further in section 5.3.

This lack of uniformity in shear stress distribution is also seen in the joint separation prior to failure, Figure 101, where the joint separation is greatest nearer to the edge of the part. This plot also highlights that the deflection within the joint is much greater than the deflection within either the floor or sill from the diverging section curves immediately above and below the joint compared to the almost identical profile curves within the floor and sill. The reduced curvature of the separation curves between test one and two show the reduction in sill bowing as a result of the sill stiffener.

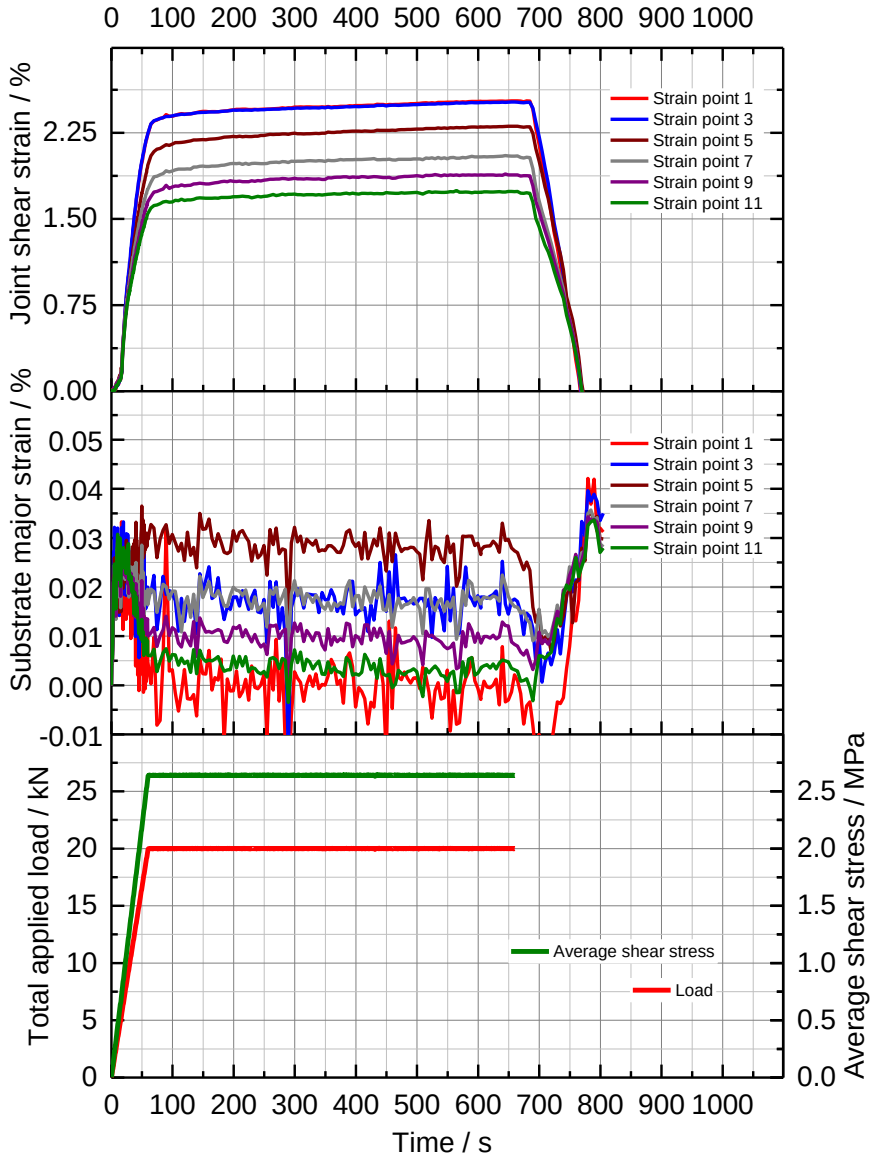

Figure 103 Demonstrator results test two, PU 1510 adhesive

5.2.3. Demonstrator test three results

Test three was performed using 3M™ SA9816 adhesive, unfortunately upon loading the part calibration issues with the DIC were experienced. Due to the lack of available time to recalibrate before the end of the day the test was run without the DIC, rather than leaving the partially cured adhesive until the next day. The test failed at 15.5 kN, which is slightly lower than that predicted in Table 34. This is unsurprising giving the variation in bondline temperature distribution identified within section 5.1.4. It can be seen from the load vs. crosshead displacement plot, Figure 104 that at 10 kN load there is some evidence which suggests adhesive creep with the crosshead displacement increasing by 0.27 mm over the 5 minute hold. A section of the failure surface is shown in Figure 105, where the adhesive

failure surface varies between regions of CFRP material failure and regions of high porosity. This highlighted the problem of uneven temperature distribution during the cure process and explains why the average bond strength may be lower than predicted, due to low strength porous regions.

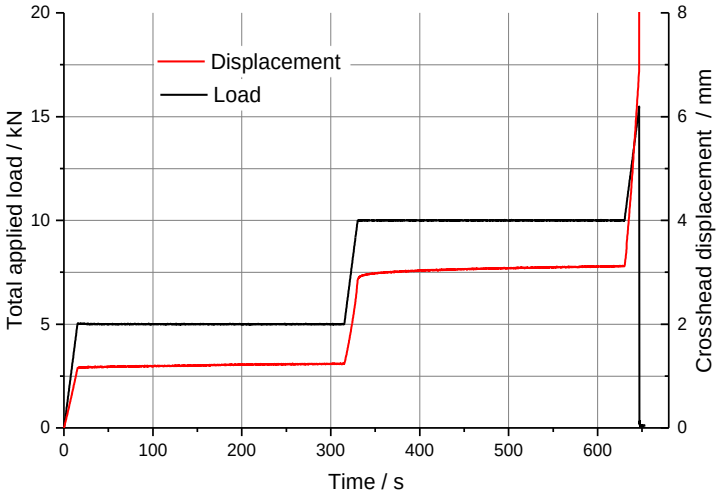

Figure 104 Test three 3M™ SA9816 load and crosshead displacement

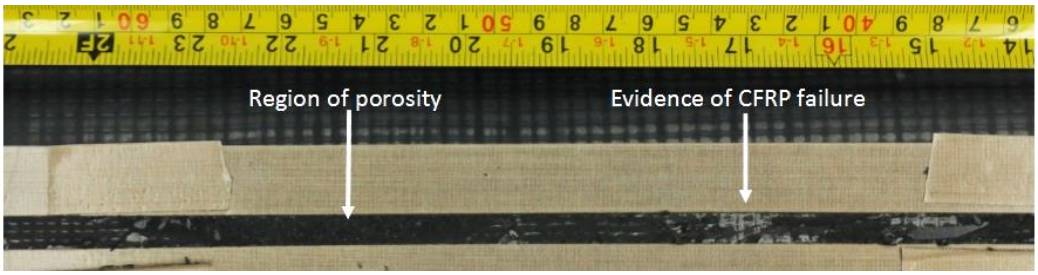

Figure 105 Test three 3M™ SA9816 demonstrator component section of failure surface

5.2.4. Demonstrator test four results

The results from test four are shown in Figure 107, with the additional bolted, sill restraint present as shown in Figure 89. The joint failed at 15.2 kN, which was similar to the failure load of test three with comparable curing conditions. The joint shear strain plot, Figure 107 shows following the 5 minute hold at 10 kN there was greater shear strain at the edge of the joint compared to nearer the centre. Unsurprisingly the joint creep over the DIC measurement region is much greater nearer the part edge where the joint shear strain is greater, with shear strain increasing by approximately 25 % over the duration of the 10 kN hold. Substrate major strain appeared slightly greater than with test two, despite the lower load with the greatest major strain trends appearing near to the inside edge of the joint compared to the outside with test two. The change in major strain distribution was predicted to be a result of the inside

regions of the joint achieving a greater degree of cure compared to the outside region around the cut notch where heating efficiency was lower despite the compensation in coil current applied. This conclusion was supported by analysis of the failure mode, where a large region of material failure was observed inside of the notch, indicative of a strong bond region. Thus, greater load is transferred to the substrate where the adhesive is stronger, explaining the change in major strain distribution. There is still however an increase in major strain of approximately 25 % compared to test two despite the applied load being 50 % lower, this may be attributable to the change in sill restraint, preventing some of the assembly rotation in previous tests altering the floor strain distribution, later shown in Figure 110. The joint separation plot is shown in Figure 106, it was highlighted that joint separation is much greater near to the outside edge of the joint, with a discontinuity surrounding the region of the notch supporting the previous conclusion relating to substrate major strain distribution. The break in the “above joint” line is due to a poor DIC speckle pattern around a region of adhesive spew. It was also observed that with the additional sill restraint the separation plot for test four is considerably straighter compared to test two in Figure 101 showing the improvement in loading condition and reduction in out of plane deflection.

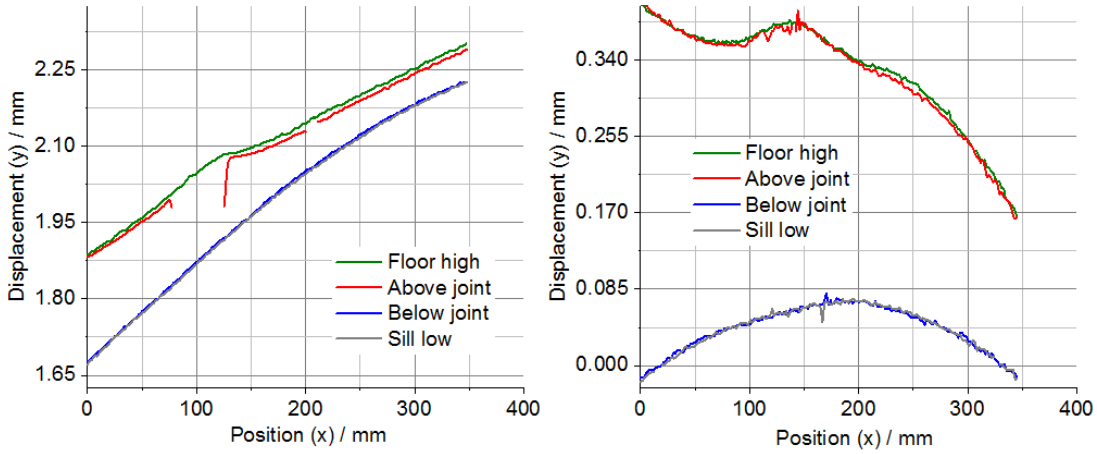

Figure 106 Joint separation immediately prior to failure 3M™ SA9816 test four (left) and PU 1510 test five (right)

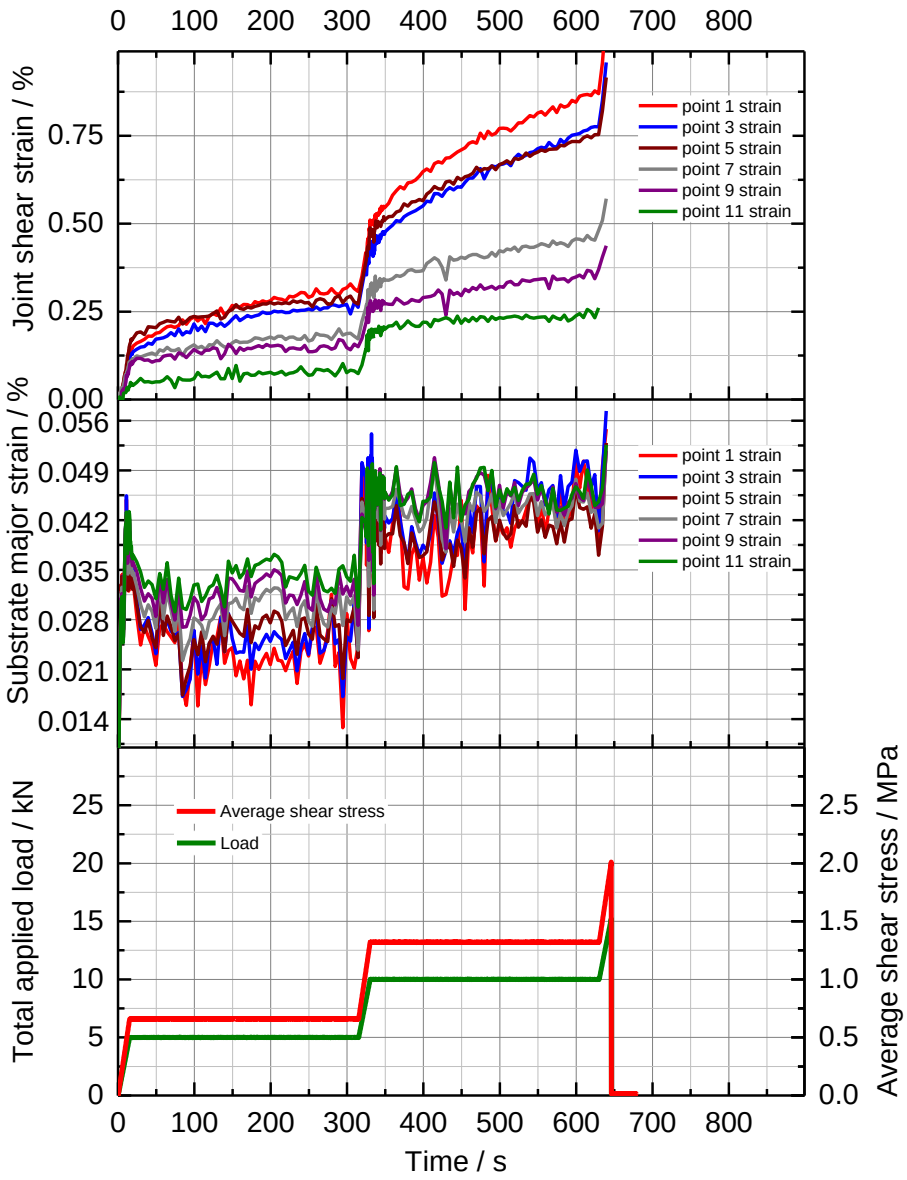

Figure 107 Demonstrator results test four 3M SA9816

5.2.5. Demonstrator test five results

Test five results using PU 1510 adhesive are presented in Figure 108, unfortunately a power failure on the DIC system during the test resulted in the loss of measurement data prior to approximately 570 s into the test. As a result, unloaded frames in the start condition were lost. To compensate the system was unloaded and the unloaded frame used as a start reference, with raw data values subtracted from those recorded during the test. This correction was applied to all of the presented data for test five. It was noted that the joint did not fail under 20 kN load however there is a very similar pattern of adhesive shear strain creep at 20 kN load compared to test two. The absolute shear strain values are lower, which is likely to be a result in the change of the start condition frame, failing to account for initial creep in

the joint prior to restarting the DIC. Substrate major strain is of similar magnitude to test two as would be expected. The distribution of peak major strain appears to change, peaking nearer to the edge of the part rather than around the notch in test two. This was attributed to the increased restraint of the sill compared to test two. The joint separation, Figure 106, also appears much greater towards the edges of the joint and is of similar magnitude to test four.

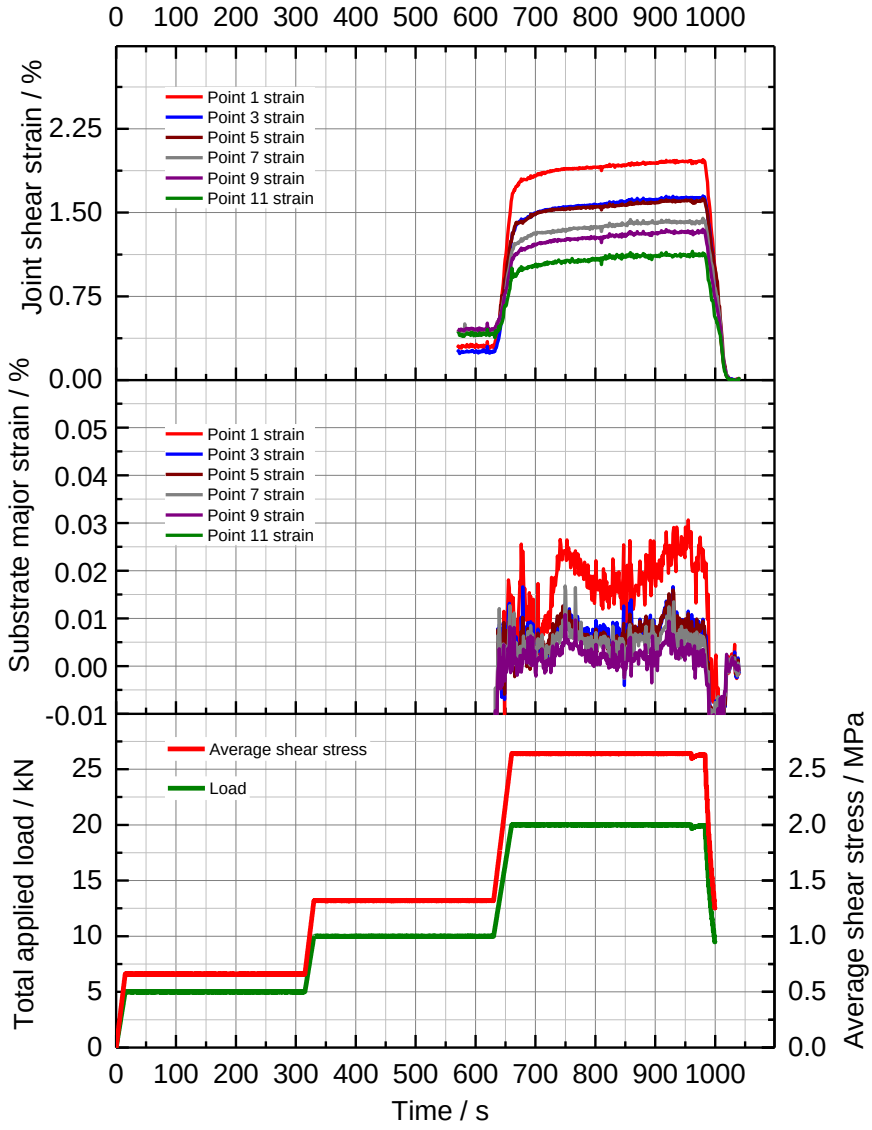

Figure 108 Demonstrator results test five PU 1510

5.2.6. Results comparison – demonstrator testing

The separation of the joint was considered as one of the most significant outputs of the demonstrator testing. Excessive joint separation of a primary bonded structure during manufacturing is likely to determine the suitability of the joining technique, indicative of insufficient handling strength. In order to express the resultant joint separation immediately

prior to failure, or in the final frame of the test where the joint did not fail, the y-displacement section raw data above the joint was subtracted from that below the joint for each test performed. As such the separation in the y-axis of the joint can be compared directly for each test over the length of the joint monitored by the DIC, presented in Figure 109. The region monitored can be visualised in Figure 97 and qualitatively represented, relative to the fixture in Figure 110. Whilst it is challenging to pinpoint the exact position of the monitored area along the bond a significant understanding of the joint behaviour can be gathered.

It is shown in Figure 109 that for all tests a similar profile of joint separation was observed, with greatest separation nearest to the edge of the assembly. This highlights the existence of stress concentrations at the edges of the assembly. Test 1 showed by far the greatest joint separation, largely explained by the reduced restraint and bowing compared to subsequent tests. The rotation and bowing of the sill resulting in increased stress concentrations along the joint as well as a loading of the adhesive into peel, magnifying stress states and contributing to failure at a much lower load than predicted with greater separation prior to failure. The introduction of the sill stiffener in test two reduced the joint separation by a factor of three with the same adhesive, without failure, adding confidence to the previous conclusion. This is deduced by comparing the separation profile for tests one and two. The profile and magnitude of joint separation for test four is similar to test two, despite the change in adhesive and lower failure load. The joint separation of test 5 appears greater than that for the same adhesive and maximum load in test two, however due to the loss of the DIC start frame the data for this test may contain some uncertainty.

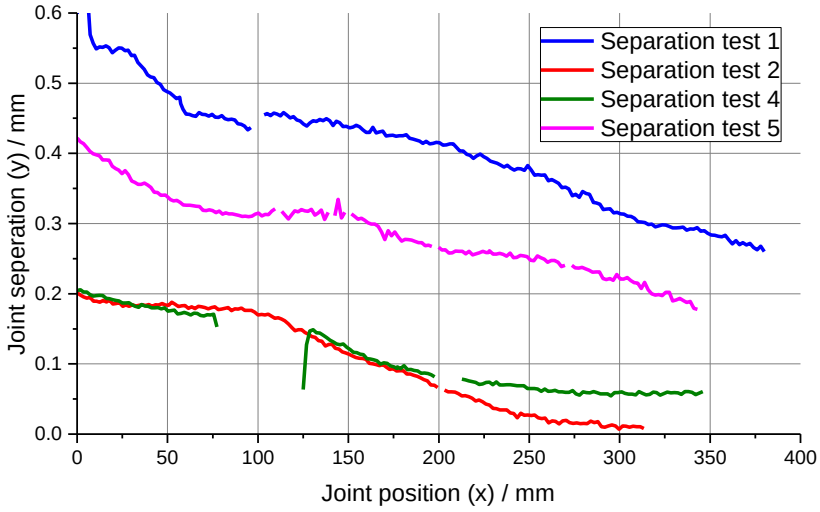

Figure 109 Combined joint separation plots, all tests

Comparing the substrate major strain changes and joint separation plots for each test shows how the changes in restraint made a significant difference to the test method over the course of the investigation. The initial addition of a steel stiffener above the sill preventing bowing of the sill and some rotation. Further the addition of a bolted restraint between the sill and fixture dramatically reduced lifting of the assembly and bowing of the sill in test three, four and five. To highlight these changes the surface deformation in the z-axis, out of plane, is shown in Figure 110 for each restraint method shown. The images are taken at the final loaded frame of each test, immediately prior to failure, if the joint failed.

It is evident in Figure 110 that out of plane displacement peaks at approximately + 17 mm with the straps as the only sill restraint, with the sill and joint moving towards the DIC cameras during the test. The addition of the steel stiffener to the top of the sill reduced this very little between test one and two although did reduce the bowing of the sill as previously shown. The out of plane movement and rotation is primarily attributed to the design of the test fixture and lack of stiffness in the straps. Adding a bolted steel restraint inside the sill dramatically reduced the out of plane deflection to within a few mm, approaching an order of magnitude lower than without the bolted stiffener.

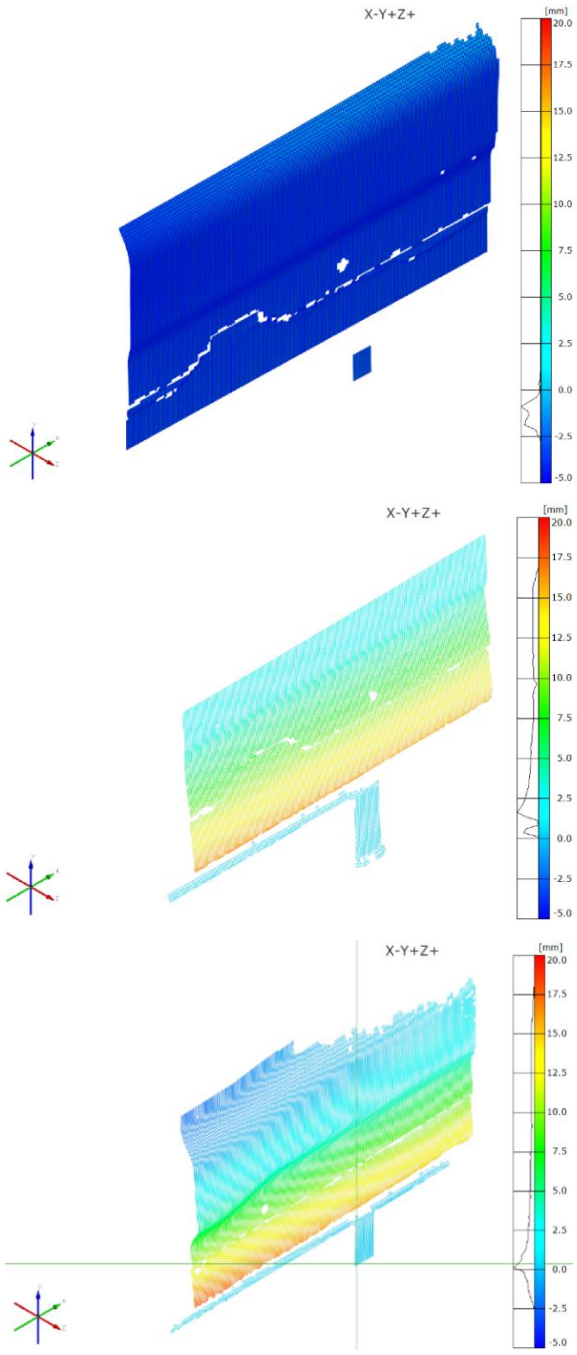

Figure 110 Out of plane (z-axis) displacement, test one (bottom), test two (middle) and test three (top) images taken at final frame of test

5.3. Further investigation – creep

Based on the data collected in section 5.2 one of the important considerations that emerged was the observed creep over the periods of applied load. In a primary bonded structure, partially cured to develop handling strength, creep could result in a distortion of the structure during the manufacturing processes prior to full cure. This could either result in complete failure of the structure or tolerance issues during manufacture. As a result, it was important

to identify whether at constant load the creep continued until joint failure or the creep rate reduced with time. To investigate this further three-hour long creep tests were performed, with SLS joints held under constant load for the duration of the test. The extension of the joints over the duration of the test was monitored. The three-hour duration was considered a compromise between available experimental time and a duration considered sufficient for a substantial proportion of BIW assembly to take place within a manufacturing environment.

SLS adhesive specimens were produced from 50 mm AL/TS-CFRP substrates with a 12.5 mm overlap and three samples in each batch. Both PU 1510 and 3M™ SA9816 adhesives were used with 0.3 mm beads. The specimens were cured using the same induction heated parameters and induction coil as detailed in section 5.1.2, for the demonstrator component work. The feedback controller was used in this case to control the heating profile with an in bondline thermocouple in the same way as chapter 4. An identical batch of specimens was oven cured following the induction cycle for 1 hour at 100 °c in the case of PU 1510 and for 1 hour at 130 °c in the case of SA9816. This enabled a comparison to be made between the creep behaviour of a partially cured joint, cured to generate handling strength and a fully cured joint.

Surface preparation was performed using an IPA wipe on both substrates. 5754 aluminium was used with P596 primer for PU 1510 and PT3 coating for 3M™ SA9816 adhesive. This was identified as a suitable surface preparation for coupon level work in chapter 4. TS-CFRP substrates were also the same as those used within chapter 4. An Instron 25 kN servo-hydraulic test machine was used for the investigation. The joints were all loaded to 812.5 N, this equated to a shear stress of 1.3 MPa upon the samples, with the test machine operating in load control. This provided an equal shear stress to the average shear stress upon the demonstrator sub-assembly joint when 10 kN load was applied. The load was held for 3 hours. The tests were conducted in a temperature-controlled environment at 25 °c. The results, with joint extension based on crosshead displacement, are shown in Table 36.

Adhesive	Cure Condition	Sample no	Sample failed	Time to failure /min	Crosshead extension at test end /mm
3M™ SA9816	Induction, 60 s at 130 °c	**1**	**Yes**	**10**	**1.1**
		2	**Yes**	**179**	**0.6**
		2	No	N/A	0.1
3M™ SA9816	Induction, 60 s at 130 °c plus oven at 130 °c for 1 hour	1	No	N/A	0.1
		2	No	N/A	0.1
		3	No	N/A	0.1
PU 1510	Induction, 10 s at 150 °c	1	No	N/A	0.1
		2	No	N/A	0.1
		3	No	N/A	0.1
PU 1510	Induction, 10 s at 150 °c plus oven at 100 °c for 1 hour	1	No	N/A	0.1
		2	No	N/A	0.1
		3	No	N/A	0.1

Table 36 Creep results PU 1510 and SA9816 under a load of 1.3 MPa for 3 hours

It is shown in Table 36 that PU 1510 adhesive, with both cuing conditions, demonstrated negligible creep over the three-hour test duration. A maximum crosshead displacement of 0.1 mm was observed in all cases. Importantly the PU 1510 joints did not fail. It was not possible to attach an external extensometer due to the operation of the servo-hydraulic test machine. As such the crosshead displacement provided an indication of joint extension. However, this measurement is affected by factors such as thermal expansion of the test machine and should only be used as an indication of joint extension.

Oven cured 3M™ SA9816 also showed negligible creep, with a maximum displacement of 0.1 mm in all cases. The induction cured SA9816 specimens, however, showed great variability. One specimen broke following approximately 10 minutes under load, with another specimen breaking just before the end of the three-hour test. The final specimen did not break and showed negligible creep equal to 0.1 mm crosshead displacement. A similar failure mode, exhibiting relatively low porosity, was observed upon both failed surfaces with 3M™ SA9816 adhesive. Based on previously observed temperature differentials within coupon sized Al/CFRP joints in section 4.3.3 it was predicted that small variations in curing temperature may significantly affect the creep behaviour of 3M™ SA9816.

The important conclusion to be taken from the creep investigation was that both PU 1510 and 3M™ SA9816 adhesive joints did not always fail as a result of creep, following an induction cure. Considering the best-case result for partially cured 3M™ SA9816 where one joint did not fail with an extension equal to that of the fully cured joint, it follows that with further

optimisation of curing parameters and temperature distribution this result could be achieved consistently during manufacture. Further it should also be considered that the creep tests represented a worst-case scenario, with the following important considerations.

- The load case applied to the creep specimens approximates a load of 10 kN being applied to the demonstrator sub-assembly joint. It must be considered that this load, equal to approximately 1 tonne of weight is substantially greater than the BIW mass of any of Jaguar Land Rover's vehicles, discussed in chapter two. As such, it is unlikely that a load this high would ever be applied to a partially cured, primary bonded, BIW joint during manufacture.
- It is unlikely that the weight of the BIW during manufacture would ever be loaded onto any one joint in particular, with the BIW usually supported in more than one location.
- It should be considered that even if the weight of the BIW was loaded onto one joint alone, it is very unlikely the load would be held for a period of three hours as performed in the creep tests. This situation may apply for short durations, for example when the BIW is moved from one location to another.

As a result of the above considerations it was concluded that creep of a partially cured, primary bonded structure did not appear a significant manufacturing concern provided excessive temperature distribution deviation during cure could be avoided. However, this would need to be evaluated further over a range of loading conditions and structure temperatures to gain increased confidence. Further, knowledge of the load cases BIW joints may be exposed to during manufacture should be considered prior to performing this further work. At the time of writing this information was not available due to a manufacturing process for a primary bonded CFRP intensive structure not existing within Jaguar Land Rover.

5.4. Conclusions – component level demonstrator

Chapter five has demonstrated that rapid curing thermoset structural adhesives, combined with electromagnetic induction heating, can produce rapid handling strength generation upon CFRP/CFRP automotive assemblies. It was shown with a 10 s dwell using PU 1510 and 60 s dwell with 3M™ SA9816 a shear load of 20 kN and over approximately 15 kN respectively could be applied to the sub-assembly joint, with reduced overlap, prior to failure. Relative to the total BIW mass, which is generally in the order of a few hundred kilograms (106), the required handling strength of a primary bonded structure in industry is likely to be

substantially lower than this. This shows that the work has demonstrated handling strength requirements can be met, within the required high-volume automotive industry cycle time of under one minute. The component level work also highlighted that as the CFRP component geometry becomes larger the induction heating process becomes more efficient with the available equipment. This was evident by the requirement for spacers to reduce the electromagnetic field strength during the programming step. This emphasises the importance of analysing CFRP component fibre architecture and component geometry on a specific application basis, to optimise induction heating processes and efficiency. It was also seen that despite the larger geometry CFRP components uneven temperature distribution was a significant problem with the single sided induction coil used as seen with coupon scale development in section 4.2.1. This highlighted the need for improved design principles and validation when specifying coils for CFRP induction heating applications in future work, rather than directly applying principles used for metallic substrate heating coils.

Creep appeared to be a primary concern based on component level test data which may prevent adoption of primary bonded structures within industry. If primary bonded, partially cured automotive assemblies deformed significantly during manufacture this could cause significant problems with structure tolerances and related quality issues. It has been identified in subsequent creep validation that this was only a significant concern with 3M™ SA9816 at partial cure, showing significant variation in time to failure under load. As such, based on a generally cohesive failure mode, it was predicted that small variations in cure conditions, as a result of uneven temperature distributions may significantly affect the time to failure under load for partially cured 3M™ SA9816. This further stressed the importance of improved coil design to create uniform temperature distributions for adhesive curing applications. Providing this can be achieved, creep at 25 °c would not appear a significant issue over the timescales required, and loads expected for high-volume manufacture. Further evaluation over a range of temperatures and loads is required to provide increased confidence in this conclusion.

A final consideration concerns the stress concentrations, which were predicted to account for some of the variation in substrate major strain and joint shear strains observed within this chapter. It would be approaching impossible to design a sub-assembly test avoiding any stress concentrations. Further, within an industrial application, stress concentrations are likely to initiate joint failure. As such, determining the magnitude and location of stress concentrations

for primary bonded structures on a case by case basis may be vital, ensuring sufficient handling strength is generated within manufacture. This requires extension of the developed technique beyond the consideration of shear loading alone, considering the case where multiple load cases are present, forming an area for further work.

5.5. Proposed industrial solution

It has been shown within this chapter that induction heating technology can be used to accelerate adhesive cure and achieve substantial handling strength generation in under one-minute cycle time. This was a primary requirement for the manufacture of high volume, primary bonded joints. This sub-section was included to provide a high-level evaluation of the business case surrounding the proposed joining solution. The approach taken was primarily to compare the costings of an induction cured, primary bonded joining technique upon a CFRP intensive joint to an existing joining technique used by Jaguar Land Rover. The comparable technique in this case was riv-bonding, the combination of SPR's and structural adhesives, used by Jaguar Land Rover for the manufacture of aluminium body structures. For more details on this technique refer to section 2.4.2.

It was assumed for the purposes of illustration that the CFRP intensive solution consists of an aluminium sill bonded to a CFRP floor panel. The phased introduction of multi-material joints being consistent with the emerging "right material in the right place" design ethos discussed in section 2.2. The components considered were the same geometry as the demonstrator test component shown in Figure 82. The CFRP component is assumed to be a TP-CFRP, requiring the addition of plasma surface treatment to generate a cohesive failure mode as shown in section 3.3. This was not required with the TS-CFRP components used earlier in this chapter, however represented a more demanding surface pre-treatment requirement and a worst case pre-treatment scenario for the business case.

The key features of the process for both a riv-bonded aluminium intensive assembly and a CFRP intensive, primary bonded assembly are detailed within Table 37. It was assumed that in order to meet high volume cycle time requirements and minimise labour costs, the process would be entirely automated. Thus, the application of robotic systems to the industrial solution is paramount to the development of the business case.

	Existing technology (aluminium intensive joint)	**Proposed new technology (CFRP/aluminium joint)**
Sill material	Aluminium	Aluminium
Floor material	Aluminium	TP-CFRP
Primary joining technology	Riv-bonded solution, Rivet + structural adhesive	Primary bonded solution, structural adhesive only
Required surface treatment upon aluminium surfaces	None – assumed contamination is controlled and structural adhesive formulated to bond in presence of expected metallic surface contamination as 3M 3M™ SA9816 (92).	Assumed adhesive can be formulated to bond to expected aluminium surface contamination.
Required surface treatment upon TP-CFRP surfaces.	No CFRP present	Atmospheric plasma surface treatment. Assumed other contamination e.g. mould release is strictly controlled through manufacturing.
Primary method of handling strength generation	Blind rivets inserted during manufacture, see Figure 111. Only single sided access possible through sill which makes SPR's impractical. Blind rivets provide a suitable alternative.	Electromagnetic induction curing of structural adhesive in under one-minute cycle time.
Adhesive cure method	Structural adhesive cured during E-coat cycle.	Adhesive cured through combination of initial induction process and paint oven thermal cycle.

Table 37 Process comparison – riv-bonding compared to primary bonding

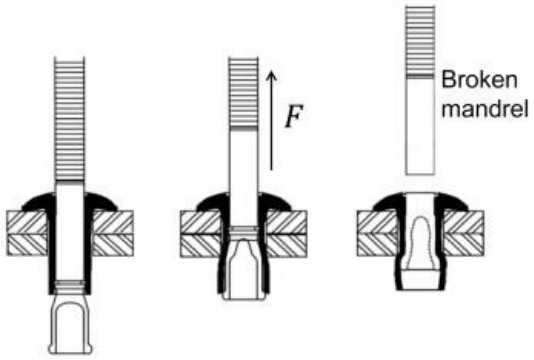

Figure 111 Blind rivet insertion (left) through pre drilled hole, load applied causing rivet to flare (centre) leading to fracture of stem (right) (107)

5.5.1. Industrial process steps for a primary bonded joint

A simplified illustration of how the primary bonded industrial solution was visualised to look is shown within Figure 112. This shows the process steps of component pre-treatment, adhesive application and rapid adhesive curing which lead to a completed sub-assembly.

- **Step 1 (Pre-treatment and adhesive application);**

Within the first stage it was assumed that the floor component would be robotically loaded from stillages into a fixture upon a production line conveyer system. Further, the floor was assumed to be held rigidly in place by the fixture system and moved automatically to the next step at a defined time increment equal to the process tact time. It was assumed that surface contamination upon the CFRP component would be strictly controlled during manufacture, not requiring an abrasion pre-treatment as discussed within section 3.2.1. Once the floor was held in position by the fixture the adhesive would be applied to the bondline by a robot mounted dispenser head. The robot head would also plasma treat the bond surface ahead of adhesive application in the same operation. This is illustrated within Figure 113. This required adhesive dispensing equipment is readily available and used within Jaguar Land Rover's existing manufacturing processes. Adhesive is pumped from bulk 200 L containers and mixed within the dispenser head. The required plasma treatment unit would be similar to that used within chapter 3, described in section 3.1 and is also commercially available.

- **Step 2 (Adhesive cure);**

Following adhesive application and pre-treatment in stage one, the assembly was assumed to move along the production line into stage two. In this stage the aluminium sill components would be picked up from stillages by a pneumatic attachment head on a robotic arm. The robotic arm would place the sills repeatably in the required position on the adhesive bond. It was expected that additional pneumatic fixture devices may be required to hold the sill once positioned by the robot. This would enable the robot to release the sill prior to curing cycle, leaving the same robot free to position the sill on the opposite side of the assembly. Once the sills are in position it was envisaged that an induction coil would move up by pneumatic actuators under the floor, applying moderate pressure to the floor/sill joint to help ensure a consistent bond thickness. Once the coil was in position the induction cycle would commence, initiating the accelerated curing process in a single step

and the development of handling strength. Once the required handling strength was achieved the coil would be retracted. This process would commence simultaneously with both sills. As a result, two induction heating systems would be required. Alternatively, a single system capable of supporting two induction coils. This equipment is also commercially available and would only require moderate development to meet the proposed requirement.

- **Step 3 (Completed sub-assembly);**

Once step two was complete the subassembly would be ready for subsequent assembly operations. The sills would be held in place entirely by the partially cured adhesive, which would generate final strength either over time or during a paint oven cycle.

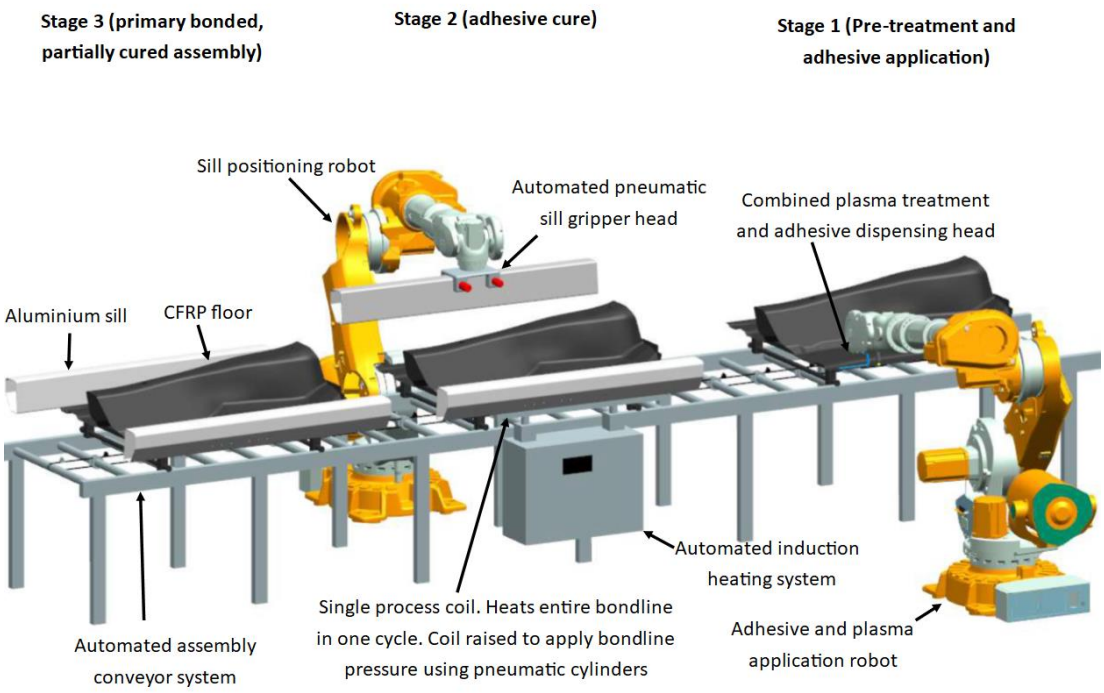

Figure 112 Illustration of proposed industrial solution

It was concluded that all of the primary equipment required for the proposed industrial solution is commercially available with little further development required. The main requirements for future development include optimised induction heating coils for CFRP heating and enhanced adhesives for rapid curing with CFRP and multi-material bonding applications. Refer to chapter four for more detail on the need for these two requirements.

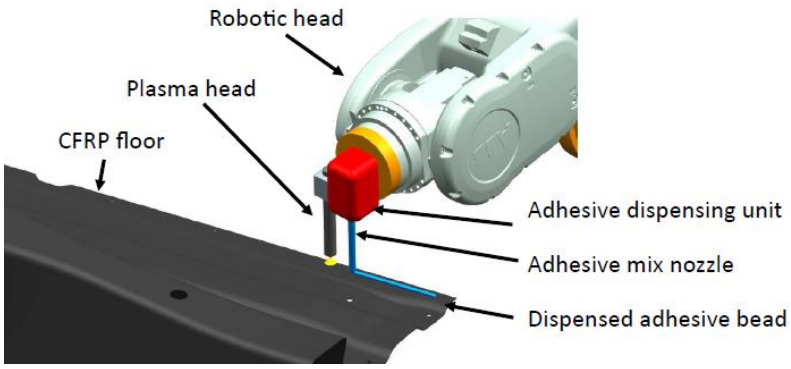

Figure 113 Combined plasma pre-treatment and adhesive application

5.5.2. Process control measures

One of the key barriers identified to the introduction of primary bonded structures within the automotive industry was achieving confidence in the reliability of the adhesive joint. With Jaguar Land Rover's existing manufacturing strategy the structure would be sufficiently supported by the SPR's if the adhesive joint were to fail, reducing the risk of structural failure. However, with a primary bonded joint the redundancy afforded by the SPR's is not present. As such, within this subsection, a variety of quality control processes which could be applied during the manufacture of primary bonded joints were discussed. The combination of these processes offers opportunities to reduce the risk of a joint failure, creating greater confidence in the primary bonded joining strategy.

- **Preliminary quality control processes;**

The potential consequences of excessive surface contamination upon adhesive bond strength were highlighted within section 3.2.1, being both highly detrimental to bond strength and failure mode. To reduce this risk, it was determined that a primary bonding strategy should be designed to either reduce contamination to acceptable levels, function in the presence of excessive surface contaminants or remove the contaminants entirely prior to bonding. To control contaminants procedures would need to be implemented during component manufacture. For example, this could include highly controlled, repeatable application of substances such as mould releases or controlled internal mould releases. Further, critical surface contaminants could be excluded from the manufacturing area, such as silicon sprays and components could be protected from additional contaminants prior to assembly by protective packaging. Alternatively, an adhesive could be formulated to bond in the presence of contaminants, in a similar way to many metal bonding adhesives (92). If either of these

methods were considered impractical an alternative strategy would be to adopt an abrasion surface preparation, removing the contaminant entirely from the bonding surface. This was shown to be one of the most effective methods of contamination removal in section 3.2.1. To ensure consistency of bonding surfaces an automated contact angle analysis system may be advantageous. This unit could measure the surface energy of the material prior to adhesive bonding and flag up any unexpected deviations, indicative of excessive surface contamination. It was identified in section 3.2.1 that this process is most reliable at identifying surface contamination if applied prior to any plasma treatment. Through processes such as these, the risk of excessive surface contamination significantly reducing joint strength can be greatly reduced.

- **Step 1 Pre-treatment and adhesive application control processes;**

The primary risk at this stage in the manufacturing process was identified to be adhesive not being applied to the joint, either through an equipment blockage of failure. Advanced automated dispensing systems employ sophisticated metering systems to ensure the required adhesive flow is achieved, with gear pumps providing one of the most accurate systems (62). Feedback loops are paramount to ensure dispensing is within specification, for example should adhesive viscosity change with facility ambient temperature. Exact monitoring of adhesive flow during the application process can help ensure a repeatable adhesive application and help identify potential joint defects. Adhesive dispensing monitoring systems could be used to flag the joint up as requiring human inspection, where dispensing parameters were outside of a pre-set confidence limit. For example, if a pressure drop in the adhesive flow was identified during dispensing. An additional control measure may be the implementation of imaging techniques which could identify any failure of the robot to dispense a bead. For example, a still image taken in a repeatable position under predefined lighting levels could be taken after adhesive application and compared to a benchmark image. A script could be written to compare adhesive bead colours to a pre-defined acceptable range. This may also enable identification of an off ratio adhesive mix, or failure of a bead to be dispensed. Further work would be required to develop this approach. It would also be recommended to mix glass beads within the adhesive during dispensing, ensuring tolerance issues could not result in complete squeeze out of adhesive within a joint, as well as helping

ensure a joint with a bond gap comparable with the design criteria. The combination of these control processes during dispensing would significantly reduce the probability of joint failure.

- **Stage 2 Induction heating control measures;**

Within the induction heating stage, two critical to quality issues were identified. The first was ensuring repeatable component positioning. In this case advanced fixturing systems would generate confidence that all components align repeatably, including positioning in relation to the induction coil. It was proposed that these fixtures would be pneumatic, enabling rapid clamping and release of components when required. Electrical sensors could be incorporated to ensure fixtures had reached their specified position prior to commencing the cure cycle. The second key element considered was the requirement to achieve a consistent and uniform heating effect along the adhesive bondline. This was shown in section 4.2 to be critical to consistent joint strength. To achieve a uniform bondline temperature distribution, effective coil design was identified as a fundamental requirement. As such, this area would require significant development as part of the industrial process design. It was also determined that this must be completed with respect to a specific component geometry and CFRP layup. Further, the specification of induction heating equipment with sufficient temperature monitoring and feedback control would be vital to ensuring a consistent joint temperature distribution.

Many industrial heating systems implement infrared pyrometers to monitor material temperature during heating and adjust heating parameters through a feedback loop as required. It would also assist in joint quality control to rigorously understand the heating process window during initial equipment set up. This could be completed with additional in-bondline thermocouples using a similar procedure to that detailed within section 5.1.4. This can enable a heating process window to be established, including the range of power input to achieve a specified bondline temperature. This data can later be used for process monitoring. For example, if the required heating power to achieve a specified temperature oversteps this acceptable process window the system could flag up a requirement for manual intervention. This could assist in the avoidance of overbaked, reduced strength adhesive. An example of a potential cause could be a manufacturing inaccuracy or component damage causing an artificially increased bondline thickness. This would require a greater power input to achieve a specified temperature on the reverse of the joint, flagging up a requirement for

manual intervention. The use of external infra-red cameras was also considered, these would enable the monitoring of continuous regions of the joint during heating. With suitable development these thermal images could be compared to an acceptable series of predefined thermal images, again identifying regions of the joint which may have been exposed to an inadequate heating cycle, requiring rework. These processes were believed to offer significant opportunities to increase confidence in the resultant primary bonded adhesive joint.

- **Stage 3 Completed joint inspection methods;**

Once the joint is produced there are further quality assurance methods which were considered. One method would be to create physical joints as part of the manufacturing process. For example, incorporating test coupons produced concurrently with the structure. These could then be removed at a predefined point and destructively tested. In the case where a significant reduction in joint strength identified, the structure could then be removed for rework and analysis of the cause of the problem. Non-destructive test methods such as ultrasonic evaluation were also considered, the subject of much discussion and development in recent years and may help to provide additional confidence in the integrity of a primary bonded joint (108). However reliable non-destructive adhesive joint test methods are limited by presently available technology, future opportunities may emerge within this area in the future.

5.5.3. Costing implications

A high-level comparison between the equipment cost of a riv-bonded (rivet and structural adhesive) production facility and the proposed primary bonded facility, shown in
Figure 112, is presented within this sub-section. Costings were based on initial estimates, in many cases scaled from the procurement of the induction heating equipment used for the experimental work within chapter four and five, discussed further in portfolio submission three. Table 39 presents a comparison between the equipment costs for the two solutions. It was assumed in Table 39 that a single rivet installation gun can be used for the installation of all rivets used on both the left and right side of the aluminium floor/sill sub-assembly. This however would depend upon the number of rivets specified within the assembly design. It can be seen that the total equipment expenditure for the proposed primary bonded solution is in the region of £215,000 higher the existing solution, or £615,00 higher including an estimate of the quality assurance equipment costs discussed in section 5.5.2. Quality

assurance equipment was considered separately, this is due to the requirement being dependant on the probability and consequence of joint failure. It should be considered however, that this is an initial estimate and more accurate quotations would be required with specific geometry to improve the accuracy of this estimate.

It could be assumed that the adhesive cost would be comparable between a primary bonded solution and a riv-bonded solution, with structural adhesive already applied during riv-bonding. A saving in rivets was approximated to be £0.3 per assembly (109), based on an estimate of 10 rivets per assembly and assuming a comparable cost between blind rivets and SPR's. One estimate calculated that approximately 0.0022 kWh of energy is required for the installation of a single SPR (109), thus an assembly of 10 SPR's uses approximately 0.022 kWh, equating to approximately £0.00176 (110). This was assumed to be similar for blind rivets. The primary bonded solution avoids both of these costs associated with rivet installation.

By comparison, the energy requirement for induction heating is much more difficult to quantify, being heavily material dependant. Simulation or experimental evaluation would be required to accurately estimate this value. In order to provide an approximation, the system parameters used in section 5.1.4 were considered, however this is the case of a CFRP/CFRP joint. The system used, detailed in section 4.1 had a maximum power consumption of 23 kW (111). The heating parameters that were used for the demonstrator component testing are shown in Table 38 , in this case the PTFE spacers were added to slow the heating rate. The effect of removing these was estimated to reduce the power consumption to a factor of one third. The effective bond length of 120 mm used in section 5.1.4 was scaled by the 2240 mm bond length on both sides of the sub assembly. It was equated using these scaling parameters the energy cost of the induction cured component would be approximately £0.0419.

The atmospheric plasma treatment surface preparation is assumed to be power from a 13 amp power supply, based on the equipment used within chapter 3. Treatment speed estimated at 50 mm/s equates to approximately £0.0031 of energy per component. Other consumables are considered negligible, with compressed air already in place within the factory and the head controlled by the robot, required for adhesive dispensing.

Based on this estimate the variable cost difference between the proposed primary bonded, induction heated component and the riv-bonded component is an approximate saving of

£0.257 per component. Based on 100,000 vehicles produced per year an approximate eight year payback time is required to offset the extra £215,000 required equipment, or 26 years to offset the required equipment and quality assurance equipment. Whilst upon first inspection this appears a high value, it should be considered that the primary bonded solution provides an enabling technology to incorporate lightweight materials into high volume body structures. This technique avoids many of the disadvantages associated with mechanical fasteners, highlighted in section 2.4.2.

	Max power output / kWh	Power output	Time/s	kWh	kWh (no spacers)	Estimated cost (no spacers)	Scaled by bond length
Ramp phase	23	45.00 %	12	0.0345	0.0115	£0.0009	£0.0171
Dwell phase	23	13.00 %	60	0.049833	0.016611	£0.0013	£0.0248
						Total £/ component	£0.0419

Table 38 Estimate of energy input for an induction heated sub assembly

There are many influencing factors which may influence the business decision towards either a primary bonded solution or the existing riv-bonding solution. The primary aim of this sub-section was to highlight some of the likely cost implications involved. It is likely that with further supplier engagement the equipment costs of the proposed technique could be reduced notably.

		Estimated individual cost	Riv-bonded solution (AL/AL)	Primary bonded solution (AL/CFRP)	Cost increase (Riv-bonded) – (primary bonded)
Required equipment	Conveyer system equipment	£200,000	£200,000	£200,000	£0
	Adhesive dispensing robot	£100,000	£100,000	£100,000	£0
	Atmospheric plasma treatment unit		£0	£40,000	£40,000
	Adhesive dispensing equipment	£75,000	£75,000	£75,000	£0
	Rivet installation gun	£50,000	£50,000	£0	-£50,000
	Rivet installation robot	£100,000	£100,000	£0	-£100,000
	Induction coil	£5,000	£0	£10,000	£10,000
	Induction heater control system	£150,000	£0	£300,000	£300,000
	Induction coil pneumatic positioning system	£15,000	£0	£15,000	£15,000
	Sill positioning robot	£100,000	£100,000	£100,000	£0
	Sill gripper head	£10,000	£10,000	£10,000	£0
				Cost increase	**£215,000**
Optional, quality assurance equipment	Additional dispensing feedback equipment	£40,000	£0	£40,000	£40,000
	Dispensing monitoring camera	£20,000		£20,000	£20,000
	Additional fixturing	£5,000	£0	£10,000	£10,000
	Control pyrometers and feedback system (induction heating)	£20,000	£0	£40,000	£40,000
	Thermal camera monitoring	£100,000	£0	£200,000	£200,000
	Non-destructive testing (ultrasonic)	£150,000	£0	£150,000	£150,000
				Cost increase	**£460,000**

Table 39 Comparison between estimated riv-bonded system costs and primary bonded solution capital costs

6. Project conclusions and opportunities for further work

The continued introduction of lightweight materials, such as fibre reinforced composites, to the automotive body in white has been identified as key future requirement of the high-volume automotive industry. Further, the development of suitable joining techniques has been recognised within the industry as a key enabling technology to allow the introduction of such lightweight materials. The literature review which was conducted identified that primary bonded (adhesive only) joining methods bring advantages for the joining of lightweight, multi-material, automotive structures compared to traditional mechanical fastening techniques. As such, the development of structural adhesive joining techniques, with a particular reference to high-volume multi-material joints, is of great interest to Jaguar Land Rover as the project sponsor. A primary emphasis was placed upon the joining of carbon fibre reinforced composites (CFRP) for this work, an area of ongoing research interest within Jaguar Land Rover and the wider automotive industry.

Two key barriers towards the adoption of high-volume, primary bonded, CFRP structures were identified within chapter two. The first was a requirement for optimal surface pre-treatment methods for thermoset (TS) and thermoplastic (TP) CFRP's, performed prior to adhesive bonding. This was identified as a prerequisite to produce strong, durable adhesive bonds upon low energy CFRP surfaces where various surface contaminants are often present following manufacture. The second barrier related to the cycle time limitations of high-volume manufacture. Often structural adhesives have lengthy cure cycles, through which the adhesive generates strength. However, within high-volume manufacture it is generally considered that a cycle of one minute or less is acceptable in order to generate joint handling strength. Once sufficient strength is developed, fixtures can be removed, and the assembly can progress further along the production line. Thus, a primary industrial requirement is a method to accelerate the cure of structural adhesives during manufacture, meeting a one-minute cycle time to generate sufficient joint strength. The joint strength requirement being component and manufacturing process specific.

Atmospheric pressure plasma treatment (APPT) was identified as a potentially suitable method for the pre-treatment of CFRP prior to structural adhesive bonding. The process was of particular interest to Jaguar Land Rover at the start of the project. Various aspects of this process were considered within chapter three. These included; optimal process parameters and suitability for high-volume manufacture, ability of the process to remove surface

contamination and the effect upon joint durability of the APPT process for both TS and TP-CFRP substrates. The resultant effects upon surface free energy (SFE), single lap shear (SLS) adhesive bond strength and failure surfaces were analysed. It was identified that the process can effectively increase the SFE of TS-CFRP surfaces from approximately 35 mJ/m^2 untreated to approximately 67 mJ/m^2 on average following treatment. However, with the epoxy adhesive used for the investigation the APPT process was not required, upon an uncontaminated TS-CFRP surface, to produce a fully cohesive joint failure mode and a failure strength of approximately 30 MPa. Knowledge of the achievable SFE, following a variety of surface pre-treatments, has provided valuable knowledge for the selection of alternative adhesive systems for bonding the candidate materials in later work.

APPT was shown to influence the proportion of undesirable adhesive failure mode upon a TP-CFRP surface through control of the APPT speed and working distance. The TP-CFRP failure mode was observed to change from fully adhesive failure without APPT to a combination of material and cohesive failure following APPT. The influence upon the TP-CFRP surface and subsequent adhesive failure mode change was identified through a surface free energy increase from approximately 48 mJ/m^2 untreated to 65 mJ/m^2 with optimal APPT. A change in surface chemistry was also identified through x-ray photo electron spectroscopy, with surface oxygen content increasing from 16.3 % untreated to a maximum of 29.7 % following APPT, contributing to the change in failure mode through the creation of oxygen containing functional groups on the TP-CFRP surface. The requirement to minimise the proportion of adhesive failure upon a joint failure surface is of significant importance to industry and was shown to reduce strength loss upon joint ageing within hot/wet environments from 37.9 % to 28.9 % untreated and with APPT treated respectively. It was observed that the slowest treatment speed investigated did not yield the lowest strength loss, potentially due to degradation of the polymer surface. The reduction in strength loss post ageing was attributed to the generation of stronger adhesion forces. Further, knowledge of the required APPT and SFE parameters to achieve an optimal surface condition contributes to reduced cycle time and increased manufacturing efficiency for Jaguar Land Rover, through the efficient introduction of the APPT process.

The ability of APPT process to remove surface contamination which may be expected upon CFRP surfaces was shown to be limited in section 3.2.1. This disproved previous suggestions within literature and the sponsor company that the process may be effective at

contamination removal prior to adhesive bonding. Applying plasma treatment to remove a water-based mould release contaminant, for example, can reduce the bond strength from approximately 31 MPa on average with an uncontaminated TS-CFRP surface to 16 MPa following APPT treatment upon the contaminated surface. Where the joint was formed directly onto the contamination without pre-treatment an average bond strength of 25 MPa was identified, highlighting the reduction in joint strength as a result of APPT treating the contaminant.

It was identified that whilst a significant reduction in SFE may not necessarily be identified post APPT as a result of treating a contaminated surface, the resultant bond strength is often critically reduced. Bonding to the untreated and contaminated surface in many cases results in a higher joint strength than bonding to the APPT treated surface where contamination is present. This is an important result for Jaguar Land Rover, which if it had remained unidentified could result in the incorporation of a process not able to perform to manufacturing requirements, as such risking unnecessary capital expense, manufacturing delays and the risk of in-service joint failure. It was identified that abrasion is often the only failsafe method of surface contamination removal prior to adhesive bonding from the pre-treatment methods investigated. In all cases abrasion restored bond strength to approximately the uncontaminated levels in the presence of contaminants. Alternatively, it may be possible to control the type and level of surface contamination present through the CFRP manufacturing process, rather than implementing abrasion process to remove surface contamination.

Electromagnetic induction heating was identified within chapter two as a suitable method for rapidly heating CFRP and metallic substrates. As such, the process held potential for accelerating the cure of thermoset structural adhesives in view of the high-volume manufacturing cycle time requirements. Induction heating equipment was specified and purchased as detailed in section 4.1.2. Subsequently an extensive test methodology was developed in section 4.1 and 4.3.1 to identify the achievable joint strength for specified heating profiles using various polyurethane and epoxy structural adhesive candidates. Four leading adhesive manufactures were engaged to supply potentially suitable rapid curing adhesive products for the specific industrial requirement. The key requirement was to achieve a partial degree of cure and strength through an initial heating cycle not greater than one minute, known as handling strength. This partial strength generation is sufficient for

manufacturing requirements, with final cure developed at a later stage of manufacture such as a paint oven bake. Due to handling strength requirements being largely component and assembly specific a specific target did not exist. As such, the main aim of the work was to identify the maximum handling strength within the available cycle time which could be achieved.

It was identified that mean handling strengths in lap shear of up to 8.8 and 3.9 MPa could be achieved in up to one-minute cycle time with polyurethane and epoxy adhesive systems respectively, when tested at 50 °c. The bondline temperature at the point of tensile test, or load application in a manufacturing environment, can significantly affect the strength of the partially cured joint. For example, 3M™ SA9816 produced approximately 1.8 MPa lap shear strength after a 60 s dwell at 130 °c when tested at 30 °c, compared to 0.6 MPa when tested at 80 °c. This is an important consideration where a primary bonded structure moves though the production line, in that as the bondline temperature varies the handling strength will also vary. For example, if the structure moved through a paint oven at elevated temperature the joint may not be able to resist the loads upon it, if insufficiently cured and the structure may deform. This assumes that the rate of residual cure development within the oven was not great enough to generate sufficient additional strength prior to deformation. This is a significant finding and highlights the need to validate this property of an adhesive when used for a primary bonding application within industry, data which was not previously available from adhesive suppliers.

Another important consideration identified was the high variability in experimental results for some of the analysed adhesive products. For example, with Sika 7666/522 a residual error standard deviation of joint strength, σ=1.62 MPa was calculated. This compared to a mean joint strength of approximately 3.75 MPa following a 60s dwell at 110°c, when tested at 50 °c. This leads to great uncertainty when predicting joint strength for a given curing profile. For a primary bonded automotive joint, confidence is vital for the technology to be adopted into a production application. As such adhesives which produce low variability in handling and final strength may be preferable to those with higher ultimate performance and higher variability. Similarly, within industry, consideration should be given to methods to reduce joint strength variability, such as achieving a consistent substrate surface condition, precise adhesive application specifications and control over curing temperature profiles. Methods which can be used to achieve this were discussed within section 5.5.2. In later work, standards for

acceptable handling strength variability would need to be considered. These would inevitably be based on production requirements and component specific geometry.

It was also identified that a trade-off exists between maximising the rate of cure development and the risk of overheating the adhesive, which can reduce its fully cured performance. As such, close control over bondline temperature distribution is vital to achieve optimal joint strength development. This was found to be much more challenging when induction heating CFRP compared to aluminium. The induction heating effect upon CFRP was influenced by many factors including component geometry and laminate fibre type and architecture. Effective design principles for induction heating coils used for CFRP heating can aid optimal development of adhesive handling strength. For example, using multiphysics simulation packages to optimise the induction coil design to achieve target heating profiles on CFRP substrates. Where sub-optimal induction coils were used for heating CFRP localised joint overheating was observed. This was shown to result in reduced fully-cured adhesive joint properties. Examples of this can be seen in sections 4.2.1 and 5.2.

The use of thermokinetic modelling to simulate the adhesive cure process during manufacture was demonstrated in section 4.4.2. This approach provides a rapid method to establish the required induction heating profile to achieve a specified degree of adhesive cure. Through the use of developed relationships between adhesive mechanical properties and degree of cure the model can be used to establish the required cure profile for a specified handling strength. Thus, should the joint handling strength requirements change, a revised cure profile can be quickly established. A further extension of this concept could be applied to the entire automotive assembly process, leading to the prediction of adhesive cure and joint mechanical properties through a multitude of heating and dwell phases. As a result, thermal processes can be introduced to ensure only the minimum energy input is applied to deliver the minimum required degree of cure and joint mechanical properties. As such, the use of thermokinetic cure modelling can provide substantial time savings through avoiding repeated experimental data collection and cost savings through the optimisation of cure cycle's and thermal processes. These are both substantial benefits to Jaguar Land Rover relating to the introduction of primary bonded structures.

Finally, the primary bonded technologies developed were demonstrated through a full-sized CFRP sub-assembly of a floor to sill joint from a demonstrator Jaguar vehicle within chapter

five. A bespoke fixture was designed and manufactured to support the assembly and apply a shear load of 20 kN to the joint between a floor and sill. Two adhesive products were selected, one epoxy and one polyurethane and the adhesive joint was induction cured using the parameters developed within the experimental work. A failure load of up to 20 kN was sustained over a reduced bondline area compared to the design joint overlap. This load was well in excess of a typical BIW weight, following an adhesive cure cycle of up to approximately one minute. This highlighted to Jaguar Land Rover that handling strength and cycle time limitations are achievable for a primary bonded CFRP structure using rapid curing adhesives combined with electromagnetic induction heating.

To conclude, key industrial challenges relating to the introduction of high-volume, primary bonded, adhesive joints were identified and subsequently addressed throughout this project. This included optimised surface pre-treatment techniques for CFRP and methods to accelerate adhesive cure, generating rapid joint handling strength. Optimal solutions were identified as well as important industrial considerations to maximise the industrial performance and cost effectiveness of the developed adhesive bonding techniques. Together, these conclusions contribute towards the introduction of primary bonded structures within the challenging field of multi-material automotive structure joining at high-volume. This represents an innovative potential solution to a key industrial problem within Jaguar Land Rover and the wider automotive industry.

6.1. Contribution to innovation

Throughout this work a number of key contributions to innovation were made, these include;

- The determination of the atmospheric plasma surface pre-treatment process suitability for high-volume, structural adhesive joining applications upon FRP substrates. This detailed understanding extended beyond that of previous studies in relation to a specific, high-volume, joining application. Further, the work discounted previous theories relating to the process suitability for surface contamination removal prior to adhesive bonding. Evaluating suitable surface pre-treatments for CFRP adhesive bonding was a primary requirement of Jaguar Land Rover at the start of this project.

- The application of electromagnetic induction heating to accelerate adhesive cure upon CFRP components for high-volume joining applications. This process was shown

to be able to deliver suitable heating rates to meet manufacturing cycle times for the generation of adhesive joint handling strength upon CFRP components. High-volume applications of induction heating for CFRP based adhesive curing within the automotive industry had not been previously identified.

- The identification of a joining process for CFRP intensive, lightweight automotive structures within Jaguar Land Rover. This was a key requirement of the sponsor company prior to the commencement of this project. The process was demonstrated through the joining of multiple full-sized CFRP sub-assemblies from a demonstrator Jaguar vehicle.

- The application of thermokinetic cure modelling to aid in the design of thermal process during the manufacture of a primary bonded automotive structures. This process can help to ensure sufficient joint handling strength is generated at all stages of the manufacturing process. Further, it can contribute to minimising unnecessary energy input during manufacture and reducing experimental time in designing manufacturing processes for primary bonded structures.

6.2. Opportunities for further work

A number of considerations evolved throughout the course of this project which provide scope for further research and development;

1. It was identified that an optimal adhesive for a CFRP intensive, high-volume, primary bonded automotive application does not exist at present. An optimal adhesive would possess such features as not requiring any surface preparation, for example. This would avoid a key step in the production process in order to produce a strong and durable adhesive joint. For example, such an adhesive would be able to bond to surfaces contaminated with mould release, in a similar way to metal bonding adhesives have been formulated to bond in the presence of stamping lubricants. Structural bonding to thermoplastic substrates without surface treatment is another opportunity for development. Further, a number of adhesives exist which produce exceptionally high bond strengths upon CFRP surfaces but are not suitable for the accelerated cure cycles required for high-volume manufacture. As a result, the potential exists to develop an adhesive specifically for the present requirement of

high-volume manufacture and rapid adhesive cure upon CFRP intensive and multi-material substrates.

2. The design of optimal electromagnetic induction coils was identified as critical in achieving uniform bondline temperature distribution when heating CFRP. This was essential if the rate of cure development was to be maximised without effecting the fully cured adhesive properties. The CFRP component geometry and fibre architecture within the laminate were identified to influence the induction heating effect. As a result, the potential exists for improved design guidelines for the design of induction coils to rapidly heat CFRP composites and multi-material joints for rapid adhesive cure

3. Creep was identified as a possible manufacturing concern for a primary bonded automotive assembly where joints are partially cured to generate handling strength. Specifically, whether a primary bonded structure would excessively distort through the manufacturing process due to the loads applied to it. A limited investigation was performed to identify the effects of creep and it was identified that creep appeared not to be a significant concern, providing adhesive cure conditions could be tightly controlled. An extended sturdy would be advantageous and provide additional information to industry, beneficial for the manufacture of primary bonded automotive structures. This would particularly extend to a range of load application temperatures and loading cases.

4. The use of single lap shear adhesive testing provides a convenient test method, widely used within the automotive industry. The method also represents many automotive joint applications. However, much discussion surrounds the generation of stress concentrations within the test geometry which can affect the apparent mechanical properties of the adhesive. A geometry–independent test method would be preferable to calculate true adhesive properties. However, combination of such test methods with rapid curing techniques and CFRP interfaces is a significant challenge. Thus, the opportunity exists to develop improved test methods for rapid curing adhesive evaluation upon CFRP substrates. This would enable more accurate adhesive properties to be evaluated for input into CAE programmes, for example.

5. Thermokinetic cure modelling has been identified as a valuable technique for the design of optimal induction cure profiles to achieve required mechanical joint properties. However, this requires evaluation of the relationship between degree of cure and various adhesive properties over a range of temperatures. Techniques to develop this area provide an opportunity for further work with many benefits to be gained in terms of manufacturing process design. This would extend the technique presented in section 4.4.2 to multiple load cases.

7. References

1. Vehicle Certification Agency. *Cars and Carbon Dioxide*. [Online]. 2017. [Accessed 27/06/2017]. Available from: http://www.dft.gov.uk/vca/fcb/cars-and-carbon-dioxide.asp
2. Department for business energy and industrial stratergy. *Greenhouse gas inventory summary factsheet*. [Online]. 2016. [Accessed 23/08/2017]. Available from: https://www.gov.uk/government/uploads/system/uploads/attachment_data/file/574505/Overview_2014_v2.0.pdf
3. European Commisson. *Climate Action - Reducing CO2 emissions from passenger cars*. [Online]. 2017. [Accessed 27/06/2017]. Available from: https://ec.europa.eu/clima/policies/transport/vehicles/cars_en
4. White M, editor. Lightweight Vehicle Technology, 2012, 02/05/2012, Castle Bromwich UK: Jaguar Land Rover Ltd, 2012.
5. Hughes D. *Automotive Council - technology road mapping exercise conversation*. Personal communication. 2017. [18/08/2017].
6. Davies G. Materials for consideration and use in automotive body structures. Oxford: Butterworth-Heinemann, 2012.
7. Autocar. *Under the skin of the new range rover sport*. [Online]. 2013. [Accessed 27/06/2017]. Available from: https://images.cdn.autocar.co.uk/sites/autocar.co.uk/files/styles/gallery_slide/public/All-New_Range_Rover_Sport_BIW_Front_34.jpg?itok=wob4a-vS
8. Hirsch J. Recent development in aluminium for automotive applications. Transactions of Nonferrous Metals Society of China. 2014;24(7):1995-2002.
9. Davies G. Materials for Automobile Bodies. Oxford: Butterworth-Heinemann, 2012.
10. Gurit. Guide To Composites. Isle of Wight, UK: 2012.
11. Mallick PK. 6 - Thermoset–matrix composites for lightweight automotive structures. Materials, Design and Manufacturing for Lightweight Vehicles: Woodhead Publishing; 2010. pp. 208-231.
12. Boeman RG, Johnson NL. Development of a cost competitive, composite intensive, body-in-white. Society of Automotive Engineers. 2002;1905(01).
13. Composites World. *Automotive CFRP: The shape of things to come*. [Online]. 2013. [Accessed 27/06/2017]. Available from: http://www.compositesworld.com/articles/automotive-cfrp-the-shape-of-things-to-come
14. BMW AG. *Life module from CFRP: An innovative cabin*. [Online]. 2017. [Accessed 27/06/2017]. Available from: http://www.bmwgroup-plants.com/en/shared-content/production/bmw-i-composition.html
15. Cunningham J. *Lightweight materials help automotive sector meet tough targets*. [Online]. 2013. [Accessed 29/06/2017]. Available from: http://www.materialsforengineering.co.uk/engineering-materials-features/lightweight-co-operation/48591
16. Begemann W. Hybrid lightweight construction for optimum component design. [Press release]. *Verband deutscher maschinen - und anlagenbau* (Mechanical engineering industry association). 2016.
17. Gardiner G. *Is the BMW 7 Series the future of autocomposites?* [Online]. 2016. [Accessed 11/09/2018]. Available from: https://www.compositesworld.com/articles/is-the-bmw-7-series-the-future-of-autocomposites
18. Thryft A. *Faster, cheaper compoites for automotive manufacturing*. [Online]. 2016. [Accessed 30/06/2017]. Available from: https://www.designnews.com/materials-

assembly/faster-cheaper-composites-automotive-manufacturing/109833708545390/page/0/1
19. Gardiner G. *HP-RTM on the rise*. [Online]. 2015. [Accessed 30/06/2017]. Available from: http://www.compositesworld.com/articles/hp-rtm-on-the-rise
20. Mallick PK. 5 - Thermoplastics and thermoplastic–matrix composites for lightweight automotive structures. Materials, Design and Manufacturing for Lightweight Vehicles: Woodhead Publishing; 2010. pp. 174-207.
21. Headley M. *Auto Industry Explores Thermoplastics*. [Online]. 2016. [Accessed 10/06/2017]. Available from: http://compositesmanufacturingmagazine.com/2016/09/thermoplastic-composites-draw-automotive-industry-interest/6/
22. Reynolds N, Balan Ramamohan A. High-Volume Thermoplastic Composite Technology for Automotive Structures. Chichester, UK: John Wiley & Sons Ltd; 2013. pp. 29-50.
23. BWM Group. *EUROCARBODY AWARD 2015*. [Online]. 2015. [Accessed 29/06/2017]. Available from: https://news.bmw.co.uk/article/eurocarbody-award-2015-goes-to-the-carbon-core-body-of-the-new-bmw-7-series/
24. Thatcham Research. *BMW 7 Series*. [Online]. 2016. [Accessed 15/08/2018]. Available from: https://www.thatcham.org/files/First_Sights_June2018/Thatcham%201st%20BMW%207%20Series%20-%20G11.pdf
25. BWM Group. *The All-New BMW 7 Series:*. [Online]. 2016. [Accessed 15/08/2018]. Available from: http://www.bmwusanews.com/newsrelease.do?&id=2361&mid=
26. Reed Exhibitions. *Future of lightweight construction depends on right material mix: Lightweight Technologies Forum in Düsseldorf to premiere at ALUMINIUM and COMPOSITES EUROPE 2016*. [Online]. 2016. [Accessed 27/06/2017]. Available from: http://www.reedexpo.com/fr/Press-Releases/2016/Future-of-lightweight-construction-depends-on-right-material-mix-Lightweight-Technologies-Forum-in-Dusseldorf-to-premiere-at-ALUMINIUM-and-COMPOSITES-EUROPE-2016/
27. Modi S, Stevens M, Chess M. *Mixed material joining advancements and challenges* [Online]. 2017. [Accessed 29/05/2017]. Available from: http://www.cargroup.org/publication/mixed-material-joining-advancements-and-challenges
28. Pereira-da-Costa A, Botelho E, Costa M. A Review of welding technologies for thermoplastic composites in aerospace applications. Journal of Aerospace Technology and Management. 2012;4(3):255-265.
29. Yousefpour A, Hojjati M, Immarigeon J-P. Fusion Bonding/Welding of Thermoplastic Composites. Journal of Thermoplastic Composite Materials. 2004;17(203):303-341.
30. JEC Composites Group. *Induction welding: an automated joining process for composites*. [Online]. 2008. [Accessed 23/09/2014]. Available from: http://www.jeccomposites.com/news/composites-news/induction-welding-automated-joining-process-composites
31. Benatar A, Gutowski TG. Methods for fusion bonding thermoplastic composites. SAMPE Quarterly. 1986;18(1):35-42.
32. Balle F, Wagner G, Eifler D. Ultrasonic metal welding of aluminum sheets to carbon fibre reinforced thermoplastic composites. Advanced Engineering Materials. 2009;11(1-2):35-39.
33. Ageorges C, Ye L. Resistance welding of thermosetting composite/thermoplastic composite joints. Composites Part A: Applied Science and Manufacturing. 2001;32(11):1603-1612.

34. Bayerl T, Duhovic M, Mitschang P, Bhattacharyya D. The heating of polymer composites by electromagnetic induction – a review. Composites Part A: Applied Science and Manufacturing. 2014;57(0):27-40.
35. Ageorges C, Ye L. Fusion bonding of polymer composites : [from basic mechanisms to process optimisation]. London: Springer, 2002.
36. Moser L. Experimental analysis and modeling of susceptorless induction welding of high performance thermoplastic polymer composites. Dr.-Ing thesis. Kaiserslautern, Germany: Inst für Verbundwerkstoffe, 2012.
37. Duhovic M, Mitschang P, Maier M. Advances in simulating the processing of composite materials by electromagnetic induction In: Corporation LST, editor. 9th European LS-Dyna Conference 2013; Livermore, CA 94551 USA, 2013.
38. Ahmed TJ, Sravrov D, Bersee HEN, Beukers A. Induction welding of thermoplastic composites- an overview. Composites Part A: Applied Science and Manufacturing. 2005;37:1638-1651.
39. Ye S, Cramer NB, Stevens BE, Sani RL, Bowman CN. Induction Curing of Thiol-Acrylate and Thiol-Ene Composite Systems. American Chemical Society. 2011;44:4988-4996.
40. Mitschang P, Velthuis R, Emrich S, Kopnarski M. Induction heated joining of aluminium and carbon fibre reinforces nylon 66. Journal of Thermoplastic Composite Materials. 2009;22(767):767-800.
41. Buxton AL. Welding Technologies for Polymers and Composites. The Joining of Plastics and Polymer Composite Materials. Cambridge, United Kingdom: IMechE Seminar, 24/10/2002. 2002.
42. Villegas IF, Moser L, Yousefpour A, Mitschang P, Bersee HE. Process and performance evaluation of ultrasonic, induction and resistance welding of advanced thermoplastic composites. Journal of Thermoplastic Composite Materials. 2013;26(8):1007-1024.
43. Benatar A. 12 - Ultrasonic welding of plastics and polymeric composites. Power Ultrasonics. Oxford: Woodhead Publishing; 2015. pp. 295-312.
44. Beehag A, Jackson A, Hou M, Paton R, inventors; Advanced Composite Structures Limited, assignee. Welding of functional components to polymer composite components. US patent. 2012, 12/07/2012.
45. ACS Australia. *Materials and Manufacturing*. [Online]. 2017. [Accessed 30/06/2017]. Available from: http://acs-aus.com/index.php/materials-and-manufacturing
46. Lionetto F, Balle F, Maffezzoli A. Hybrid ultrasonic spot welding of aluminum to carbon fiber reinforced epoxy composites. Journal of Materials Processing Technology. 2017;247:289-295.
47. Hughes D. Associate Professor, WMG. *Automotive body joining technical accreditation scheme module discussion*. Personal communication. 2017.
48. Mallick PK, Jandali G. Vibration welding of a unidirectional continuous glass fiber reinforced polypropylene GMT. Composites Part A: Applied Science and Manufacturing. 2005;36(12):1687-1693.
49. Dukane IAC LLC. *Automotive Welding Solutions*. [Online]. 2017. [Accessed 03/07/2017]. Available from: http://www.dukane.com/us/AP_Auto.htm#Classic
50. Dukane IAC LLC. *What is Vibration Welding?* [Online]. 2017. [Accessed 03/07/2017]. Available from: http://www.dukane.com/us/PVI_What.htm
51. Wu C-Y, Benatar A, Mokhtarzadeh A. Comparison of Ultrasonic Welding and Vibration Welding of Thermoplastic Polyolefin. Welding in the World. 2012;56(1):69-75.
52. Messler Jr RW. Chapter 2 - Mechanical Joining. Joining of Materials and Structures. Burlington: Butterworth-Heinemann; 2004. pp. 45-104.

53. Khoshravan MR, Samaei M, Paykani A. Numerical investigation on the position of holes for reducing stress concentration in composite plates with bolted and riveted joints. Theoretical and Applied Mechanics Letters. 2011;1(4):041005.
54. Gay A, Lefebvre F, Bergamo S, Valiorgue F, Chalandon P, Michel P, et al. Fatigue of Aluminum/Glass Fiber Reinforced Polymer Composite Assembly Joined by Self-piercing Riveting. Procedia Engineering. 2015;133:501-507.
55. Heimbs S, Schmeer S, Blaurock J, Steeger S. Static and dynamic failure behaviour of bolted joints in carbon fibre composites. Composites Part A: Applied Science and Manufacturing. 2013;47:91-101.
56. Kroll L, Mueller S, Mauermann R, Gruetzer R, editors. Strength of self piercing riveted joints for CFRP/aluminium sheets. 18th International Conference on Composite Materials; 2011, Jeju Island, Korea.
57. Di Franco G, Fratini L, Pasta A. Analysis of the mechanical performance of hybrid (SPR/bonded) single-lap joints between CFRP panels and aluminum blanks. International Journal of Adhesion and Adhesives. 2013;41:24-32.
58. Pramanik A, Basak AK, Dong Y, Sarker PK, Uddin MS, Littlefair G, et al. Joining of carbon fibre reinforced polymer (CFRP) composites and aluminium alloys – A review. Composites Part A: Applied Science and Manufacturing. 2017;101:1-29.
59. Ueda M, Miyake S, Hasegawa H, Hirano Y. Instantaneous mechanical fastening of quasi-isotropic CFRP laminates by a self-piercing rivet. Composite Structures. 2012;94(11):3388-3393.
60. Blaga L, dos Santos JF, Bancila R, Amancio-Filho ST. Friction Riveting (FricRiveting) as a new joining technique in GFRP lightweight bridge construction. Construction and Building Materials. 2015;80:167-179.
61. Nagel P, Meschut G. Flow drill screwing of fibre-reinforced plastic-metal composites without a pilot hole. Welding in the World. 2017;61(5):1057-1067.
62. Lucas da Silva, Ochsner A, Adams R. Handbook of Adhesion Technology. Berlin: Springer, 2011.
63. Lu Y, Broughton J, Winfield P. A review of innovations in disbonding techniques for repair and recycling of automotive vehicles. International Journal of Adhesion and Adhesives. 2014;50:119-127.
64. Roussak OV, Gesser HD. Applied chemistry : a textbook for engineers and technologists. New York: Springer, 2013.
65. Ford Motor Company. *Engineering Material Specification.* Dearborn, Michigan. Ford Global Technologies Inc. 2003.
66. Adhesivesandglue.com. *What is the surface energy and surface tension?* [Online]. 2017. [Accessed 04/07/2017]. Available from: http://www.adhesiveandglue.com/surface-energy.html
67. Kruss GmbH. *Owens, Wendt, Rabel and Kaelble (OWRK) method*. [Online]. 2017. [Accessed 24/08/2017]. Available from: https://www.kruss.de/services/education-theory/glossary/owens-wendt-rabel-and-kaelble-owrk-method/
68. Davis GD. Contamination of surfaces: Origin, detection and effect on adhesion. Surface and Interface Analysis. 1993;20(5):368-372.
69. Ebnesajjad S, F. EC. Surface treatment of materials for adhesive bonding. London, UK: Elsevier, 2013.
70. Hnilica J, Potočňáková L, Stupavská M, Kudrle V. Rapid surface treatment of polyamide 12 by microwave plasma jet. Applied Surface Science. 2014;288(0):251-257.
71. Fanelli F, Fracassi F. Atmospheric pressure non-equilibrium plasma jet technology: general features, specificities and applications in surface processing of materials. Surface and Coatings Technology. 2017;322:174-201.

72. Encinas N, Abenojar J, Martínez MA. Development of improved polypropylene adhesive bonding by abrasion and atmospheric plasma surface modifications. International Journal of Adhesion and Adhesives. 2012;33(0):1-6.
73. Gesche R, Kovacs R, Scherer J. Mobile plasma activation of polymers using the plasma gun. Surface and Coatings Technology. 2005;200(1–4):544-547.
74. Akram M, Jansen KMB, Ernst LJ, Bhowmik S. Atmospheric plasma modification of polyimide sheet for joining to titanium with high temperature adhesive. International Journal of Adhesion and Adhesives. 2016;65:63-69.
75. Law V, Mohan J, O'Neill F, Ivankovic A, Dowling D. Air based atmospheric pressure plasma jet removal of FreKote 710-NC prior to composite-to-composite adhesive bonding. International Journal of Adhesion and Adhesives. 2014;54:72-81.
76. Dickie R, Bauer D, Ward S, Wagner D. Modeling paint and adhesive cure in automotive applications. Progress in Organic Coatings. 1997;31(3):209-216.
77. Ali SM. Ultrasonic and thermo-kinetic characterization of curing epoxy resin. PhD thesis. The University of Nottingham. 2013.
78. British Standard. BS EN 1465:2009. *Adhesives. Determination of tensile lap-shear strength of bonded assemblies.* London, UK. BSI. 2009.
79. Kemal Apalak M, Davies R. Analysis and design of adhesively bonded corner joints: fillet effect. International Journal of Adhesion and Adhesives. 1994;14(3):163-174.
80. British Standard. BS EN 15870:2009. *Adhesives —Determination of tensile strength of butt joints (ISO 6922:1987 modified).* London, UK. BSI. 2009.
81. Masterbond. *Strength Properties of Epoxy Compounds*. [Online]. 2017. [Accessed 31/07/2017]. Available from: https://www.masterbond.com/properties/strength-properties-epoxy-compounds
82. Woodward R. Development of innovative composite joining technologies for high volume automotive body in white structures. EngD portfolio submission. WMG - University of Warwick: 2016.
83. Sika AG. SikaPower 490c, Product Data Sheet. Structural and crash resistant two component adhesive. 2014.
84. Woodward R. Development of atmospheric plasma surface treatment for high volume, composite intensive automotive body structures. EngD portfolio submission. WMG - University of Warwick: 2016.
85. Laerd Statistics. *One-way ANOVA*. [Online]. 2017. [Accessed 28/09/2017]. Available from: https://statistics.laerd.com/statistical-guides/one-way-anova-statistical-guide.php
86. Davis M, Bond D. The importance of faliure mode identification in adhesive bonded aircraft structures and repairs. Aircraft Structural Integrity Section Directorate General of Technical Airworthiness. Melbourne, Australia: Royal Australian Air Force, 2008.
87. CASA XPS. *XPS Spectra* [Online]. 2013. [Accessed 06/09/2017]. Available from: http://www.casaxps.com/help_manual/manual_updates/xps_spectra.pdf
88. Walker M. University of Warwick physics department photoemission facility manager. *XPS Analysis discussion*. Personal communication. 2017. [28/07/2017].
89. Hofsetter D. Project leader, R&D adhesive systems, Sika Technology AG. *Sika 490c*. Personal communication. 2015. [12/10/2015].
90. Surface finishing equipment group. *Specification - what is Garnet Abrasive?* [Online]. 2017. [Accessed 30/08/2017]. Available from: http://www.sfeg.co.uk/abrasives-and-spares/abrasive-media/expendable-abrasives/garnet-abrasive
91. Waite C. Materials Engineering, Engineering Technical Services (ETS), Jaguar Land Rover Ltd. *Email conversation - Specification for handling strength*. Personal communication. 2016. [10/06/2016].

92. 3M Ltd. Two part Epoxy Adhesive SA9816 (NPI503), Preliminary Technical Data Sheet. 2011.
93. 3M Ltd. 3M Structural Adhesive SA 9820 - Data Sheet. 2009.
94. Henkel Ltd. Teroson PU1510 - Technical Data Sheet. 2014.
95. Lohmann GmbH & Co. KG. DuploTEC 10400 SBF Preliminary data sheet. 2015.
96. ASTM International. ASTM D3518 / D3518M-13. *Standard Test Method for In-Plane Shear Response of Polymer Matrix Composite Materials by Tensile Test of a ±45° Laminate.* West Conshohocken. 2013.
97. Kapp J. Advanced Application Engineer: Composites, 3M PLC. *Induction curing results discussion*. Personal communication. 2016. [14/09/2016].
98. Sikkel B. Senior Specialist, Adhesives, Coatings and Sealants Group, 3M Automotive and Aerospace Solutions Division. *Results discussion*. Personal communication. 2017. [19/01/2017].
99. Sundrum C, Friedland R, Stahl J. *Results discussion and product optimisation* Personal communication. 2016. [16/12/2016].
100. British Standard. BS EN ISO 11357-5:2014 *Plastics. Differential scanning calorimetry (DSC). Determination of characteristic reaction-curve temperatures and times, enthalpy of reaction and degree of conversion.* London, UK. BSI. 2013.
101. Knauer W. Physicist, Customer Training, Netzch GmbH. *Simulation of adhesives*. Personal communication. 2017. [09/06/2017].
102. Netzch Thermokinetics. Manual - User Guide. 2006.
103. Niks S. *Hem Flange Bonding: Part 1*. [Online]. 2012. [Accessed 29/08/2018]. Available from: http://www.adhesives.org/resources/knowledge-center/aggregate-single/hem-flange-bonding-part-1
104. McCormick N, Lord J. Digital Image Correlation. Materials Today. 2010;13(12):52-54.
105. GOM. Aramis user manual - software. Braunschweig, Germany: GOM, GmbH, 2013.
106. White M, Mustard B, Hutchinson A, Morrey D, Winfield P, Raugei M, et al., editors. Future Automotive Body Structures, 2014, Heritage Motor Center, Gaydon: Institution of Mechanical Engineers.
107. Min J, Li Y, Li J, Carlson BE, Lin J. Mechanics in frictional penetration with a blind rivet. Journal of Materials Processing Technology. 2015;222:268-279.
108. Adhesives.org. *Non-destructive evaluation* [Online]. 2018. [Accessed 06/08/2018]. Available from: http://www.adhesives.org/adhesives-sealants/adhesives-sealants-overview/structural-design/joint-testing/non-destructive-evaluation
109. Briskham P, Blundell N, Han L, Hewitt R, Young K, Boomer D. Comparison of self-pierce riveting, resistance spot welding and spot friction joining for aluminium automotive sheet. SAE International. 2006(2006-01-0774).
110. Department for business energy and industrial stratergy. *Quarterly energy prices*. [Online]. 2018. [Accessed 22/08/2018]. Available from: https://assets.publishing.service.gov.uk/government/uploads/system/uploads/attachment_data/file/720379/QEP_Q1_2018.pdf
111. EFD Induction. Minac 6–12–18–25 SH, Technical Description. Skien, Norway: 2016.